New Horizons in Ocular Surface & Dry Eye Evaluation

Karl Mark Obszanski

Doctor of Philosophy

Aston University, March 2019

KARL OBSZANSKI ASSERTS HIS MORAL RIGHT TO BE IDENTIFIED AS THE AUTHOR OF THIS REPORT.

Thesis Abstract

Although considered to be the most important of all the human senses, the delicate nature of the human eye gives rise to many potential defects that could impact the quality of sight and if left untreated eventually lead to permanent vision loss. Scientists and engineers have studied human vision with a desire to better understand and diagnose conditions that may compromise sight. With the never-ending advancement of technology, new avenues of exploration are continually becoming available which can offer the potential for reduced invasiveness whilst extracting even greater diagnosis fidelity. Nevertheless, even with new technological possibilities, many potential solutions are not suited to day to day clinical environments and may be cost prohibitive or simply unreasonably complex to perform. In many cases subjective observation techniques introduced over a century ago still find favour today and may be preferred over newer methods due to large accessibility and low training requirements.

This thesis is an exploration of cutting-edge technical approaches and developments with the intention of applying them in an original yet rational fashion to achieve mainstream use in real day to day clinical settings for the provision of superior dry eye diagnosis capabilities. The following research will be focused on identifying anterior eye conditions, in particular dry eye which is growing in prevalence and affecting younger age groups. Rather than restricted, in depth focus on a particular technique, this work will consider several unique approaches and lay a strong argument for their viability and subsequent clinical testing in separate, future work.

Chapter 2 focuses on improving the commonly used technique of sodium fluorescein viewing with custom created blue excitation and yellow emission filters. Although such subjective fluorescein observation techniques have existed for many years, the custom filters offer a large improvement in viewing performance, filter efficiency and slit lamp hands free usage, and are ready to scale to production with 1,000 units already manufactured and a further 16,000 units on order.

Chapter 3 describes research on determining the thickness and degradation of the transparent tear film over the course of a blinking cycle. To date, many attempted measures have produced results with an accepted value in the region of 5 µm. Tear dynamics; refresh, spreading and degradation behaviours are key in providing insight into the stability and premature breakdown leading to dry eye disease, all of which are demonstrated as possible with confocal and interferometric technologies being examined and an average tear film thickness value 3.28 µm and degradation rate of $0.048 \pm 0.034\ \mu m^{-2}$ being achieved.

Lastly, chapter 4 introduces a new anterior eye assessment instrument based on the technique of persistence of vision that is capable of enhancing the ability to detect tear film break up time in a new low cost, non- invasive device. A plethora of additional anterior eye examinations such as corneal topography and slit lamp viewing capabilities are also made possible with this new projection method. The POV scope is a distinctive new approach to anterior eye viewing and gives the ability to capture high resolution, high contrast images that in the near future may be coupled to a machine learning platform to provide a clear diagnosis for common conditions including the multifactorial and inconsistent signs and symptoms of dry eye disease.

Acknowledgements

It is with great kindness and gratitude that I would like to thank the many people that were with me on this important journey of investigation and research. My two supervisors, Dr Thomas Drew and Professor James Wolffsohn provided great direction and fuelled my enthusiasm thereby allowing my imagination to flourish while remaining balanced with the appropriate amount of realism.

From the very beginning, master technician Graham Davis has been instrumental in transforming my ideas from drawings on paper into real world devices that convert abstract research into reality. Following on, a big contribution of this was the generous time spent by the technicians of Aston vision sciences department- Kim, Tony, John and Matt for allowing me to use the laboratories and instruments usually at short and inconvenient notice. Special mention must also be given to Ian Routledge from Armstrong Optical for free of charge equipment loans and Richard Furnival at First Press Plastics who believed in my ideas and provided his time as well as professional contacts in the form of Peter and Graham from Colour Flow UK. Together we were able to make something truly special out of nothing.

Finally, the eternal patience and support of my partner Karina Krawczyk who simply by being within arm's reach, had to put up with being the Guinee pig and sitting through many hours of frustrating experiments and failures in my search for a breakthrough. Thank you for making this work worth something!

Table of Contents

List of Figures

List of Tables

Nomenclature

ACD	Anterior Chamber Depth
AI	Artificial Intelligence
CE	Conformité Européenne
CL	Contact Lens
COC	Cyclic Olefin Copolymers
COP	Cyclic Olefin Polymers
CW	Central Wavelength
D	Dioptre
DED	Dry Eye Disease
IPL	Intense Pulsed Light
IR	Infrared
LASIK	Laser-Assisted in Situ Keratomileusis
LED	Light Emitting Diode
Lm	Lumens
MG	Meibomian Gland
MGD	Meibomian Gland Dysfunction
OBE	Optical Bench Equipment
OCT	Optical Coherence Tomography
OEM	Original Equipment Manufacturer
PCB	Printed circuit board
PCTF	Pre corneal tear film
PLTF	Pre Lens Tear Film
POTF	Post Lens Tear Film
POV	Persistence of Vision
PRK	Photorefractive Keratectomy
qDot	Quantum Dot
RI	Refractive Index
SMD	Surface Mount Device
SMILE	Small Incision Lenticular Extraction
STP	Standard temperature and pressure
TF	Tear Film
TFLL	Tear Film Lipid Layer
TFT	Tear Film Thickness
TRL	Technology Readiness Level

1. Introduction

Vision is one of the five sensory inputs of the human body and is considered by many to be the most important of all [1, 2]. A majority of people will live their lives with healthy sight which allows for high quality, independent and fulfilling life-styles. However, the immense complexities of how vision works are hidden, oblivious to most, and taken for granted. Unfortunately, it is only when vision problems develop that individuals start to take notice.

The complex nature of the human eye and its' intricate workings opens the door for enough potential complications to fill a large textbook and as the world's population continues to grow and age, the instance of visual difficulties is increasing [3-5]. If, due to genetic birth defects, accidental injuries or adverse environmental exposure, one or more of the elements begins to function with reduced efficiency or completely ceases to work, serious consequences for visual acuity can become quickly apparent and without medical intervention, may become irreversible.

Visual impairment is defined by the International Statistical Classification of Diseases into one of seven categories according to severity of vision loss as listed in table 1.1; category 0 being normal healthy vision, 1 and 2 referring to mild to severe impairment with 3 to 5 progressively worsening blindness [4, 6]. As of 2010 it has been estimated that worldwide across all age ranges 39 million of are blind [7]. Many diseases are progressive with patients becoming aware of issues early and able to seek appropriate remedies. However, silent diseases such as glaucoma [8, 9] or diabetic retinopathy [10] are typically not immediately apparent to the subject and may only become known during the next eye exam or once vision is compromised sufficiently to become apparent to the patient. Unfortunately damage sustained is typically permanent. It is for such reasons that the College of Optometrists recommends bi-annual eye examination intervals as a means of preventative care, with shorter periods between tests for at high risk patients groups [11]. Counter-intuitively, US studies have shown that 51.9% of adult diabetes sufferers have missed their recommended primary care visit interval [10].

Within the developing world, restricted access to affordable care is the major factor in the high levels of untreated patients; in many instances the visual impairment is caused by reversible conditions such as uncorrected refractive error and advance cataracts, affecting 43 and 33 percent of those visually impaired respectively [7]. Current estimates place the global number of people suffering visual difficulties at 285 million - 90 percent of which are in developing countries [7, 12]

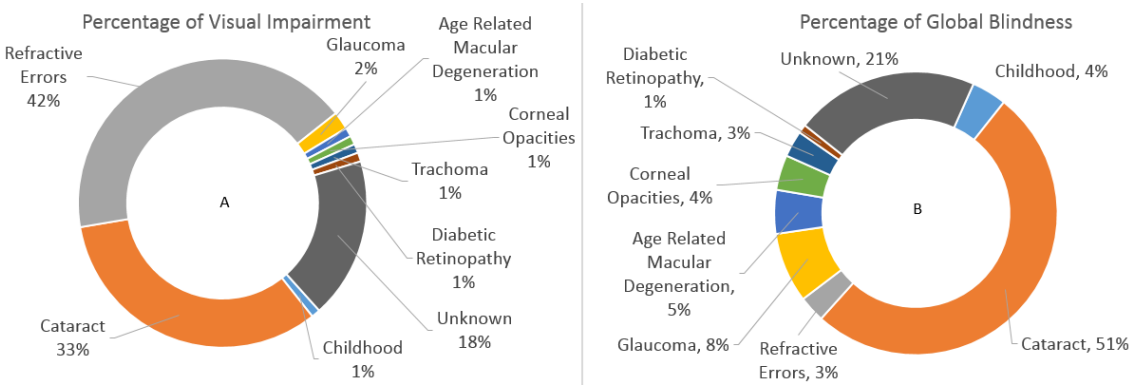

Figure 1-1: [A] Global causes of visual impairment [B] Global causes of blindness. Self- drawn with data compiled from Global estimates of visual impairment: 2010

Care for those affected normally falls on the immediate family members and adds to the burden of reduced independence and inevitable lower quality of life. Globally, reduced productivity attributed to blindness has been calculated at 20- 25 billion US Dollars annually and with most of those affected in the developing world, this adds a signification additional drain on already disadvantaged societies [13]. Even in the UK, it is estimated that 1.93 million people experience sight loss with an additional 250 people beginning to lose their sight every day [1, 14].

Amongst the commonly encountered illnesses broken down in figure 1.1, tear film disorders such as Meibomian Gland Dysfunction (MGD) and Dry Eye Disease (DED), are growing in frequency and severity [15, 16]. Due to behavioural and environmental changes as well as modern lifestyles, dry eye disease which was traditionally confined to older generations and post- menopausal women, is now beginning to manifest itself in younger populations [2]. Triggered by a premature breakdown of the protective tear film that covers the ocular surface, dry eye is a complicated and underappreciated disease which may initially begin as nothing more than itchy or inflamed eyes [17], but unless recognised and treated early DED will evolve into a progressively debilitating chronic condition that will require the patient to administer lifelong stabilising medications with no cure being a real possibility [18]. Indeed ocular surface disorders such as DED are recognised as the leading cause of patient complaints and visits to vision clinics corresponding to increased global disease prevalence [19].

Vision may be the most cherished of the senses, but few people have anything more than a simple understanding of the complexities that give rise to sight [20, 21]. Drilling down deeper into the science of the eye opens many avenues of overwhelming knowledge and wonder that

can be baffling in their detail. Currently there have been over 165 anterior segment conditions identified [22] - too large a scope to allow for sufficient scientific focus in a single thesis. Instead the research within this body of work will confine itself to investigating new approaches and techniques for anterior eye diagnosis and in particular tear film assessment. General knowledge of the anterior eye will be necessary to gain an appreciation of how the various components choreograph their roles and this leads on to an introduction to the human tear film, both of which are covered below.

Contemporary methods and instruments for dry eye evaluation together with industry trends will then be discussed before moving on to new pioneering techniques and forms of assessment devised by the author. It is the aim of this thesis to not only add useful knowledge to this field of science, but ultimately to demonstrate new tangible techniques that allow for the provision of high-quality eye care to a greater number of the world's population.

Table 1-1: International Statistical Classification of Visual disturbances and blindness [6]

<table>
<tr><th rowspan="2">Category</th><th rowspan="2">Description of visual impairment</th><th colspan="2">Observed Visual Acuity</th></tr>
<tr><th>Worse than:</th><th>Equal to or better than:</th></tr>
<tr><td>0</td><td>None to mild</td><td>-</td><td>6/8
3/10 (0.3)
20/70</td></tr>
<tr><td>1</td><td>Moderate</td><td>6/8
3/10 (0.3)
20/70</td><td>6/60
1/10 (0.1)
20/200</td></tr>
<tr><td>2</td><td>Severe</td><td>6/60
1/10 (0.1)
20/200</td><td>3/60
1/20 (0.05)
20/400</td></tr>
<tr><td>3</td><td>Blind</td><td>3/60
1/20 (0.05)
20/400</td><td>1/60
1/50 (0.02)
5/300 (20/1200)</td></tr>
<tr><td>4</td><td>Blind</td><td>1/60
1/50 (0.02)
5/300 (20/1200)</td><td>Light perception</td></tr>
<tr><td>5</td><td>Blind</td><td colspan="2">No light perception</td></tr>
<tr><td>9</td><td colspan="3">Undetermined or unspecified</td></tr>
</table>

1.1. The Anterior Eye

The anterior eye as drawn in Figure 1.2, not only includes obvious components such as the cornea, sclera, pupil and iris, but also concealed adnexa mechanisms which have the primary role of protecting and maintaining the health of the cornea and collectively fall under the definition of the ocular surface as defined by Gipson: [*…the ocular surface] includes the surface and glandular epithelia of the cornea, conjunctiva, lacrimal gland, accessory lacrimal glands, and meibomian gland, and their apical (tears) and basal (connective tissue) matrices; the eyelashes with their associated glands of Moll and Zeis; those components of the eyelids responsible for the blink; and the nasolacrimal duct* [23]. Functional deterioration of the components can lead to a downward spiral of progressively worsening ocular health and persistent conditions ranging from bacterial infections (such as blepharitis and conjunctivitis) through to serious vision disturbing aliments such as keratoconus or corneal dystrophies.

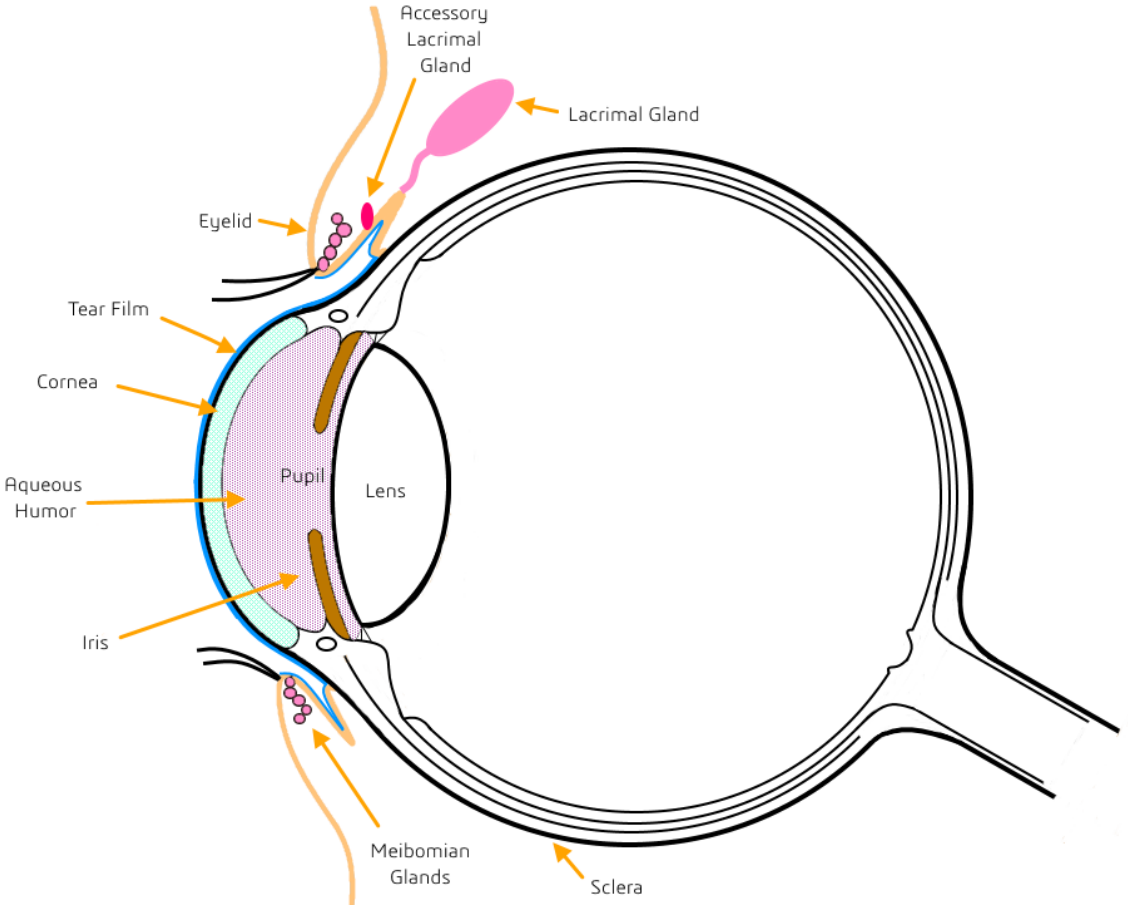

Figure 1-2: Anatomy of the Anterior Eye

Although being anatomically separate to the eye, the eye lids work in tandem to perform several critical functions that aid vision. Eyelids are the protective overcoats which, by means of blinking, keep the eye lubricated and displace foreign bodies that may have gathered on the surface. During a blink cycle the orbicularis oculi muscle works to lower the eyelid and the levator palpebrae superioris muscle counteracts to re-open [24]. Three distinct regions have been identified within the lid margin; a band of cornified epidermis; a mucocutaneous junction zone and finally the stratified epithelium of the palpebral conjunctiva [25]. The limited structural integrity of the human tear film means it must constantly be refreshed through the act of blinking and contaminates that have landed on the exterior of the eye are pushed down toward the lacrimal canal for drainage [26]. Experiments by Nakamoi and co. measured a blink rate of 20.1 ± 1.6 per minute, with a maximum blink interval periods of 11.4 ± 1.1 seconds for healthy eyes under relaxed conditions with freedom to blink as and when desired [27]. Lower blink rates have been associated with increased tear osmolarity [28].

Meibomian Glands (MG), embedded on the underside of the tarsal plates of both the top and bottom eye lids embody modified sebaceous glands which are responsible for lipid fluid secretion that promote tear film stability and longevity between blinks [29, 30]. Although the upper and lower lids were once considered as being duplicate, it has been found that the lower lid contains roughly 20 – 30 MGs, compared to 30 – 40 MGs for the upper, “wiper” lid [31]. Meibomian Gland Dysfunction (MGD) is a broad term given to changes in glandular function and secretion which give rise to a negative alteration in tear film composition [32]. MGD has been linked to the two main forms of dry eye disease; evaporative dry eye [32] and aqueous deficient dry eye [33].

Working in harmony with MGs are the lacrimal glands located higher up under the brow, which together create a fine lubricating liquid composed of three constituents termed the lipid, aqueous, and mucin layers- the last being produced by the conjunctiva as seen in figure 1.2. Antibacterial enzymes such as Lysozyme and Lactoferrin, help ward off infection and are included with the above ingredients [34, 35]. Hyposecretion from the lacrimal and meibomian glands has been linked to increased tear osmolarity- a condition of reduced tear film aqueous component [28] and as one of the prime indicators of dry eye disease [36].

Lining the underside of the eyelids and covering the sclera up to the corneal limbus, is a smooth transparent membrane which reduces friction of the eyelids as they pass over the eyeball and facilitates comfortable and effortless blinking. Composed of two layers; an epithelium containing goblet cells for mucin tear film layer production and a second inner stroma layer [37],

the conjunctiva and cornea provide an even surface to promote the uniform spread of the tear film over the exposed eyeball [38].

Twenty mucin varieties have been identified as being secreted by the goblet cells found in the conjunctiva and one of the core roles is considered to be maintaining cleanliness of the ocular surface [39]. Debris or foreign bodies that make their way into the depths of the tear film are captured and drained away through the nasolacrimal ducts [38]. For mucins to perform their role they must be free to disperse across the surface of the eyeball and any reduction in the goblet cell number will directly affect their efficiency [38].

Surrounding the central cornea is a white collagenous skin known as the sclera. Comprising of tough interlocking fibres interwoven with tiny blood vessels, the sclera stretches around the eye in all directions and covers roughly 85% of the total surface [40]. Being no more than 1 mm thick, the main roles of the sclera are to help maintain the round shape of the eye, protect the subtle internal mechanisms as well as provide an interface upon which six main extraocular muscles can attach to various points around the eyeball which give the ability to precisely control eye movement [41].

Conjoining with the sclera at the limbus is the cornea, which although being similar in composition, is completely transparent. Composed of six cell layers [42] arranged in a longitudinal direction, the cornea is designed to minimise opacity and allow maximum light radiation of between 400 – 650nm to pass through to the retina [43]. Although the cornea is filled with the greatest nerve density of any tissue within the human body [44], to achieve total clarity, it is also avascular and all nutritional requirements are satisfied through tear film molecular absorption. The cornea is curved in shape and roughly 12 mm in diameter with an average 0.5 mm thickness at the central apex [45]. Along with protecting the intricate components within the eye, the main function of the cornea is in fact first stage refraction of light before reaching the crystalline lens. The curvature of the cornea gives it about two thirds, or 40 dioptres of the total 60 dioptres focusing power of the eye [46]; any variations to the curvature of the cornea leads to complications that affect visual perfection with common examples including long sightedness, near-sightedness, and astigmatism. To assist with TF adhesion and to act as the first line of ocular defence [47, 48] the corneal and scleral epithelia comprise of transmembrane mucins termed Epitectin, extending up to 500nm into the tear film [49, 50]. It is these transmembrane mucins which help with spreading the TF over the surface of the eyeball and prevent premature collapse of TF.

It has been demonstrated by Nakamori et al. that blinking is influenced by ocular surface conditions, environmental factors and psychological state [27]. Corneal damage arising from events such as prolonged contact lens use, refractive corrective surgery (LASIK/ SMILE/ PRK) or diseases such as dry eye cause corneal desensitization leading to fewer blinks and a consequential compromised flow and hyposecretion of the tear fluid [16].

Myopia, one of the most common refractive conditions, appears from a disparity between axial eye length and refractive power [40]. This results in incoming light not being focused correctly onto the retina and indistinct images interpreted by the brain- figure 1.3. The condition is thought to affect up to 20 – 30% of North American, Australian and European populations, but is distressingly high in East Asia where frequency is reported in 90% of school leavers [51]. It is currently accepted that negative change of the sclera plays a central role in the advance of myopic disorders [40] and although considered to be a benign condition that is remedied with simple corrective lenses, the increase in prevalence may not only be due to genetic predisposition but also to modern changing lifestyles, educational pressures and a reduction in time spent outdoors [51, 52]. Indeed, refractive error is one of the major causes of preventable visual impairment which affects 42% of the global population [7].

Found within the boundaries of the cornea is a coloured ring of muscle fibres which controls the size of the central opening; the pupil. Filled with melanin pigment to reduce intraocular phantom light scatter, the colour of the strands are dependent on melanin concentration with lower amounts giving rise to a lighter blue eye colour and higher concentrations giving rise to darker browns [26]. Substantial performance differences have been found between lighter and darker Iris pigmentation: in a large study performed by Nischler and colleagues, subjects were exposed to various lighting conditions and visual displays and were graded depending upon their response. It was found that levels of Iris pigmentation have significant effects on intra ocular stray light and corresponding contrast sensitivity, giving rise to hazy or unclear vision. People with lighter irides suffered from greater stray light and a reduction in contrast which resulted from the higher translucence of the lighter blue coloured irises [53].

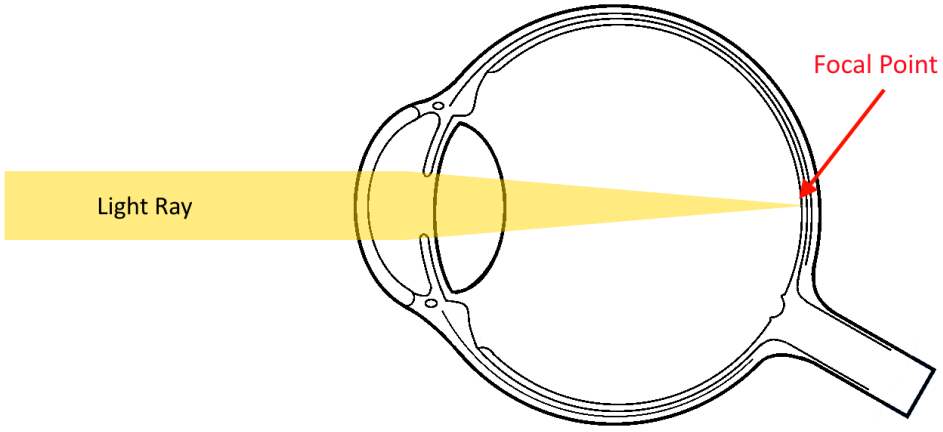

A: Emmertropic condition- images formed on the retinal surface giving rise to clear, sharp vision

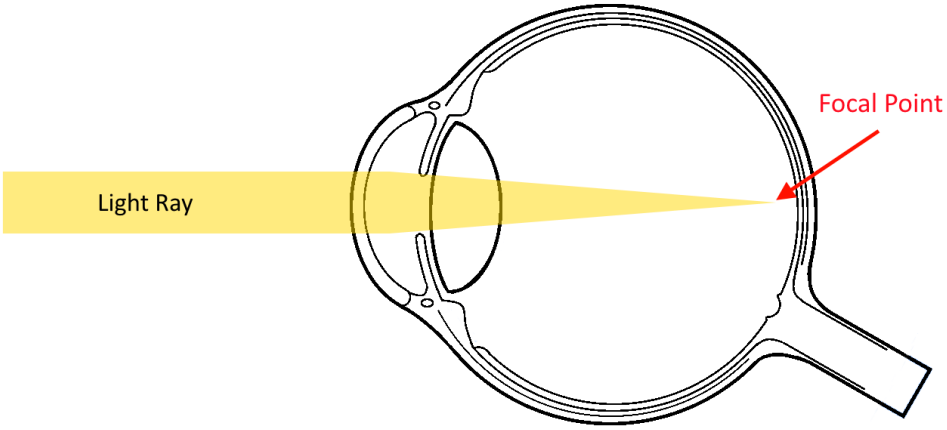

B: Myopic condition- images formed short of the retinal surface due to disparity between corneal strength and eye ball axial length leading to poor, blurry vision

Figure 1-3: Normal, healthy eye (a) compared to (b) myopic eye (short sightedness)

Contained within the iris are an opposing pair of muscles which allow for controlled opening and closing of the central pupil, similar in operation to a camera aperture. Contraction of radial smooth muscles intertwined within the fibres of the iris cause the pupil to be pulled into a larger diameter opening. In situations of high brightness a separate sphincter muscle which follows the inner perimeter of the Iris acts as the polar opposite and works in tandem with the radial smooth muscles to ensure appropriate light levels reach the retina without causing damage [41]. At controlled luminescence levels, it has been found that pupil size decreases with age [53] which is thought to be a result of a reduction in accommodation abilities as one grows older- a smaller pupil gives rise to reduced light scatter entering the eye and subsequent greater depth of field thereby acting as a compromised remedy to poor vision resulting from myopic conditions [54-56].

Filling the void between the anterior and posterior chamber is a fully transparent fluid called the aqueous humour which is produced in the ciliary epithelium and helps keep the eyeball inflated through maintaining an average intraocular pressure of 15.5mmHg ± 2.6mmHg [57]. Main constituent components are; carbohydrates, amino acids, organic and inorganic ions, and water. The aqueous humour fluid acts as a medium to transport vital nutrients to cellular structures as well as removing waste, thereby fulfilling the traditional roll of red blood cells in almost all other parts of the body [57].

To the rear of the pupil sits the secondary, elastic lens composed of a central nucleus with surrounding cortical zones of proteins in a layered , onion- like arrangement [58]. Encapsulated within a biconvex elastic collagen sack attached to tiny fibres running around the perimeter like spokes on a bicycle wheel known as the Zonules of Zinn, the crystalline lens is suspended in permanent concentric position with regard to the pupil. This supple lens fulfils two roles; firstly it works in tandem with the cornea to form sharp images on the retina and secondly it acts as a bandpass filter- reducing transmission of radiation that falls outside of the visible spectrum of 450 to 600nm [59]. For distance viewing, the ciliary muscle pulls the zonules tight, and the attached elastic capsule of the crystalline lens is coerced into a thinner, flatter shape. Upon near target focal stimulation, the ciliary muscles relax, reducing the pull on the zonular fibres and allow the elastic capsule to adopt a progressively convex shape thus increasing lens power and allowing near object light rays to be precisely focused on the retina- a process termed accommodation [58, 60]. The internal lens proteins continue to accumulate with age and over time axial lens length increases, reducing both flexibility and transparency [61]. The older, thicker lens is stiffer and resists the pull of the zonules and the ability of the eye to accommodate will progressively decrease eventually resulting in a refractive condition termed presbyopia, where the subject is no longer able to focus on close objects and can only be remedied with a reading correction such as with spectacles, contact lenses or surgical options [41]. As one ages, a lifetime of UV-B and oxidation damage results in an accumulation of denatured protein cells turning the originally transparent lens a cloudy brown colour which severely hinders vision and reduces contrast [58]. This is called a cataract and although easily cured if access to proper medical facilities are available, it is unfortunately the largest cause of preventable blindness, affecting roughly 20 million people around the world [62]. In India alone cataracts are responsible for roughly 80 percent of vision complaints and this number continues to increase by 3.8 million cases per year. To clear the growing waiting list of patients, roughly 6 million cataract operations would need to be performed each year, a figure that currently stands at 1.7 million per annum [62].

1.2. The Human Tear Film

Homeostatic Tear film (TF) dynamics is recognised as a key component to clear uncompromised vision and is a topic that has been heavily studied for many years. Yet uncertainty and continual disagreement over the nature, thickness and even structure of the pre- corneal tear film (PCTF) still resides in the field today [63-66]. One element is the prohibitive expense of instruments that are necessary to perform objective TF observations. Both contact and non-contact techniques for the evaluation of the PCTF have been developed and refined to help gain an insight into the behaviour and thickness of the invisible medium that forms the outmost boundary to the human eye. Yet as much as tear film composition has been studied and momentary tear film thickness values obtained, the ability to record a continuous and repeatable in vivo tear film behaviour during the entire inter- blink period is lacking.

The TF is a transparent, lubricating and nutritional fluid which covers the entire exposed eye surface [39]. Primarily secreted by both meibomian and lacrimal glands in tandem with the conjunctiva, the carefully balanced formula is composed of three primary components; lipid, aqueous, and mucin [67]. Four distinct varieties of tear have been identified: closed- eye tears, basal, emotional and reflex tears, each comprising of different primary ingredient concentrations [50]. Nevertheless all perform the important janitorial and preservation roles of continuously removing debris and external microbes during each blink, as well as providing constant nutrition to the cornea [47].

The TF was traditionally believed to compose of three distinct overlapping belts forming a solution that anchored itself to the cornea and was refreshed entirely with each blink [31, 68]. With the evolution of instrumentation and knowledge, observations now point to a complex multi- coating model with varying thickness and concentration gradients towards the boundaries of each ingredient [69]. A thin 15 – 157 nm lipid outer film rests atop a thick aqueous solution composing the 90% majority of the total 4.5 µm tear film thickness [39, 63, 70, 71]. Submerged towards the lower depths of the aquatic fluid is a viscous 0.5 µm mucin- corneal epithelium which increases in concentration the closer it comes in to contact with the cornea.

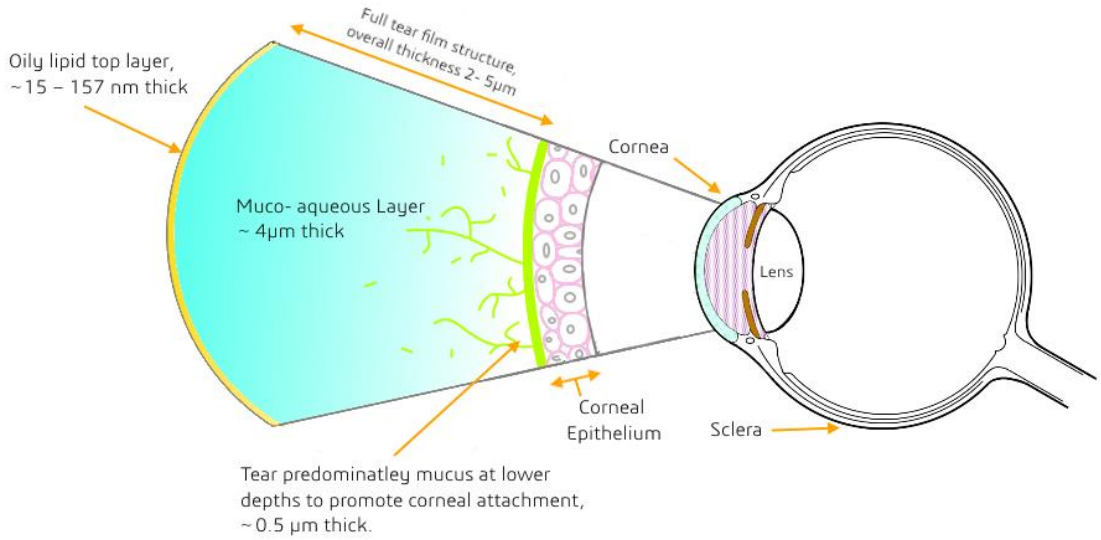

Figure 1-4: The human tear film composition and structure

Each of the three ingredients has a particular role and an upset in the synergy between any may lead to a variety of symptoms which are collectively called dry eye. If TF disruption continues to worsen, patient symptoms may develop from mild ocular inflammation and redness to ever increasingly severe afflictions such as chronic pain, compromised visual acuity and eventual permanent ocular surface damage [36, 72, 73].

Measuring at a mean 40nm depth [71], the oily hydrophilic lipid coating [39] is the outermost film and provides a smooth low friction surface for eyelid operation and has the role of helping the tears spread evenly over the eyeball surface as well as reducing evaporation of the aqueous layers beneath [32, 74-76]. Evaporative Dry Eye (EDE) is triggered by loss of water from the eyeball surface and fluorescein dye imaging by King- Smith and colleagues have suggested that the premature TF breakup is the result of defective tear film lipid layer (TFLL) regions where the composition of the TFLL was compromised due to bacterial lipases working to digest cholesteryl esters or waxes [77, 78]. Indeed, it has been measured by Craig and Thomlinson that upon artificial suppression of the lipid layer, a fourfold increase in evaporation rate of 5.90 $gm^{-2}h^{-1}$ compared to 1.42 $gm^{-2}h^{-1}$ can be expected [75]. Patients suffering from Sjögren's syndrome- a genetic condition consequential in reduced glandular secretion throughout the body, have been found to have an increased tear evaporation rate which may promote corneal surface inflammation and increase tear film instability leading to a hastening of premature TF evaporation [79]. Conversely, a thicker lipid layer also poses TF stability issues as studies point

to an inconclusive relationship between lipid layer thickness and rates of evaporation, indicating that other factors such as lipid layer structure and composition are equally important contributors in maintaining a healthy TF [71].

Just below the outer lipid coat, the secondary muco- aqueous layers are to be found. Secreted by the lacrimal glands, the aquatic nature of the fluid helps lubricate the eye and transport debris down to the lacrimal sac as well as allowing the free flow of oxygen and nutrients essential to the health of the cornea [80, 81]. Proteome sampling has uncovered the existence of over 1,500 varieties of proteins with more than 200 peptides (shorter amino acid chains) present within the aqueous layer [82, 83].

Found in the lower depths of the aqueous layer and with progressively increasing concentration is the mucin layer which straddles directly on top of the cornea. Produced by the goblet cells present on the conjunctiva [39, 84], mucin is primarily composed of O-glycosylated glycoproteins, 80% of which are carbohydrate by mass [23]. Goblet cell secretion is stimulated by the conjunctiva and cornea [85]

Current research indicates no distinct boundary between the aqueous and mucin layer and thus it is difficult to directly estimate an aqueous layer thickness [86]. Khanal and colleagues introduced biomarkers in the form of fluorescent quantum dots into a subjects' eye of varying lipophilic or hydrophilic fluid absorption characteristics [70]. Depending on pre- defined absorptive properties, the qDots were found to separate into the three individual TF layers that washed from the eye at differing rates depending on the layer in which they were found, indicating layer refresh independence- something that had not previously been considered. This coupled with regular blinking every 4- 5 seconds, natural vibrational saccades of the eye and the constant dynamic motion of the TF fluid, all combine to make *in-vitro* observations of the TF a very difficult task [87]. Moreover, patients which are considered as suffering from dry eye typically experience on average double the blink rate of 33.9 min^{-1} compared with 14.3 min^{-1}, thereby adding further complication to any observations [88].

Many techniques varying from mathematical modelling, optical coherence tomography (OCT) in combination with statistical estimators (Statistical Decision Theory), tear film osmolality and surface fluid evaporation have all been employed to assess tear film thickness (TFT), with obtained values varying by as much as an order of magnitude between approaches [64-66, 89-91]. Both contact and non – contact methods, as well as computer models, have been devised and tested, but an agreed golden standard of relatively low cost, easy to obtain, repeatable and

reliable single technique for tear film thickness testing and dry eye evaluation is frustratingly elusive [36].

Original estimates by Prydal suggest overall tear film thickness is between 34 – 45 µm [65]. This thickness value however has been challenged by other researches using different techniques for measurement. Debated invasive contact measurements have yielded values from 4.5 to 8.5 µm [90], all the way down to 3 µm using newer interferometric methods employed by King- Smith and company [92]. Current best agreed values of complete TFT have been achieved through the use of pre- corneal tear film reflection spectra and various OCT techniques of questionable accuracy. Thickness values of between 2 to 5 µm are viewed as the standard [92-97]. Table 1.2 below shows thickness results obtained from previous studies.

Table 1-2: Tear film thickness values obtained from previous studies

Method	Measured TF Thickness (Overall)
OCT in combination with Statistical Decision Theory [64]	20µm - 150µm
Confocal Microscopy without Oil Immersion [65]	Roughly 41 - 46 µm
Spectral Oscillation with Contact Lens Worn (Interference Method) [89]	Average 1.4 to 3.9 µm for five subjects wearing CL
Spectral Oscillation without Contact Lens (Interferometric Method) [89]	2.94 µm
Coloured Interference Fridges [98]	0.1 - 0.52 µm
Angle Dependent Fridges (Interferometry Method) [99]	Estimated as 10 µm or less
Angle- Dependent Fringes (Laser Interferometry) [65]	34 - 45 µm
Interferometry [92]	3 µm
Wave Dependent Fringes- Interferometry [100]	Healthy Eye 6 ± 2.4 µm, ADDE Patients 2.0 ± 1.5 µm
Confocal Microscopy with Oil Immersion [65]	Roughly 40 µm (mostly mucus)
Fluorescein Addition and drainage [90]	10 - 20 µm
Glass fibers Against Cornea [91]	6.5 µm

1.3. Dry Eye

Dry eye Disease (DED), also known as Keratoconjunctivitis sicca (KCS) is a global health issue [101] affecting aforementioned parts of the anterior eye and tear film and can manifest itself as a number of co- dependent symptoms ranging from minor discomfort, visual compromise right through to persistent pain severely interfering with daily activities [102, 103]. Patients experiencing long term DED risk worsening progression which can lead to serious visual complications involving corneal epithelial defects, superficial punctate erosions, conjunctival and corneal scarring, and chronic pain [104]. Furthermore, dry eye patients often exhibit measurable shortages of tear film defensive compounds such as lysozyme and lactoferrin [35] which increase the risk of acute and chronic infections such as acne rosacea and blepharitis [104, 105]. DED was formally identified as a disease state over 30 years ago and scientific understanding and awareness of the condition has evolved greatly since the original global definition put forward by the NEI/ Industry report of 1995 [73]. Subsequent technological advancements coupled with an increasing prevalence have added to the growing body of research and a corresponding evolution of the definition of the disease as its understanding is increased. The latest revision of the definition being put forward in the 2017 TFOS DEWS II report as [73]:

"Dry eye is a multifactorial disease of the ocular surface characterized by a loss of homeostasis of the tear film, and accompanied by ocular symptoms, in which tear film instability and hyper-osmolarity, ocular surface inflammation and damage, and neuro-sensory abnormalities play etiological roles."

Because of the multidimensional ethology of dry eye and varying experiences of sufferers, the appearance of DED is sub-classified into evaporative dry eye (EDE) or aqueous- tear deficient dry eye (ADDE) components, with most sufferers being somewhere on the spectrum between these two states [73]. Evaporative dry eye is typically the consequence of conditions affecting the eyelid including blink-abnormalities, mucin deficiency, MGD or even negative effects induced from contact lens wear [74]. Aqueous deficient dry eye is usually the result of lacrimal gland deficiency giving rise to a lower tear volume than found in healthy patients; this triggering reactionary inflammatory responses leading to the loss of the homeostatic tear film. Discomfort experienced by DED suffers is difficult to quantify and the condition manifests itself on a wide continuum of possible mutually reinforcing phenomena, the most common of which tends to be a dry, burning sensation of the eye ball, soreness and sensitivity to light [106, 107]. Other

reported complaints are foreign body sensation, red eyes and counterintuitively, watery eyes due to tear hypersecretion.

1.3.1. Evaporative Dry Eye

Defined as the premature evaporation of a healthy volume of secreted tear, EDE may be the consequence of both intrinsic and extrinsic factors.

Examples of intrinsic contributory elements may be caused, but not restricted to:

- damaged anterior structures due to defects or injury,
- meibomian gland dysfunction caused by a gland blockage by bacterial infection such as posterior blepharitis [108],
- reduced/ incomplete blinking due to long term visual display unit (VDU) exposure. This in turn leads to a reduction in surface nourishment through excessive ocular surface drying, insufficient tear secretion and inefficient spreading of tears over the eyeball [39, 109].

Extrinsic factors such as the wearing of contact lenses greatly contributes to DED and it has been estimated the risk of developing dry eye is between 2 and 3 times greater for contact lens wearers compared with a healthy control group [110, 111]. The insertion of a contact lens has the effect of splitting the tear film into two; a pre- lens TF and a post- lens TF which is sandwiched between the inside surface of the lens and the cornea. Prolonged wearing of contact lenses may damage goblet cell sites and affect tear film stability with over 50% of CL wearers reporting dry eye symptoms [18, 112-114]. Other extrinsic factors may include low humidity, dusty environments, use of topical anaesthetics and in some cases vitamin A deficiency [115].

1.3.2. Aqueous Tear Deficient Dry Eye

Divided into either Sjögren's syndrome (SS) or non- Sjögren's syndrome modalities, ADDE is a consequence of insufficient tear fluid secretion from the lacrimal glands leading to a hyperosmolar tear film condition. SS patients exhibit a rare auto immune disease which reduces expression function of all fluid secreting glands within the body. Lacrimal glands are normally affected causing hypo- secretion of the tear and a sub- normal ocular surface wetness [116]. Sufferers of SS are by their very nature more pre-disposed to experiencing ADDE.

Non- SS sufferers of dry eye tend to be afflicted by a reduced sensitivity of the cornea, such as from laser corrective eye surgery, protracted contact lens use or even external viral infections. Nerve endings within the cornea send prompts to both the eyelids and lacrimal glands to blink and secrete fresh tear fluid. The reduction in corneal sensitivity stimulates fewer blinks which diminishes tear turnover and exposes corneal epithelium cells to the atmosphere, leading to inflammation.

Aqueous or evaporative dry eye is neither mutually inclusive nor mutually exclusive but may exist on an overlapping spectrum of the two condition states. Evaporative dry eye tends to be more prevalent with meibomian gland dysfunction, being the major cause of 35% of patients experiencing aqueous tear deficiency [72, 75, 117-119].

1.4. Dry Eye Prevalence

DED prevalence studies vary from region to region, partly due to the asymptomatic nature of the condition as well as the heterogeneous adopted definitions of what constitutes dry eye in different countries as well as discrepancies of age groups used in each study cohort [120]. It has been postulated that high instances of episodic dry eye exist, but coupled with the varying criteria used to assess dry eye (e.g. types of questionaries' employed and/or inconsistencies between data gathering devices), it is challenging to quantify a definitive figure on the global number of affected patients [121, 122].

Various research conducted in differing territories have seen large variations in reported results [120]. For example; US Studies conducted by Schaumberg and company in 2003 and 2009 found that 6.8% of the US population, equivalent to 16.4 million people, suffered from some form of DED with a greater tendency to affect women and an increasing instance with age [123, 124]. Separate studies conducted in Indonesia and Australia suggest occurrence of 27.5 and 17% of the female populations respectively [15, 125]. Table 1.2 lists a breakdown of the population-based studies which have reported the prevalence of DED in different countries. The fundamental difficulty of early stage dry eye diagnosis leads to great numbers of overlooked patients as can be seen in Table 1.3, suggesting a generally low-test sensitivity (the number of true positives cases correctly identified).

Within the research community it was formerly accepted that older generations were most susceptible to DED, with post- menopausal women being disproportionally affected due to hormonal changes leading to decrease tear secretion compared with male counterparts of equivalent age [124]. New evidence put forward by the Vision council 2016 Digital eye strain report shows 73% of US patients below the age of 30 demonstrating symptoms of digital eye strain, higher than any other age group [126]. Such a large example of eye strain in the younger generations may be linked with the relatively recent explosion of portable digital technology, allowing users to have access to screens at all times of the day (and night); this has prompted an accompanying change in user vision habits from yesteryear outdoor activities, which stimulate both near and far distance viewing, to more contemporary indoor digital viewing habits and long periods of concentrated near vision. This is forcing an ocular adaption leading to a rise in myopic and dry eye cases due to the reduction in blinking rates and constant near focus viewing [27, 127-130].

Table 1-3: Prevalence of dry eye in various populations and age ranges

Study	Region	Publication Year	Cohort Size	Age Range	Dry Eye Prevalence	Definition Of Dry Eye
US Women's Dry Eye Prevalence [124]	USA	2003	39,876	45 to 84	7.80%	Either previous diagnosis of dry eye or sever symptoms (dryness/ irritation constantly/ often)
Salisbury Eye Study of Older Americans [131]	USA	2000	2,420	65 to 84	14.6%	1 of 6 symptoms on questionnaire, Schirmer < 5 mm, RBS $\geq$ 5
Beaver Dam Eye Study [132]	USA	2000	3,722	48 to 91 (mean ± SD, 65 ± 10 yrs.)	14.4%	Positive DED result if patient answered yes to "For the past 3 months or longer, have you had dry eyes?"
Blue Mountains Study [15]	Australia	2003	1,075	50- 90	16.6%	Administered questionnaire. DED positive result if three or more symptoms regardless of severity, or one moderate to severe score.
Shihipai Eye Study [133]	Taiwan	2003	1,361	65 & above	33.7%	Modified dry eye symptom questionnaire, BUT $\leq$10 s, FLS $\geq$ 1, Schirmer $\leq$ 5 mm, MGD $\geq$ 1*
Lifestyles Associated with Dry Eye[133]	Japan	1999	5,98	Mean 31.3 Years	33.0%	30 questions followed by self-diagnosis test messages
Prevalence of Dry Eye [134]	Iran	2014	1,008	40 - 64	8.70%	OSDI score ≥23**, TBUT $\leq$10 s, Schirmer test ≤5 mm, FLS ≥1, and RBS of cornea and/or conjunctiva ≥3 (Oxford Grading Scheme)
Prevalence and risk of Dry Eye Symptoms [125]	Indonesia	2002	1,210	21 & above, (mean ± SD, 37 ± 13 yrs.)	27.50%	Six item frequency of dry eye questionnaire

** = presence of plugging of gland orifices or telangiectasia at lid margins,*
*** = total points in questionnaire multiplied by 25 and divided by total number of responses*

1.5. Diagnostic Challenges of Dry Eye

The greatest frustration associated with diagnosing dry eye is the weak relationship between symptoms reported by sufferers and objective indications of the disease [107, 131, 135]. It is not uncommon for patients to demonstrate classic signs of short breakup time, high osmolarity or blocked meibomian glands and perplexingly have no dry eye symptoms [136, 137]. This links with work conducted by Narayanan and company that mild to moderate instances of dry eye give rise to low correlations between clinical techniques [138].

DED can be a self-perpetuating ailment with levels of severity shifting over time [36, 114]. Conditions which befall other parts of the human body may also impact on the eye. Systematic Lupus erythematosus, Scleroderma and Sjögren's syndrome are known to affect ocular health and tear evaporation rate [79, 139]. To complicate matters more, patients may be episodic with symptoms varying throughout the day suggesting environmental or activity related factors contributing to DED symptoms [73, 140, 141]. Underlying all this is a lack of correlation between patient reported symptoms and clinical signs [142-144].

Indeed, it may be easy to mistake symptoms of DED with allergic conjunctivitis and to complicate matters more, both conditions may occur simultaneously [108]. Dry Eye is therefore such a complicated condition that it is commonly often overlooked by clinicians and underdiagnosed in many global populations [135], as evident in table 1.3 which demonstrates the large difference between numbers or prevalent and diagnosed patients.

So far there is no single "gold standard" test or symptom recognised to directly correlate with DED presence and severity [36, 122]. Current comprehension of dry eye and the sensitive nature of the ocular surface demand that tests for DED presence be performed either in isolation or as recommended by the Dry Eye Workshop II which stipulates a sequence from least to most invasive testing which best preserves the natural state of the eye in anticipation of the next test [36, 143].

Many invasive/ non- invasive evaluation methods ranging from simple, but well refined, questionnaires all the way through to technologically demanding methods such as OCT imaging, interferometry and even biomarkers have been developed to help gauge ever finer aspects of ocular health [36]. A guide has been composed by the author and can be found in figures 1.5 and 1.6 showing the multitude of options available and examples of popular devices used.

The changing sands of dry eye disease manifestation between patients and clinical visits still means that there is considerable scope for diagnosis improvement, but for now patients must rely on several individual tests being conducted and overall doctor experience in correct identification of the disease.

Some tests are more revealing and correlate better than others and have been recommended under the DEWS II diagnostic methodology report as the most appropriate for the reliable diagnosis of dry eye [36].

Table 1-4: Total Prevalent and Diagnosed cases of Dry Eye Disease, Ages 20 & above, both sexes
Data sourced from [2, 145-149] AGR: Annual Growth Rate

Country	Total Prevalent Cases	AGR to 2026 (%)	Total Diagnosed Cases	AGR to 2026 (%)
China	193,756,483	0.61	60,539,295	0.61
USA	22,816,768	1.88	16,683,227	1.88
Germany	10,959,142	0.29	5,904,236	0.57
Spain	3,038,354	1.48	1,574,850	1.48
Italy	4,226,771	0.79	2,190,834	0.79
France	8,227,386	0.8	4,373,905	1.01
UK	7,844,894	0.81	4,066,190	1.07
Japan	16,810,987	0.03	5,252,600	-0.3

1.6. Basic Dry Eye Testing and Diagnosis

Diagnosis of dry eye is oft times treated as a diagnosis of exclusion. Consequently appropriate lifestyle questions need to be initially asked to the patient before a reasonable assumption as to the presence, subtype (ADDE or EDE) and maturity of DED, can be established. Questions may include current medication, contact lens wear and history of discomfort, and should be followed by a detailed anterior eye examination [36].

If questionnaire results point to the potential presence of DED then it is recommended by DEWS II that the following sequence of testing be adhered to from least to most invasive which will help best preserve the original eye homeostasis and limit bias in results:

1. Dedicated Dry Eye Questionnaires
2. Non- Invasive Tear Film Break up Time (If fluorescein employed then this step needs to follow Osmolarity measurement)
3. Tear Film Osmolarity Measurement
4. Ocular Surface Staining

The four steps above are the minimum required to diagnose for dry eye but do not distinguish between classes of DED or severity. For that level of granularity, more particular tests will need to be employed, usually involving specialist equipment.

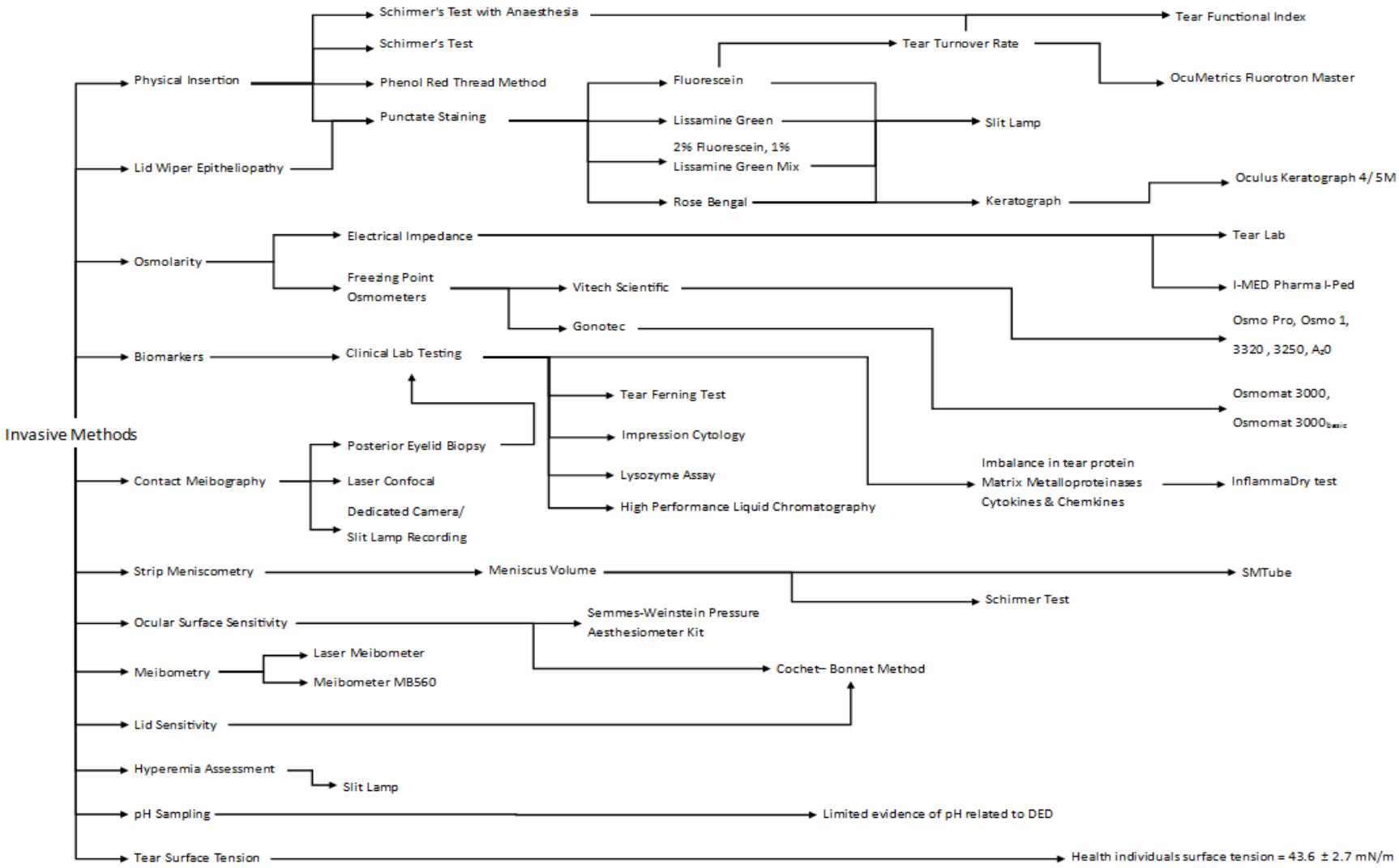

Figure 1-5: Invasive methods of anterior eye analysis [25, 36, 43, 150-156]

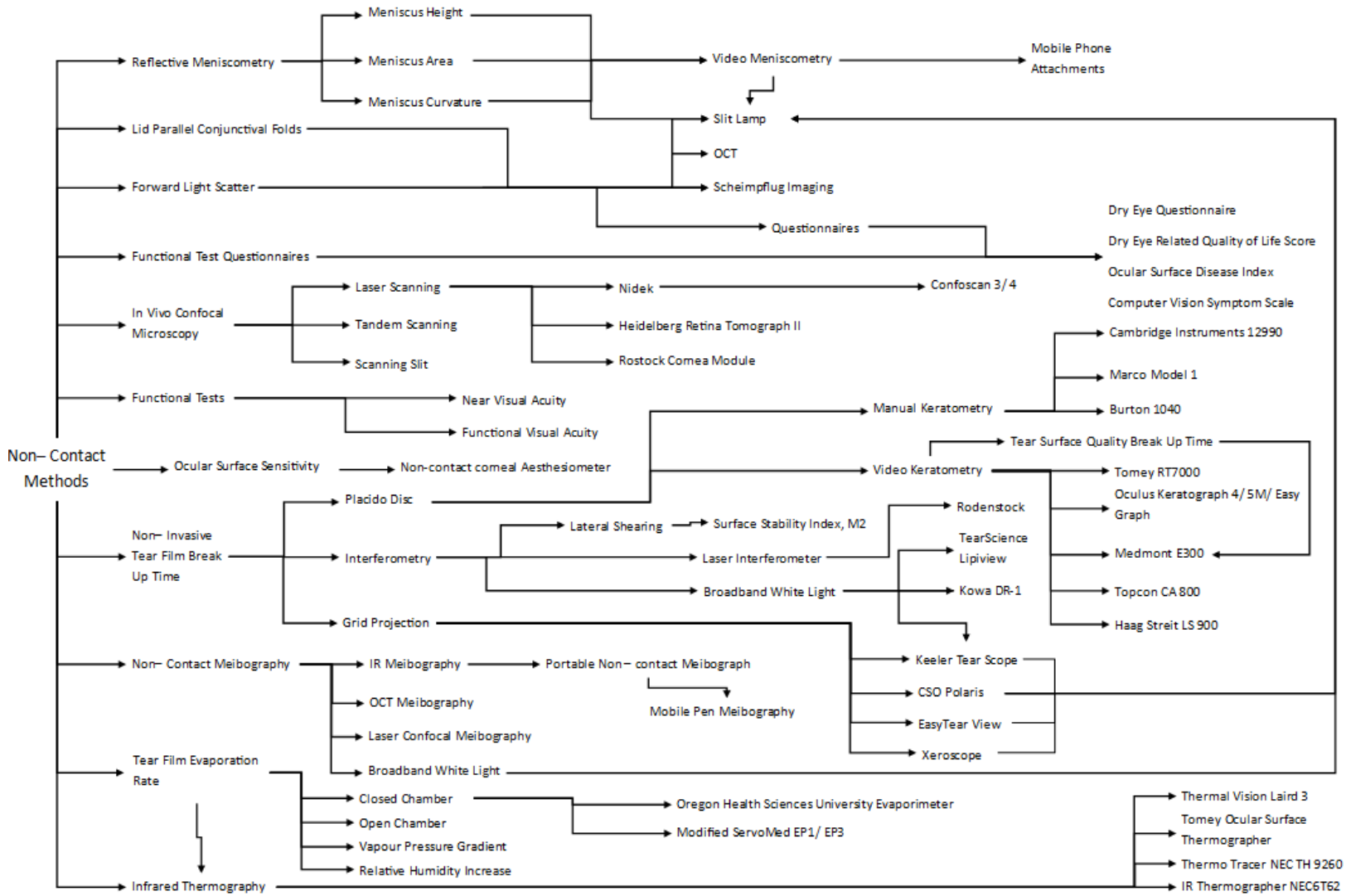

Figure 1-6: Non- Contact Methods of anterior eye inspection [36, 75, 143, 157-163]

1.7. Repeatability of Dry Eye Measurements

One of the core issues surrounding dry eye evaluation is the notorious non- linear variability between signs and symptoms of the disease. When asked, most clinicians tend to believe that current testing for dry eye to be equally erratic [142, 143, 164]. Studies carried out by Nichols and co. suggest reliability between tests may be different depending on the severity of the disease but both sensitivity and specificity will increase in severe instances of dry eye compared to healthy subjects. Nichols recommends a short time interval of a week between repeat assessments to ensure consistency between results [143]. Even differences between study cohorts (age or sex) may have an effect on obtained results [122]. Due to these discrepancies, it is useful to have an understanding of the limitations of mainstream tests used to diagnose dry eye, which may help to explain the disparity between dry eye prevalence as reported in table 1.3 earlier.

Research by Korb in 2000 attempted to recognise the tests of choice by surveying prominent practitioners in the field of tear film evaluation and clarify individual test efficacy [164]. The survey simply asked clinicians “If you could use only one test for diagnosis of the tear film and dry eye, what would that test be?” Although the wording of the survey may have been open to interpretation, the results showed no defined first choice amongst the responders and a general understanding by experienced clinicians that several tests need to be performed to correctly identify dry eye disease [164]. The favoured first tests were dry eye questionnaires and patient lifestyle histories (28%), followed by fluorescein break- up time (19%), fluorescein staining and or sequential staining (13%) and Rose Bengal staining (10%). The preferred second test was most commonly identified as the Schirmer test, with a 21% score [164]. Overall, the favoured testing strategies varied widely, even between optometrists and ophthalmologists, but they all agreed that there is no single test that is capable of clearly identifying DED.

Since the Korb survey, understanding of dry eye has continued to evolve and the latest DEWS II diagnostic guidelines published in 2017 suggest initial screening with a dry eye questionnaire (narrowed to either the Ocular Surface Disease Index [OSDI] or Dry Eye Questionnaire [DEQ-5]). If questionnaire indicates potential for DED presence, diagnosis is confirmed by testing for premature loss of homeostasis identified by a low non-invasive tear breakup time, high tear osmolarity (or significantly different osmolarity scores between the eyes), or ocular surface staining with topical dyes [36]. It is generally recommended that testing procedure be conducted from least to most invasive [36, 137]. Several common methods of dry eye evaluation and their individual merits will be discussed below.

1.7.1. Dry Eye Questionnaires

The numerous aetiologies and diverse manifestation of DED gives rise to inconsistencies between personal patient experiences and visible signs of tissue damage [131]. This is similar to a patient experiencing a migraine without any physical manifestations of injury- the pain experienced is still real.

Traditional, non- scripted interactions between clinicians and patients produced information that is difficult to categorise and standardise [36]. New tools were needed to gain an insight into patient experiences and correlate them against physical test results allowing for maximum insight into the extent of patient pathology. To facilitate this, many questionnaires have been developed and refined to help identify DED depending on patient lifestyles.

Well recognised DED tests have been listed in the TFOS DEWS II Diagnostic Methodology Report and include a range of 12 carefully designed questionnaires. Depending on patients' lifestyles, clinicians may select a preferred questionnaire over others that will narrow down potential factors of DED influence. The Ocular Surface Disease Index (OSDI) and Impact of Dry Eye on Everyday Life (IDEEL) are recognised as the most frequently employed [36, 145]. 5- Item Dry Eye Questionnaire (DEQ-5) has been identified as useful because of its short length and the Computer- Vision Symptom scale (CVSS17) is particularly appropriate for identifying symptoms of visual display unit usage [36].

Generally, it is accepted that approved dry eye questionnaires have shown to be reliable tools for the potential presence and severity of dry eye sensation [165-167]

1.7.2. Schirmer Tear Test

Perhaps the simplest test and lowest cost for distinguishing tear volume abnormalities is the Schirmer test. Originally introduced in 1903 by Otto Schirmer, the test is available in three varieties [130, 168, 169]. Schirmer I, performed without topical anaesthesia, is a measure of stimulated reflex tear flow and involves placing a folded notch of a 5 x 35 mm paper strip inside the temporal lid margin of the eye for a period of 5 minutes [36, 130]. Tear fluid is absorbed through capillary action and progressively travels the length of the paper strip which is then manually measured. So far there are no absolute cut off values and disagreements between accepted distance measurements and what can be reliably inferred still exists. An absorbed TF reading of 10mm over the course of the 5 minute test is typical of healthy eyes whereas a reading below 5 mm after 5 minutes points to potential dry eye [143].

Schirmer II test differs from the above by employing a cotton swab inserted into the patient's nasal cavity parallel to the internal wall to stimulate a reflex tearing event [130]. Schirmer III is performed similarly to Schirmer II, but rather than reflex tearing induced from nasal irritation, the patient is instead asked to stare at the sun [169]. Unsurprisingly, the Schirmer III test is no longer in prominent use. Although both Schirmer I or II can be performed with or without topical anaesthesia, large studies by Lee and Hyun in 1988 showed no significant difference between the two approaches [152].

Serious inconsistencies in results have been identified during Schirmer type I and II tests and could possibly stem from variations in the amount of notch surface inserted into the eye, the gaze of the eye during the test and whether the eye is kept open during the test [152, 170]. In addition, Schirmer strips are commercially available from several suppliers which each have unique absorption and porosity characteristics. Discrepancies have been noted between different manufacturers, leading to more confusion when interpreting results across different studies [170].

Because of this large variability, there is much discussion and doubt as to the true reproducibility of the test [152, 164]. Lee and Hyun compared the Schirmer test to the toss of a coin when used to diagnose dry eye; there was a misdiagnosis rate of only 48.4% when an individual clinician used a single measurement to make a forecast of DED presence but a 41.2% misdiagnosis rate when making predictions from a repeat five test average [152].

1.7.3. Fluorescein Tear Film Breakup Time

Fluorescein instillation into the human eye followed by blue light slit lamp observation was a approach first described by Norn in 1969 as a new technique to directly gauge tear film integrity and is still considered one of the most frequently used methods for dry eye analysis today [171, 172]. For fluorescein observation to take place, blue light of a wavelength close to 495 nm must be used to excite the chemical and create the fluorescence effect [173]. To assist with viewing, a yellow barrier filter close to 520 nm peak absorbance is placed between the subject eye and observer to exclude non-fluorescing light, thus highlighting regions of corneal damage and TF breakup [174]. Ideal fluorescence is achieved between 1 to 3 minutes post instillation and therefore viewing should take place during this interval [173].

Tear stability or Fluorescein Break Up Time (FBUT) is a term to denote the length of time beginning from a complete blink to the first appearance of dark streaks on the cornea- the longer the span- the more stable the tear film. A breakup time of 10 seconds or above is considered healthy [36] with experiments suggesting that breakup tends to occur more commonly in the temporal corneal periphery rather than the nasal periphery [175]. A second test assessing "completeness of blink" is also possible with fluorescein instillation. A distinct dark boundary line becomes visible on the inferior cornea clearly marking the lowest position of recent incomplete blinks [176].

The test is inherently subjective with the observer's proficiency in the procedure being crucial to the early detection of breakup [177]. Much disagreement exists between the reliability and usefulness of the technique which can be due to the variability of results stemming from numerous factors such as frequency and duration of blinks before testing, the location of light source, volume of instilled fluorescein as well as fluorescein concentration itself [178-181]. Fluorescein breakup time is the only method for the direct measurement of tear film stability [135], but it has also been observed that fluorescein instillation may have the effect of inducing reflex tearing [182] as well as having a direct effect on tear film integrity [183]. It has been shown that fluorescein instillation compromises tear film stability and reduces tear film breakup time, particularly in DED patients and so for this reason fluorescein instillation in the human eye is considered mildly invasive [36, 184-186].

Nakamori and co. suggests that there is a significant inverse correlation between maximum blink interval duration and blink rate and that rather than relying solely on TFBUT, it would be more appropriate to measure blink interval as this is a closer relation to overall patient comfort [27].

1.7.4. Non-Invasive Tear Film Break Up Time

Subjective limitations of FBUT may be addressed by the development of non- invasive breakup time (NIBUT) instruments which rely on the projection and monitoring of specular reflections of concentric mires reflected back from the pre- corneal tear film [158]. The integrity of the reflection is the direct function of tear film stability and unlike FBUT, is not compromised by the artificial presence of fluorescein or any reflex tearing during vital stain instillation [181].

Many instruments have been developed which range in complexity and measurement abilities. An early example is the Keeler Tearscope (*Keeler, Windsor, UK*) which used transparent films with various printed mesh patterns wrapped in front of a circular cold cathode diffuse white light source. The instrument was introduced in 1997 [187] and was designed to be held up by hand to the patients' eye as they are asked to blink. Once the tear film has stabilised post blink, the grid pattern that is projected on the tear film is sharp and regular. Over the following seconds, natural breakdown of the tear film causes distortions in the reflection which signifies the end of the test. With only a manual start- stop digital timer fitted to the instrument, the manual tear scope test is a empirically subjective measurement and relies wholly on the clinician to correctly identify early regions of breakup – a difficult ask to perform well [188]. Inter-observer variability between clinicians has been shown to reduce the effectiveness of this approach [187]. Although the Keeler Tearscope device was discontinued from the market, many copycat devices have been recently introduced such as the CSO Polaris (*CSO, Florence, Italy*) or the EasyTear View+ (*Easytear, Trento, Italy*), which work on the same principles and are still subjective in measurement.

Significantly more advanced NIBUT systems such as the CSO MS-39 (*CSO, Florence, Italy)* or Oculus Keratograph *5M (Oculus, Welzlar, Germany)* have been developed around retro illuminated static placido rings with proprietary computer algorithms for objective assessment of NIBUT. Testing is performed in the same fashion as the subjective equivalents mentioned above, but repeatability has been improved due to the removal of human decision making and smaller, less noticeable areas of repeat breakup can be identified by software mapping [189].

NIBUT values tends to be longer and show more variability between instrument suppliers than those achieved from FBUT possibly due to a combination of the destabilising effect of fluorescein in the eye as well as the proprietary algorithms used between manufacturers [158, 159]. For example, the Oculus Keratograph measures the integrity of the circular mires and triggers an end condition once a threshold of ring deterioration or eccentricity has been surpassed [158].

The competing RT- 7000 (*Tomey Corp, Aichi, Japan*) on the other hand evaluates overall ring brightness levels, which decrease over the course of the test [158]. NIBUT measurements performed by the Oculus Keratograph repeatedly measured shorter breakup times than side by side tests performed on the Keeler Tearscope, possibly due to the higher sensitivity of the software and the ability to detect smaller regions of breakup that may be difficult to recognise with the naked eye [189].

With the ability to video record patient data and track disease progression over time, objective NIBUT is considered an important tool for the detection of dry eye disease. Additional data such as corneal topography may be gathered from the circular mires, providing information on contact lens fitting and presence of astigmatism which is considered useful for vision correction [181].

1.7.5. Tear Osmolarity

A decrease in tear volume, for whatever reason, leads to an increased concentration of dissolved minerals within the remaining fluid. This relationship between compromised tear production and tear osmolarity was suggested by Gunnar von Bahr in 1941 [190] and many conditions such as MGD, contact lens wear and Sjögren's syndrome are all known to contribute to tear hyperosmolarity [76]. Evaporative dry eye and aqueous deficient dry eye will by their very nature result in tear hyperosmolarity and so it has been suggested that osmolarity be recognised as the objective "gold standard" for identifying dry eye conditions [144, 150].

Before the introduction of the Tearlabs Osmolarity System (*TearLab Corp, San Diego, USA*) in 2008, osmolarity testing was conducted by complicated freeze point depression tests and vapour pressure techniques which required large volumes of sample tear and typically forced such laborious activities to be confined to research settings [153, 191]. New handheld technology now allows clinicians to collect a 50 nL tear sample from the outer lower tear meniscus and perform automatic on the spot electrical impedance testing to give an objective osmolarity value [153, 192].

When tested, healthy eyes usually achieve an average osmolarity value of between 302.2 ± 8.3 mOsm/L, whereas mild to moderate dry eye sufferers 315.0 ± 11.4 mOsm/L. Severe dry eye cases show values as high as 336.4 ± 22.3 mOsm/L as well as a larger disparity between intra eye osmolarity values. It is postulated that the severity of the disease increases due to a poorer mixing and distribution of critical nutrients in low volume tears [36, 193, 194].

Arguments against osmolarity testing suggest a single tear sample fails to provide osmolarity information over the complete ocular surface, including the all-important cornea. Studies have also shown a greater divergence between the tear meniscus osmolarity values compared with actual osmolarity of the local tear film present on the cornea [153]. Work by Khanal and co. found a variation of up to 35 mOsm/L in consecutive readings of individuals and suggested that only after three repeat readings will a reliable tear osmolarity score be established- an expensive proposition considering the high cost of consumables required for each measurement [195]. In addition, relative humidity, time of day, temperature and inconsistencies in the actual measurement process are thought to have an effect on the reading and although osmolarity may be considered by some to be the single best marker of DED across mild, moderate and severe cases, it should not be used as the sole indicator of dry eye disease [28, 144, 153, 191].

1.8. Summary of Dry Eye Measurement Techniques

Although fundamental disagreements between testing procedures still exist today, awareness of dry eye is growing. Nichols and co. conducted retrospective studies on patient test charts to determine which dry eye tests had been performed on dry eye patients across four ophthalmic clinics and found that although each had its own regimes, there was strong overlap between preferred tests [122]. Nevertheless, the lack of consensus between methods and clearly defied cut off values of each test make identification and extend of disease progression nebulous and difficult to define [169]. Part of this reason could be the lack of standardisation between clinical trials and the variation of reliability of testing depending on the extent of disease manifestation [137, 169]

Worryingly, dry eye is seen as a difficult and 'boring' disease to treat [145]. Patients tend to be dismissive of the significance of early dry eye symptoms and tend to self-medicate with over the counter (OTC) eye drops as a first step in seeking relief [16]. OTCs fail to solve the underlying roots of disease and progression continues as detrimental patient habits continue uncorrected. Only once moderate dry eye has become established and consistent pain/ irritation experienced is professional help finally sought. Clinicians themselves express frustration towards the diagnosis and treatment of dry eye; a web- based questionnaires sent to a small number of hospitals by Turner and co. asked a range of questions on diagnosis and preferred techniques. Results revealed a range of predominantly low satisfaction and negative responses [172].

It is clear that considerable variation and confusion exists even between common, well refined testing procedures for the presence of dry eye. With no gold standard and inconsistent correlation between signs and symptoms, dry eye continues to be seen as an elusive disease, which is difficult to identify especially in the mild and moderate forms [122, 169]. DED requires a proactive and adaptive testing strategy as no single method is able to give definitive diagnosis and different assessments are necessary to hone in on the underlying cause of disease particular to a patient on the continuum of possible explanations [136, 164].

1.9. Aims of Thesis

Current techniques and medical devices offer many options for clinicians to take advantage of for the diagnosis of ocular surface conditions such as dry eye. Although DE prevalence is high, rates of undiagnosed are also high. Many of the tests described require trained professionals and only allow for subjective measurement which leads to discrepancies between diagnosis [196]. It is obvious that a single test for the accurate identification or even confident presence of the disease is still elusive [143]. Considerable opportunities exist for the evolution of diagnosis techniques mentioned above and this thesis will explore the potential for improved functionality and disease identification.

It is the upmost importance that science continues to search for ingenious, effective and affordable methods for the early diagnosis and effective treatment of anterior eye diseases and develops methodologies that will be implantable in to different sections of the global societal spectrum; be it a wealthy society where access to medicine is only a phone call away or a third world country where citizens can live several days travel by foot to the nearest point of care.

This thesis and the experiments contained within will focus on taking full advantage of the latest technological advancements and attempt to package them into devices that are low cost, require minimal training and provide highly accurate, repeatable results. It is intended that these devices will improve the level of care to many people where access to traditional practice based ophthalmological equipment is simply not possible; be it the elderly with mobility restrictions in a retirement home in England or a mother and her children in a remote village in the developing world.

The following chapters will centre on new techniques of dry eye diagnosis and improved, earlier detection. Chapter 2 will detail custom created blue excitation and yellow emission filters tuned to take full advantage of the ideal spectral profile of sodium fluorescein viewing allowing for improve viewing quality, especially in low light conditions. Chapter 3 will introduce confocal technology currently used in the industrial non- contact measurement of transparent surfaces and materials. The transparent, near invisible composition of the human tear film coupled with the close refractive indexes of adjoining surfaces (cornea and aqueous humor) pose difficult challenges for detection and coherent results have so far been difficult to repeat in clinical settings. It is hoped that the new application of proven technology may provide the resolution necessary to allow for on the spot tear film thickness measurement and assessment of patients sitting through normal eye examinations.

The final instrument will be an anterior eye examination tool for the monitoring of tear film breakup stability. Although many instruments already exist which can perform such measurements, high cost, training and examination time requirements mean that they are not always suitable for intended purpose. The new instrument will exceed the current device capabilities while being cheaper, portable and provide greater accuracy of diagnosis.

Work on these new approaches will be mostly explorative and intended to provide direction and a solid foundation for future development and eventual clinical trials rather than a conclusive solution. As such, the scope of data collection within this thesis will be limited to small cohorts and the focus primarily set on new technique/ concept discovery.

2. High Performance Diffuse, Excitation and Emission Filters for Fluorescein Observation of the Ocular Surface

The indiscriminate nature of dry eye and associated ocular discomfort has resulted in the disease becoming one of the most notorious complaints with symptoms being reported by a quarter of patients visiting ophthalmic clinics [197, 198]. For many years the complex pathological nature of dry eye has given rise to many different methods of evaluation with significant confusion and disagreement within the eye care profession as to which is the best assessment for patient symptoms [199]. Greater understanding of the disease and a continual definition refinement by international expert panels such as the International Dry Eye Workshop [73], Delphi Panel Dry Eye report [200] or the preferred practice guidelines suggested by the American Academy of Ophthalmology [201], has allowed for the development of recognised assessment techniques that yield greater accuracy and confident diagnosis guidelines. Hand in hand with ocular health questionnaires and patient histories, the most popular assessment techniques involve the instillation of topical dyes into the eye for slit lamp observation under various lighting conditions [164]. First introduced by Ehrlich in 1886, vital staining is a technique used to distinguish cells of various properties through the use of appropriate dissolvable, coloured dyes [202]. Although vital staining techniques only provide qualitative assessment of ocular abnormalities, dyes do provide a good first indication of disease presence/ severity and provide clinicians with clues as to which additional assessments should be performed to confirm suspicions [164, 203].

2.1. Commonly Used Dyes for Anterior Eye Assessment

Bismarck Brown, Methylene blue or Neutral Red are just a few examples of the many dyes which have been developed over the last hundred years to assist in clinical evaluation of the eye [202]. Negative side effects and safety concerns have rendered many obsolete [204, 205]. The high attrition rate of dyes has however led to a small remaining number of well-tailored formulas that depending on country and recommended local practices, enjoy contemporary mainstream use. In conjunction with high performance colour filters tuned to allow certain wavelengths to pass, vital dyes provide clinicians with great insight into the health of the ocular surface in a simple and relatively low cost, low risk method.

2.1.1. Rose Bengal

Perhaps one of the least pleasant dyes still in use today is Rose Bengal (RB) which is toxic in nature [206] and administration commonly gives rise to increased tearing and stinging sensations that typically necessitate prior instillation of topical anaesthetics [186]. Quality of staining is dose dependant with a recommended volume of 25µL being introduced onto the upper surface of the bulbar conjunctiva with the eye lid held back and the patient looking down to the floor [186]. Smaller doses give lower staining contrast [186]. RB is particularly effective at identifying dry eye as the dye simultaneously contrasts strongly on both the cornea and sclera and presence of the disease leads to clear punctate staining, an example of which is seen in figure 2.1 [202]. Patients with brown eyes tend to mask the red dye and contrast performance is reduced. A suitable green filter such as the Kodak Wratten 58 Green (545- 567 nm) [186] in combination with a white light source can enhance viewing [207].

Negative patient responses such as ocular irritation, reflex tearing, pain and long lasting unsightly cosmetic staining of the patients' face due to fluid overspill have been reported. Additionally, remaining RB in the eye can be subject to photo- activation from UV sources, such as sunlight, which could lead to severe pain once the patient has left the clinic and is making their way home [186]. All these factors contribute to reducing the popularity of this stain and reluctance in administration.

Figure 2-1: RB staining of cornea and conjunctiva highlighting areas of severe dry eye damage in red [208].

2.1.2. Lissamine Green

Lissamine Green (LG) is the preferred alternative to RB as it stains the same regions as RB and allows for similar observations without the painful side-effects [209, 210]. The first documented use in the human eye was by Norm in 1973 [211] and follow on experiments conducted by Manning et al. [209, 212] showed a greater patient tolerance to Lissamine Green without a difference in subjective staining scores nor the requirement for anaesthetic. An excitation wavelength of 567 – 634 nm which can be supplied by a Kodak Wratten 92 filter, has been suggested to enhance the observation of LG stained cells with the conjunctival staining appearing black against a red background [186].

As with RB, LG staining contrast is affected by instillation volume. 10 µL of LG has been found to be optimal and combined with the non- toxic nature of the dye and the strong appearance on the white sclera, LG is recognised as the prime choice for evaluation of conjunctival regions of the eye [212]. As opposed to RB, LG only stains damaged or dead cells [210] and can be used not only for detecting signs of dry eye [209], but also as a test for incorrect contact lens fit [211]. Contact lens induced conjunctival staining (CLICS) [213] demonstrated in figure 2.2a, gives clinicians an indication that lenses are inducing unnecessary limbal stresses resulting from either poor contact lens edge design or incorrect sizing for patient corneal diameter [213].

Separate to ocular surface grading, LG can be used for Lid Wiper Epitheliopathy (LWE) which is a negative condition affecting the leading edge of the top and bottom eye lids. Responsible for the even distribution of the tear film over the eyes' surface [214], a healthy lid margin contains many goblet cells which may experience degradation due to reduced surface lubrication and corresponding increased frictional component [215] as is experienced by contact lens induced dry eye sufferers. Studies by Korb et al. have found a strong relationship between LWE and dry eye symptomatic patients with 88% of positive dry eye subjects showing signs of LWE and only 18% for the asymptomatic group [216].

Although both RB and LG have limited use within the UK, surveys carried out by Korb show that both are still popular with examiners in other parts of the world where reduced choice of less invasive, alternative dyes mean they enjoy a relatively strong following [164].

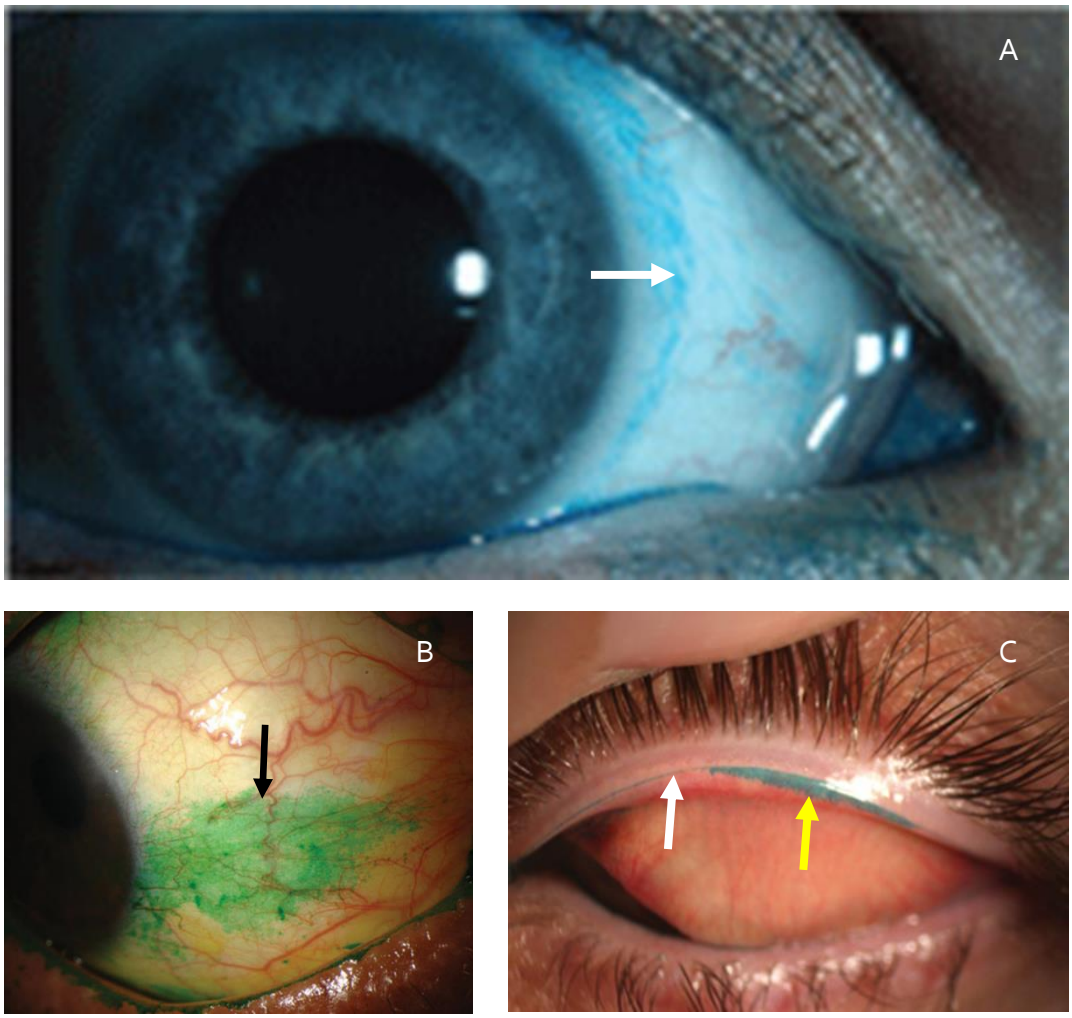

Figure 2-2: A) Contact lens induced staining due to poor contact lens edge design/ fitting, is apparent by the ring of blue dye surrounding the limbus indicating a damaged corneal epithelium [217]. (B) Damaged/ dead conjunctival cells clearly visible as green regions against the normally white sclera [218]. (C) Lid Wiper Epitheliopathy induced through dry eye conditions. Healthy lid wiper is considered a thin leading line (white arrow) whereas severe regions of frictional damage due to reduced lubrication being highlighted in the thicker staining of the lid margin (yellow arrow) [219]

2.1.3. Sodium Fluorescein

The most commonly used dye, and the main focus of this chapter, is Sodium Fluorescein which was first created by Adolf von Bayer in 1871 and applied to the human eye by Pfluger and then Straub in the 1880's [220]. In raw powder form, Sodium Fluorescein has a dark orange colour with a chemical formula $C_{20}H_{10}O_5Na_2$ and can be applied either intravenously, ingested for retinal and iris assessment, or instilled directly on to the ocular surface for common anterior eye observation [221].

Fluorescein is readily obtainable in two forms; fluorescein impregnated paper strips (requiring saline wetting prior to instillation) or a 2% solution that can be dropped on to the eye directly [186]. Impregnated paper strips are the preferred method as the individual units are low cost and are carefully manufactured to be of a predetermined concentration. The use of a single strip per eye promotes sanitary handling by eliminating cross contamination between left and right eyes of patients through the use of one strip per eye. Additionally, research has uncovered that corruption of medical fluids such as Sodium Fluorescein solutions is a common and significant problem which may lead to unintended secondary infections [222]. An example of this is the work by Kyei et al. who discovered significant bacterial and fungal contaminates including Pseudomonas aeruginosa, Pseudomonas pyocyanea and Serratia marcescens present in varying amounts in all 21 bottles of fluorescein solutions used in several Ghanaian eye clinics [223] leading to inadvertent additional distress for patients seeking care and relief from disease.

Once introduced on to the ocular surface, Fluorescein requires a wide excitation wavelength of between 420- 520 nm (central wavelength of 495nm) to induce a resultant green fluorescence in the 485- 580 nm (central wavelength 520 nm) region of the colour spectrum. The use of appropriate fluorescein blue excitation and yellow emission filters allow for simultaneous cornea and conjunctiva qualitative assessment.

Presumably, due to the limited availability of suitable filters in the late 1800s, slit lamp manufacturers tended to use Cobalt blue as the default excitation filter that was placed in front of the default white light source to stimulate fluorescence. Cobalt blue however produces sub-optimal wavelengths required for high intensity fluorescein viewing and to compensate, the brightness of the light source must be increased which leads to uncomfortable experiences for the patient and may give rise to dangerous blue light exposure scenarios. Many contemporary slit lamps are still equipped with sub- optimal blue excitation filters which although are generally within the working spectrum of fluorescein, do not produce maximum viewing performance.

In conjunction with excitation, an appropriate yellow emission filter with a peak wavelength of 510 to 520 nm is necessary to view the fluorescent light returning from the patients' eye and exclude all unnecessary blue light spectra produced by the slit lamp [174]. Modern high- end slit lamp instruments may come furnished with both blue excitation and yellow emission filters built into the body of the devices. However, many eye care practitioners who do not have access to new equipment rely on alternative low-cost handheld thin film filters which must be manually suspended in position by the administering clinician during staining tests. This is not particularly comfortable for the clinician and the filters are generally not well tuned to optimum fluorescence emission wavelengths leading to poor viewing experiences and an increased possibility of missed diagnosis.

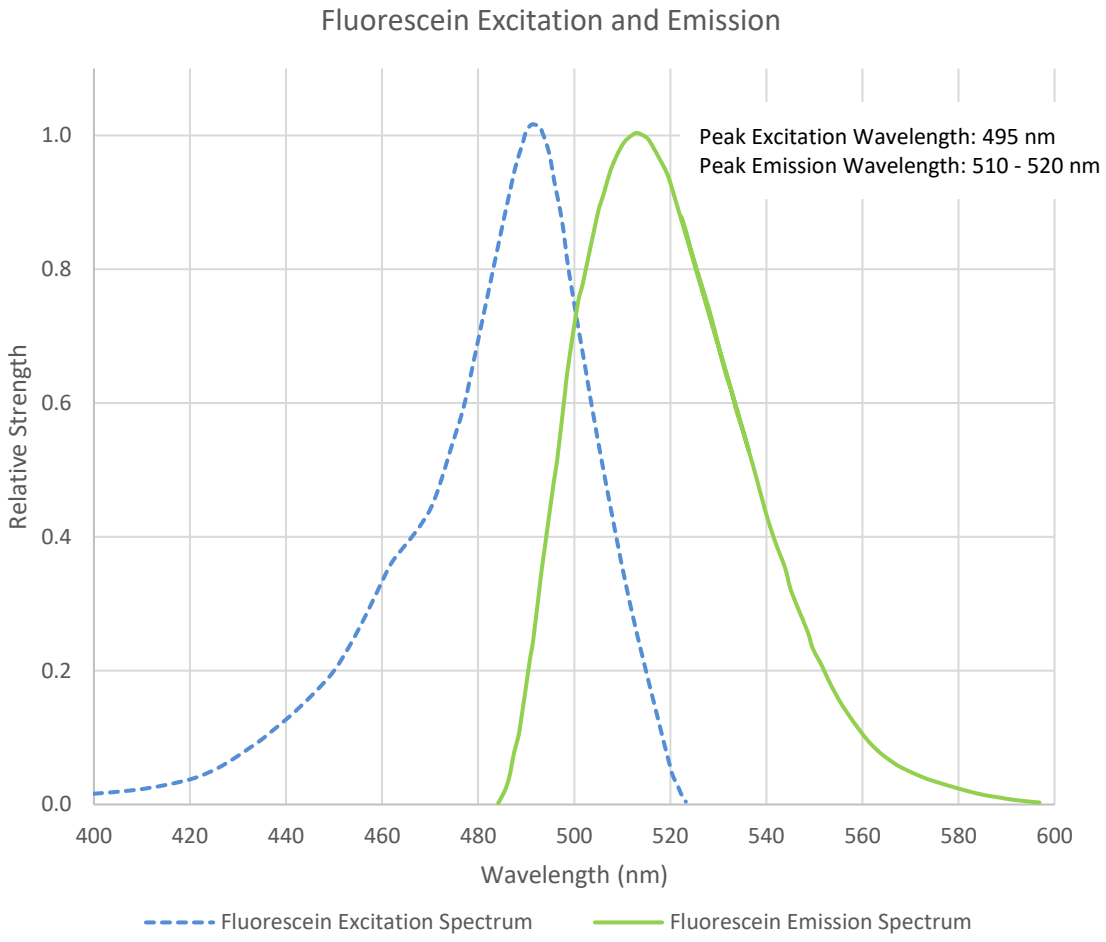

Figure 2-3: Sodium Fluorescein excitation & emission Spectrum. Adapted from [174]. Ideal excitation wavelength 495 nm, ideal emission wavelength 510 - 520 nm, with minimal overlap in-between.

Contrary to RB or LG, higher volumes of fluorescein instillation do not lead to better viewing as the dye experiences a “self- quenching” effect which leads to reduced fluorescent efficiency and a noticeable dimming of fluorescent light emanation at higher concentrations [224]. Figure 2.3 shows the ideal excitation and emission wavelength of the Fluorescein stain in the human eye under normal pH levels – typical healthy baseline values are of around pH 7.6 but increase up to pH 9 over prolonged periods of eyelid opening due to tear film carbon dioxide absorption from the air [225]. Due to changes in amount of fluorescence at different pH levels, fluorescein has the ability to be used as a pH indicator as well [226].

Typically, fluorescein allows trained clinicians to identify a whole host of abnormal manifestations such as corneal abrasions, scratches (length and position), corneal corrosions and abscesses, a few example of which are shown in figure 2.4 [202]. Although considered mildly invasive and has been shown to promote premature breakup in moderate to severe dry eye patients, FBUT is one of the most commonly used tests of tear film stability [171, 172, 183]. Lid wiper Epitheliopathy - thought to be one of the best indicators for the presence of dry eye [216] can also be performed using fluorescein similar to the earlier mentioned Lissamine green. Although conjunctival and corneal staining patterns have proved to be particularly effective markers of dry eye disease presence, this is only accurate in the most severe case examples, with less variability reported in both mild to moderate instances of dry eye as compared to healthy control patient [36]. Nevertheless, staining is still seen as one of the preferred techniques by clinicians due to low cost and ease of execution [164, 172].

In summary fluorescein is considered as the least invasive option of all three commonly used vital dyes because of the large number of tests that can be conducted and the low negative patient impact. A full summary of tests that can be performed with fluorescein can be found in table 2.1.

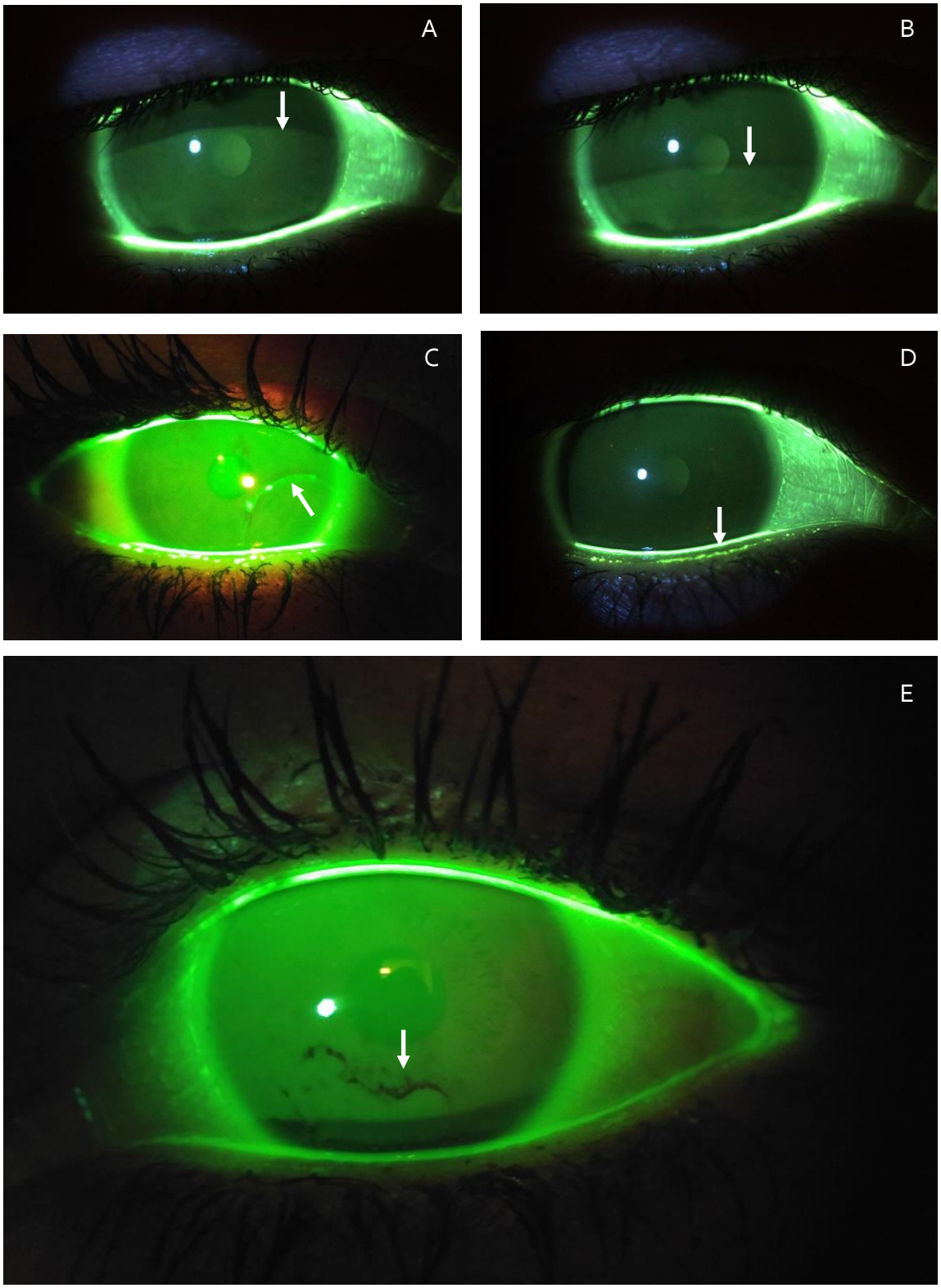

Figure 2-4: (A & B) Incomplete blink example- fluorescein boundary line showing the lowest position of the eyelid during current blink cycle. Repeated incomplete blinks leads to reduced expression from meibomian glands and compromised tear film formula (C) Foreign body visible on ocular surface (D) Tear Meniscus and scleral staining (E) Tear breakup regions shown by dark shadows on corneal inferior region. Measurement is subjective. (All images author's own work)

2.1.4. Summary of Ocular Surface Stains

Table 2-1: List of commonly used dyes and appropriate filters for viewing. Adapted from [186]

Ocular Surface Stain	Suggested Excitation Filter	Suggested Absorption Filter	Test	Invasiveness Level
Rose Bengal	Green Light Source for viewing over sclera, else White light source	Wratten 58 Green, Wratten 92 (Red) or Hoya 25A (Red) for use with white light source	• Detection of damaged/ dead epithelial scleral cells • Conjunctival Staining • Lid Wiper Epitheliopathy	High
Lissamine Green	White Light source	Wratten 92 (Red) or Hoya 25A (Red)	• Conjunctival damage assessment • Contact lens fitting issues • Lid Wiper Epitheliopathy	Moderate
Sodium Fluorescein	Cobalt blue, Wratten 47/ 47A Blue, Transmission 410-500nm.	Wratten 12 Yellow, Peak Transmission above 510nm	• Fluorescein Break up Time • Grading Staining • Tear Meniscus Profile • Fluorophotometry • Lid Wiper Epitheliopathy • Foreign Body Identification • Complete Blinking Analysis • Dendritic Ulcers	Low

2.2. Staining Classification and Grading Schemes

The subjective nature of vital staining makes it clinically challenging to consistently record abnormal ocular surface features and extent of damage. Subsequently, grading schemes have been developed to allow for comparison of patient symptoms and progression over time. Popular examples include the Oxford grading scheme [186], the National Eye institute/ Industry Workshop guidelines, the area- density index, the van Bijsterveld system, the Sjögren's International Collaborative Clinical Alliance ocular staining score and the Collaborative Longitudinal evaluation of keratoconus (CLEK) [36, 227]. Each grading scheme allows for the recording of different characteristics and at different sensitivity increments. For example the Oxford grading scheme and CLEK use a greater score dynamic range than van Bijsterveld, thereby allowing identification of smaller changes in ocular conditions [228]. No studies have been completed proving the superiority of one scheme over another [228] and since the grading charts were designed to identify staining patterns and require subjective scoring, they are not particularly useful for quantitative assessment of diseases [186].

2.3. Dye Observation with a Slit Lamp Biomicroscope

Anterior eye observation by means of a traditional slit lamp biomicroscope is a common and non- invasive procedure [229]. White light, typically from a halogen or Light Emitting Diode (LED) source, is used to illuminate the eyeball and allows for direct, magnified, binocular viewing and assessment. Typically available in two form factors- Zeiss and Haag Streit, one of the many key advantages of the slit lamp is the ability to independently manipulate the angle of the light source projected on to the eye as well as the facility to control the profile of the light beam and adjust magnification of the eye piece- usually in steps from 6X, 10X, 16X, 25X and 40X. An experienced operator may be sufficiently skilled to observe forty two individual aspects of anterior ocular health ranging from simple foreign body identification, corneal erosion or crystalline lens cortical cataract [230].

A distressed eye may present characteristics of disease and abnormalities that vary in aspects from size, colour, transparency and depth. To assist diagnosis, modern slit lamps allow five modes of illumination for optimised viewing of the affected areas [231, 232]:

1. Direct diffuse illumination – general anterior eye observation of corneal surface and crystalline lens, contact lens fitting, lacrimal reflex
2. Direct focal illumination – cataracts evaluation, vessels, nerves, corneal shape, opacity depth
3. Indirect illumination – corneal epithelium scarring, stromal defects, corneal micro cysts/vacuoles, corneal swelling, foreign bodies/ contaminates
4. Specular Reflection – observation of surfaces, principally cornea
5. Tangential – raised iris lesions

The versatility of slit lamps allow clinicians to take advantage of multiple illumination techniques that will return the best results in respect to the abnormality being observed. Modern slit lamps can also be equipped with photo/ video capabilities and patient condition progression can be recorded over time to measure treatment efficacy.

With the introduction of custom tailored synthetic dyes such as Sodium Fluorescein, Lissamine Green, or Rose Bengal into the anterior eye, along with the insertion of appropriate colour filters in the light path, this arsenal of slit lamp observations can be boosted to include hidden details not possible with simple white light observation [186]. It is common to find advanced slit lamps fitted with five manipulation/ excitation filters such as diffuse white, neutral density (grey), heat absorbing, green (red- free), and blue as well as a separate yellow emission filter located in the main body used for fluorescein observation.

2.4. Low Cost Alternative Filters

Although modern slit lamps tend to include the filter packages required for various dye viewing, not all come as part of the standard model and many manufacturers only offer filters as part of expensive additional extras. The blue excitation filter can be an additional £1,000 option on some manufacturer quotation lists and cannot be retro fitted to earlier models. In addition not all filters are of equal performance, with certain manufactures choosing to use stock components from suppliers while others such as Topcon (*Topcon, Tokyo, Japan*) develop their own high performance fluorescein filters known as the Blue Free Filter ™ which is a proprietary combination of blue exciter and yellow absorption filters that are claimed to give 1.6x brighter fluorescein viewing [233].

Although these costs may be considered acceptable for large, well-funded organisations such as hospitals or research facilities, there is a tendency to save the best equipment for those that can afford it while others have to make do as best they can. Many older slit lamps which are to be replaced as part of product life cycles are still in reasonable working order and are sent to developing nations for a second life. Although there are no official figures for the re- used equipment market, the equipment tends to be of an older specification and be missing modern upgrades such as the coloured filters necessary for fluorescein viewing.

To help with the lack of fluorescein viewing ability, companies such as Johnson and Johnson or Bausch and Lomb [234] have developed low cost, semi- disposable hand held filters such as those shown in figure 2.5 which are manually held in front of the objective lens and substitute inbuilt filters that are present with higher priced slit lamps. Needless to say, the requirement by the clinician to hold the filter in place takes up their spare hand which is an unnecessary inconvenience. Furthermore, thin film filters, tend not to be particularly tuned to the desired fluorescein excitation curve and provide inferior viewing capabilities compared to the glass counterparts. During use, film filters are often sandwiched between the eyepiece objective lenses and illumination column by the clinicians which after time results in a scratched surface of the filter and suboptimal viewing effect. Such filters also tend to become easily damaged and lost.

Figure 2-5: Low cost thin film filters for handheld use. Johnson & Johnson model includes an additional red barrier filter for Lissamine green viewing

2.5. Chapter Aims and objectives

It is clear that vital staining as part of slit lamp examinations is an important tool in the identification and grading of anterior eye diseases and in particular for dry eye where fluorescein breakup time has been identified as the one of the four homeostatic markers that is to be used to identify the disease should preferred non- contact methods not be possible [36].

Fluorescein is a popular and readily obtainable dye which allows for great flexibility in a large number of clinical tests with minimum patient side- effects. To extract maximum data during an examination, instilled fluorescein should be exposed to a blue light source whose 495 nm peak wavelength matches the spectrum of optimum fluorescein excitation (figure 2.3). This will produce maximum fluorescence at lower light intensities thus minimising both patient discomfort and the potential for retinal damage through intense blue light exposure. Secondly a yellow emission filter closely matched to the shift in wavelength between the applied blue and resulting green emission wavelengths, namely 510 – 520 nm is to be developed for hands- free operation. The emission filter must be tuned to accentuate detail and early signs of disease giving the clinician the ability to make a confident diagnosis.

Laboratoires Thea (*Clermont-Ferrand, France*) and Bausch & Lomb (*Bridgewater, New Jersey, USA*) have both expressed interest in the creation of low-cost filters for fluorescein viewing. To help differentiate between individual filter development, this chapter will be separated into two halves; the first focusing exclusively on the creation of a low-cost retrofitable pair of blue and white diffuse filters for Thea; and the second half dedicated to the development of a high-performance fluorescein emission filter to be adopted by Bausch & Lomb. A joint discussion of all filters will complete the chapter at the end.

Both development projects will have the following aims:

- Create a low cost (sub- £2), high performance filter combination alternative to exceed viewing capabilities of mainstream filters available today;
- Filters must be of universal design and retrofitable to fit as many of the Haag Strait style slit lamps variants as possible;
- Filters must be designed to be commercially viable for large volume, commercial production and distribution;
- Regarding blue excitation filter, minimise unnecessary blue light damage wavelengths;
- Show individual company logos as well as Aston University logo on the body.

2.6. Diffuse White and Fluorescein Blue Excitation Filters

The lack of an active patent in the long history of slit lamps has allowed for many manufacturers to develop custom iterations of the instruments. Standard desktop slit lamps are available in two form factors named after the original manufacturer of that style; the first being Haag Streit which houses the light source at the top of the lighting column and the second being Zeiss which has a light source in the bottom of the body. It is difficult to accurately ascertain the active number, but to the authors' knowledge there exist 29 larger slit lamp manufacturers with many more smaller producers not being known [235]. The vast majority of slit lamps have been designed with pre- selected coloured filters such as the common cobalt blue for fluorescein excitation or a separate green filter (known as red- free) for scleral/ retinal vessel viewing. Both variants are integrated into the illumination column allowing the user to change lighting conditions with simple switch selection without the need to manually insert filters.

Individual manufacturers are free to choose custom light sources in their instruments along with filters that they may consider to be appropriate for the level of performance they are looking to achieve at an acceptable cost. Light sources typically vary between Tungsten, Halogen and newer LED versions. Colour temperature, brightness and colour rendering index (CRI)- which is the ability of a light source to appropriately render colours of an object in comparison with natural light, all vary between manufacturers and models and such details need to be considered for custom filter design.

In an effort to further differentiate performance and styling between each other, manufacturers develop individual designs of their instruments with dimensions that are constantly changing. To develop a single filter that will fit popular slit lamps available from various manufacturers as well as accurately reproduce the appropriate spectrums will be challenging.

2.6.1. Blue Light Hazard

A harmful side effect of using fluorescein for observation of the eye is the requirement to use a relatively short wavelength blue light source below 500 nm and the corresponding risk of retinal damage through a process known as blue light exposure as seen in figure 2.6. Although it has been proven that intense visible light, such as normal noncoherent sunlight is capable of retinal degradation [236, 237] the high energy, short wavelength of intense blue/ violet light when shone into the human eye even for brief periods, encourages both degenerative retinal pigment epithelium and photoreceptor damage in the retina [238, 239].

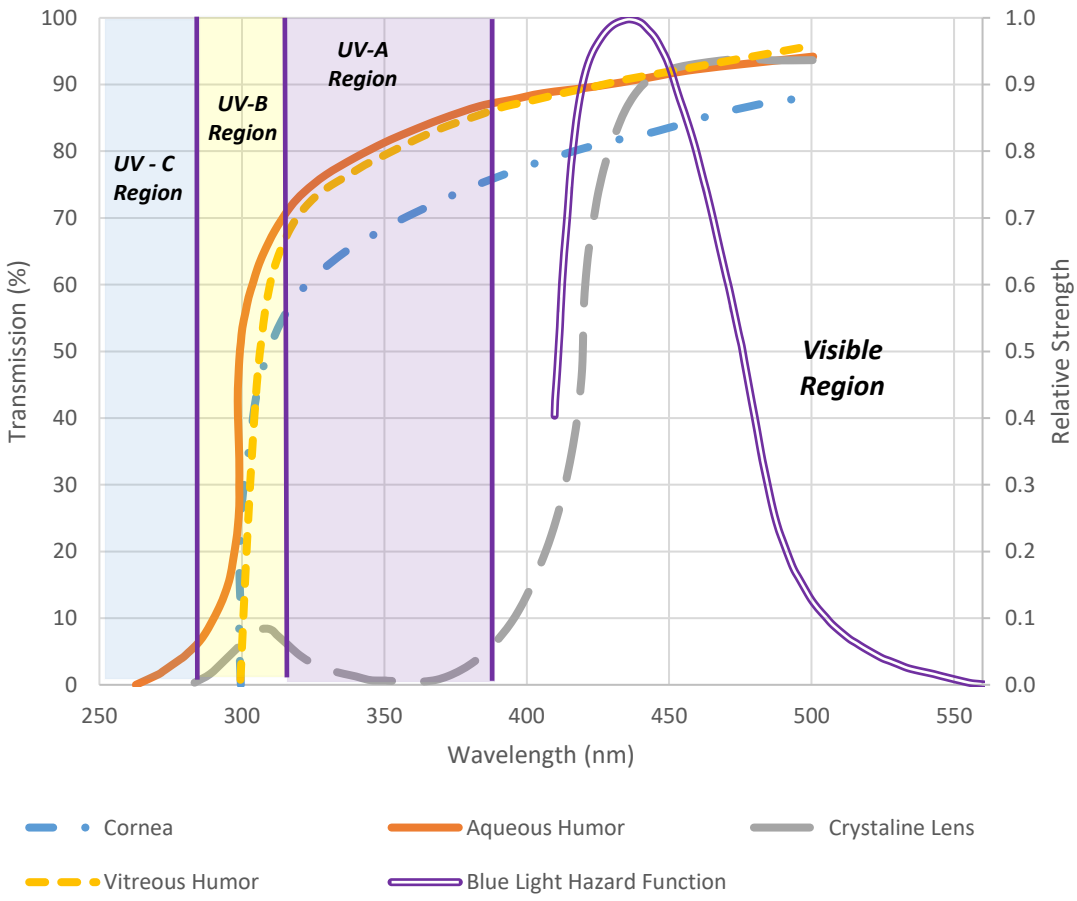

Figure 2-6: Blue light hazard overlaps the crystalline lens transmission profile (grey line) allowing light energy of 415 nm and above to reach the retina. Self-drawn with data obtained from [238, 240]

At sea level, the amount of solar energy contained in the 400 – 500 nm region is greater than in any successive 100 nm bandwidth. Solar radiation peaks at 470 nm and direct viewing of the midday sun on a bright day at sea level through a 2mm constricted pupil gives rise to a retinal irradiance of 1.6 J s^{-1} cm^{-2}. A minute of sun gawking gives rise to 96 J cm^{-2} of radiation exposure potentially leading to scotomata- permanent photochemical damage of the retina or even a possibility of uncontrolled cellular mutation [241, 242]. Modern slit lamps, such as the halogen powered Haag Streit 900, are capable of producing up to 1.2 J s^{-1} cm^{-2} under full power illumination conditions [243] and are able to exceed the maximum allowable exposure of blue light shone into a patients' eye in as little as fifteen seconds [174, 243].

Prolonged radiation into the eyes of young adult rhesus macaque monkeys by Dawson et al. demonstrated that blue light exposure of 20 J cm^{-1} causes significant changes on the fundus structure leading to retinal lesions [236]. Separately, Rapp & Smith found that UV-A light causes between 50 and 80 times greater photoreceptor damage than green light at the same light intensity [244].

Historically, carbon arc, Nernst glower and Köhler illumination were once all used as light sources for slit lamps, but evolution of the device has now settled on the common incandescent, halogen and more recently introduced LED lamps. The method of electron excitation of these newer LED sources give rise to different light spectrums and therefore differing amounts of energy in the blue light hazard region but thankfully zero emissions within the UV range. The prime consideration that must be kept in the forefront of design is the need to minimise blue light exposure and sidestep any potential fallout of retinal damage as a results of fluorescein observation and to keep observation time short to minimise exposure length.

2.6.2. Slit Lamp Pure White and Blue Filter Spectrum Data Collection

Contemporary slit lamps are typically fitted with either Halogen or LED light sources, but with no standardisation existing between manufactures, spectrum profiles of both pure white and filtered blue from common manufactures will need to be measured to gain a starting point for filter design.

An Ocean Optics Maya 200 Pro Spectrometer (*Ocean Optics, Dunedin, Florida, US*) was used for the collection of all spectral data on available slit lamps at Aston University. To achieve consistency across various test and slit lamp models, the following physical setup was employed:

1. Individual slit lamps were powered on 5 minutes prior to start of test to allow for operating brightness to be fully achieved
2. The spectrum probe was placed at 100mm from slit lamp objective lens- the average distance a patient will sit when being observed during examination
3. All spectrometer settings were maintained across all slit lamp tests: Integration time set to 0.01 seconds, 2 scans to average, Box Car width = 3, Electric Dark Correction and Non- Linearity Correction = True
4. Probe was held in place by a bespoke rig created from Thor Labs Optical Bench equipment (*Thor Labs, Newton, New Jersey, USA*)
5. Dark field measurements were taken and subtracted from the light signal in an effort to remove any stray radiation during measurement.
6. To extract maximum data, brightness of each slit lamp was progressively adjusted until just before spectrometer sensor saturation was reached, i.e. maximum brightness that can be recorded by the spectrometer before sensor overexposure.

Experimental setup is shown in figure 2.7 with results following.

Figure 2-7: Experimental setup of slit lamp spectrum measurement process. A) Probe positioned on custom platform in-line with slit lamp light path. Spectrometer settings to be kept constant across all slit lamps. B) Close up of probe and slit lamp mirror assembly- last position before light enters patients' eye.

2.6.3. Slit Lamp Spectrum Results

Data was successfully collected on a wide variety of raw white light slit lamp spectrum profiles from both halogen and LED slit lamp light sources and have been graphed in figures 2.8 and 2.9 respectfully. Transmission profiles were calculated for each sample and important indicators such as central wavelength and maximum transmission were extrapolated for each- maximum transmission and central wavelength are separate indicators of filter performance and need not occur at the same wavelength. As expected, no two slit lamp pure white light sources were the same with marked differences between manufacturers giving a large range of intensities at different wavelengths. This is most likely attributed to individual manufacturers specifying bulbs that are particular to their models as a way of generating future revenue on replacement parts and a fact that is backed up by many online suppliers offering multitudes of bulbs, both OEM and alternative manufacturer low cost equivalents [245, 246].

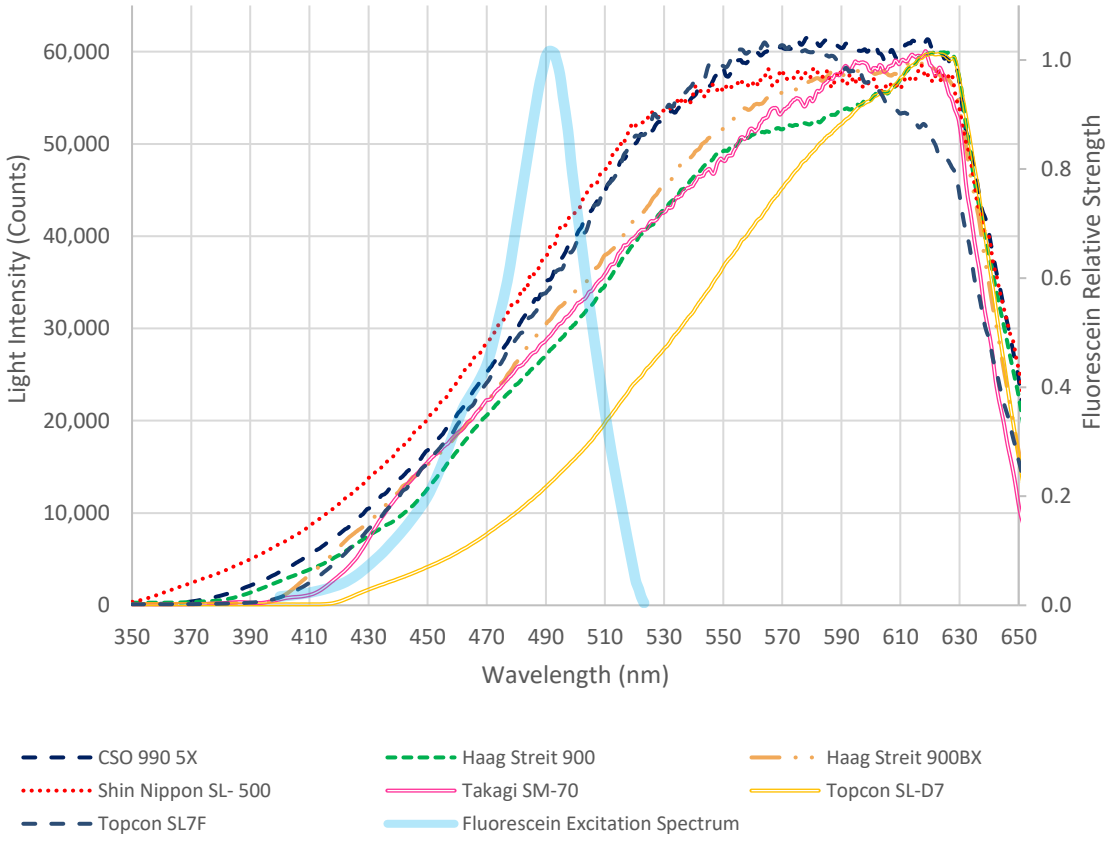

Figure 2-8: Slit Lamp White Light Source Comparison - Halogen

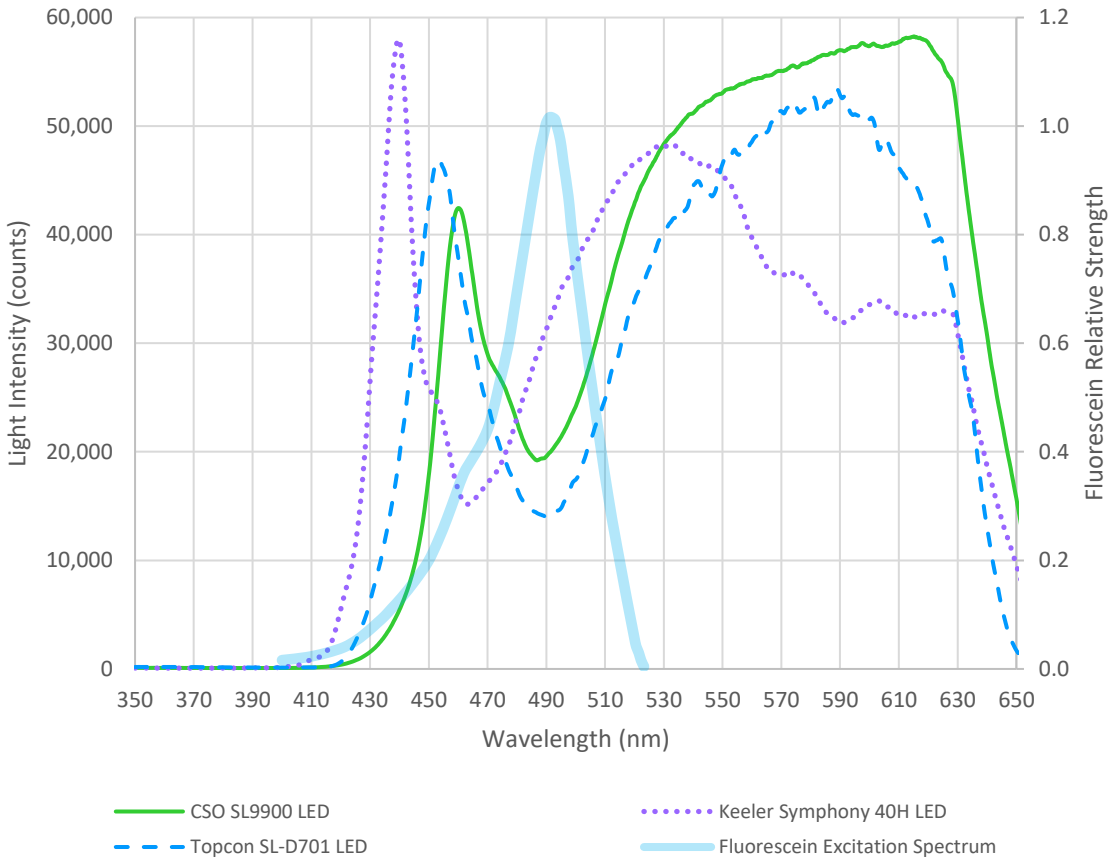

Figure 2-9: Slit Lamp White Light Source Comparison – LED

Bulb age, thermal degradation and usage cycles may also play a factor with units that are close to end of life typically experiencing lower light level outputs and shifts in radiation patterns from original factory conditions [247]. To maintain constant conditions and reduce unintended changes in experimental setup, slit lamp brightness settings were kept constant and onboard blue filters were sampled during the same procedure without changing of either the brightness of the slit lamp or the position of the probe. Figures 2.10 through 2.13 are a collection of all halogen and LED blue filters in combination with transmittance performance at various wavelengths. Although many filters have close central wavelengths of between 455 and 485 nm, each show large deviations of peak transmittance wavelengths of between 397 nm for the Shin Nippon SL-500 and 429 nm for the Topcon SL-D7. Similar divergences can be seen for LED slit lamps. Table 2.2 shows all spectrum data from tested slit lamps combined with calculated spectrum overlaps of each blue filter compared with ideal fluorescein.

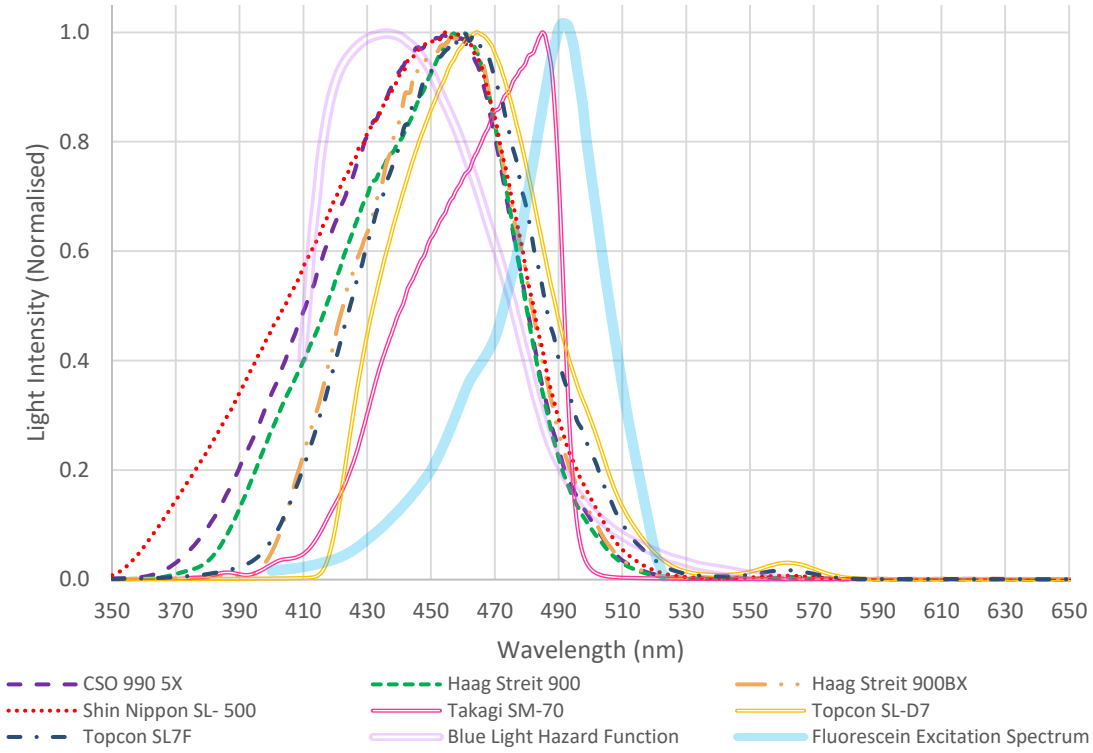

Figure 2-10: Normalised Slit Lamp Blue Light Comparison – Halogen

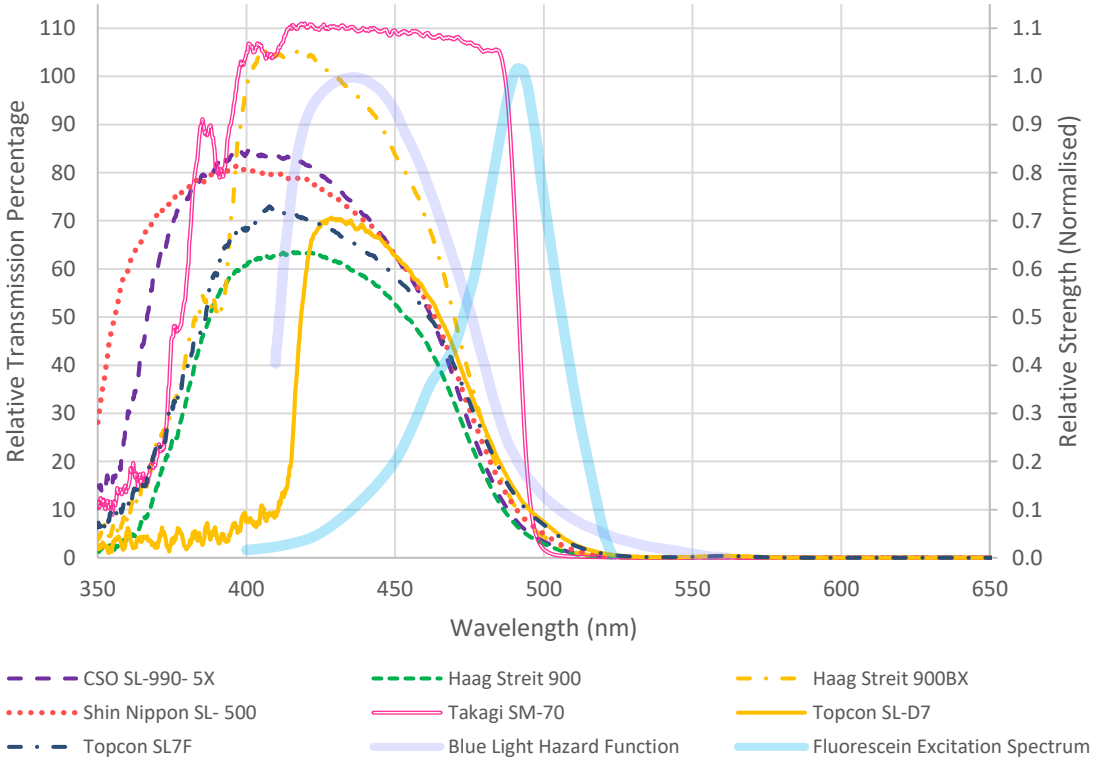

Figure 2-11: Slit Lamp Blue Filter Transmission Efficiencies – Halogen

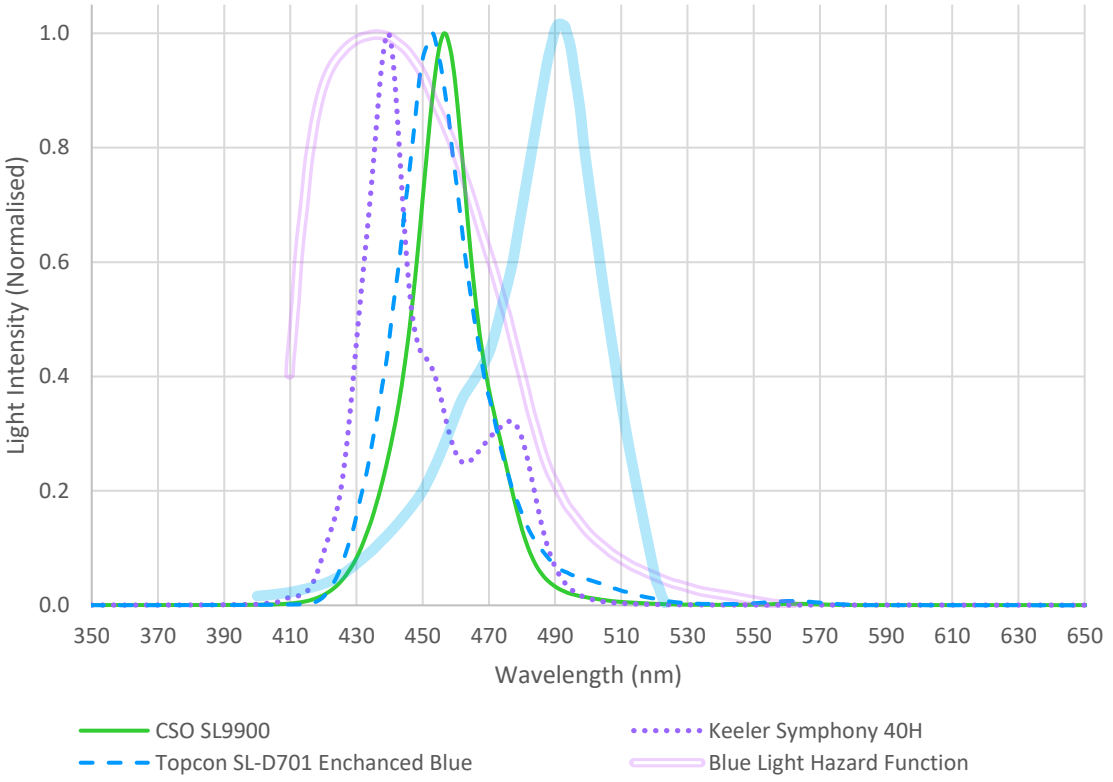

Figure 2-12: Normalised Slit Lamp Blue Filter Comparison – LED

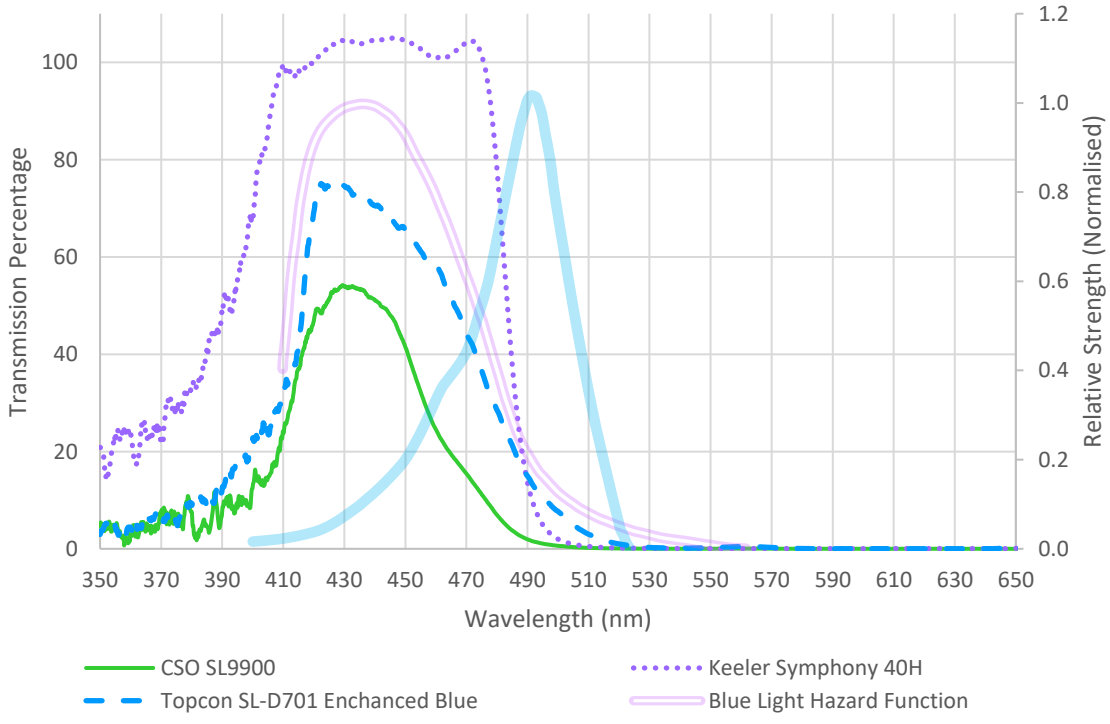

Figure 2-13: Slit Lamp Blue Filter Transmission Efficiencies - LED

Table 2-2: Comparison of Halogen and LED slit lamp filter profiles

Light Source Type	Slit Lamp Model	Central Wavelength (nm)	Peak Transmission Wavelength (nm)	Transmission Percentage at Peak Transmission
Halogen	CSO 990 5X	457	401	84.91
	Haag Streit 900	460	415	63.63
	Haag Streit 990BX	461	408	106.00
	Shin Nippon SL- 500	455	397	81.00
	Takagi SN- 70	485	420	111.00
	Topcon SL- D7	464	429	71.00
	Topcon SL7F	460	408	73.00
LED	CSO SL9000	457	430	54.20
	Keeler Symphony 40H	439	444	105.00
	Topcon SL-D701	453	427	76.00

The closest halogen blue filter to ideal fluorescein (495nm) is the Takagi SN- 70 which had a central wavelength of 485 nm. In figure 2.11, the transmittance curves of both the Takagi and the Haag Streit 900BX is confusingly above the 100 % threshold of the original white light source suggesting the blue filter itself is fluorescing to give a higher light level output than it is receiving. The Keeler Symphony 40H also demonstrates similar behaviour.

Many of the halogen filters have relatively low transmissive efficiency with the Haag Streit 900 showing only a 63.6% efficiency and the CSO SL9000 even lower with a 54.2% score. This may be indicative of a materially thicker filter used in these models and less light being able to penetrate the medium.

A large portion of blue filters are not particularly close to the ideal fluorescein spectrum and surprisingly many have peak transmission values in the low 400 nm regions where blue light hazard can pose a serious problem over longer periods of exposure. However, the light intensities of both Halogen and LED light sources is very low in these wavelengths which leaves the likelihood of ocular damage fairly low during the course of a standard slit lamp examination.

Finally, the raw white spectrums of the LED and halogen slit lamps is dramatically different with all three LED models presenting reduced spectral energy in the 450 to 500 nm region- directly in the ideal fluorescein excitation region (figure 2.9). All three of the LED blue filters in figure 2.12 produce a tighter profile than the halogen equivalents and attempt to take advantage of the left peak of the white light spectrum, with the Keeler 40H particularly excelling in being able to match the white and blue profiles at the 444 nm point and generate a second peak at 474 nm to give additional an boost of light energy closer to the desired 495 nm as shown in figure 2.14.

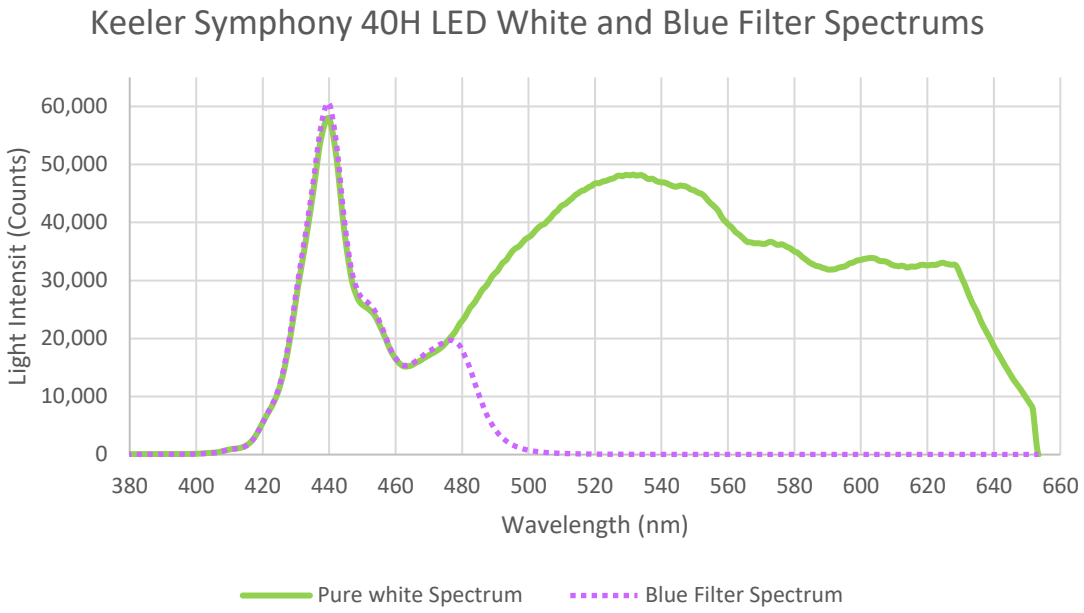

Figure 2-14: Keeler Symphony 40H LED on board blue filter compared to pure white slit lamp spectrum profile

In summary there is now a clearer understanding of current filter performance characteristics and that there is potential for improvement to better match the fluorescein excitation profile. Due to the large differences between Halogen and LED white light profiles, it is recognised that separate filters will need to be developed and tuned for either Halogen or LED slit lamps in order to produce best viewing results with whichever instrument is used.

2.6.4. Material Selection

Ultimate filter performance will not only be determined through colour, but also through physical material choice as the mechanical properties of the final polymer will influence the optical clarity, strength and durability of the production filter.

The plastic selection process should consider the real-world usage and handling of the filters. The typical environment will be in clinical settings under standard room temperatures and pressures (STP). Due to examiner convenience, it is reasonable to expect that the filters will be kept in pockets rather than in the original carry case therefore requiring scratch resistance. Material flexibility will also be necessary to be able to "clip-on" to the slit lamp during hands free operation.

Polymer optics offer many benefits over traditional glass alternatives in terms of cost, lower weight and the ability to select mechanical properties depending on the base material used [248]. The freedom to produce aspheric and complex geometric shapes at relatively low cost through the injection moulding process is a strong advantage. Additionally, resistance to shattering and breakage of plastics enhance the safety argument which together makes a strong case for the use of plastics in this potential mass-produced application.

Generally, plastics can be separated in to three families with similar properties in each:

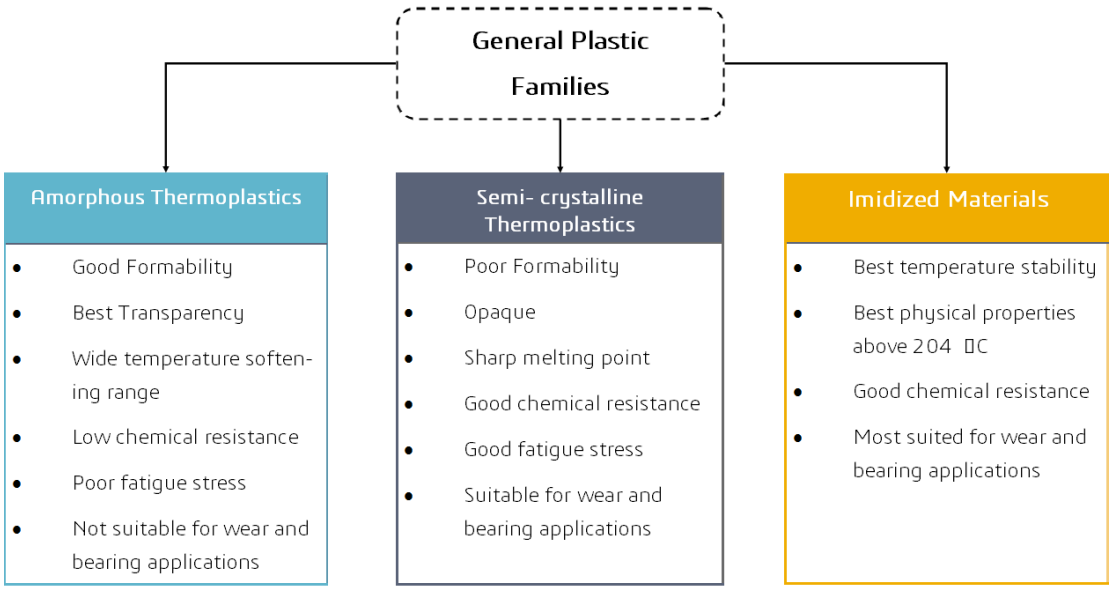

Figure 2-15: Common polymer families. Adapted from Curbell Plastics Materials selection guide [249]

Specialist plastics have been formulated to be used in optical applications with similar optical properties to glass. Cyclic Olefin Copolymers (COC) or Cyclic Olefin Polymers (COP) are two types of amorphous polymers that have high transmissibility, low birefringence and strong mechanical properties [250]. Table 2.2 shows a comparison of amorphous thermoplastics that will be considered for the use in the final design solution.

Typically, plastics are to be considered by process of elimination. These filters will no doubt be subject to potentially detrimental environments (pockets, bags, containers with other equipment, etc.) and they should be robust enough to withstand the demands placed upon them. In addition, the repetitive hanging and removal of the filters onto the slit lamps will cause fatigue in the elastic parts of the body used to attach to slit lamps and is a point that needs to be taken under consideration for materials selection.

Both fluorescein blue and diffuse white will be used exclusively for the manipulation of the slit lamp light source and therefore optical viewing parameters will focus on the best transmittance and mechanic properties available from the amorphous thermoplastics family.

It was initially planned to use COP or COC polymers, but disadvantages include high rigidity, high price and low availability which makes them unsuitable for the desired low-cost application.

Comparing user requirements with plastic offerings, the first-choice match is polycarbonate which is a common, tough and high wearing plastic used in many applications from safety spectacles through to lamp covers. Mechanical properties of polycarbonate will allow for low cost fabrication as well as providing the flexibility necessary for attachment to slit lamp appendages. Should it be deemed necessary, it is possible to obtain higher grades of polycarbonate which conform to United States Pharmacopeia and National Formulary (USP-NF) class VI designation- a toxicity and bio compatibility standard required to be met should the plastic ever be considered for large scale production and require official classification as a medical device.

The development of both the fluorescein blue and diffuse white filter will therefore proceed with polycarbonate as the selected material.

Table 2-3: Optical and Mechanical properties of potential amorphous thermoplastic materials for fluorescein blue excitation filter and diffuse white filter

	Material							
Properties	**Acrylic**	**COP**	**COC**	**Polycarbonate**	**Styrene**	**Polyester**	**PEI**	**Glass N-BK7 (Reference)**
Refractive Index (589.2 nm)	1.49	1.53	1.53	1.585	1.59	1.61	1.68	1.52
Abbe Number	58	56	58	34	31	27	19	64
Uncoated Transmittance in Visible Spectrum	92	92	92	89	88	90	50	91
Birefringence (scale of 0 to 10)	4	2	2	7	10	2	-	1
Operating Temperature (°C)	85	135	150	120	75	125	170	>400
Cost per Kg	£2.78	-	-	£2.20	£1.85	£1.79	£3.00	-

Guide

Refractive Index-light rays entering a transparent or opaque material will experience a change in speed and a corresponding change in direction as the density of the new medium is different to the source material (Coronis, 2009). The greater the change in direction, the greater the refractive index.

Abbe Number-a useful measure for dispersion of visible light as it travels through a material. Light of different wavelengths will have various angles of refraction which will cause images to become unclear and foggy. A common example is seeing rainbow fringes when looking at a light source through a section of plastic. The higher the Abbe number, the greater the clarity of the image.

Birefringence- optical polymers hold an inherent amount of stress which affects the light waves as they travel through the material. If the plastic is injected into the mould and careful consideration is not given to mould designs and cool down times, the finished units will suffer from molecule misalignment which disrupts any images that will be viewed through the material.

2.6.5. Mechanical Sizing

Haag Streit type slit lamps have light sources and coloured filters enclosed in a plastic body located in the upper half of the illumination assembly thereby allowing light to be channelled through the filters before it is reflected off the 45˚ mirror and into the patients' eye. As both the blue and diffuse white filters will need to interrupt the light path prior to being received by the patient, both will need to be positioned around the mirror assembly (see figure 2.16) which, without physical modification to the slit lamp itself is the natural area of interest. Common slit lamps were selected and measured using a Mitutoyo 500-196-20 Digimatic Vernier calliper (Takatsu-Ku, Kawasaki, Japan).

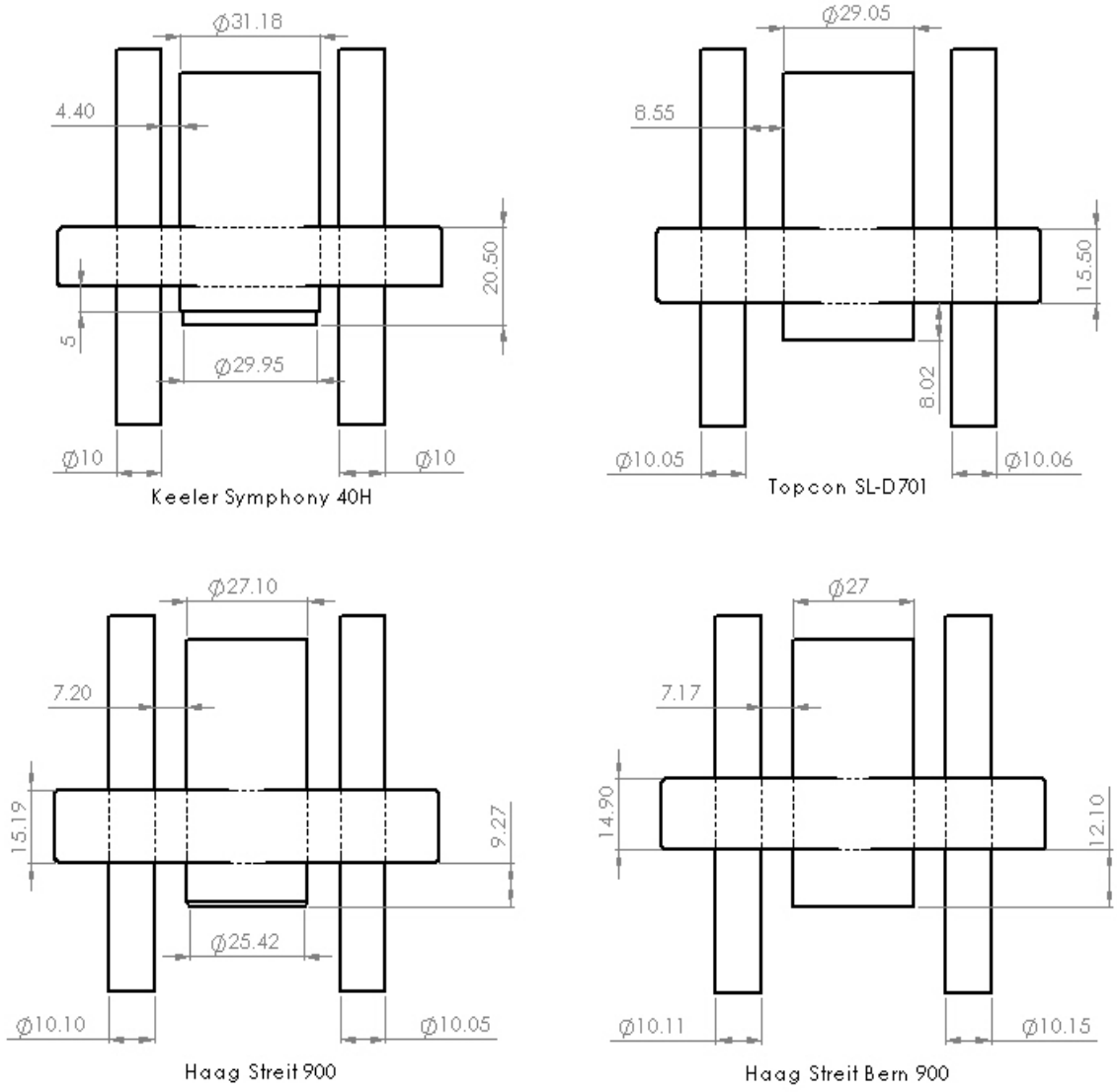

Figure 2-16: Common slit lamp mirror assembly dimensions. Uprights on both left and right are of similar dimensions across all known manufacturers and models

2.6.6. Filter Development

All filter design and development steps were carried out on the Solidworks 3D CAD package (Dassault Systèmes, Vélizy-Villacoublay Cedex – France) in conjunction with rapid prototyping facilities such as the HPC Laserscript laser cutter and the Stratasys UPrint SE Plus.

For assistance with transfer to manufacture, external injection moulding companies were contacted and vetted. Firstpress Plastic Moulders and Colour UK were selected as the development partners. The design ethos centred primarily on development of a filter matching the ideal fluorescein spectrum packaged in a body that would be easy to use with existing slit lamps and be of low cost to manufacture in large quantities.

When developing a colourant formula for injection moulding, two forms of additives are available: pigments and dyes. Pigment additives will sit between particles of plastic as it is injected into the mould. Higher concentrations lead to higher opacity which in turn lowers transmission. Alternatively, dyes will mix with the plastic polymers during injection with higher concentrations not significantly affecting transmissivity, allowing for a greater range of formulas to work with.

Various blue samples swaths were produced and shown in figure 2.17. There were three parameters that could be changed to each sample: 1) dye formula; 2) dye concentration and; 3) material thickness. Spectrum signatures of the samples are graphed in figure 2.18. Through an iterative process, the formula and performance of the filters was established and progressively tuned over a 12 month period to achieve as close a transmission profile as ideal fluorescein.

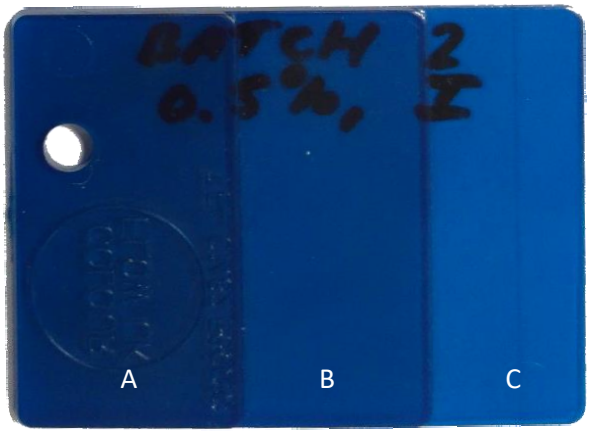

Figure 2-17: Blue colour sample. Three thicknesses available to measure from single sample- A, B & C = 3, 2 & 1 mm respectively

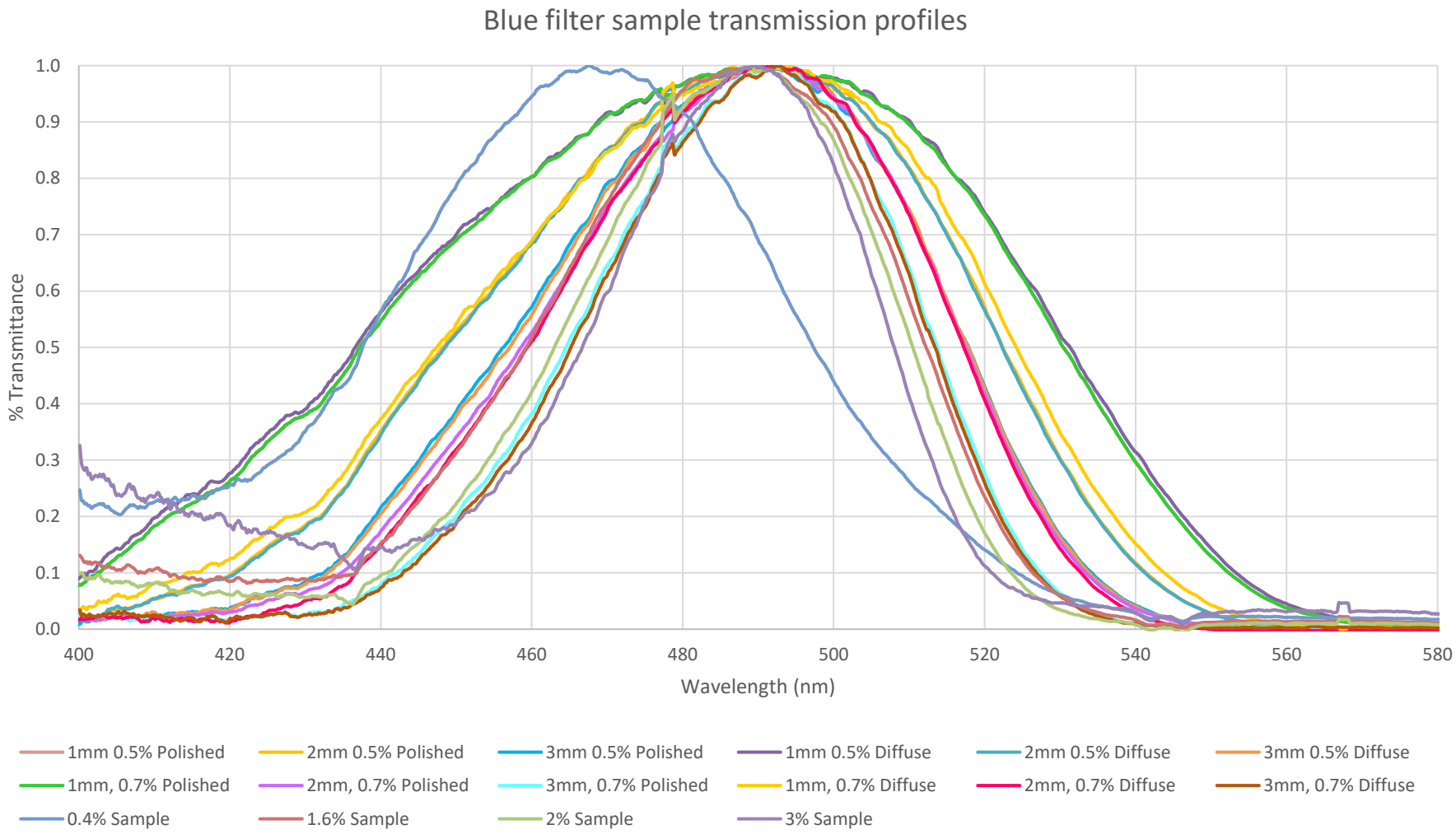

Figure 2-18: Absolute Transmittance of Blue Filter Samples

The testing of each colour swath was performed on the Ocean Optics 3000 spectrometer by placing the filter in-between the light source and probe while held in position using OBE. For Halogen testing, an Ocean Optics DH- 2000 (*Ocean Optics, Dunedin, Florida, US*) light source was used, whereas for the LED a custom build testing rig was constructed which housed a 3500k LED SMD module selected as it was the closest match to the apparent market leading Topcon SL-D7.

At the same time that colour formula was being created, the designs of the filter body were also being developed. A total of 13 design iterations were necessary to arrive at the final solution of which are shown in figure 2.19. The mounting ring and lens are a single injected unibody design with a polished finish on the lens as opposed to a sandblasted finish on the body and perimeter to minimise stray light leakage. Both Aston University and Thea company logos are recessed with polished finish to highlight them under illumination.

As the diffuse white filters only serve to evenly disperse the total white light without attenuation of certain wavelengths, it will be possible to use a single filter interchangeably between both Halogen and LED powered slit lamps. Fluorescein blue filters are however significantly affected by the different light sources due to the variation in source spectrum and therefore each filter will have small indicators which differentiate the Halogen from LED filter versions. To achieve best results, filters should only be used with labelled light sources.

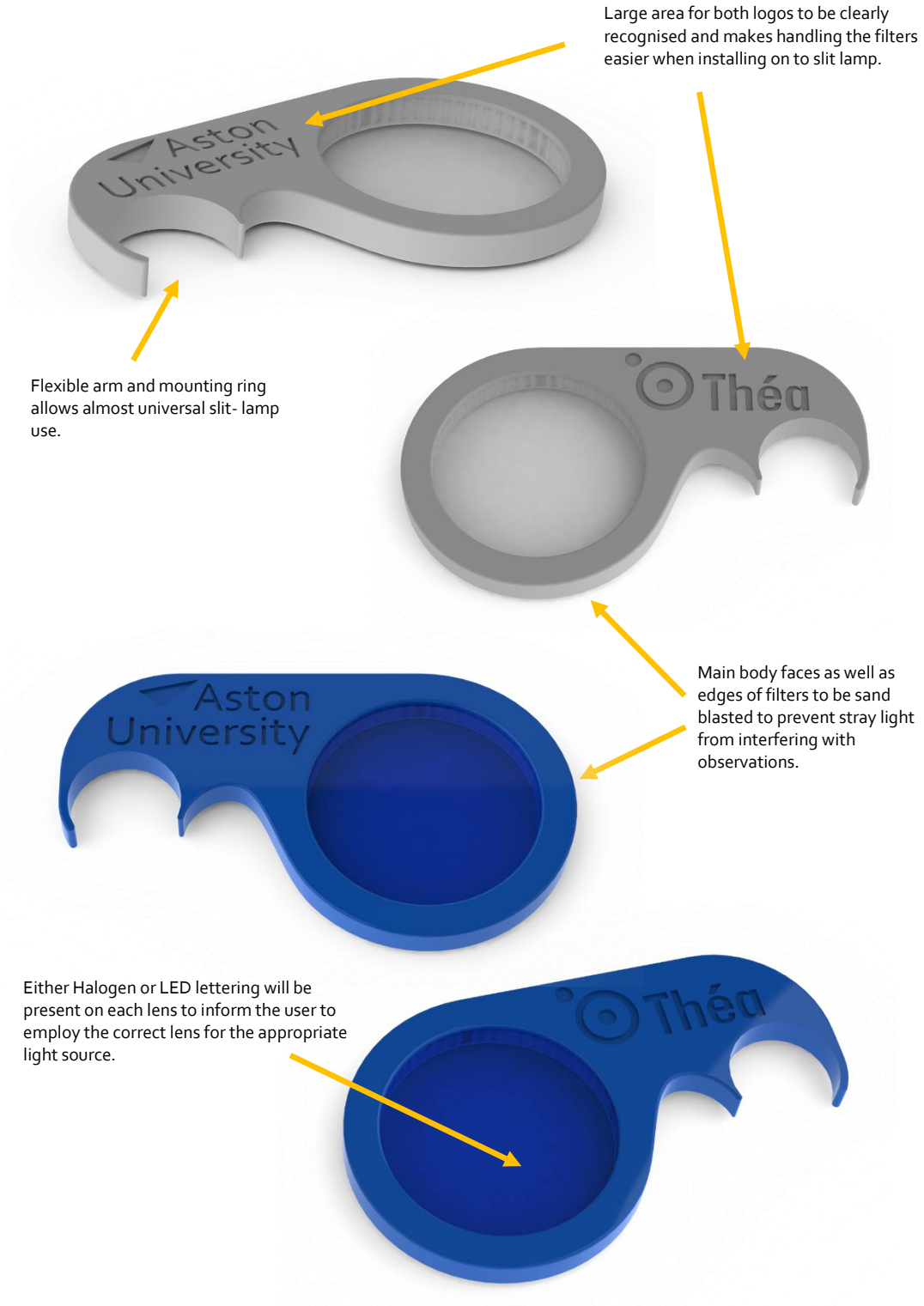

Figure 2-19: Computer renders of final blue fluorescein and white diffuse filter designs

2.6.7. Mounting Instructions

Both the Fluorescein blue and white diffuse filters are designed to fit on as wide a range of slit lamp models as possible. The uprights to the left and right of the mirror assembly have been selected as they are found almost universally between upright Haag Streit slit lamp types (figure 2.20a). With a simple clip on action, the filters can be attached and turned into position (figure 2.20b) as required and allow for high performance, hands– free fluorescein or general anterior eye viewing which greatly assists with the inspection of the eye and the identification of previously hidden details.

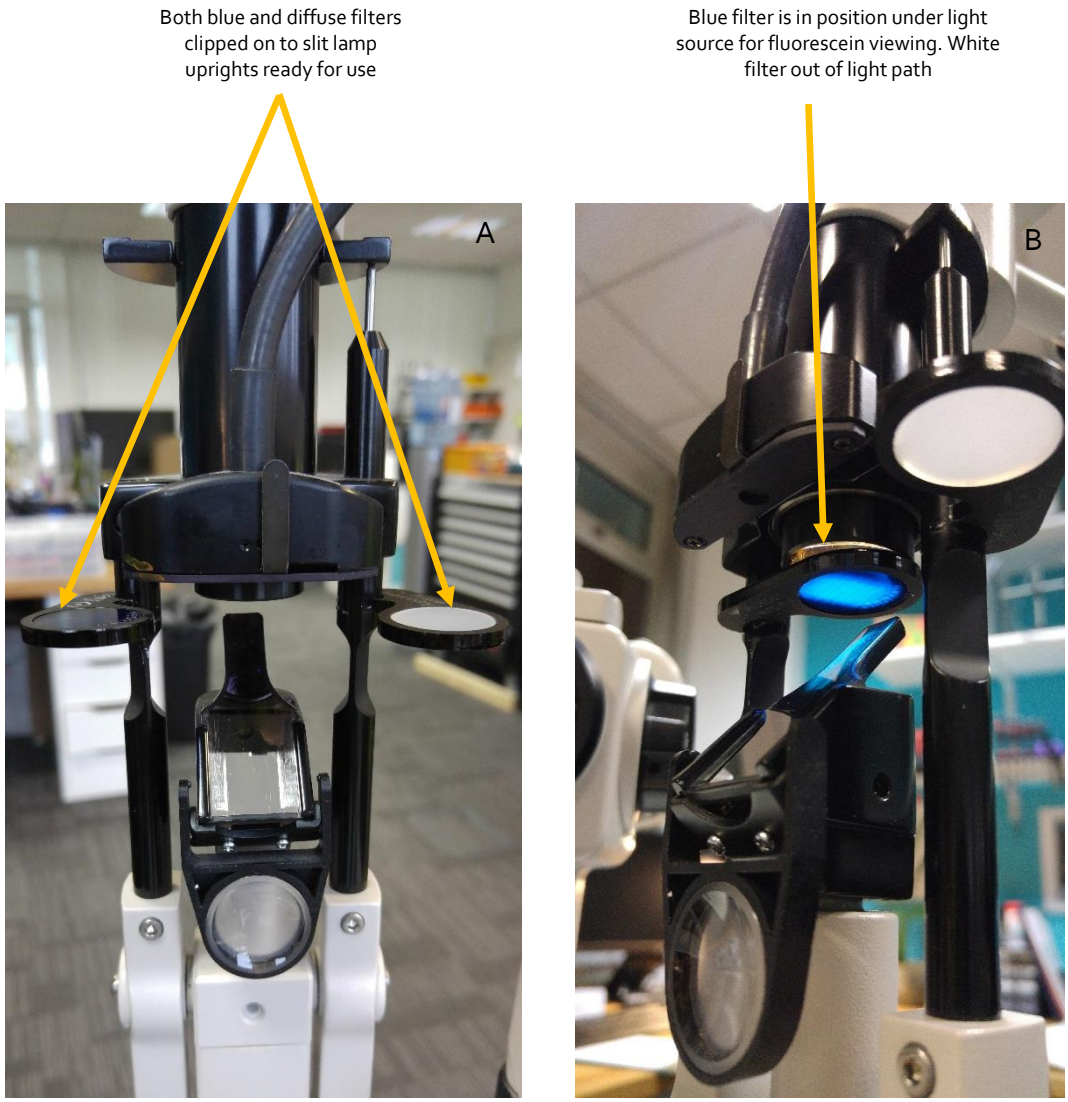

Figure 2-20: Custom developed blue and white filters in position on Topcon SL-D7 Slit Lamp. (A) shows how filters can be clipped on to the upright and moved out of the light path during general observation. (B) shows the blue filter in the path of the light source when fluorescein excitation is necessary

2.6.8. Results

It is not uncommon to find traditional halogen slit lamps being used alongside modern LED equivalents and although both instruments work well when general anterior eye observation is being conducted with the relatively simple white diffuse filter, performance significantly deviates when coloured filters are inserted into the light path. This is essentially due to the way white light is produced by the respective bulbs and is significant enough that a blue filter which shows strong performance under a halogen light source may not work so well under an LED alternative.

Table 2.4 is a full comparison of all slit lamp fluorescein filter spectrums available at Aston University with the custom developed filters included at the bottom of each light source type. The least squares method was used to calculate areas under the graph and compare with overlap of ideal fluorescein excitation. There is clearly a large discrepancy between different slit lamps with fluorescein spectrum overlap being surprisingly low under several models.

With a central wavelength of 485 nm and 64.1% of light transmitted within the ideal fluorescein spectrum, the best performing slit lamp is the Takagi SN- 70. The Keeler Symphony 40H was the best in the LED category. It was intended to compare best performing slit lamps of each type to the newly developed filters, however due to the Takagi no longer being available for use, the Topcon SL-D7 was selected as the nearest alternative.

Table 2-4: Comparison of halogen, LED and custom blue fluorescein filter spectrum and transmission performance properties

Light Source Type	Slit Lamp Model	Central Wavelength (nm)	Peak Transmission Wavelength (nm)	Transmission Percentage at Peak Transmission	Percentage of Blue Filter Spectrum Overlap in Ideal Fluorescein Spectrum	Overall Percentage of blue light transmitted within Ideal Fluorescein Excitation Spectrum
Halogen	CSO 990 5X	457	401	84.91	52.50	36.40
	Haag Streit 900	460	415	63.63	51.50	34.50
	Haag Streit 990BX	461	408	106.00	54.50	40.70
	Shin Nippon SL- 500	455	397	81.00	56.70	38.90
	Takagi SN- 70	485	420	111.00	64.30	64.10
	Topcon SL- D7	464	429	71.00	70.40	42.60
	Topcon SL7F	460	408	73.00	65.00	41.00
	Custom Blue CB6002	478	471	36.00	93.00	49.30
LED	CSO SL9000	457	430	54.00	32.20	23.76
	Keeler Symphony 40H	439	444	105.00	33.80	49.40
	Topcon SL-D701	453	427	76.00	34.70	43.28
	Custom Blue led CF5814	473	487	21.71	97.90	29.20

Guide

Central Wavelength (nm) – midpoint wavelength of the total allowable transmission spectrum

Peak Transmission Wavelength (nm) – wavelength at which maximum amount of light energy is allowed to pass through the filter.

Transmission Percentage at Peak Transmission- maximum amount of light energy compared with unfiltered light source allowed to pass through filter at peak transmission wavelength.

Percentage of Blue Filter Spectrum Overlap in Ideal Fluorescein Spectrum – amount of blue filter spectrum coverage within the excitable wavelength range of fluorescein

Overall Percentage of blue light transmitted within Ideal Fluorescein Excitation Spectrum – total amount of transmitted energy within ideal Fluorescein spectrum

2.6.9. Custom Halogen Fluorescein Filter

Halogen light sources generally exhibit a continuous rising profile of light from the blue to the red end of the spectrum. Figure 2.14 shows the performance of the custom Halogen filter compared with existing glass filters found in common slit lamps. Spectrum of the custom filter peaks at 480nm, whereas ideal fluorescence is achieved at 495 nm.

Using least squares method to calculate areas under graphs 2.22 and 2.23 and compiling in to table 2.4, the custom blue halogen filter (highlighted in blue) attains a 93% coverage of the ideal fluorescein spectrum but due to the wall thickness of 3mm, achieves only a 36% overall transmittance value. Light is greatly attenuated as it passes through the thick filter medium. A reduction in filter wall thickness was attempted as a way of improving transmissivity. However, a bleeding effect was noticed and greater amounts of white light were able to pass through the filter lens. Correspondingly, fluorescence levels seemed to decrease dramatically. To overcome this deficiency of lower transmissivity, the clinician will need to increase slit lamp brightness values which during testing allowed for good viewing capabilities.

Takagi SN-70 is the best performing slit lamp tested. Over 64% of filtered light falls within the ideal fluorescein excitation spectrum and allows for best viewing results from the available models. During testing however, the Takagi was not available and instead the Topcon SL-D7 was used. Figure 2.21 shows images of Topcon filters compared directly with the custom created blue filter captured by external camera. Camera exposure and slit lamp brightness was fixed for all tests. Images A and B show the pure blue filters side by side and a significant difference is visible. The Topcon, with a central wavelength of 464 nm is a darker and more intense violet blue, whereas the custom filter is much lighter and mellow colour. This is to be expected as lower wavelengths will produce colours closer to an ultra violet colour. Images C and D are taken under the same brightness conditions, but this time with fluorescein dye instillation. Image D which uses the custom filter emanates a brighter green glow and regions of tear film breakup are visible- even without the yellow filter being employed. Images E and F are taken with the onboard Topcon yellow emission filter placed in the return light channel and mimics typical real world fluorescein testing practices. Onboard Topcon blue and yellow filters in image E produce a clear fluorescence over the full ocular surface with the brown iris appearing cloudy again the green foreground. Image F, taken with the custom blue filter in combination with the Topcon yellow does produce stronger fluorescence and a clearer Iris definition. An incomplete blink can be identified through the faint black line apparent slightly below the central horizontal plane of the pupil.

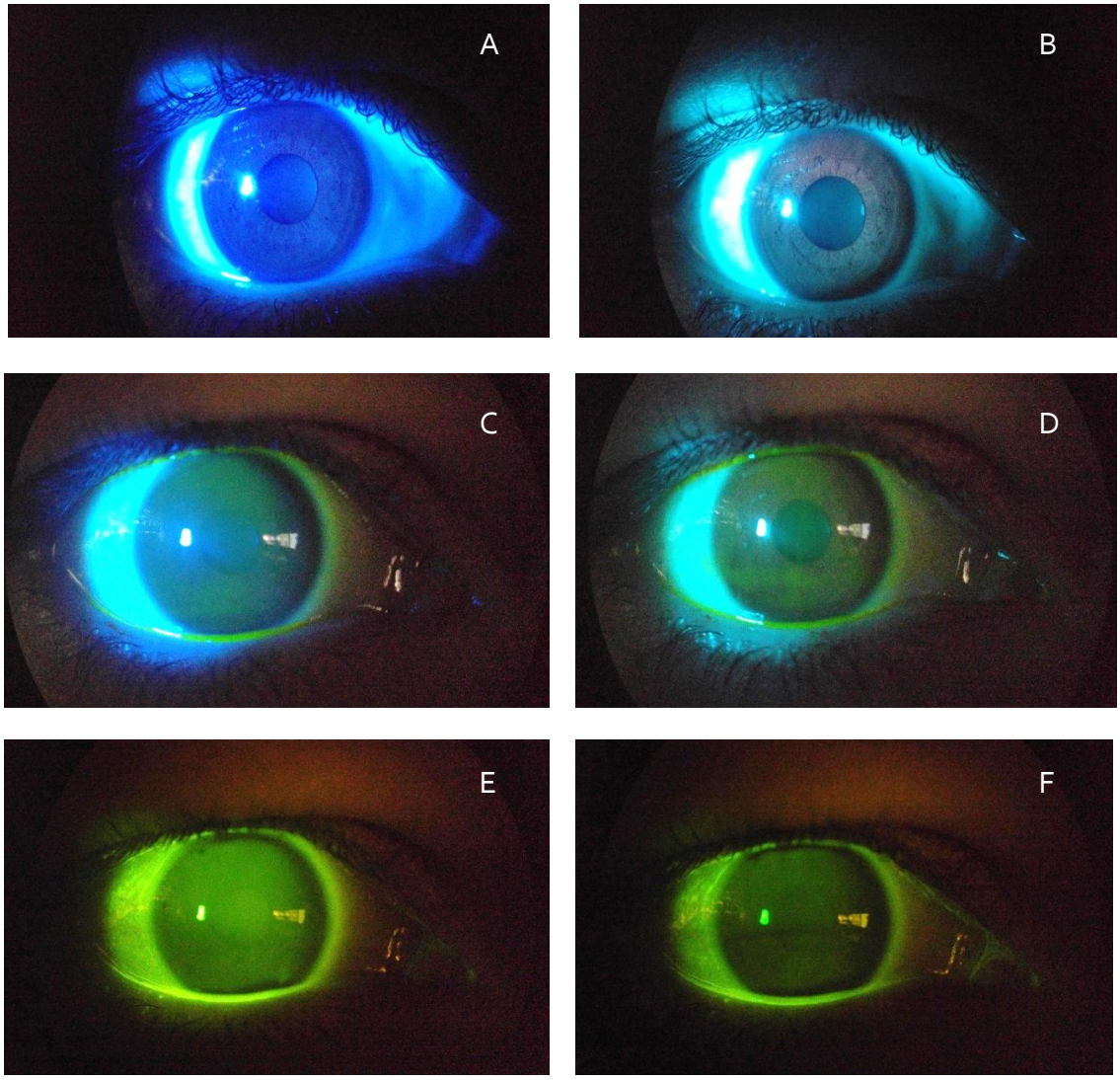

Figure 2-21: Comparison of filter performance - Topcon SL- D7 Slit Lamp test with various filter combinations. A) Topcon blue filter only B) Custom blue filter only c) Topcon blue filter with fluorescein instilled D) Custom blue filter with Fluorescein instilled E) Topcon blue filter with onboard Topcon yellow filter & Fluorescein F) Custom blue filter with onboard Topcon yellow filter & Fluorescein (Regions of TF breakup are also visible but may not be apparent in the printed images).

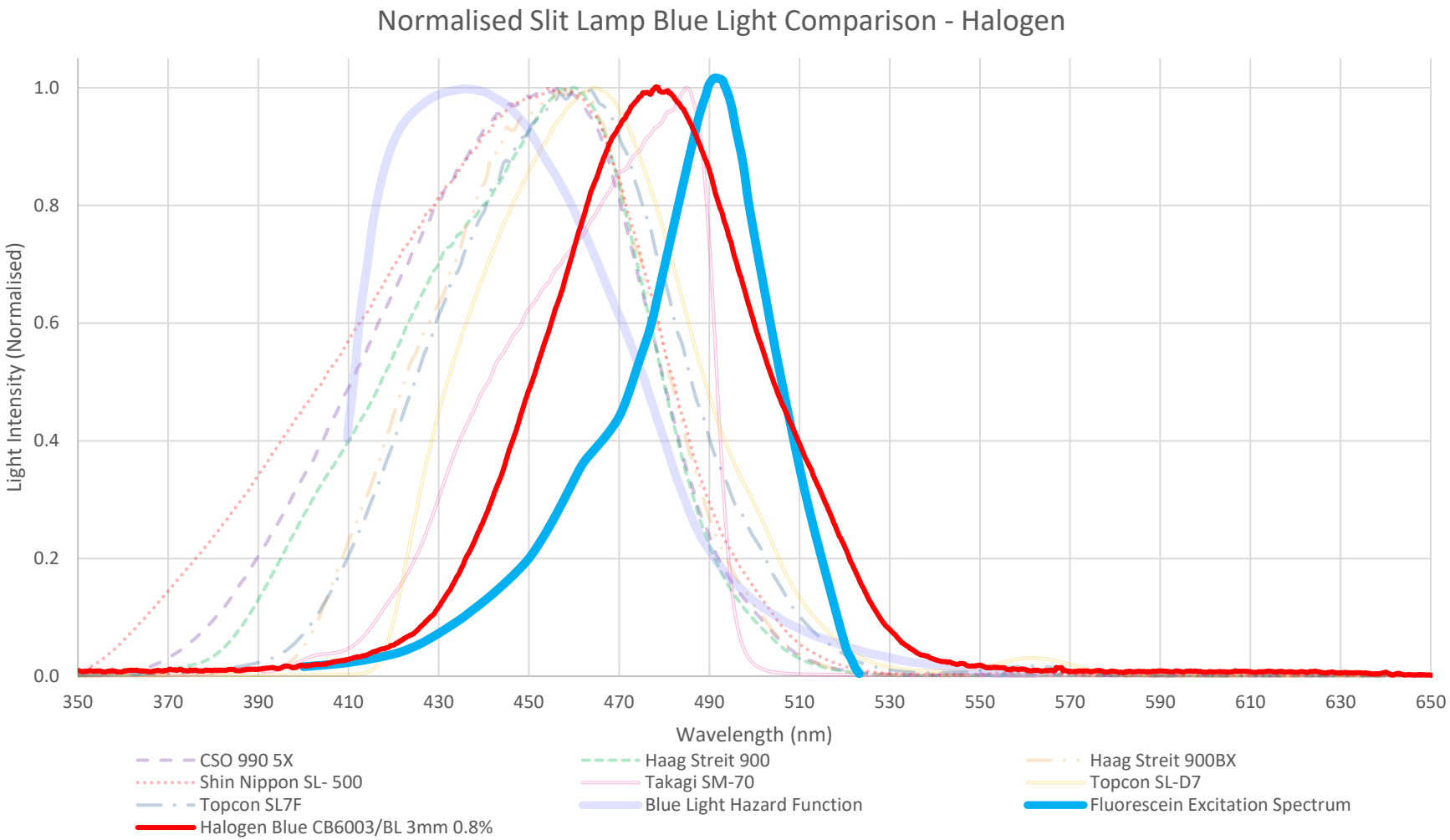

Figure 2-22: Custom 3 mm Fluorescein filter spectrum comparison to ideal fluorescein and commercial slit lamp models

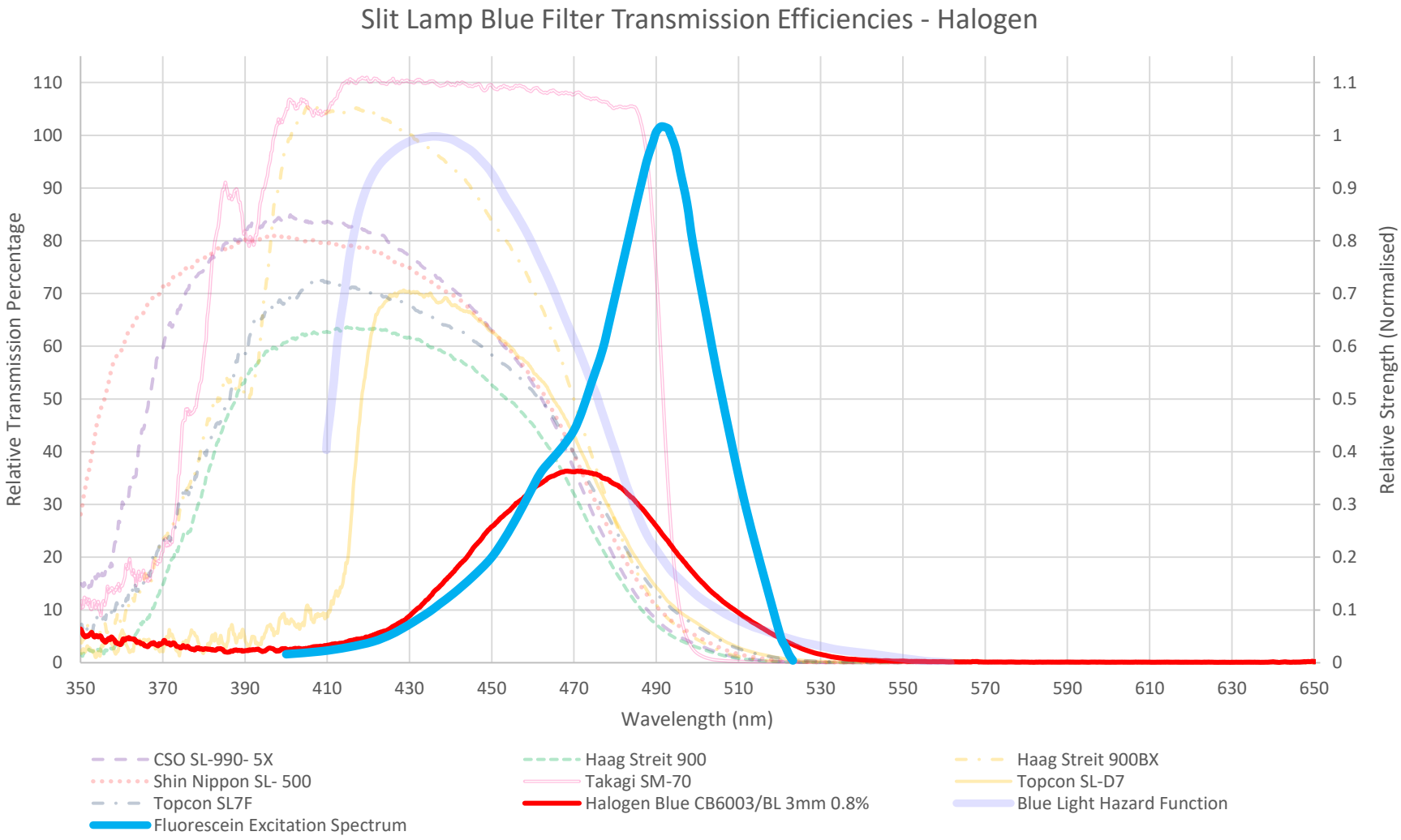

Figure 2-23: Custom 3 mm Halogen Fluorescein filter transmission performance compared with commercial slit lamps

2.6.10. Custom LED Fluorescein Filter

The LED spectrum posed more of a challenge as the raw trace of LED light output has a large peak at the 450 nm range, a dip in the important 490 nm region and then picks up again after 510 nm. Instrument manufactures such as Topcon, which is regarded to have the industry leading advanced LED blue/ yellow filter combination, overcome these energy deficiencies by tuning the blue excitation filters to a central wavelength nearer to 450 nm, directly where the first peak emission of the LED light source is registered and thereby compensate for the loss of light energy at 490 nm (figure 2.9). Negative consequences to this however, is that the emitted spectrum is closer to the blue light hazard region and may cause health issues over repeated long periods of exposure.

In attempts to harvest maximum light energy, the custom LED colour formula was designed to work at two peaks – the LED 450 nm peak and the fluorescein 490 nm peak. Although there is less energy at 490 nm, the filter can take advantage of light from a larger area of the spectrum and gives very strong fluorescence performance compared to the more expensive glass filters found in commercial slit lamps.

Compared with ideal fluorescein peak of 495nm, the custom blue filter testing resulted in a central wavelength of 473 nm with a remarkable 97.9% coverage of the ideal Fluorescein spectrum- figure 2.25. Absolute filter performance is again severely handicapped by the low filter transmission properties with a value of only 29.2% within the fluorescein region. Peak transmission occurs at 487 nm, but only has a 21.7 % efficiency at this wavelength- figure 2.26.

From the list of commercial slit lamps, the best performing instrument from the available LED slit lamp models is the Keeler Symphony 40H, achieving a shorter peak wavelength of 444 nm but a superior 49.4 % of light transmitted over the ideal fluorescein band. The Keeler 40H is the only slit lamp tested which demonstrated a two peak blue filter spectrum, allowing a greater amount of white light to be used in fluorescein excitation. Custom LED Filter testing proceeded with the LED Keeler Symphony 40H with all images in figure 2.24 captured by means of the onboard camera supplied with the slit lamp instrument. During testing it was apparent that unlike the halogen cousins, custom LED blue filters produced considerably darker images compared to the Keeler competition. Again, material thickness and dye concentration are the main culprits behind this.

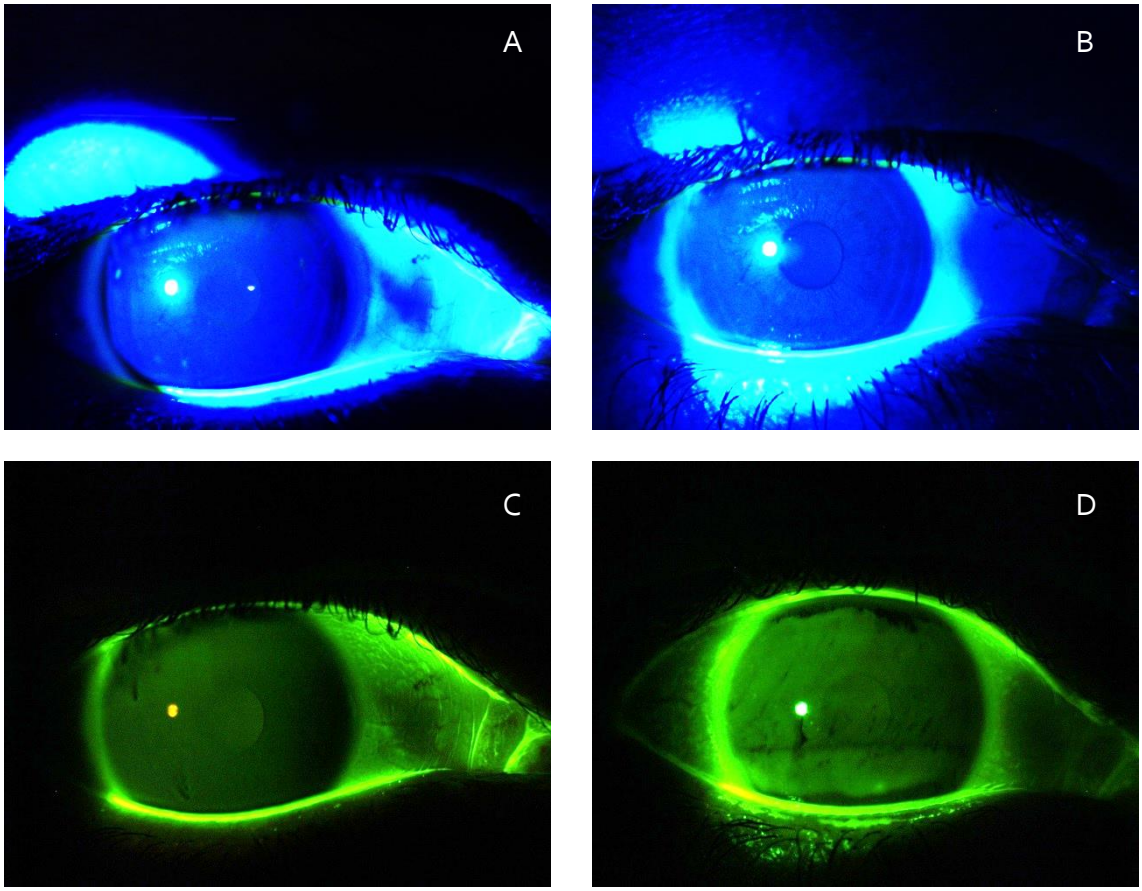

Figure 2-24: Blue filter performance comparison- Fluorescein instilled in to patient eyes and imaged using Keeler 40H LED slit lamp with onboard camera. (A) Keeler slit lamp onboard blue filter. (B) Custom Blue LED filter, slit lamp brightness increased. (C) Keeler Blue filter in combination with onboard Keeler yellow filter. (D) Best image captured of custom blue filter in combination with onboard Keeler yellow filter. NOTE: Both C & D have been colour boosted equally to help with printed viewing.

Fluorescein imaging through the custom filter can be seen in Figure 2.24d. Dark regions on the cornea signify tear film break up and contrast level are very high making identification of such regions relatively easy. Although the custom filter did produce good fluorescence, slit lamp brightness was turned up to maximum to be bright enough for viewing. The author believes that slit lamp images were generally darker with custom filter and fluorescence effect tended to weaken quicker under custom filter viewing. An important issue to discuss is the poor quality of the onboard slit lamp camera to capture images. When regular white illumination is used, the onboard camera is able to capture high quality images. However, in cases of low light such as those experienced during fluorescein observation, the light being captured becomes disturbed and attenuated slightly by the onboard Bayer filter located in front of the CMOS ship found in colour cameras. A by-product of this is a misrepresentation of real world viewing results and a reduced image contrast. Fluorescein viewing is therefore superior looking though the slit lamp binocular scope compared with on screen digital capture.

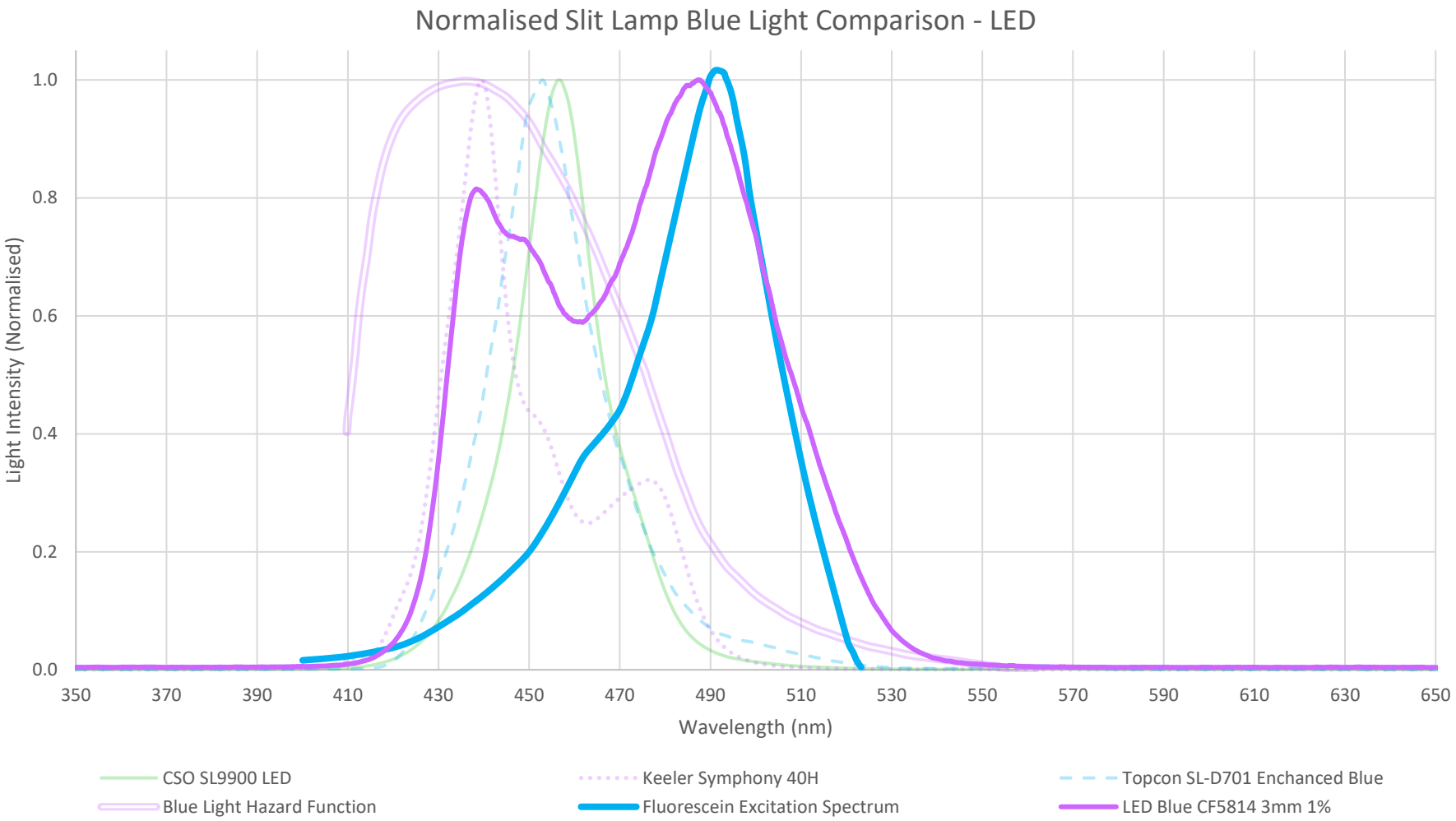

Figure 2-25: Custom 3 mm Fluorescein filter spectrum comparison to ideal fluorescein and commercial slit lamp models

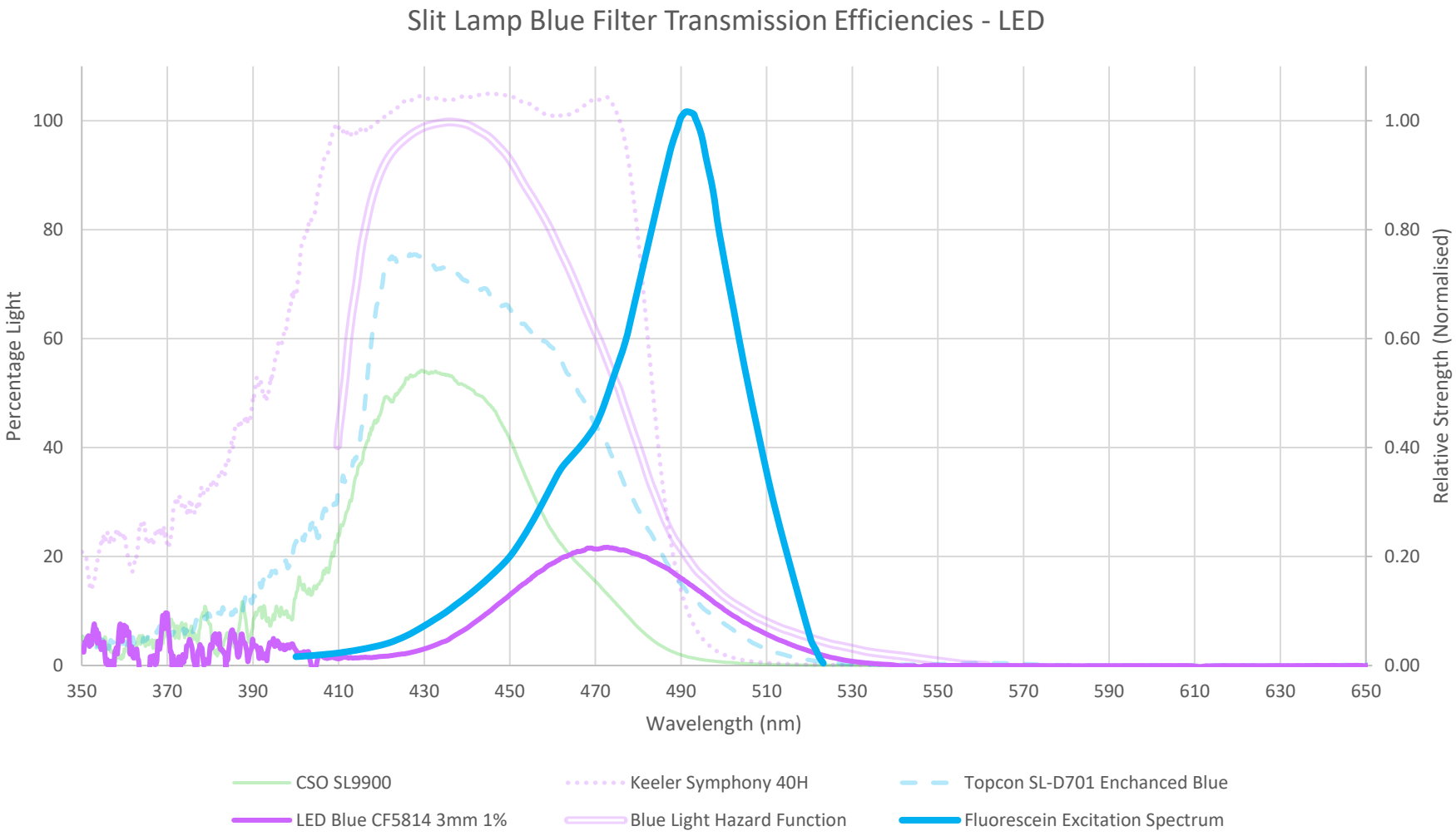

Figure 2-26: Custom 3 mm LED Fluorescein filter transmission performance compared with commercial slit lamps

2.7. Yellow Emission Filter

Once fluorescein has been instilled into the eye and a blue light source of appropriate wavelength is shone onto the surface, fluorescence will become apparent. Viewing of the eye under these conditions is possible, but the introduction of a simple yellow barrier filter which matches with the spectral emission signature of fluorescein as illustrated in figure 2.3, allows for more insightful observation due to better contrast of areas of damage such as tear breakup, punctate staining, or corneal abrasions- such regions appear as green against a dark background where fluorescein begins to pool.

Fluorescein breakup time is not only a key diagnostic test that has been identified by the TFOS DEWS II workshop as a key global metric for the identification of the presence of dry eye [36]; it is also seen by many clinicians as one of the preferred tests for doing so [122]. When asking a patient to hold their eyes open for as long as possible, the tear film begins to break down after some time by thinning and evaporation, causing localised regions of increased fluorescein concentration leading to the self-quenching effect and a lowering in fluorescence levels. These areas appearing dark under observation [173, 251]. Figure 2.4 is an example of tear breakup.

Whereas pure blue light may be used to identify regions of fluorescein pooling in cases of corneal scratches, it does not allow for easy tear film break up observation. A yellow barrier filter does and with that comes the need to develop a highly tuned filter to match fluorescein emission. Unlike the excitation filters which were dependent on light source type, the yellow emission filter is responsible for the blocking of reflected light from the patient eye and should therefore be immune to differing light sources.

2.7.1. Existing Yellow Filter Spectrum Data

Yellow emission filters are installed into slit lamps as part of an optional upgrade at the time of purchase and not all, especially older examples, are equipped with this additional hardware.

Ordinarily, the yellow barrier filter is found within the main body of the slit lamp and is able to influence light collected from the objective lens before it passes to the binocular view finder. As the filters are buried within the instrument itself, it has not been possible to make direct measurements of filter characteristics without disassembling the apparatus- something that was not feasible. In work by Peterson et al. the yellow filters of a Takagi SM-70 and Haag Streit slit lamps were directly measured and steep emittance curves, peaking between 525 and 550 nm and with transmission value above 90% were measured [173], thus providing a useful indication of performance required by the custom filters.

Slit lamps that are missing the inbuilt filters lack important fluorescein viewing abilities and a work around has been developed by the use of hand-held thin film filters that are to be kept in position by clinicians during observation, see figure 2.5. Theoretically, there exist many commercially available alternative thin film filters which may have better fluorescein barrier properties than the two mentioned above. A sample booklet from a renowned coloured film manufacturer called Lee Filters (*Hampshire, United Kingdom*) was acquired and filters of desired characteristics were tested to provide a starting point.

As before, the Ocean Optics Maya 3000 Pro Spectrometer (*Ocean Optics, Dunedin, Florida, US*) was used for the collection of all spectral data on all yellow thin film filters. To maintain uniformity across tests, a custom rig was built using Thor Labs Optical Bench equipment (*Thor Labs, Newton, New Jersey, USA*) which held the filter in place during data collection. The DH-2000 (*Ocean Optics, Dunedin, Florida, US*) Halogen light source was selected as a constant light source across all filter specimens. Spectrometer settings remained constant across tests: Integration time set to 0.325 seconds, 2 scans to average, Box Car width = 3, Electric Dark Correction and Non- Linearity Correction = True. Dark field measurements were taken and subtracted from the light signal in an effort to remove any stray light radiation during measurement.

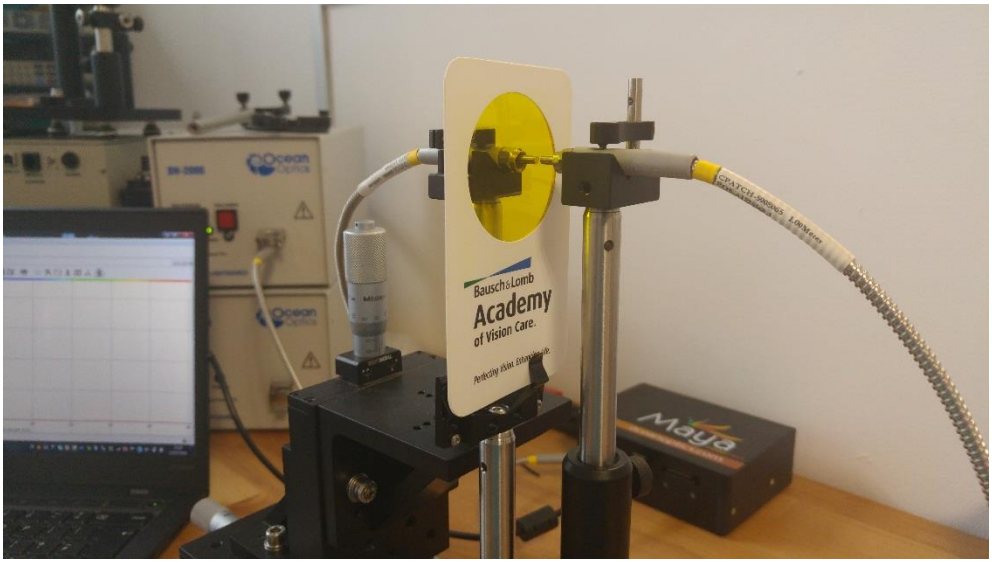

Figure 2-27: Data collection of thin film filter performance.
Each filter held in position with Thor Labs optical bench equipment.

2.7.2. Thin Film Spectrum Results

A total of nine thin film filters were tested, with all results shown in figure 2.28 below. Mean thickness of samples was 0.1 mm, giving rise to transmissivity values of 80% or greater- figure 2.29.

The Bausch and Lomb (B&L) filter revealed a steep rising gradient in the 480 nm region and good coverage of fluorescein emission while the competing Johnson & Johnson filter produced a gentler profile rising from the 480 nm region and increasing steepness post-525 nm which does not overlap with fluorescein emission particularly well. It does however follow the profile of Lee Filter 015 (Deep Straw) almost identically and there is a very large likelihood that both are one and the same. A similar claim can be made for the B&L filter which closely followed the Lee 101 yellow filter. Results shown in figure 2.28.

Two green filters, 139 Primary Green and 738 Jas Green were selected as part of this test regiment and surprisingly produced closer emission spectra to ideal fluorescein than many of the yellows. Lee 738 Jas Green was a close colour match with Lee 139 Primary Green providing an identical trace to fluorescein emission but shifted right by 20 nm. Transmissivity of Lee 139 was low at only 35% transmitted due to the nature of the darker colour which may compromise viewing.

Good information was deduced from this exercise that was used as a starting point to develop the custom yellow dye.

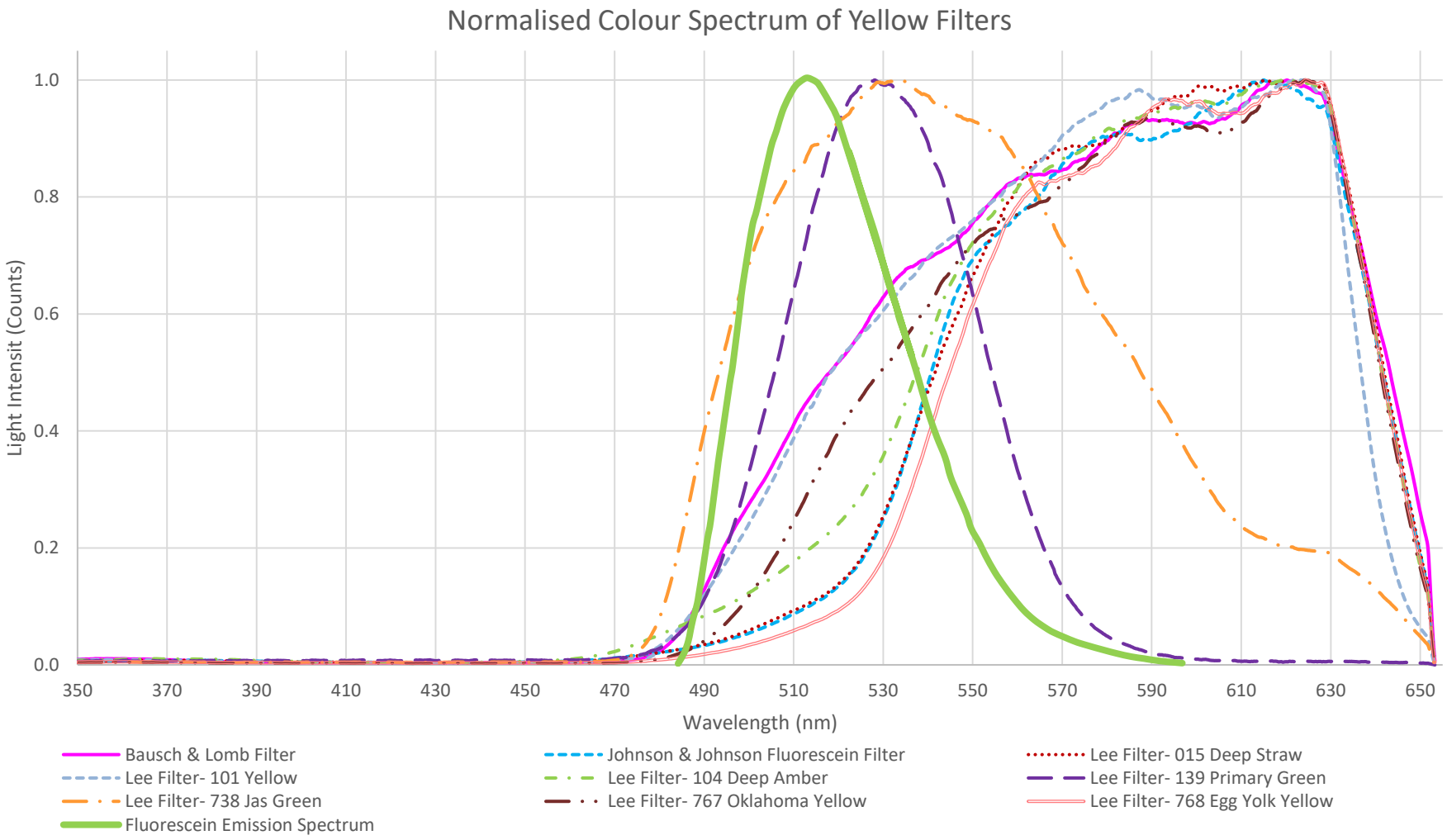

Figure 2-28: Yellow filter specimen colour spectrums

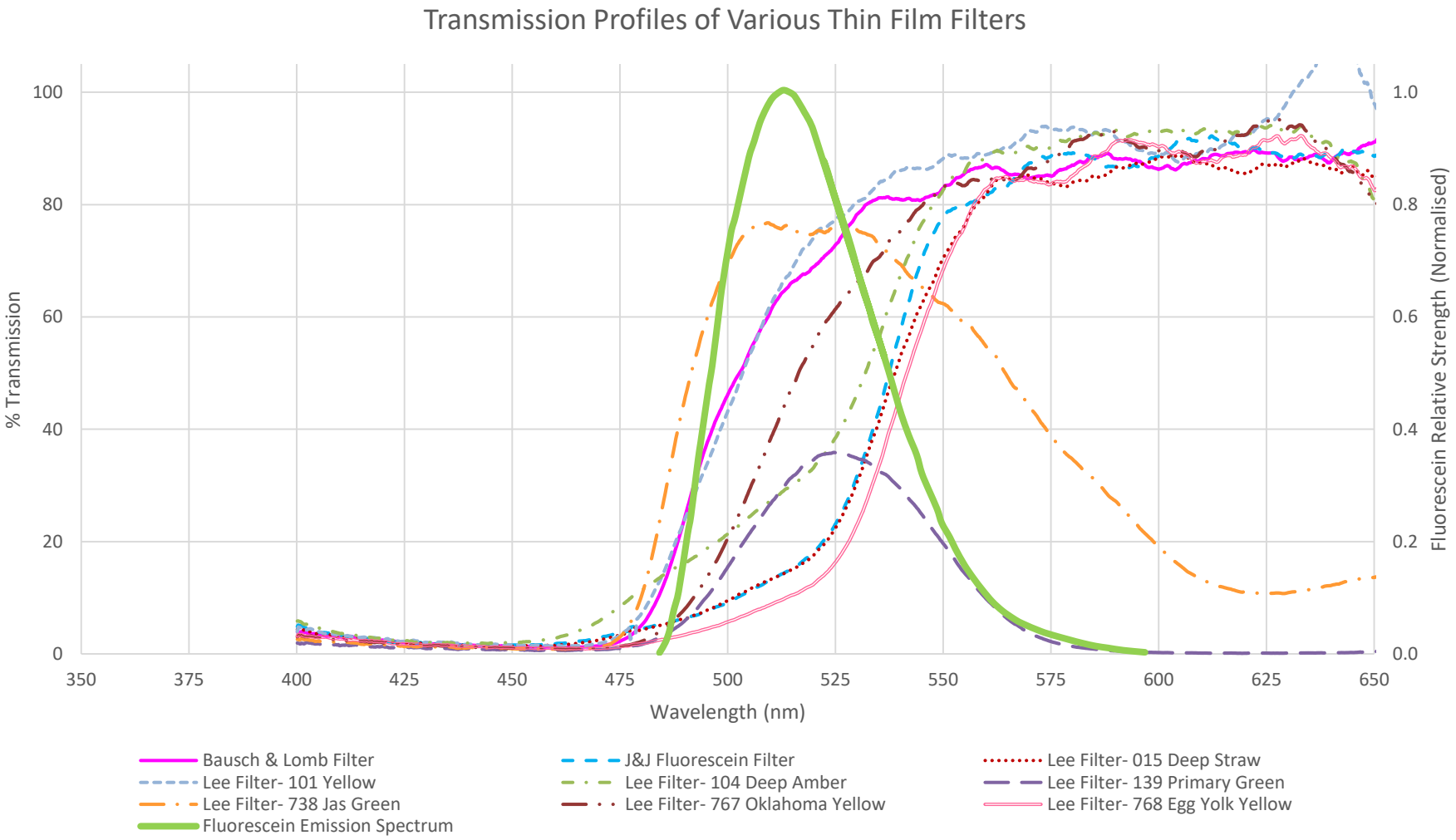

Figure 2-29: Thin Film transmission profiles of early selected specimens

2.7.3. Materials Selection

The emission filter must be placed in the viewing path to filter the reflected light from the patients' eye and therefore maximum optical quality is of prime importance. Referring to table 2.3, birefringence- a measure of distortion as light travels through a material, is an important aspect to consider. Demands are different to the blue excitation filter which focused on colour influence, rather than visual quality. Acrylic, with a much lower birefringence value and higher abbe number was selected.

2.7.4. Mechanical Sizing

Slit lamps with inbuilt fluorescein viewing capabilities typically house emission filters within the main body just behind the objective lens and are moved into position during dye testing by mechanical swing action. The position of the custom yellow filter is consequently restricted to being located in a similar location.

Available university slit lamps were measured by means of a Mitutoyo 500-196-20 Digimatic Vernier calliper (Takatsu-Ku, Kawasaki, Japan). Dimensions are shown in figure 2.30. Measurement results show that many slit lamps share objective lens profile and dimensions, which are similar across models/ manufacturers and range between 25 – 28 mm in diameter. The objective lens on CSO, Keller and Topcon slit lamps tend to protrude from the main body and allow removal for maintenance purposes. Haag Streit Bern slit lamps do not share this common design feature and instead have a chamfered, single piece body which tapers down to meet the objective lens, making any attachment difficult.

With the only alternative to mount the yellow filter being the binocular view finders, the decision was taken to develop around the objective lens but excluding Haag Streit slit lamps as their profiles will require a one off solution and not be compatible with the majority of slit lamps model available. It was considered a better solution to be compatible with a larger volume of available slit lamps rather than a wide range of slit lamp manufacturers.

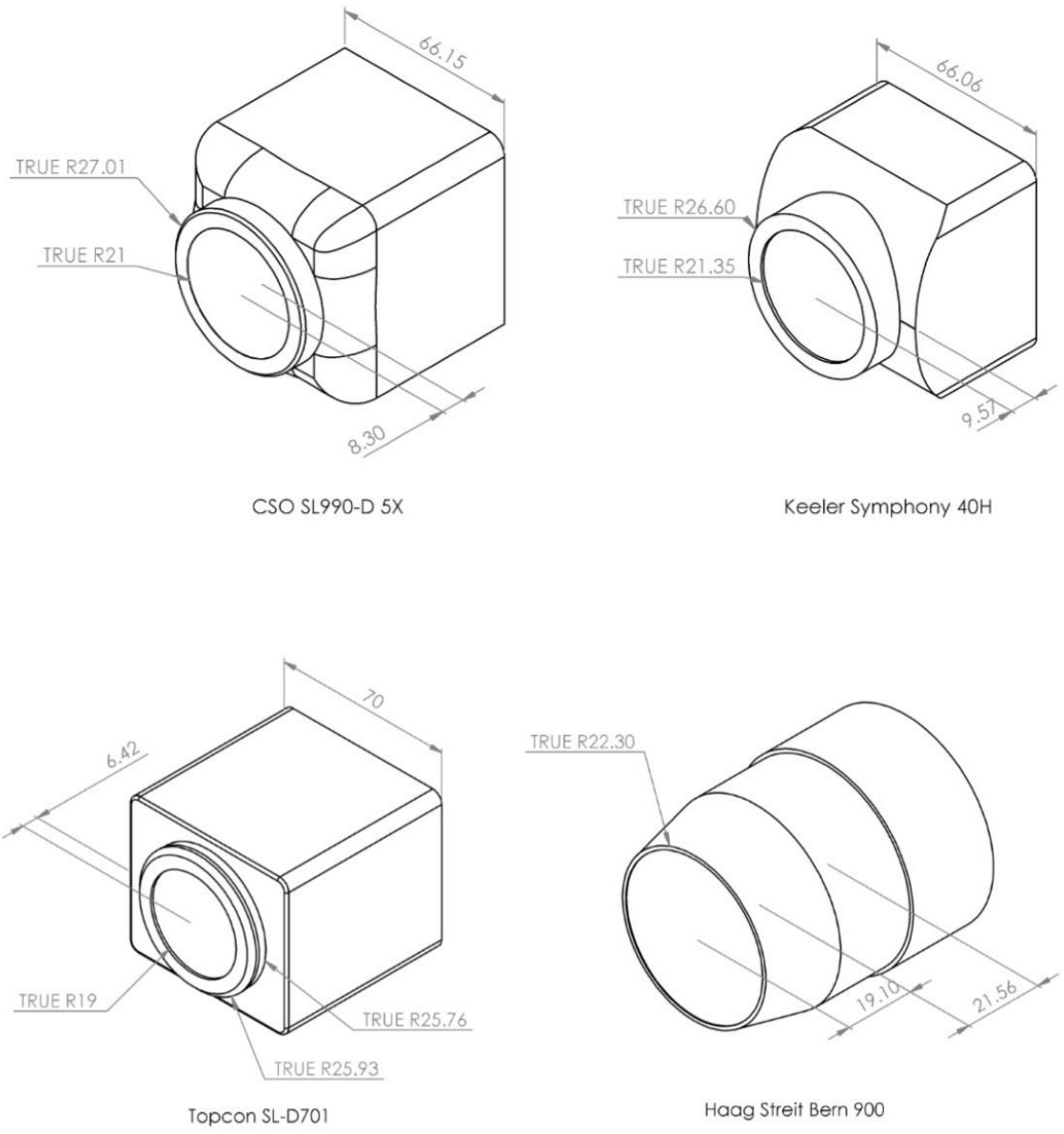

Figure 2-30: Objective lens profiles and physical dimensions of available slit lamps at Aston University

2.7.5. Emission Filter Development

As before, all filter design and development steps were carried out on the Solidworks 3D CAD package (Dassault Systèmes, Vélizy-Villacoublay Cedex – France) in partnership with Firstpress Plastic Moulders and Colour UK.

Optical clarity, hands free operation and fluorescein spectrum matching were considered main driving factors. Both Aston University and Bausch & Lomb logos must be present on the filer.

Thin film spectrum results were used to decide a starting point for dye mixing and 22 design concepts with 12 colour mixes were iterated over a one and a half year period. Spectrum testing was performed on the Ocean Optics 3000 Pro (*Ocean Optics, Dunedin, Florida, US*) in combination with the DH- 2000 light source and OBE.

Similar to blue filters, the yellow emission filter feature a single, one piece injection moulding body with institution logos located on front and rear faces. Small raised dimples were added to the front surface of the filter to help minimise lens contact with table surfaces and reduce the risk of scratching. To help maintain design consistency the body was sandblasted to the same finish as both blue and white diffuse filters. However, unlike fluorescein excitation filters which are strongly influenced by light source type, the emission filter is not susceptible to such issues and so a single version which works on both slit lamp light source types was created.

The yellow filter is designed to be clipped on to the front plane of the objective lens which was accomplished through the addition of flexible arms that straddle the slit lamp profile and keep the filter firmly in place. Manufacture of the aluminium mould commenced allowing acrylic prototype units to be created. Early units of the filter would fail due to poor elasticity of the material and the support arms which hold the filter to the objective lens were prone to snapping. Acrylic, although having excellent visual properties, proved too brittle for this application. Arm thickness was increased which made matters worse. It was decided to switch to polycarbonate which was able to solve this issue of flexibility but at the cost of added birefringence.

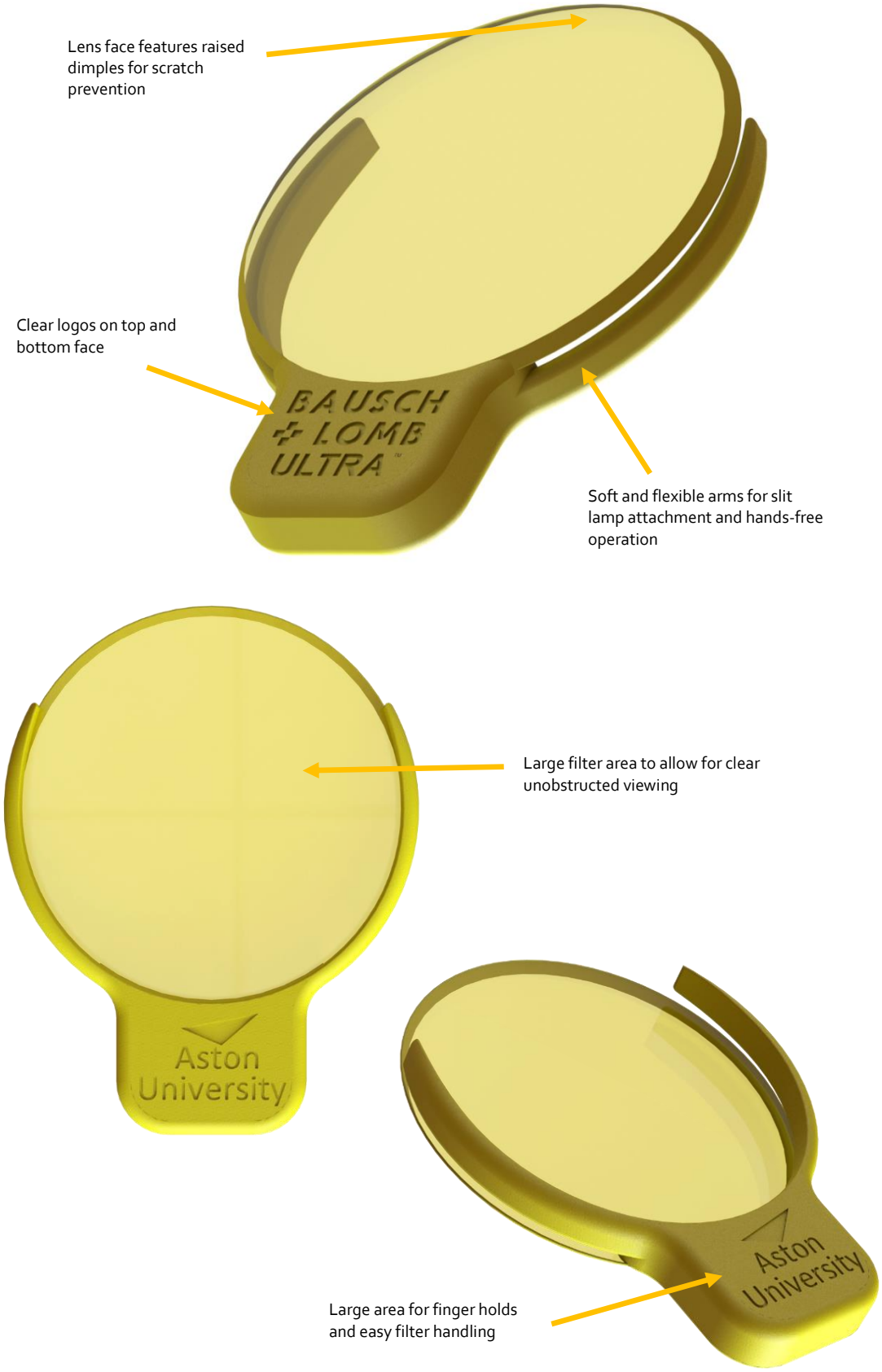

Figure 2-31: Renders of custom Fluorescein emission filters

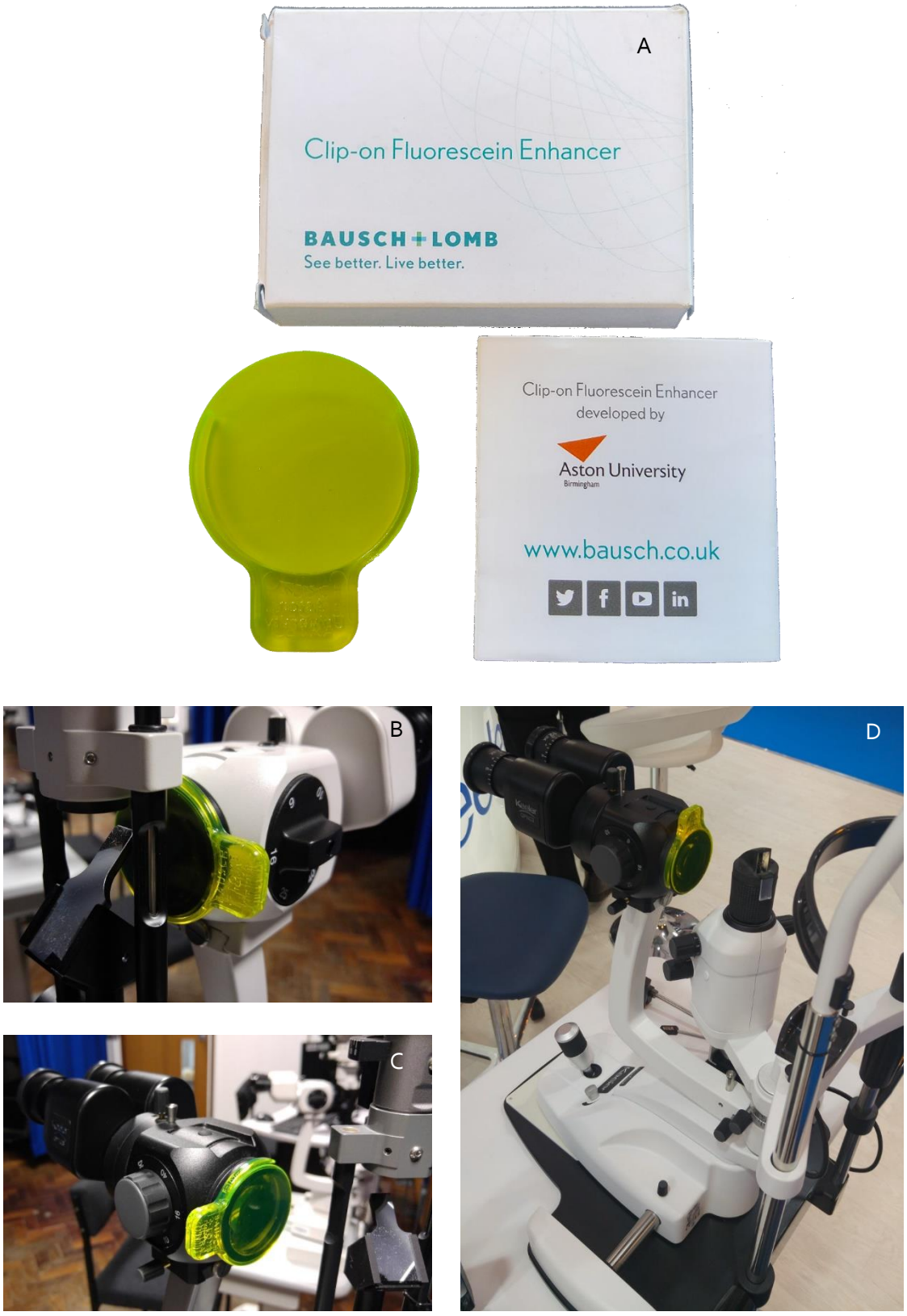

Figure 2-32: Yellow filter on slit lamps A) Custom filter complete Bausch & Lomb distribution kit including instruction booklet. B) Filter mounted to CSO CS9900 C) Filter mounted to Keeler Symphony 40H D) Filter mounted to Keeler Zeiss style slit lamp

2.7.6. Yellow Fluorescein Emission Filter Results

With the slit lamp light source not having a strong bearing on the performance of fluorescein emission, it was possible to create a single filter that could be used interchangeably between models. The attachment method is simple and the change from acrylic to polycarbonate material has allowed flexibility within the arms to fit many slit lamp models. The filter has been successfully fit tested on over ten slit lamp variants including Zeiss style slit lamps. Unfortunately, Haag Streit 900 models with cone shaped objective lenses proved too dissimilar to other models and therefore could not be currently accommodated but an adapter collar could be developed at a later stage to allow for use.

Filter performance is graphed in figures 2.34 & 2.35. As the glass filters of modern day instruments are embedded within the main body of slit lamps it is impossible to measure their specta. Spectrometry was conducted comparing handheld B&L and J&J thin film filters which act as replacements for slit lamps not fitted with onboard filters. The custom yellow filter shows a closer match to ideal fluorescein emission spectrum and a transmissivity of over 90% for the area covered by fluorescein than either of the two thin film filters available.

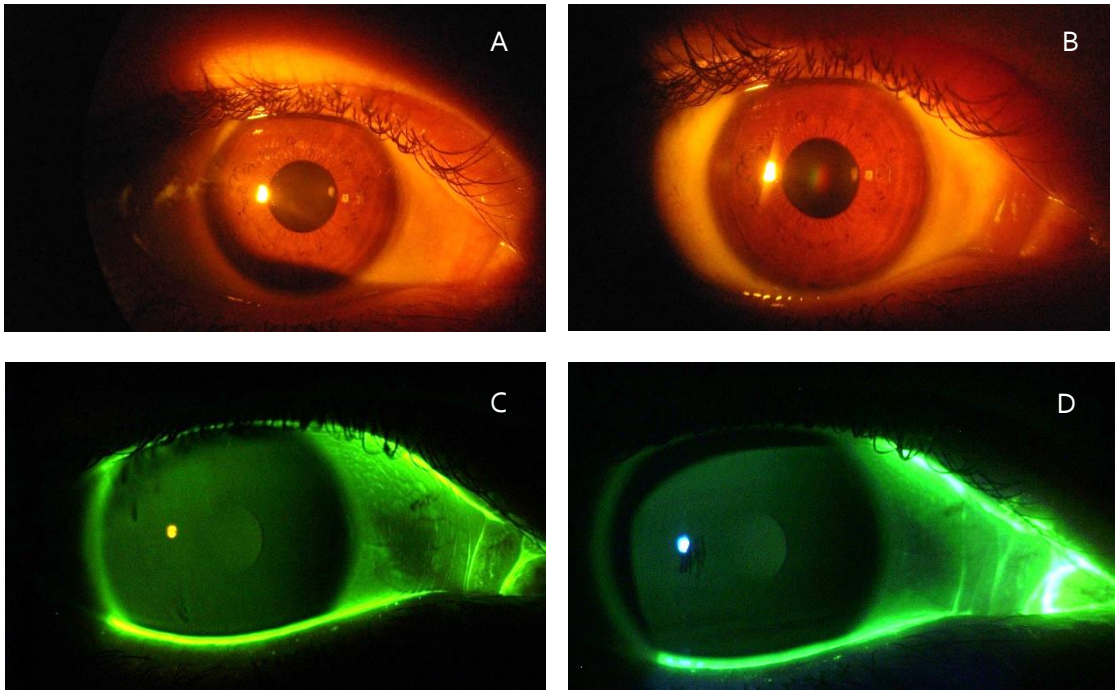

Figure 2-33: A) Topcon pure white light shone onto patients' eye with onboard Topcon yellow filter in return path B) Topcon pure white light source with custom yellow filter inserted in return path C) Topcon blue with Topcon yellow filter after fluorescein instillation D) Topcon blue with custom yellow after fluorescein instillation

Testing was conducted on the Topcon SL-D7 slit lamp. Unlike before, an external mobile phone camera (*LG G4, Seoul, South Korea*) was used to capture images with exposure and shutter speed fixed throughout all tests. Figure 2.33 shows examples of Topcon filters on the left compared with custom equivalents on the right. Images A and B are direct comparisons of yellow filter visual quality. Pure white light was used to illuminate the patients' eye without the addition of fluorescein. Although the image is bright and definition of iris features are clear, there is a greater amount of haze and distortion visible through the custom yellow filter. This is predominately due to the birefringence stresses introduced into the polycarbonate material upon rapid cooling after the injection moulding process causing molecular misalignment. Steps had been taken to control the temperature and injection speed which has greatly reduced the hazing effect, but only a material change would be able to fully overcome this.

Fluorescein was instilled into the patients' eye and the onboard Topcon blue filter was used as the excitation source. Image 2.33C is captured though the onboard Topcon yellow filter. A small region of early tear film breakup can be seen at the 7 and 10 o'clock positions with small dark regions appearing. Image 2.33D employs the custom yellow filter which produces a greater contrast image. High fluorescence regions such as the lower meniscus and lacrimal canaliculi give rise to brighter greens against a darker Iris. Early breakup regions are visible in the 9 o'clock position and overall performance of the custom yellow filter is very strong.

Figure 2-34: Custom yellow filter colour spectrum compared with existing thin film filters and ideal Fluorescein emission spectrum in green

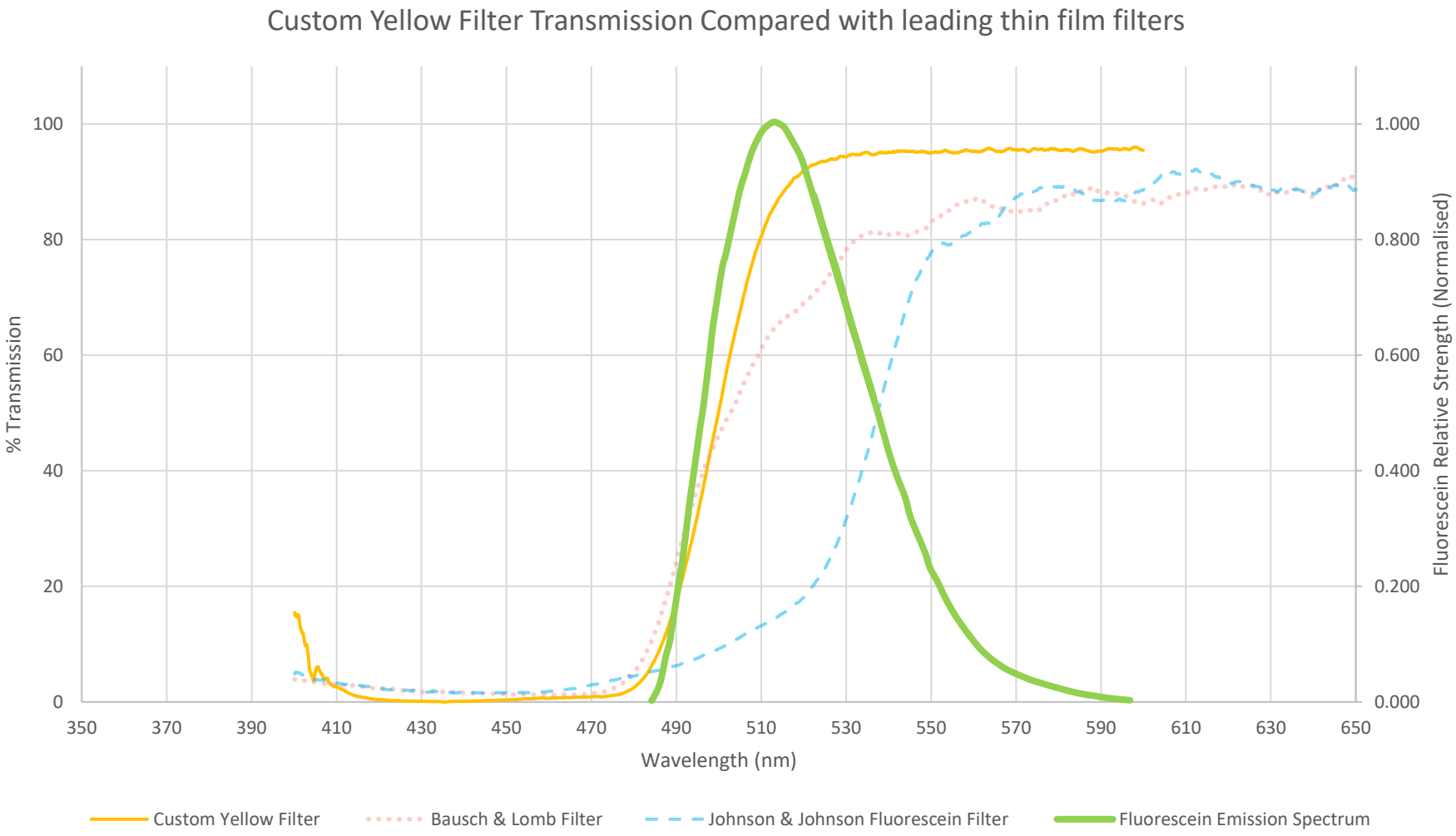

Figure 2-35: Custom yellow filter transmission comparison to existing thin film filters

2.8. Custom Blue and Custom Yellow Filters Testing

When custom blue and yellow filters were combined for fluorescein viewing results proved disappointing. Figure 2.36 shows that the ocular surface is illuminated uniformly with light, but unlike when in combination with onboard filters, fluorescence is not present. Tear film breakup cannot be measured and although spectrometer results promised strong performance, this was not the case in real life.

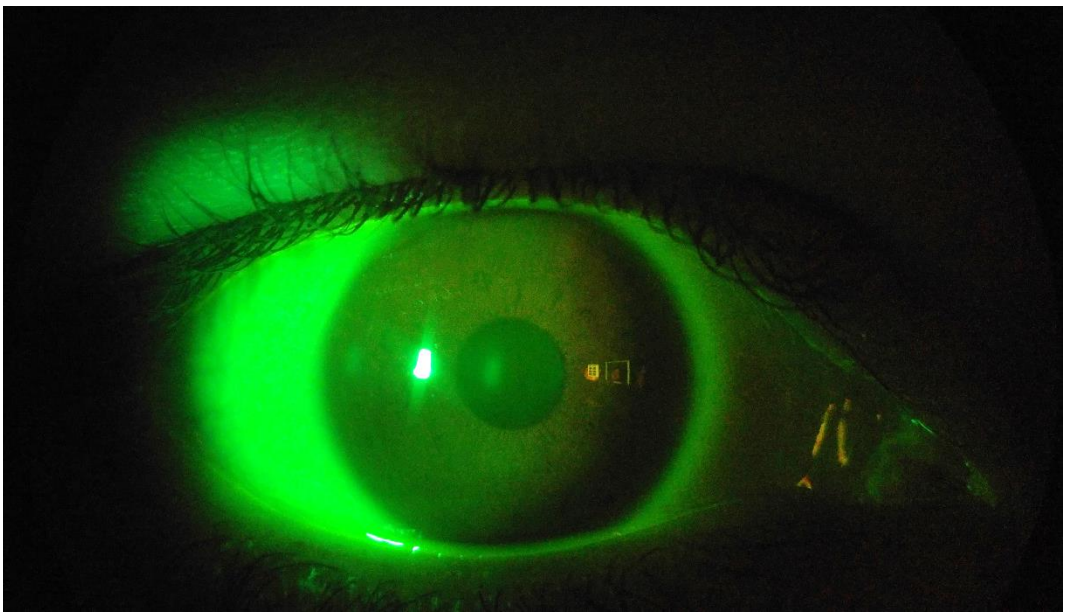

Figure 2-36: Custom blue and yellow filters in combination for fluorescein viewing

Reasons for this point to the very close excitation and emission spectra of both filters used together causing a major reduction in image contrast. Due to the blue excitation peak being 487 nm with the yellow transmission peak being 520 nm, this leaves only a small amount of colour difference to be detected by the observer. Additionally, the significant overlap of the blue and yellow filters seen in figure 2.37 means that much of the energy generated by the blue is cancelled out by the yellow. To boost contrast, a greater difference between excitation and emission may need to be developed with a shaper boundary between both filters to minimise overlap- something that may not be entirely possible with simple, low cost plastic filters.

2.9. Final Custom Filter Performance Results

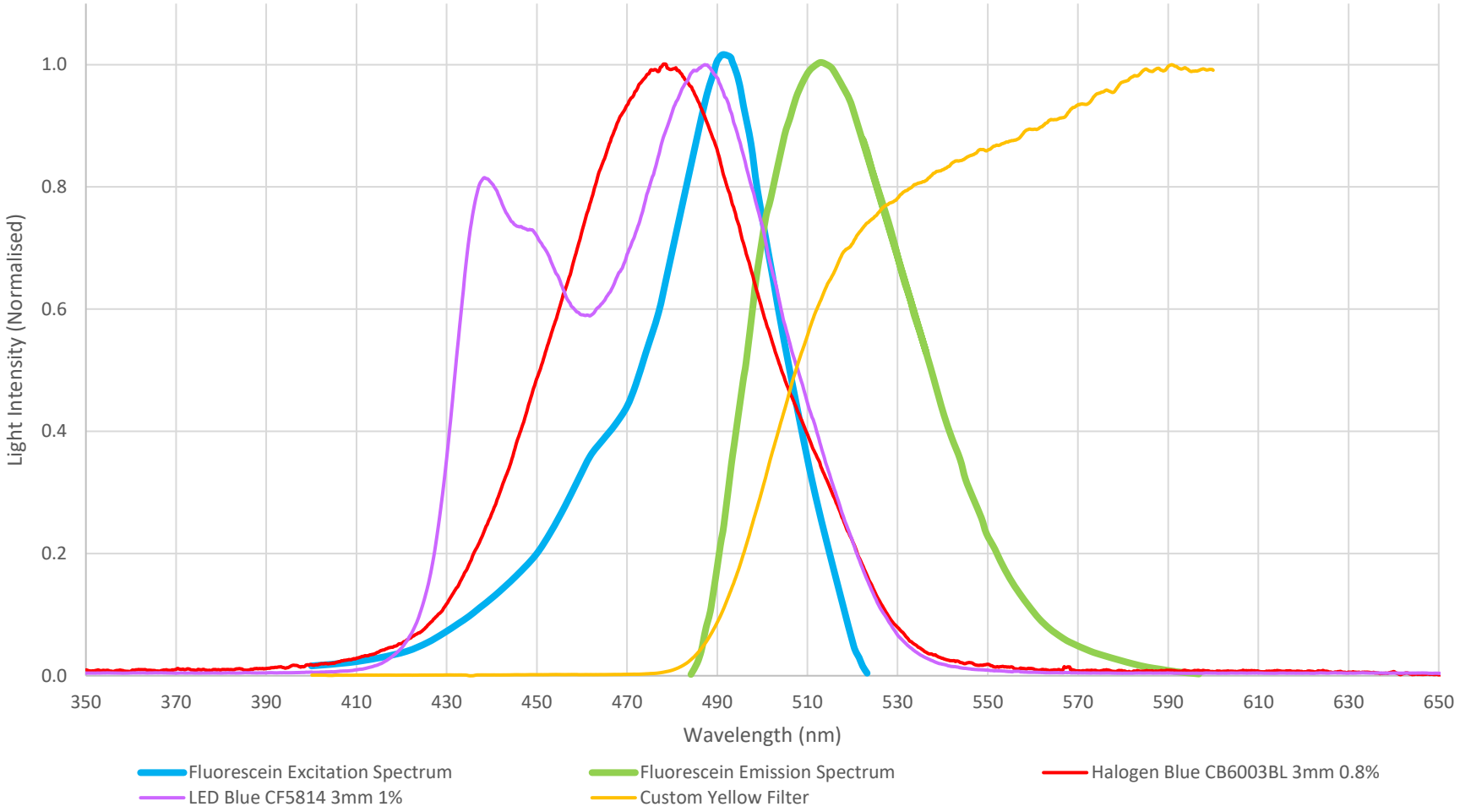

Figure 2-37 Final custom blue & yellow filters performance compared to ideal Fluorescein excitation and emission

2.10. Discussion

The use of topical dyes in anterior eye examination is a common and low cost procedure that enjoys worldwide acceptance [122, 172, 211]. With regards to dry eye diagnosis, a fluorescein breakup time of below 10s is considered one of the core indicators for the presence of dry eye disease [36]. Many modern slit lamps may be equipped with onboard filters for various dye viewing, although efficiency with respect to ideal Fluorescein leaves much to be desired.

Although it would have been ideal to create a single blue filter that can accept both light sources, the sheer range of halogen or LED combinations with various colour temperatures and brightness levels leaves no option but to have two individual filters, each of which are tailored to work with either a halogen bulb or the newer LED bulbs. Final custom filter performances of both blue and yellow versions are shown in figure 2.37.

Under the current scope of work, blue filter design was focused to be compatible with Haag Streit upright slit lamp models and future work can incorporate adapter components to allow for fitting to the Zeiss equivalents. The excitation filters are attached to various slit lamp models by means of the uprights that are present either side of the mirror assembly and the vast majority of slit lamps share common dimensions. CSO slit lamps uprights are of a significantly different design and the filters are unable to attach in the position required for good operation but variations could be created to overcome these restrictions.

Tuning custom blue filter colour spectra to ideal fluorescence has proved a success with 93.0 and 97.5% coverage for the Halogen and LED filters respectively. Nevertheless, low transmission values offset performance with slit lamp brightness levels needing to be increased to compensate. A similar effect was observed with diffuse white filters; under equal brightness levels custom white filters allowed far less light to pass and images of the ocular surface were dark, but produced stronger viewing once light levels increased. It has proven difficult to objectively measure amount of fluorescence produce by custom filters due to the subjective nature of fluorescein observation as well as poor camera properties. However, a positive of these custom filters is the reduced amount of transmittance in the blue light hazard region which means that even with the slit lamp brightness turned to maximum, dangerous light energy is restricted from reaching the patients' eye.

In cases where LED light sources are used, many instrument manufacturers tune the blue filters to work within the higher energy region closer to 450nm, rather than 490 nm, as LED output at this point in the spectrum exhibit greater light and therefore stronger fluorescence. The larger

spacing between the excitation and emission spectra tends to give rise to superior contrast viewing which is beneficial when trying to identify regions of similar fluorescence.

For end user assistance, small indicators on the lens of each filter identify the light source to be used with that filter version and although in some cases the user may not experience a difference in visual performance, there will be slit lamp models where visual acuity will be dramatic.

Separate to the blue stimulation, the second half of fluorescein observation relies on a yellow emission filter that is placed in the returning light path from the patients' eye. Development focused on improving on currently available thin film filters available from B&L and J&J.

Spectral data of custom yellow filters seen in figures 2.34 and 2.35 show very high performance and this is supported by in vivo testing captured in figure 2.33. Not only is the filter capable of high fidelity viewing but the physical design allows for attachment to many slit lamp models and convenient hands-free use.

In partnership with First Press Plastics Ltd. an initial 1,000 unit batch was manufactured in May 2017 at a cost of £0.98 each plus a one off tooling cost of £4,299 and have since been distributed to students and clinicians for testing. Positive feedback has given impetus to B&L to officially CE mark the filter as a class 1a medical device and manufacture another 16,000 units with the intention to begin global distribution. Not only is this an acceptance of the technology by a major manufacturer in the ophthalmic industry, but it is a strong opportunity for Aston university to promote its' reputation on the world stage. At time of writing, negotiations are continuing with regard to the licencing and distribution rights of the filter.

Although the filters produce strong viewing results individually, when used in combination performance is poor. Both blue excitation and yellow emission filters must work in tandem to produce strong fluorescence and block unwanted spectra. Images taken of custom filters when used together show little fluorescence and low contrast. At this point it is unclear as to why this is the case and may be a result of the low transmissivity values of the blue filters restricting the amount of energy reaching the yellow filter. Secondly, there is a strong overlap of the excitation and emission spectrums when both custom filters are used together – figure 2.37. This overlap may in fact be creating a cancellation effect where the intruding regions produce reduced fluorescence and only the areas of the spectrum that are free of overlap give light. This would also serve as an explanation as to why slit lamp filter manufacturers develop blue filters that act in the 470 nm range rather than the target 490 nm – not only is the amount of light energy

available higher in this wavelength region (especially with LED light sources) but there is an overall improved image colour clarity due to increased contrast arising from the larger wavelength separation.

A way to solve this performance deficit would be to attempt to replicate cut off filter characteristics where the blue filter would allow a peak transmissivity in the 460 to 490 nm wavelength range and then drastically reduce to zero at 500 nm. The yellow filter would also have a low transmissivity at 500 nm and then a sharp increase in the 510 nm and above. Although this would serve an improved viewing experience, it is simply not possible with low cost plastic filters where colour properties of dyes are difficult to control in fine increments.

A reasonable alternative may therefore be to investigate substitutes to the traditional yellow emission filters. Spectrum testing on 139 Primary Green and 738 Jas Green yielded colour signatures with very close results to ideal Fluorescein excitation, see figure 2.28 and may be interesting areas of research for next stage of filter tuning. The steep increase in transmittance of 139 Primary green in the 500 nm region lends itself well to the desired cut of filter performance mentioned above.

Furthermore, although fluorescein may be the strongest available dye for corneal staining, a new formula proposed by Korb et al. suggests a 2% fluorescein and 1% Lissamine green mix which would provide simultaneous corneal and scleral viewing capabilities [211]. If this be the case, then a single excitation filter that can would provide high quality imaging capabilities of both the cornea and sclera through a single dye instillation would form the next avenue of research.

3. Non- Contact Approaches to Tear Film Thickness Measurement

Tear film (TF) dynamics, recognised as a key component to clear, uncompromised vision is a topic that has been heavily studied for many years and yet uncertainty and continual disagreement over the nature, thickness and even structure of the pre- corneal tear film (PCTF) still resides in the field today [63-66]. One consistent trait is the expense of custom instruments that are typically built to be capable of performing such intricate observations. Both contact and non-contact techniques for the evaluation of the pre- corneal tear film have been developed to help gain an insight into the behaviour and thickness of the transparent medium that forms the outmost boundary to the human eye. Yet as much as the tear film composition has been studied and momentary tear film thickness values obtained, ability to record a continuous thickness profile during the entire inter- blink period is lacking.

The tear film is a dynamic system subject to constant change- refreshing, mixing and thinning between every blink [76]. Blinking has a profound influence upon the structure, stability, and function of the tear film [252]. Discrete ingredient compositions within the fluid are subject to separate rates of refreshing [70] making the ecosystem fluctuate constantly without a single instance of when it can be considered at baseline.

It has been suggested that tear film thinning is subjected to three phenomena working together; (1) evaporation of the tear film from the surface of the eye, (2) inward/ outward flow into the ocular surface (3) minor flow parallel to the ocular surface [253].

Physical extrinsic factors such as environment and humidity may be contributing influences but it is in fact contact lens (CL) wear that has been proven to have significant impact of the tear film with up to 50 % of wearers reporting symptoms of dry eye [112, 254]. A study by Nichols and colleagues revealed that contact lens wearers described dry eye experiences with a five time greater frequency than spectacle wearers and twelve times greater than in individuals without visual correction [113]. However, on the positive side, patient opinion of CLs include a personal perception of better physical appearance, self-confidence and freedom to perform leisurely activities without interruption [255-257]. As of 2013 the number of UK wearers stood at 3.7 million suggesting that 1.35 million experience induced dry eye symptoms [258].

As a CL is inserted into the eye it becomes sandwiched between the pre and post lens tear film. Nichols et al. used interferometry to measure pre- lens tear film thinning rates at 2.8 seconds

faster compared to control groups and postulated that lipid layer undergoes electrostatic binding to the lens surface and consequent compromise of the upper tear film layer, leading to increased TF evaporation rates [254].

Voluntary withdrawal from contact lens wear has been identified as largely due to persistant dryness and discomfort [259]. Therefore, material scientists are continually evolving lens composition to form new soft hydrogel, gas permeable and hybrid lens material combinations that will promote greater oxygen permeability and comfortable mechanical properties. Nevertheless, reduced tear film thickness and instability issues due to contact lens wear is a serious problem and a leading cause of extrinsically induced dry eye.

Dry Eye disease may take many forms, but association between signs, symptoms and objective measurements are weak [39, 143]. Fluorescein break up time may be considered to be a direct measurement of tear film stability [135] nevertheless high variance between results are puzzling to clinicians [143, 188]. Invasive forms of measurement such as Schirmer testing or phenol red thread test lead to unintended disruption of the tear film [152].

Many techniques varying from Statistical Decision Theory OCT, tear film osmolality and surface fluid evaporation have all been employed with acquired tear film thickness (TFT) values varying by as much as an order of magnitude between approaches [63, 64, 66, 89]. Both contact and non– contact methods, as well as computer simulation models, have been devised, tested and listed in table 3.1. Reflex tear production resulting from contact approaches renders obtained results as suspect to unintended stimulus [260]. So far, an agreed gold standard of relatively low cost, easy to obtain, repeatable and reliable techniques for tear film thickness measurement and dry eye evaluation is still elusive [36].

Current best agreed values of complete TFT have been achieved through the use of pre- corneal tear film reflection spectra and various OCT techniques. Thickness values of between 2 to 5 μm are viewed as the standard for healthy eyes [92-94, 96].

3.1. Interferometry

Based on the principles of constructive and destructive wave generation as light is passed through various media, interferometry was first used by Doane in 1989 to estimate the thickness of the PCTF [261]. Once hailed as “the most promising non-invasive method” for tear film thickness measurement [262], interferometry has evolved from the original Michelson interferometer of the late 1800s and developed into three principle approaches; angle-dependent fringes; thickness- dependent fringes and; wavelength- dependent fringes [262].

Reflection spectra can be captured by video recorder and appear as different colour fringes depending on the thickness of the lipid layers. Colour and consistency of fringes have been found to have a significant correlation between other dry eye testing methods such as tear break up time and fluorescein staining [263]. Lipid layer interference patterns have been classified by Yokoi et al. on a grade scale of 1 to 5 which give an indication of the severity of dry eye [263]. Grade 5, severe dry eye, is the absence of the lipid layer altogether.

Certain interferometric systems have also been designed with low numerical apertures giving rise to a circular field of view as large as 8 cm which have been used to monitor distribution and spread of the lipid layer between blinks [253]. Interferometry has also been used in the attempted determination of in vivo intra-ocular pressure and axial eye length with mixed results [264, 265].

Large discrepancies exist between recorded tear film thickness values achieved through various interferometric methods- see table 3.1 and the technique has been superseded by advent of OCT in the early 90’s.

3.2. Optical Coherence Tomography

In 1991 Huang et al. demonstrated the first ex- vivo OCT system for the observation of retinal arteries on principles based upon time of flight of an optical signal as it is transmitted or reflected from biological tissue [266]. By 1995, Carl Zeiss Meditec introduced OCT on a commercial scale [267], and it is now considered as important a tool as the common slit lamp.

OCT works on the principle of low coherence interferometry in conjunction of an appropriate light source (wavelength typically 1,300 nm for anterior chamber imaging) which gives the capability of high resolution, through tissue imaging [268].

During a scan, the patient is sat with their head on a chin rest and their eye focused on to a target within the machine. This is a similar sitting position to slit lamp observations. The OCT is focused on to the eye and captures cross- sectional images of semi- transparent or even opaque media.

Early OCT instruments, such as the Stratus and Visante OCTs (*Carl Zeiss Meditec, Inc., Dublin, CA*) relied on time domain sampling methods which worked on the principle of a modified Michelson interferometer measuring backscattered light from the medium being scanned. A sinusoidal sweeping mirror scans the object and optimising filters coupled with high speed analogue to digital converters compile the signal into a digital representation depending on reflected light values at different depths of the sample [269]. The Stratus OCT is capable of sampling 400 axial scans per second at a resolution of 10 µm [270].

Fourier Domain OCT was developed second to Time Domain OCT and relies on a similar principle except that a single line charged coupled device has been introduced together with a diffraction grating. The single line of pixels produce a long, but thin image, while the diffraction grating allows for measurement of a wide range of light frequencies. Fourier transforms translate captured data into quantified light values at varying depths within the materials being measured. For example the Cirrus HD-OCT (*Carl Zeiss Meditec, Inc., Dublin, CA*) is capable of 20,000 axial scans per second at an improved resolution of 5 µm [270].

Swept Source OCT is the latest advancement in imaging and takes advantage of a short cavity laser capable of changing output wavelengths in 1 µm increments. During each scan, an onboard laser, which operates beyond the sensitivity of the human eye, sweeps along its capable range of wavelengths and the signal returned from the object is interpreted by a CMOS camera in conjunction with photodiode detectors. Once received, the signal is processed using Fourier transforms similar to the earlier described systems [271]. The overall benefit of Swept Source

OCT is a fast, wide field scan capable of deeper penetration depths due to the lower signal attenuations of the varying wavelength laser. Swept source instruments are therefore capable of measuring multi-layers in a single wide field pass, e.g. the Triton OCT (*Topcon, Tokyo, Japan*).

Many OCT systems are available from various manufacturers and are capable of producing similar data outputs. The main OCT parameters of interest to an ophthalmologist are [272-274];

- Depth, width and angle of anterior chamber
- Pachymetry mapping
- Corneal distortions such as Keratoconus
- Iridocorneal Angle
- Refractive surgery flaps
- Corneal wound healing
- Tear prism and volume estimation

OCT technology is still considered to be developing and continual advances in tissue penetration depth, efficiency of light sources and measurement speed will only serve to increase the capabilities of this technology [275]. Cost of these devices remains prohibitively high and refractive index changes of the various mediums of the eye (cornea, aqueous humor, crystalline lens, etc.) and image de- warping requirements are all sources for introducing error into the measurement. Nonetheless, OCT devices are now considered an indispensable tool for optical diagnostics.

Table 3-1: List of existing tear film thickness achieved though available technologies

Tear Film Thickness Measurement, Non- Invasive Methods		
Method	**Measured TF Thickness (Overall)**	**Notes**
OCT in combination with Statistical Decision Theory [64]	20µm - 150µm	Statistics used to estimate thickness of noisy signal acquired by OCT scan
Confocal Microscopy without Oil Immersion [65]	Roughly 41 - 46 µm	Images obtained very unclear and left author guessing as to what they are
Spectral Oscillation with Contact Lens Worn (Interference Method) [89]	Average 1.4 to 3.9 µm for five subjects wearing CL	Higher refractive index step change introduced through contact lens insertion allows for clearer signal capture
Spectral Oscillation without Contact Lens (Interferometric Method) [89]	2.94 µm	Difficult to acquire TF signal without contact lens. Data captured on single subject.
Coloured Interference Fridges [98]	0.1 - 0.52 µm	Able to measure contact lens film thickness of 0.1 - 1.1 µm
Angle Dependent Fridges (Interferometry Method) [99]	Estimated as 10 µm or less	Momentary thickness values from fringe photographs
Angle- Dependent Fringes (Laser Interferometry) [65]	34 - 45 µm	Could not obtain direct measurements due to involuntary eye movements. Their equipment could detect fringes of thicknesses 6 - µm to 300 µm. Eyes needed to be anesthetized
Interferometry [92]	3 µm	Unknown layer assumed to be tear film
Wave Dependent Fringes- Interferometry [100]	Healthy Eye 6 ± 2.4 µm, ADDE Patients 2.0 ± 1.5 µm	Momentary thickness values 5 seconds post blink taken as baseline

Tear Film Thickness Measurement, Invasive Methods		
Confocal Microscopy with Oil Immersion [65]	Roughly 40 µm (mostly mucus)	Added acetylcysteine to disperse mucus layer and noticed a decrease in film thickness.
Fluorescein Addition and drainage [90]	10 - 20 µm	Different polymers show varying amounts of Fluorescein retention on the eye skewing results and application variability can increase TF thickness
Glass fibers Against Cornea [91]	6.5 µm	Claim that Lipid layer is thinner than a ray of light and evaporation from ocular surface is 3µl/ hr cm2

3.3. Low cost alternative methods of tear film assessment

The majority of equipment listed in table 3.1 is expensive and in most cases confined to experimental situations. New devices available from Micro Epsilon and Precitec that are packaged in smaller footprints are available in industries such as the automotive and aerospace fields but may be suited for inter- disciplinary use in the biomedical field. An introduction to their working methods will be discussed below.

3.3.1. Confocal Chromatic

The fundamental setup of the Micro Epsilon confocalDT (*Ortenburg, Germany*) & Precitec CHRocodile 2 S/ 2 SE (*Baden- Baden, Germany*) systems consists of a controller complete with light source and onboard spectrometer. Depending on the nature and thickness of the observation to be undertaken, separate interchangeable probe heads each with particular working distance, depth of field, and resolution are connected by means of flexible optical fibre (maximum length 50 meters), thereby allowing for adjustable placement and angle with regard to the object being measured.

Polychromatic white light (either from the onboard LED or separate external Xenon light source) is pumped into the top of the probe and passes through several lenses within the body designed to aberrate the incoming light into its monochromatic constituents which are expelled axially into individual wavelengths at differing distances leaving the tip of the probe as seen in figure 3.1.

Each wavelength leaving the probe is assigned a particular distance value by factory calibration and when light is reflected from the surface being measured the spectrometer grating is able to register discrete wavelengths and compute the corresponding distance/ thicknesses that are being witnessed. Software correction for material refractive index (RI) and Abbe number coefficients can be processed in real time and depending on the controller and probe combination, up to 6 surface peaks with a measuring rate of 70 kHz can be achieved with the confocalDT equipment.

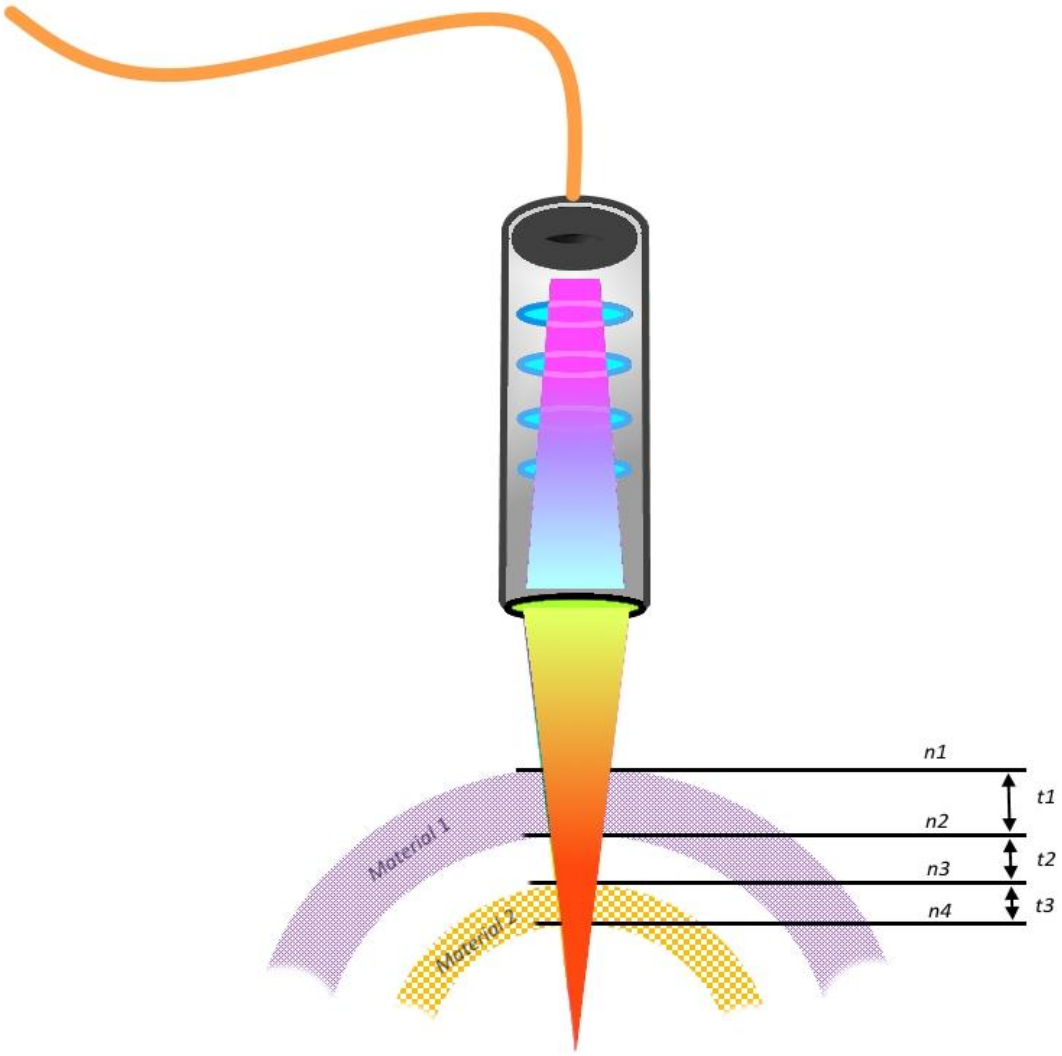

Figure 3-1: Micro Epsilon measurement principles. Wavelengths of light echoes from the surface of the sample (n1 and n2) and are reflected back into the probe. The return signal from a sample's surface is registered by the controller and the difference in wavelengths give rise to a thickness value, t1. Illustration drawn by author.

Transparent, opaque and specular surfaces can be inspected. It is worth noting that as the measurement rate is increased, the return signal of each measured surface becomes weaker and harder for the controller to distinguish from noise. The opposite is true if the scanning rate is low and the exposure too high - the grating becomes saturated due to the overpowering signal and measurement errors arise.

Instruments capable of chromatic measurement are the Micro Epsilon confocalDT IFC 2451/ 2461MP and the Precitec CHRocodile SE with appropriate probes fitted.

3.3.2. Precitec Interferometric Measurement Principles

Phase difference between source and return light signals is the technique employed by the Precitec CHRocodile SE equipment to calculate the thickness of samples with interferometric methods. Interferometric measurement is not possible with the Micro Epsilon hardware.

Polychromatic light is generated by the controller light source and focused on to the sample through the probe which is connected by fibre optic cable, just as in confocal measurement techniques. Figure 3.2 shows incident light being reflected back into the probe from each material interface that is encountered leading to varying propagation path lengths and corresponding phase shifts between returned signals. Material thickness and density influences the phase of the returning light waves leading to constructive or destructive interference between received signals and corresponding intensity variations. Fourier transforms of the registered signals are corrected for refractive index and abbe number of the material being measured and thickness values generated in real time.

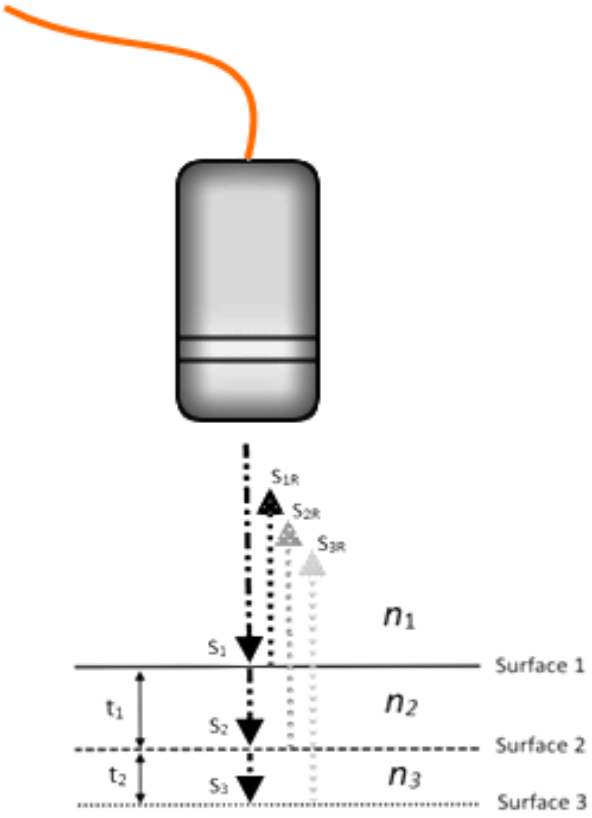

Figure 3-2: Precitec CHRocodile SE Interferometric measurement principles. Constructive and destructive wave superposition allow various transparent media to be identified provided return signal sufficiently strong.

Depending on the probe- controller combination, thickness values of roughly 1.5 µm to 250 µm with a resolution of 10 nm can be achieved provided there is a degree of difference in RI of neighbouring materials. The capability of the system is further enhanced by allowing a ± 2 mm real time variation in the working distance in relation to the probe head and the object being assessed which is beneficial when observing the human eye that experiences saccades and natural body movements due to breathing.

Table 3.2 provides a comprehensive summary of both Micro Epsilon confocalDT and Precitec CHRocodile SE equipment capabilities as well as the measurement principles that can be employed by either hardware.

Table 3-2: Micro Epsilon & Precitec hardware specification Data taken from Micro Epsilon Catalogue OCT 2015[276], Precitec Optical Sensors OCT 2014 [277] & Optical Probes Catalogues APR 2016 [278]

	Micro Epsilon		Precitec		
Controller	**IFC 2451**	**IFC 2461MP**	**CHRocodile SE**		
Measurement Mode	Confocal Chromatic		Confocal Chromatic/ Interferometric		
Multi Peak Measurement	2 Peaks	6 Peaks	3 Peaks		
Light Source	Internal White LED		Internal White LED		
Measuring Rate	Adjustable 0.1/ 0.2/ 0.3/ 1/ 2.5/ 5/ 10 kHz	Adjustable 0.1/ 0.2/ 0.3/ 1/ 2.5/ 5/ 10/ 25 kHz	0.032/ 0.1/ 0.32/ 1/ 2/ 3.2/ 4 kHz		
Safety; EMC	CE		CE		
Interference Emission	EN 61 000-6-3/ DIN EN 61326-1 (Class B)		DIN EN 61326-1:2006/ DINEN 61010-1:2002-08		
Interference Resistance	EN 61 000-6-2/ DIN EN 61326-1				
Cost	£5,339[5]	£6,630[5]	£7,629[6]		
Sensor Model	**Chromatic IFS 2405-0.3**	**Chromatic IFS 2405-3**	**Chromatic 5002399**	**Chromatic 5002508**	**Interferometric 5005000**
Measuring Range	0.3 mm	3 mm	2 mm Distance/ 3 mm Thickness[2]	12 mm Distance/ 18 mm Thickness[2]	3- 180 µm
Start of Measuring Range	6 mm	10 mm	≈ 61mm	≈ 54mm	≈ 27mm
Spot Diameter	6 µm	9 µm	12.5 µm	30 µm	40 µm
Linearity (Displacement Measurement)[1]	0.15 µm ± 0.05% Full Scale Output	0.75 µm ± 0.025% Full Scale Output	6 µm	15 µm	20 µm
Linearity (Thickness Measurement)	0.3 µm ± 0.1% Full Scale Output	1.5 µm ± 0.05% Full Scale Output	0.066 µm	0.39 µm	0.01 µm
Resolution[3]	10 nm	36 nm	66 nm	390 nm	10nm
Weight	140 g	225 g	315 g	281 g	21 g
Maximum Tilt Angle[4]	± 34°	± 44°	± 15°		± 5°
Cost	£3,143[5]	£2,870[5]	£2,511[6]	£2,469[6]	£2,104[6]

1) Ability to discern details in perpendicular (left and right) direction to axial path of beam
2) Refractive Index n = 1.5
3) Average from 512 values @ 1kHz, near the centre of measuring range
4) Decreasing on the limits
5) Prices correct April 2016
6) Prices correct October 2017

3.4. Eye Parameter definition

Both confocal and interferometric instruments are capable of measuring distance and wall thickness through various transparent and opaque materials by evaluating the returning light waves and performing refractive index corrections through the media being analysed. For accurate measurement to take place, the refractive index and abbe's number of the media needs to be entered into the controller and specified ahead of time.

Work by Tiffany found that temperature plays a major role in refractive index properties of the tear film lipid layer which varies between an RI of 1.46 – 1.53 between 25 and 45 °C [279]. For the purpose of testing a value of 1.5 will be used for the lipid layer.

Over the course of the following tests the data in table 3.3 was taken as the standard for Human Eye Refractive Index and Abbe values:

Table 3-3: Refractive Index and Abbe Number of Human Eyes

Material	Refractive Index @ 587 nm	Abbe Number
Silicone Hydrogel Contact Lens [280]	1.375	45
Tear Film [281]	1.337	50.2
Tear Film Lipid Layer [279]	1.46 – 1.53	Unknown
Cornea [280]	1.3771	57.1
Aqueous Humor [281]	1.3374	61.3
Crystalline Lens [280]	1.36 - 1.41	47.7
Vitreous Humor [280]	1.336	61.1

3.5. Aims & Objectives

Low cost, in vivo assessment of anterior eye and tear film properties is considered clinically useful and may provide reliable, cross spectrum parameters such as distribution, thickness and evaporation rate which may be markers as to the presence of dry eye [92, 282]. Traditional equipment requires high investment and is restricted to specialist clinics or settings. The small footprint and low cost may allow this technology to reach a larger patient audience.

What follows is a series of studies each involving in depth assessment of three non- contact chromatic and interferometric devices (Precitec CHRocodile SE alongside the Micro Epsilon confocalDT IFC 2451 and IFC 2461MP units) with a particular focus on obtaining real time visualisation of full in- vivo cross section TF dynamics including;

1. Central corneal thickness measurement
2. Continuous, in vivo tear film thickness and thinning behaviour
3. Contact lens effect on tear film thickness
4. Saline submerged contact lens thickness measurement
5. B scanning possibilities of the anterior eye.

The following studies were conducted at different points over the course of 21 months as controller and probe combinations were not available at the same time. Room temperature was between 20- 23°C and ambient daylight conditions were standard- STP conditions. A large range of tests were conducted over this period with learnings from earlier experiments used to enhance later tests. Every effort was taken to ensure identical setups between equipment and ensure a fair comparison between trials. All studies were approved by Aston University Ethics Committee and conformed to all tenets of the Declaration of Helsinki.

A full list of the various tests performed and the equipment combination used is listed in table 3.4 below. Not all assessments could be performed on each instrument due to loan time restrictions. It is the authors' intention to understand the limits of both low cost confocal and interferometric technologies in the application of anterior eye and dry eye diagnosing capabilities.

3.6. Experiment A: Tear Film Thickness Assessment

The anterior eye is very sensitive to any form of contact, but parameters of corneal thickness to tear film thickness could provide great insight into the health of the eye. Low cost, non- contact measurement could provide a solution to diagnose or assess many aspects of eye health. Device testing was therefore particularly focused on achieving as many different data points of the anterior eye in the hope that it could be used in mainstream medicine as an accessible, low cost device.

Thor Labs (*Newton, New Jersey, USA*) optical bench equipment (OBE) with micrometre stages was employed to allow for precise linear positioning of the probe in relation to the subjects' head which was held in place using a modified slit lamp chin rest. Slit lamp joy stick adjustment allowed multi- dimensional positioning of the probe in relation to the patients' eye. Experimental setup shown in figure 3.3.

The single subject varied between long hard and short quick blinking patterns. Test were initially conducted on the corneal apex of the right eye by manual positioning with regard to achieving the strongest signal to noise ratio. The experimental aim was to record the raw basal tear film thickness and thickness behaviour between blinks of a single subject.

Next, various regions of the cornea and sclera, such as inferior and temporal areas, were then focused upon in an attempt to achieve tear film data from as many points as possible and compare with corneal values. Tear film thinning gradient could be used to estimate tear film evaporation break up time as well as be used as an associated measure of DED.

Table 3-4: Controller and probe combinations tested under experiment A

	Micro Epsilon ConfocalDT				Precitec		
Controller	IFC 2451		IFC2461		CHRocodile SE		
Probe	0.3mm	3mm	0.3mm	3mm	2mm	12mm	180µm

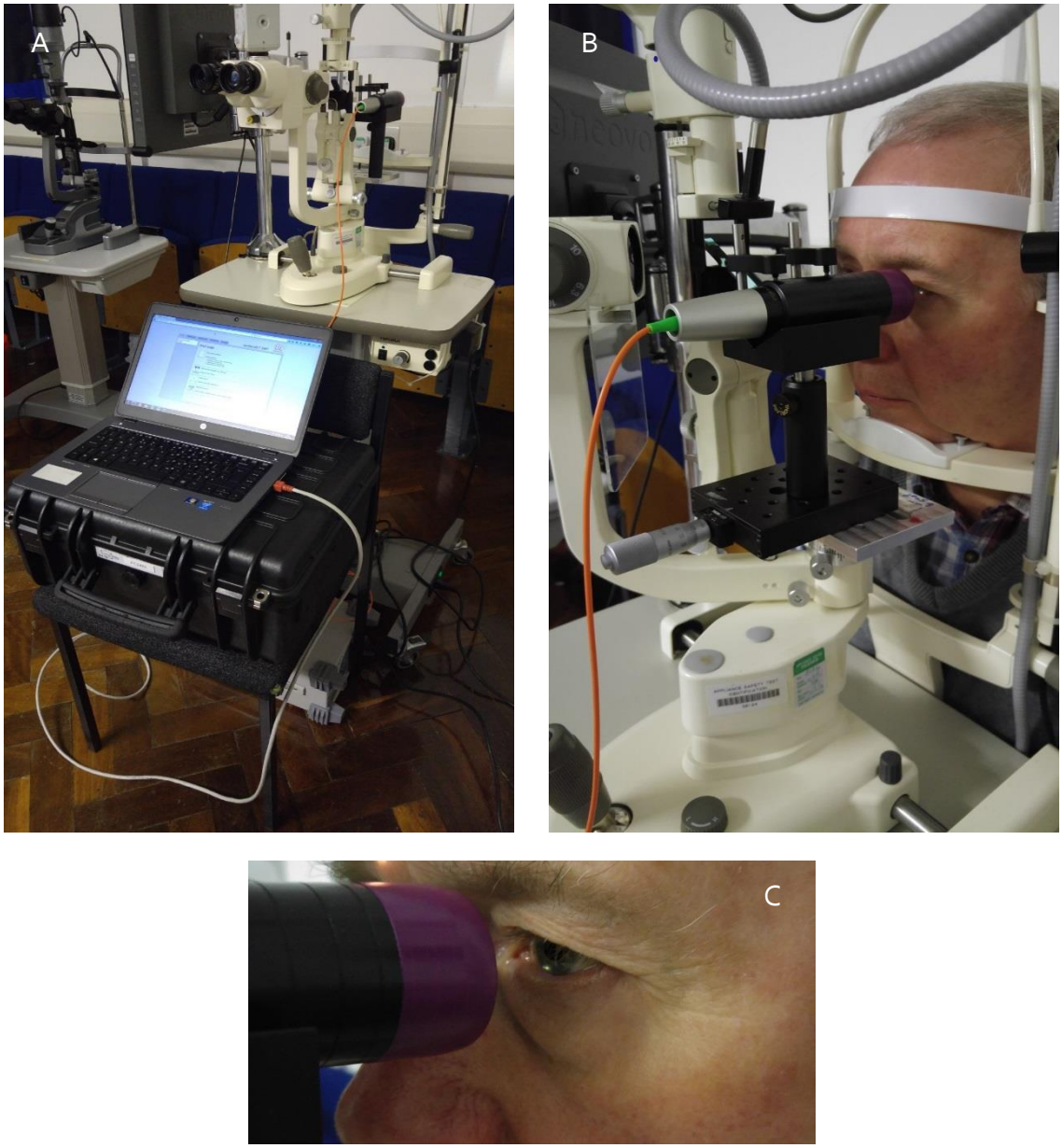

Figure 3-3: Tear film thickness measurement apparatus. A) Slit lamp with probe mounted and data collection terminal prepared. B) Patient held in position with slit lamp chin rest. Probe mounted on OBE micrometre stage to allow for distance calibration adjustment with respect to the eye C) Small white dot visible on inferior cornea indicating position of measurement area.

3.6.1. Experiment A Results

Data obtained using the Precitec CHRocodile SE interferometric instrument of the raw tear film at corneal apex proved to be the most revealing with other instruments failing to measure a thickness. Figure 3.4 is the best example of the dynamic TF being captured over the course of a blink cycle. A momentary thickness spike at 7 seconds is registered as the upper lid meniscus passes by the centre of the cornea. This corresponds with models constructed by Brown who suggests a two- step tear film spreading process over the ocular surface [283] as well as previously mentioned quantum dots (qDot) experiments which suggest different layers of the tear film refresh independently [70]. The upswing of a blink induces capillary action which pulls the tear film over the ocular surface followed by a redistribution of the upper lipid layer, creating a stable barrier to the environment [39, 283].

At 7.2 seconds a continuous decreasing signal indicates that the TF is roughly 4.4 µm at the start of the interval between blinks and decreases at a steady rate of 0.1198µms^{-1} until the next blink. Unfortunately, the TF signal registered by the controller was lost at 15 seconds before the second blink could be captured in this instance. This is typically the result of a decrease in signal to noise ratio as the medium being measured approaches the lower limits of what is capable to be measured by the probe.

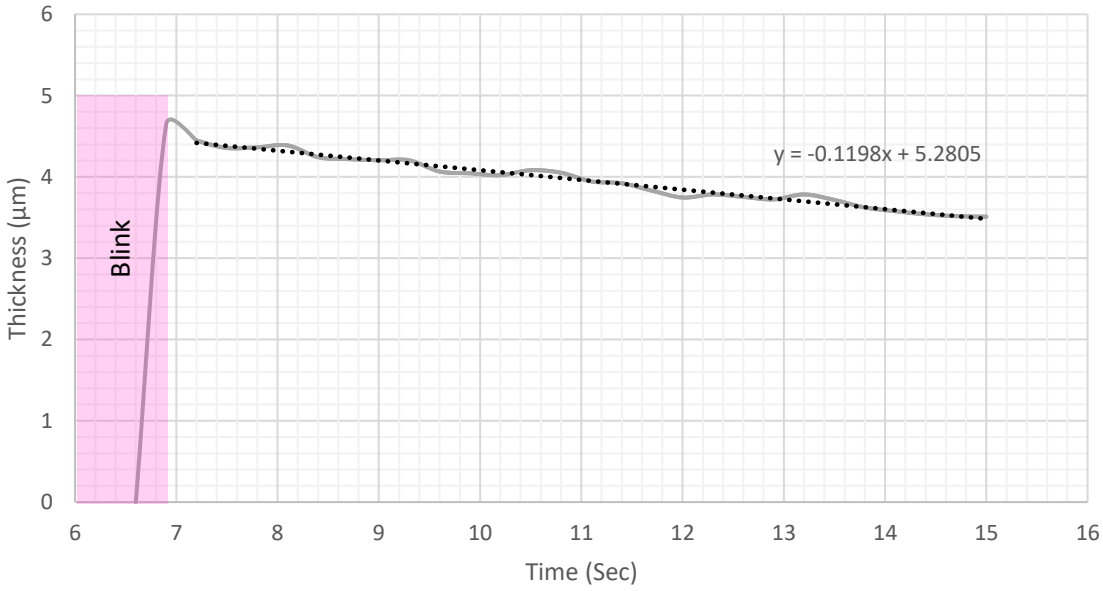

Figure 3-4: Tear Film thickness after blink (t= 7s) then thinning over time

Figure 3.5 shows an intermittent signal trace which was the more common experience as the instrument struggles to lock on to the tear film which shares a refractive index very close to that of the cornea (1.337 vs. 1.3771) [280]. Between 83 to 96 seconds, the TF is slowly thinning at a rate of 0.0434 μms^{-1} as gravity and surface evaporation take their toll on the fluid. The blink first completes at 98 seconds. TF is 3.28 µm moments after eyelid has passed upwards and degrades at 0.0507 μms^{-1}. Indeed over repeated tests, similar TF behaviours can be observed; as the upper lid rises, a small short increase (bump) in thickness is recorded, indicating that the upper tear film meniscus has passed the measurement area. Just after this the TF signal slightly decreases as the film settles and spreads evenly over the eye. Gradual thinning now proceeds until the next blink begins.

Over the course of the tests it was observed that the tear film thinning rate ranged considerably from as high as 0.1198 μms^{-1} down to 0.0205 μms^{-1} once TF stability has been reached over the ocular surface. This does seem particularly inconsistent, but this is probably due to the tests being carried out at different times of day and not consecutively. Various elements such as fatigue, previous blinking rate and even temperature conditions are known to affect tear film behaviour [284]. When blinks were recorded consecutively, the results proved much more consistent. Mean tear thickness achieved over the course of five tests was 3.28 ± 0.522 µm.

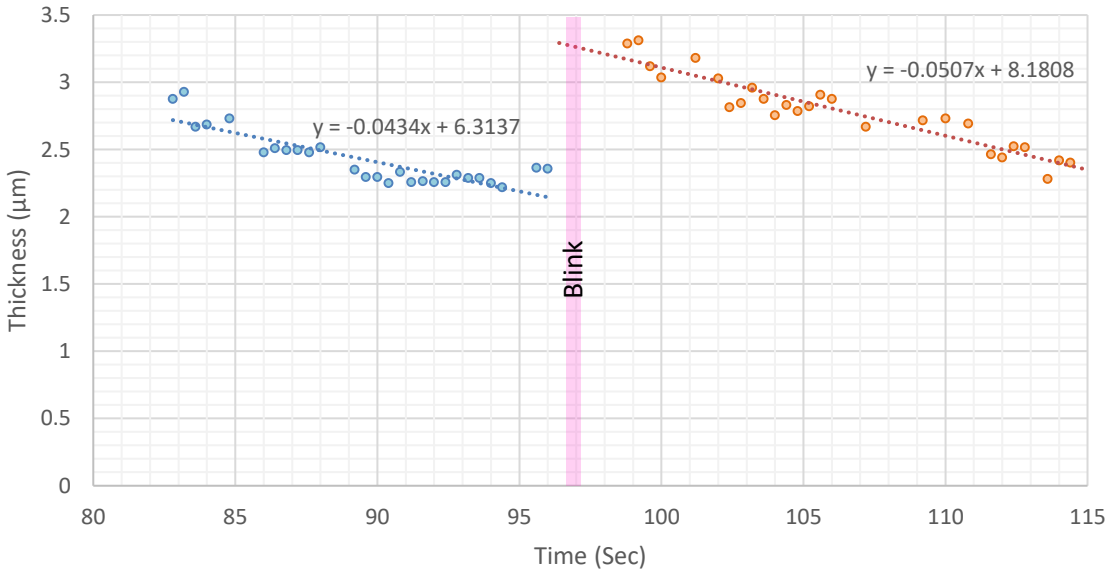

Figure 3-5: Tear film thickness changing over time.

3.7. Experiment B: Tear film thickness with artificial tears

Second stage testing involved adding Thealoz Duo (*Clermont- Ferrand, France*) lubricating eye drops to measure the changing effect on TFT and thinning rate. Experimental setup was identical to Experiment A above. An individual eye drop was added to the right eye of a single subject and they were then sat with their held in a chin rest. Probe distance to eye was adjusted using an OBE micrometre linear stage. The Micro Epsilon IFC2461 with both 0.3 and 3 mm chromatic probes was tested alongside the Precitec CHRocodile SE controller with all three probe combinations.

Table 3-5: Controller and probe combinations tested under experiment B

	Micro Epsilon ConfocalDT				Precitec		
Controller	IFC 2451		IFC2461		CHRocodile SE		
Probe	0.3mm	3mm	0.3mm	3mm	2mm	12mm	180µm

3.7.1. Experiment B Results

The TF surface proved just as elusive to detect with the lubricating fluids as without and signal strength was again intermittent and only the Precitec CHRocodile SE interferometric device was capable of observing the tear film- the confocal technology proved to be lacking with regards to these observations. Out of seventeen test attempts, only two sets of measurements were stable enough to produce degradation results and are shown in figures 3.6 & 3.7.

Surprisingly the thickness results yielded a lower mean TFT of 2.98 ± 0.243 µm across two data captures which is lower than the values achieved on the raw tear film in experiment A. However, a significantly slower thinning rate of 0.0185 μms^{-1} for the artificial tears vs. 0.1198μms^{-1} for natural tears was noted thus suggesting that the stability of the tear is enhanced and an overall improvement in patient comfort is achieved through tear longevity as opposed to a simple volume increase as originally speculated.

It is reasonable to expect the artificial tears to be progressively wiped from the ocular surface post instillation through natural blinking action and the reduced thinning rate could be a mechanism by which the artificial tears are able to maintain a longer half- life with the stable tear film triggering fewer blinks and thereby minimising the rate of attrition.

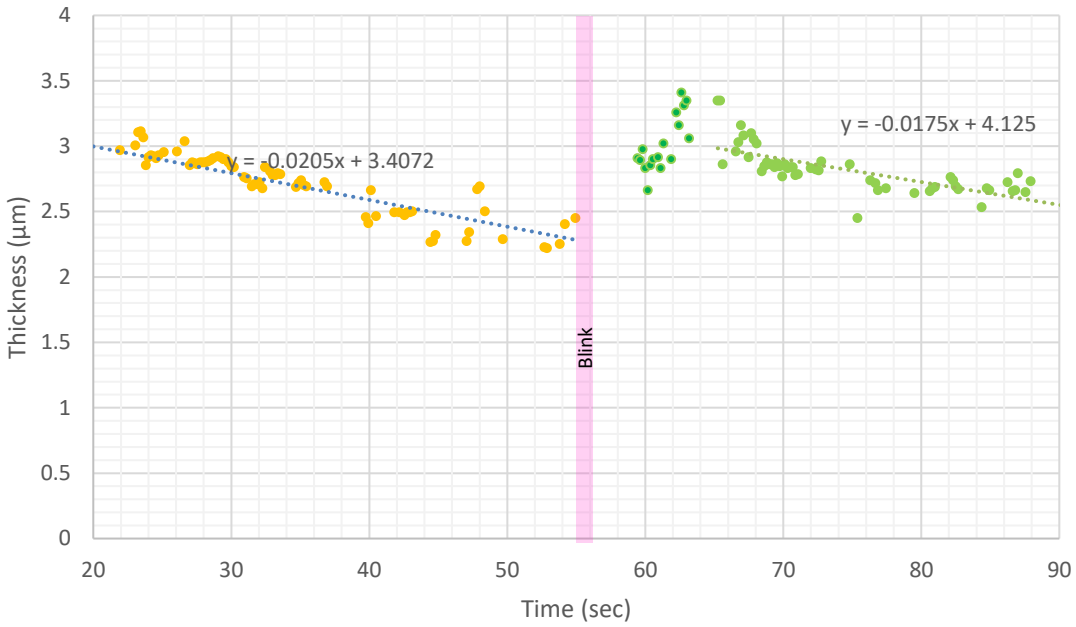

Figure 3-6: Capture 1; Tear film thickness and thinning measurements after instillation of Thealoz Duo artificial tears

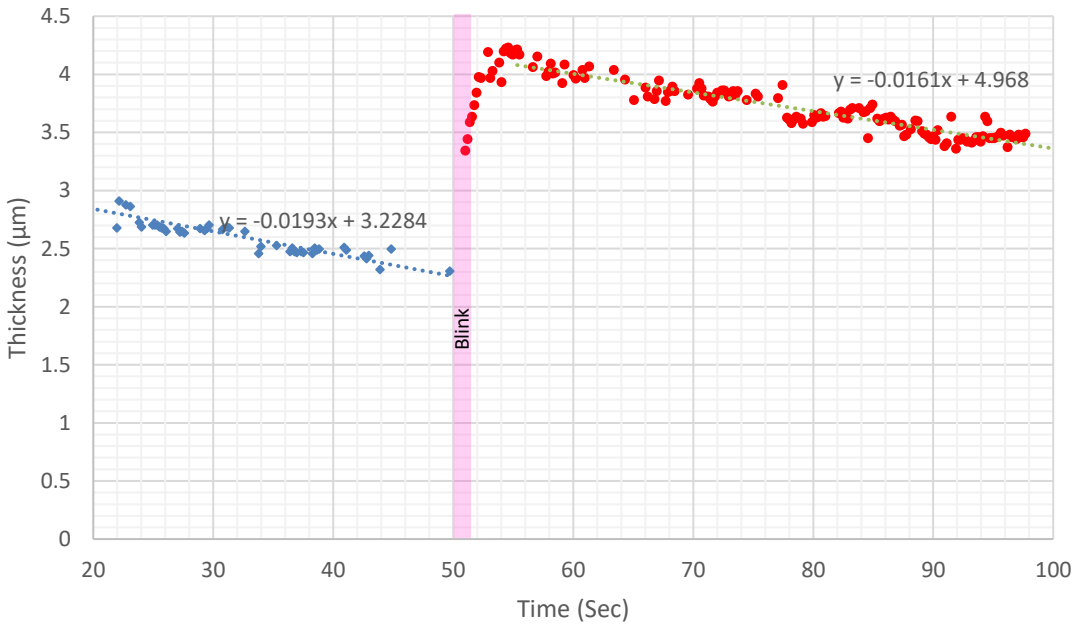

Figure 3-7: Capture 2; Tear film thickness and thinning measurements after instillation of Thealoz Duo artificial tears

3.8. Experiment C: Tear film thickness with contact lenses

Contact lenses of varying strengths and material compositions were inserted into the eye in attempts to measure pre & post contact lens tear film thicknesses and thinning rates. Experimental setup mimicked that of experiment A above- a single patient was sat in the chin rest and a contact lens was inserted. Measurements were attempted immediately and once again after an elapsed period of time.

Although the refractive index of many lenses vary in material composition, a static value of 1.3750 was selected and maintained consistent for all tests [280]. The corneal apex was selected as this gave rise to the least complications when having to consider the angle of incidence of the probe in relation to the surface being measured. Positioning was achieved by manual alignment of specular reflection from the apex. This point was the same as used in the raw tear film measurements and provided a useful comparison of thickness, degradation and blinking meniscus behaviour between the non- invasive measurements and the invasive nature of the lens being inserted into the eye. Initial insertion of the lenses prompted reflex tearing and only once this had settled did investigations commence.

Table 3-6: Controller and probe combinations tested under experiment C

	Micro Epsilon ConfocalDT				Precitec		
Controller	IFC 2451		IFC2461		CHRocodile SE		
Probe	0.3mm	3mm	0.3mm	3mm	2mm	12mm	180µm

3.8.1. Experiment C Results

Tear Film thickness observation with an inserted contact lens was far easier to achieve, but again only with the Precitec interferometric probe. Preliminary testing showed a drastic improvement in the recognition of the tear film over the course of the 120 second testing period. Depending on the lens, the signal received from the instrument was very strong with a consistent, high signal to noise ratio and the tear film was registered from blink to a minimum thickness of ≈ 1.4 µm before the signal was lost. Depending on the quality of captured data, between two to five blinking patterns over the course of 120 seconds were recorded as can be seen in figures 3.8 to

3.12. Different lenses showed variation of mean TFT for 2 seconds after a blink and also thinning time. Average TFT with lens measurements was 4.3 µm, but large discrepancies were evident between lens manufacturers with J&J Acuvue Moist lenses typically giving rise to a much thicker TF and J&J Acuvue Hydraclear a slower thinning time over the course of the inter- blink period- figure 3.13.

It was initially hoped that with insertion of a CL, the instrument could capture pre/ post tear film as well as the lens thickness. This proved not to be possible as signal attenuation was too high for reliable echo recognition. As a CL is inserted into the eye, the natural material properties of the lens cause absorption of the surrounding TF and the refractive index of the lens is now a mixture of the original lens composition material and absorbed TF fluid. Certain lenses, such as the J&J Oasys did register a steady second surface during testing in the range of 130µm, but it is not clear what this surface may be. It must also be noted that tear film degradation testing requires greater control as differences in blinking behaviours of current blinks (long hard blink, quick blink and open eye inter- blink time) all have an effect on the TF thickness on the following blink. It was typical to see the tear film thickness considerably increase upon the next blink, following a long period of not blinking, as demonstrated in figure 3.8. As the eye became irritated due to prolonged ocular surface drying, reflex tearing tended to increase TFT greatly post following blink.

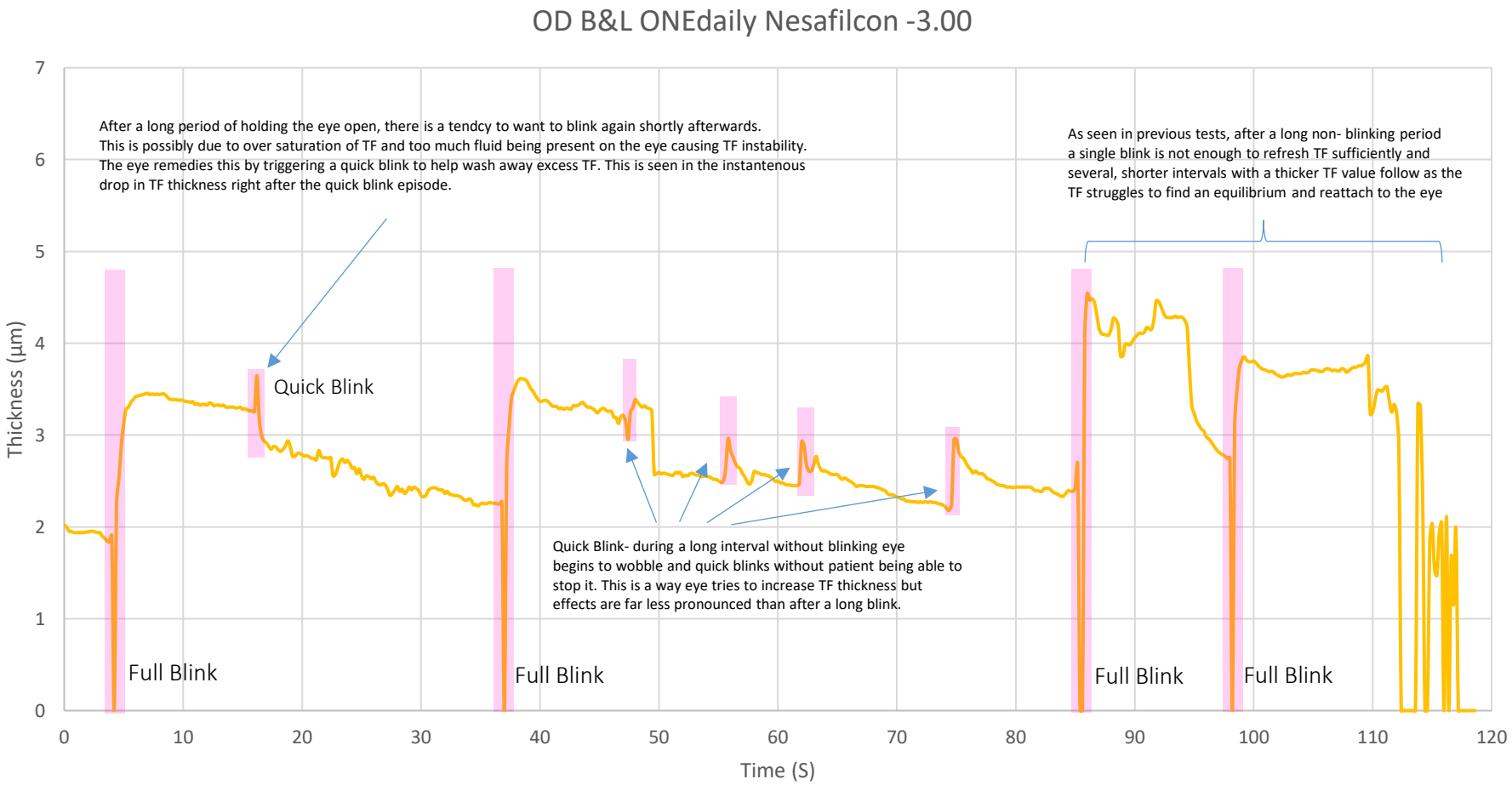

Figure 3-8: Tear Film Thickness on B&L One Daily Contact Lens over time

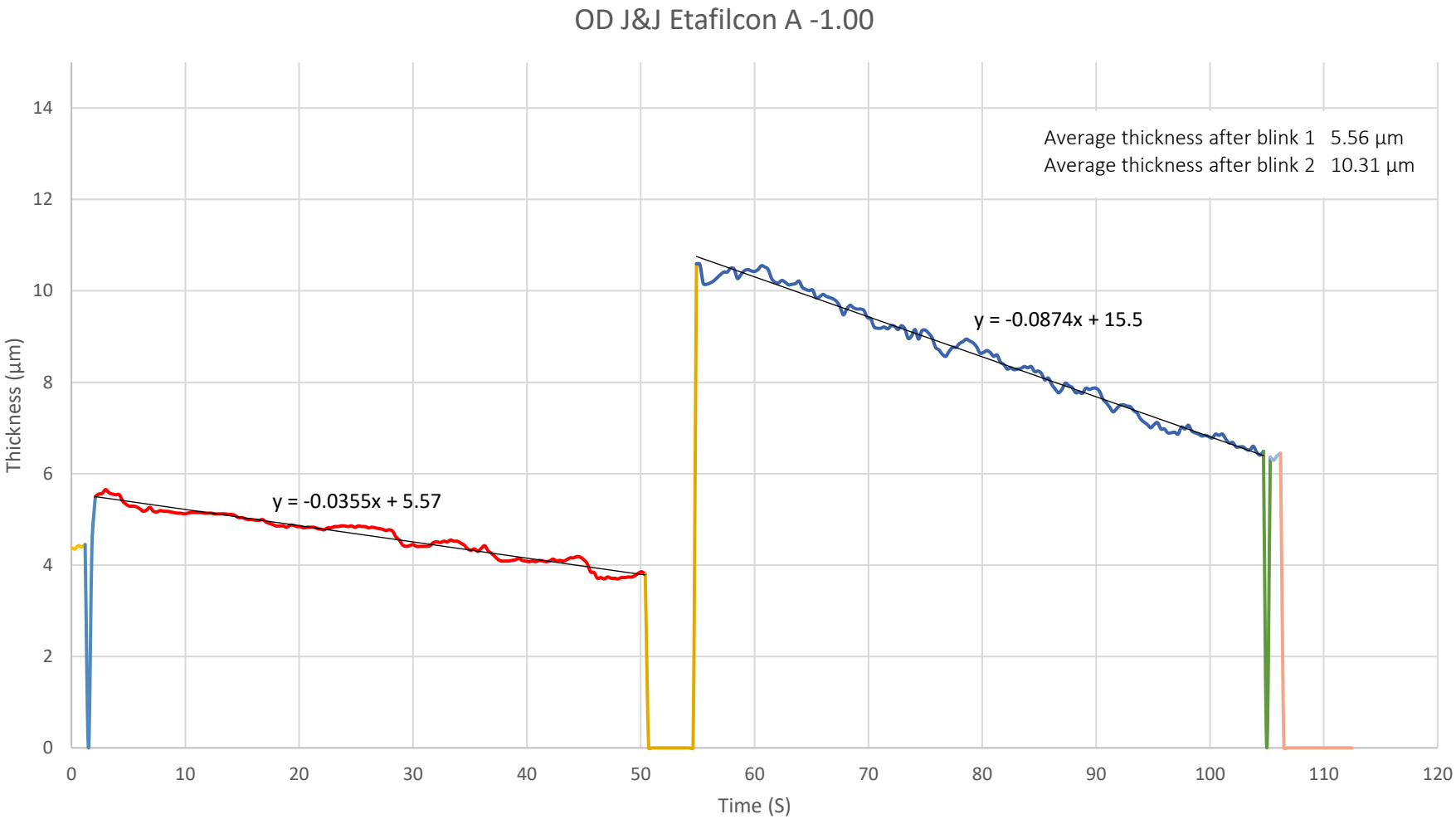

Figure 3-9: Tear film thickness and thinning rate with Johnson and Johnson Etafilcon Lens. Variation in tear film thickness is significant after each blink and no single value can be assumed to be the absolute thickness

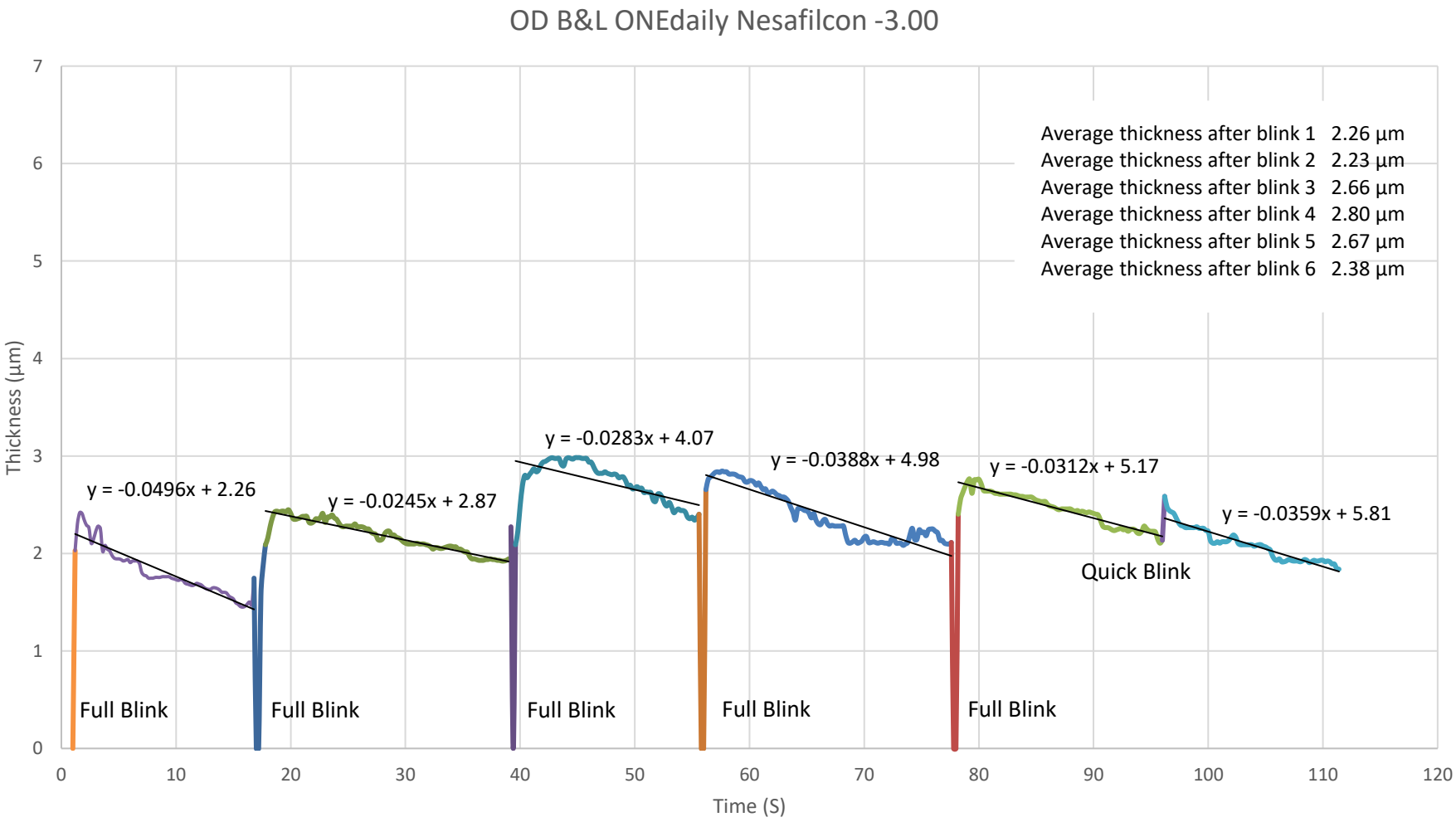

Figure 3-10: Tear film thickness and thinning rate with B&L Nasofilcon lens

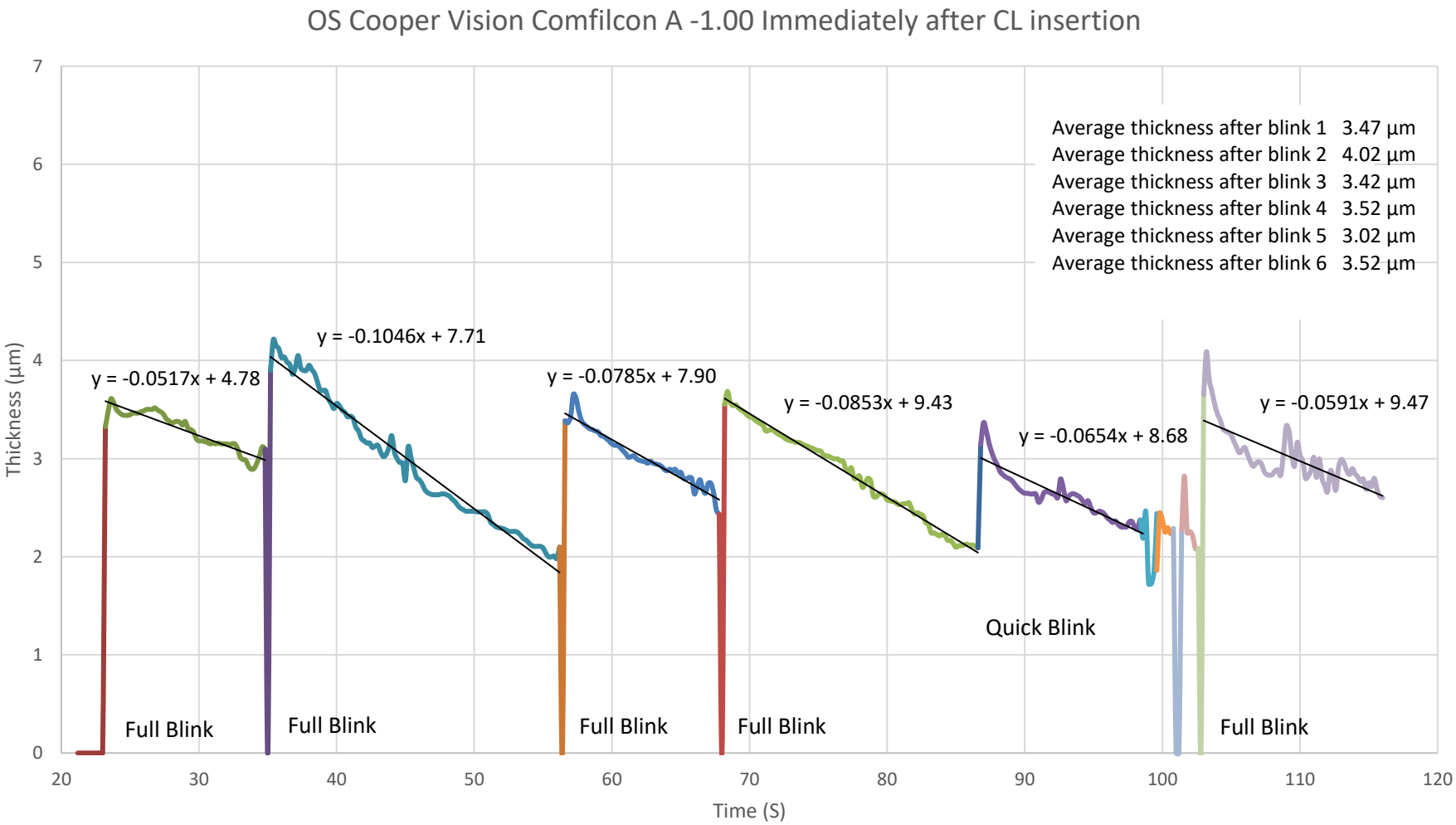

Figure 3-11: Tear film thickness and thinning rate with Cooper Vision Comfilcon immediately after insertion

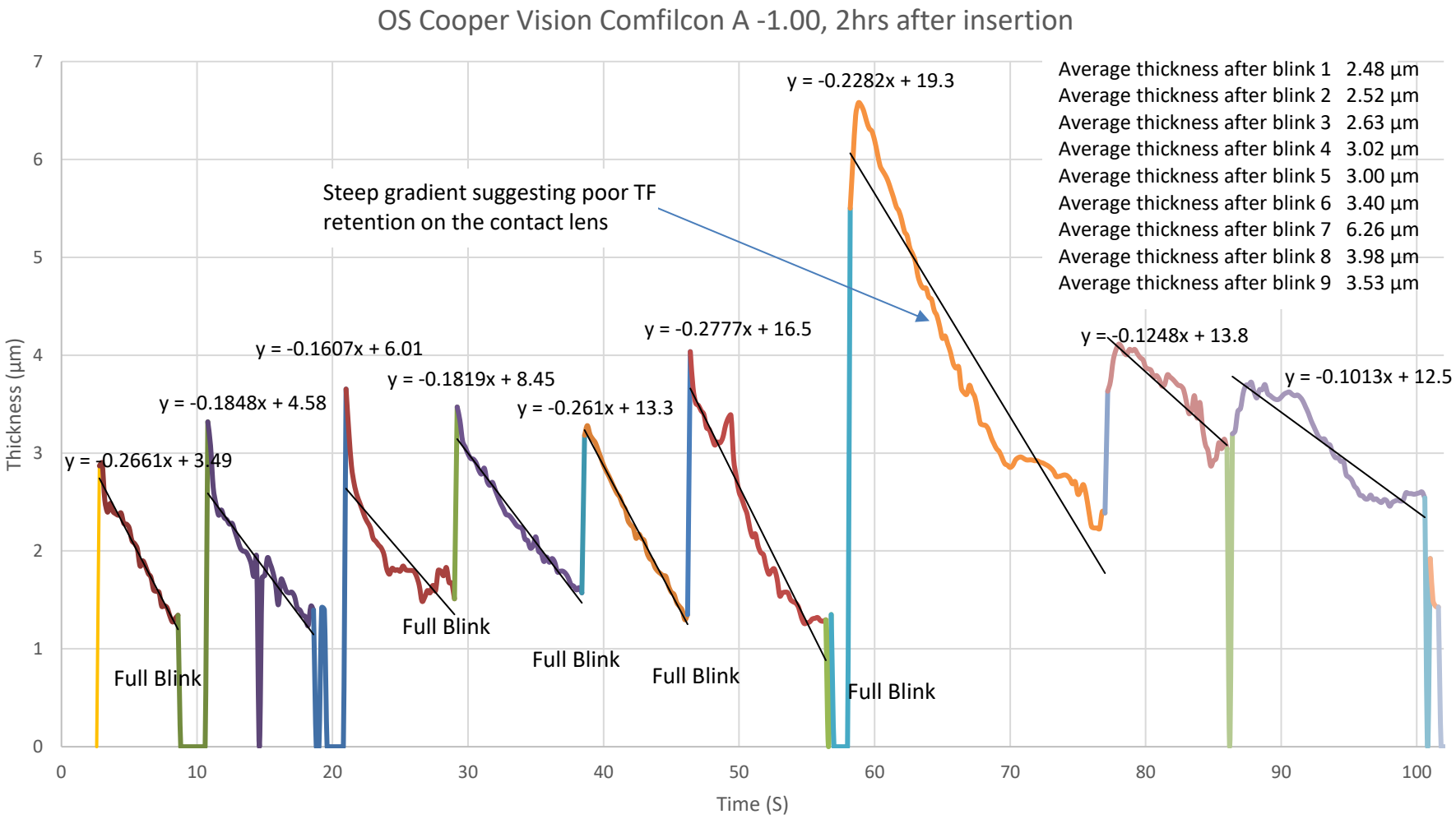

Figure 3-12: Tear film thickness and thinning rate with Cooper Vision Comfilcon 2hrs after insertion

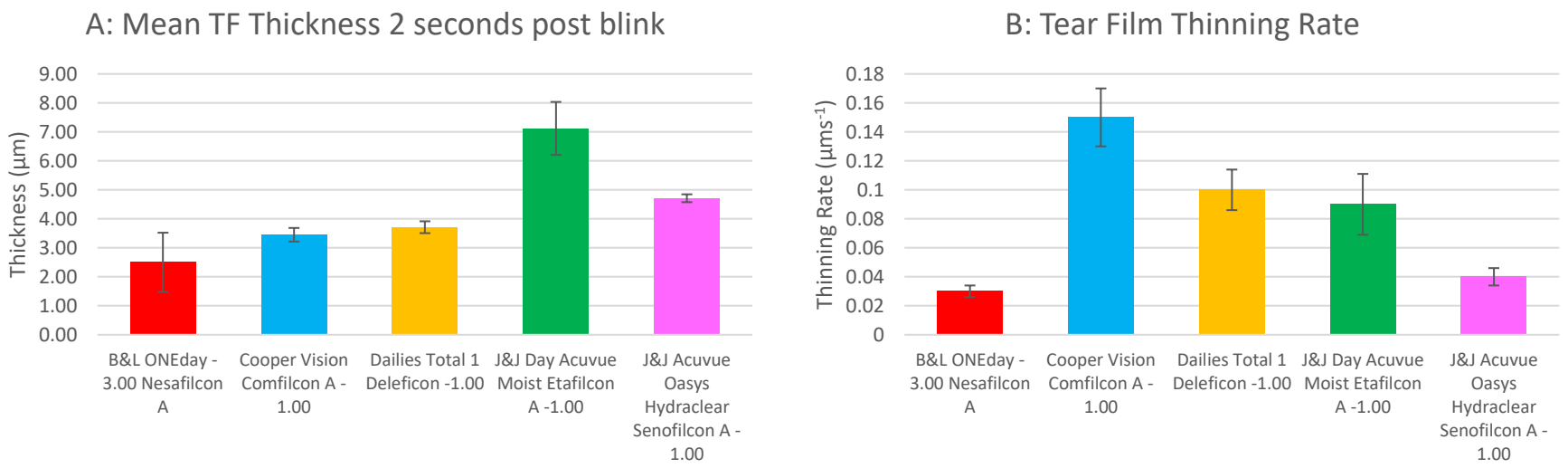

Figure 3-13: (A): Comparison of Tear Film Thickness over a 2 second period post blink with inserted contact lenses. (B) Corresponding tear film thinning rates between blinks on various contact lens materials

Table 3-7: Contact lens mean TF thickness and thinning rates

Contact Lens	Mean TF Thickness 2 Seconds after blink	Standard Deviation	Standard Error		Mean Tear Film Thinning Rate	Standard Deviation	Standard Error
B&L ONEday -3.00 Nesafilcon A	2.50	±0.241	1.021		0.03	±0.010	0.004
Cooper Vision Comfilcon A -1.00	3.45	±0.909	0.235		0.15	±0.077	0.020
Dailies Total 1 Deleficon -1.00	3.71	±0.868	0.205		0.10	±0.060	0.014
J&J Day Acuvue Moist Etafilcon A -1.00	7.12	±2.040	0.914		0.09	±0.048	0.021
J&J Acuvue Oasys Hydraclear Senofilcon A -1.00	4.71	±0.431	0.136		0.04	±0.018	0.006

3.9. Experiment D: Central corneal thickness & anterior chamber depth

Anterior chamber depth (ACD) is a crucial parameter to help determine risks of closed angle glaucoma and is known to fluctuate in length and volume throughout the day as variations in intraocular pressure push on the posterior face of the crystalline lens [285]. Current methods of measuring ACD include the use of Scheimpflung imaging [275], ultrasound techniques [286] and OCT scanning [274, 287, 288].

Central corneal thickness was measured by focusing on the naked eye at the same corneal apex as in earlier tests. Chin rest and the OBE was again used for positioning. All data was captured on a single subject. Corneal refractive index used was 1.377 from earlier established values [280].

Table 3-8: Controller and probe combinations tested under experiment D

	Micro Epsilon ConfocalDT				Precitec		
Controller	IFC 2451		IFC2461		CHRocodile SE		
Probe	0.3mm	3mm	0.3mm	3mm	2mm	12mm	180µm

3.9.1. Experiment D Results

When attention was turned to central corneal thickness, the Micro Epsilon confocalDT IFC2451 controller in combination with IFS2405- 3 mm probe registered a steady reading of 508.951 ± 0.36 µm in line with expectations of 0.534 mm [45]. Figures 3.14 & 3.15 are screenshots of the measurement screen. A peak to peak value of 0.00071mm indicates a strong signal from both anterior and posterior surfaces with little error. Instrument loan time restrictions prevented corneal thickness testing with the second IFC2461 controller, but surfaces were easy to recognise and the signal proved very consistent over a long time period. It would be reasonable to say that the IFC2461 controller coupled with the 12 mm probe would be easily capable of registering corneal thickness across repeated measures.

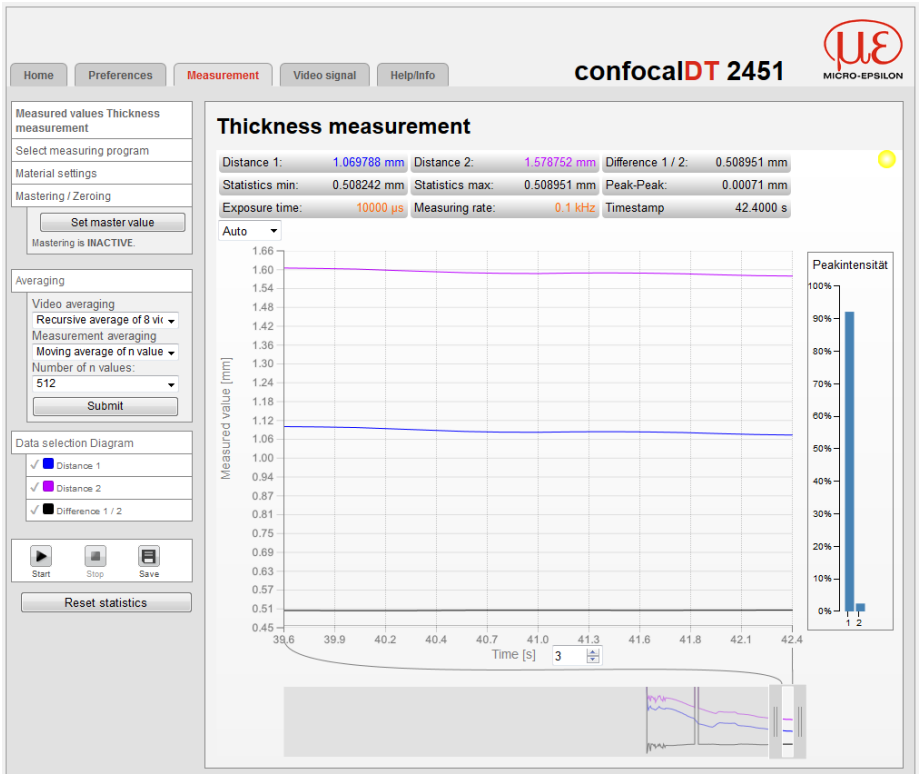

Figure 3-14: Screenshot of ConfocalDT 2451 measurement results for corneal thickness measurement. Pink and blue lines are identified surfaces. Black line is calculated material thickness.

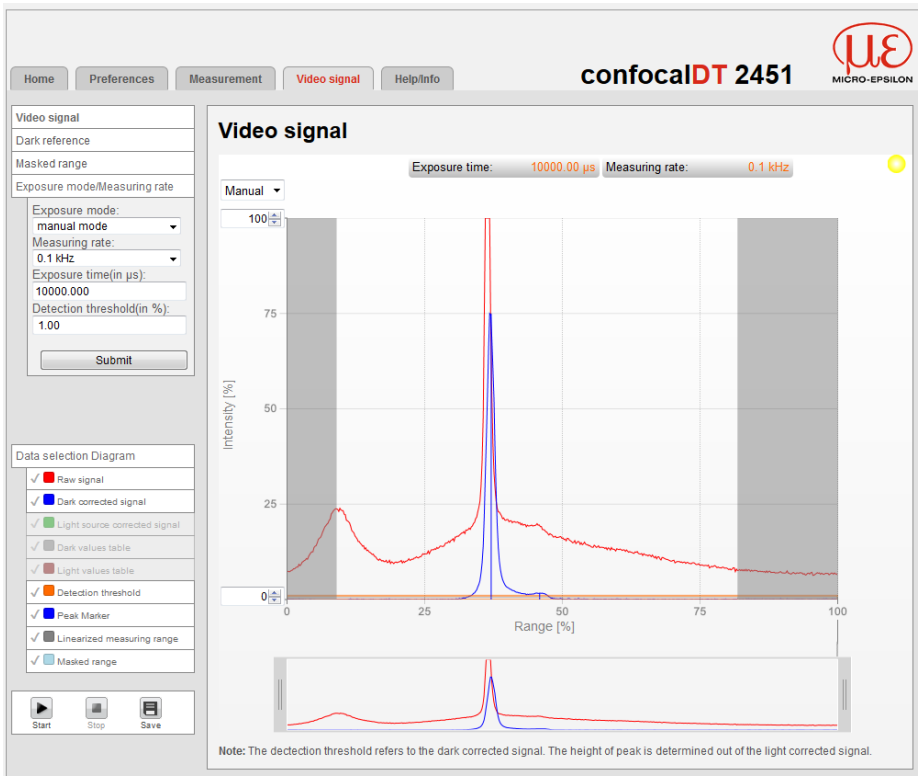

Figure 3-15: Screenshot of ConfocalDT 2451 return signal strength. The first peak indicates the anterior cornea and the second, the posterior surface. Notice how much weaker the second peak is which is due to attenuation as light energy is absorbed by cornea material

The Precitec CHRocodile SE instrument in combination with either the 2 mm or 12 mm confocal probes was not capable of easily distinguishing the rear surface of the cornea. Figure 3.16A is the trace from the 2 mm probe. Although the first peak (corneal epithelium) is clear, the second (corneal posterior) is much weaker and is shrouded in noise. A reliable corneal thickness value could not be generated from the 2 mm probe.

Secondary investigations into deeper anterior eye dimensioning continued with the 12 mm probe and although signal strength was significantly reduced, a single reading of 4.204 mm was achieved for corneal epithelium to crystalline lens distance, also known as anterior chamber depth (ACD). Expected value sit between 2.9 and 3.6 mm [289]. Repeated test could not reproduce these results. Although the recorded measurement was outside of accepted range, the reading includes the thickness of the cornea. Once subtracted a closer value of 3.67mm is achieved. However, it must be noted that the anterior chamber is filled with aqueous humour fluid which is of a different refractive index than the cornea. The same is true for the crystalline lens. Just like the confocalDT equipment, the CHRocodile SE controller can only allow for a single refractive index input per test, with such a restriction preventing the true measure of multi medium tissues.

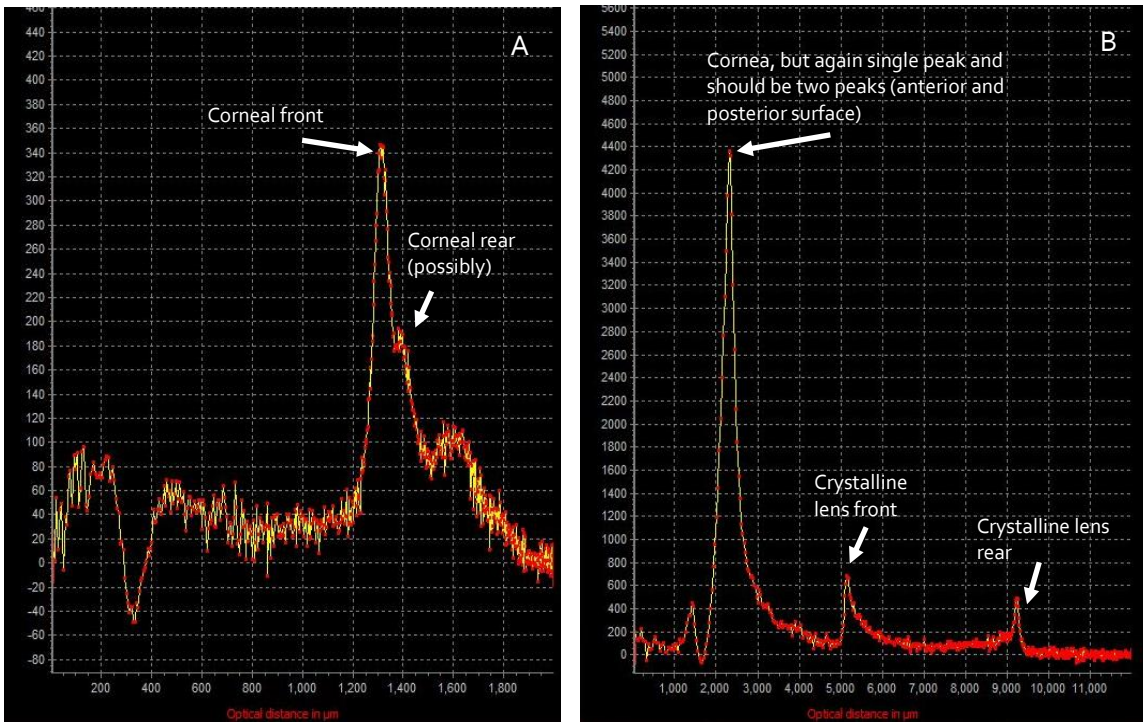

Figure 3-16: A) 3 mm probe signal capture. There is much noise in the trace but a clear peak Is visible in the 1,300 region. A second, weaker peak which could be the corneal posterior surface is present in the 1,400 region. B) 12 mm probe with several peaks clearly visible. First peak is corneal epithelium but posterior surface not registered. Not possible to see corneal thickness. Following peaks are estimated to be crystalline lens front and rear surfaces.

3.10. Experiment E: Contact lens thickness

When a contact lens is inserted into the human eye the tear film fluid is absorbed by the lens and inflates to its manufactured shape. Different contact lens materials will absorb differing amounts of fluid and the TF itself splits into two layers- the pre- lens tear film (PLTF), which keeps the surface of the lens smooth and hydrated, and the post- lens tear film (POTF), which acts as a cushion between the lens and the cornea [282].

To accurately assess real world contact lens central thickness it is therefore best to measure lenses in their native environment which mimics the human eye as closely as possible.

A custom designed, self-centring lens plate was created in Solidworks 2015 (*Dassault Systems, Vélizy- Villacoublay, France*) and 3D printed on a Stratasys UPrint SE (*Eden Prairie, Minnesota, United States*). The plate was inserted into a 35mm polystyrene culture dish (*Corning Glass Works, Coming, New York, USA*) and placed over a USB Celestron digital microscope with onboard white LED light source (*Celestron, Torrance, California, United States*). The microscope was intended to be used to ensure correct lens placement and that the centre of the probe was focused on the centre of the lens, as shown in Figure 3.17. Saline solution of 0.9% concentration was added to the dish to a level that ensured full submersion of the lens.

Individual lenses from various manufacturers were placed into the plate and position was checked with the microscope. Software settings including exposure time and averaging were all modified systematically to achieve best signal to noise ratios.

Lenses of varying compositions and strengths were tested consecutively. As probes have a restricted measurement angle to the surface (Precitec CHRocodile SE is especially sensitive, allowing only ±5° off axis), all measurements were conducted on central lens thickness. Three axis OBE was employed to allow for precise positioning of probe in relation to contact lens. All tests were allowed to run over the course of 10 seconds once a steady reading has been registered to allow for averaging functions to have enough data points to generate a steady measurement value.

Table 3-9: Controller and probe combinations tested under experiment E

	Micro Epsilon ConfocalDT				Precitec		
Controller	IFC 2451		IFC2461		CHRocodile SE		
Probe	0.3mm	3mm	0.3mm	3mm	2mm	12mm	180µm

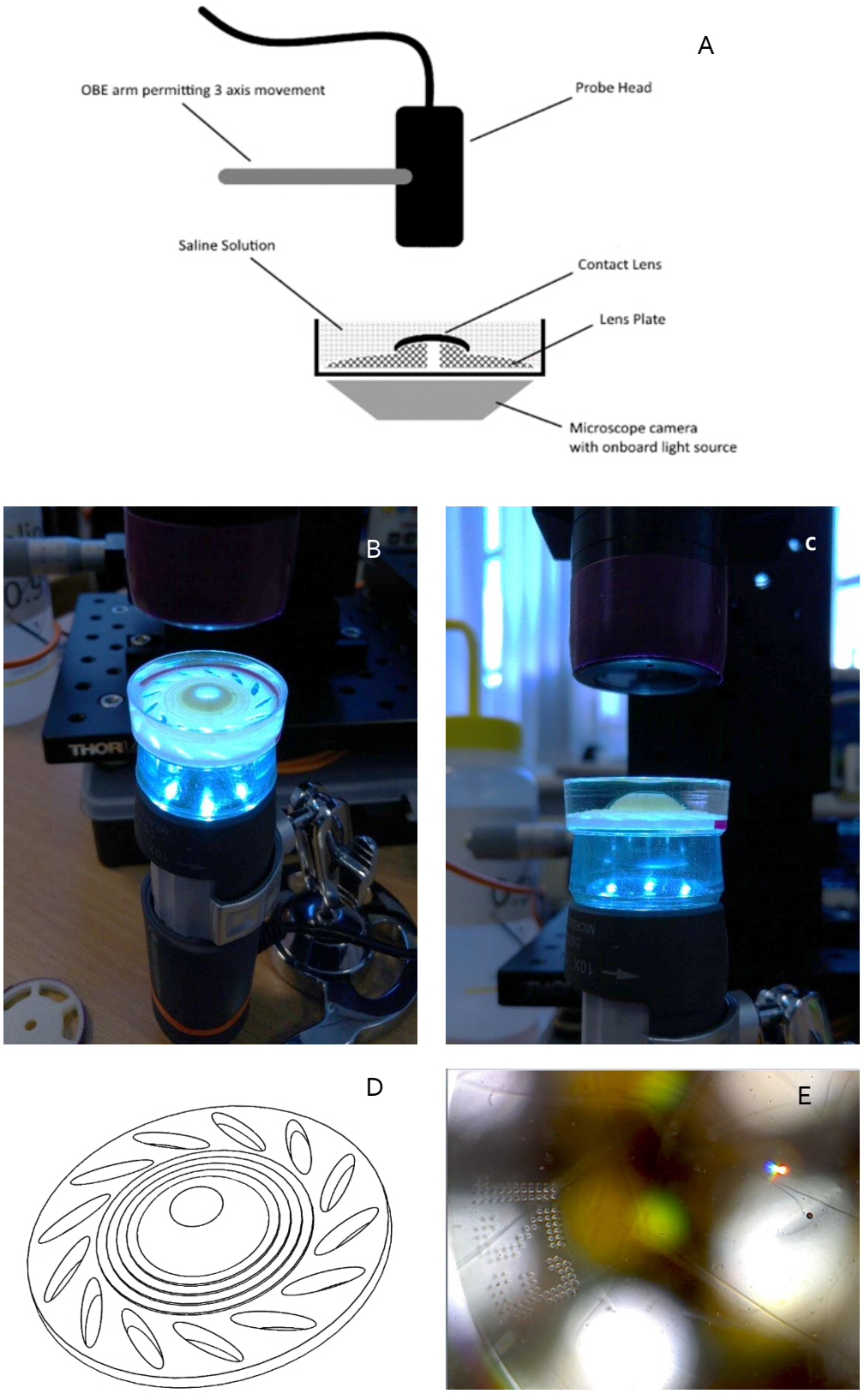

Figure 3-17: A) Contact lens measurement apparatus setup B) Saline test well placed on top of camera and illuminated from below. C) When placed in Saline, the lens has an extremely close refractive index to the solution, making it appear almost invisible, but outline can be boosted but lower light source D) Placeholder disk created to hold contact lenses in position E) Contact lens viewed from below suspended in saline solution. Rainbow dot shows measurement position. Edge of lens with identifying inscription can be seen on left.

3.10.1. Experiment E Results

Recognition of the lenses was not straight forward due to the lenses quickly absorbing the saline solution that they were submerged in. Although this is an expected phenomenon and produces correctly shaped lenses, this posed a problem for the instruments as the relatively uniform RI between the lenses and saline solution have the consequence of causing the lens to become in essence invisible to the probe. Various techniques were attempted, but what yielded the best results was a slight tilt of the probe head in relation to the contact lens surface. In addition, the underside light source provided by the USB camera allowed for greater recognition of the lens surfaces by the probe. The confocalDT instruments proved superior in detecting lens dimensions during complete submersion. Table 3.13 is a list of all lenses tested and their measured thicknesses on various controllers.

In table 3.13, column 5 lists manufacturer provided thickness values for -3.00D powered lenses [290]. Micro Epsilon confocalDT IFC 2415 was capable of measuring the J&J Acuvue Moist lens to the exact dimensions, 0.0844 mm ± 85nm, as provided by the manufacturer. A similar level of accuracy is obtained when measuring the Alcon Air Optic Aqua lens, (0.08 actual, vs. 0.073 ± 49nm measured). With lenses, of powers ≠ -3.00, verification of results is not possible as dimensional data is not obtainable from manufacturers. Precitec CHRocodile SE chromatic performed poorer with obtained values showing greater discrepancy compared with the confocalDT equipment. CHRocodile SE Interferometric measurement produced poor signal to noise ratio with most tested lenses failing to be recognised. This could be due to a weaker source signal from the controller that is diminished by passing through the saline to reach the lens. Equally, the Precitec CHRocodile SE equipment is more sensitive to the angle of incidence and misalignment, with only a ±5˚ degree of freedom between probe and sample whereas ±45˚ was allowed for the confocalDT. This increased alignment sensitivity could have been enough to cause readings to fail.

Table 3-10: Results of central contact lens thicknesses through various controllers and scanning methods. Actual lens values taken from the ACLM Contact Lens Year Book 2013 [290]

				Central lens thickness submerged in 0.9 % Saline as measured (mm)			
Manufacturer	**Lens Name**	**Primary Material Composition**	**Lens Power**	**Actual Dimension [All lenses at -3.00 Dioptres] [1]**	**Micro Epsilon confocalDT IFC 2415 [3mm Chromatic]**	**Precitec CHRocodile SE [2 mm Chromatic]**	**Precitec CHRocodile SE [180µm Interferometric]**
Alcon	Air Optix Aqua	Lotrafilcon A	- 3.00	0.08	0.0731 ± 0.0000490	1.53085	N/T
Alcon	Dailies Aqua Comfort Plus	Nelfilcon A	- 3.00	0.10	N/T	N/T	Failed
Bausch & Lomb	Bio True One Day	Nasofilcon A	- 3.00	0.10	N/T	N/T	Failed
Cooper Vision	Proclear 1 Day Multifocal	Etafilcon A	- 10.00	0.09	0.06.14 ± 0.000236	N/T	N/T
Cooper Vision	N/A	Comfilcon A	+ 3.00	N/A	0.2.05 ± 0.0000250	0.25261	N/T
Johnson & Johnson	1Day Acuvue True Eye	Narafilcon A	- 1.00	0.085	0.0804 ± 0.000675	0.83017	0.08685
Johnson & Johnson	Acuvue Oasys for Presbyopia	Senofilcon A	+ 1.25	0.07	0.07.47 ± 0.0000120	0.131911 - 0.14762	N/T
Johnson & Johnson	1Day Acuvue Moist	Etafilcon A	+ 6.00	0.084	0.223 ± 0.0000310	0.2234	Failed
Johnson & Johnson	1Day Acuvue Moist	Etafilcon A	- 3.00	0.084	0.08.44 ± 0.0000850	0.65779	N/T
Johnson & Johnson	Oasys Hydraclear	Senofilcon A	-1.00	0.07	N/T	N/T	0.06578
Johnson & Johnson	Oasys Hydraclear	Senofilcon A	- 9.00	0.07	N/T	N/T	Failed

1) Central contact lens thickness related to a standard lens power of -3.00 dioptres

2) N/T = Lens not tested on particular instrument

3.11. Experiment F: Contact Lens recognition in unopened packaging

Manufacturers of CLs must ensure quality control of their manufacturing processes and guarantee that any finished contact lens units that are being distributed to customers must contain a lens. In rare occasions customers have purchased their CLs only to find empty packets without any lenses present due to packaging faults. Recognition of lens presence in unopened packaging is therefore a desirable test and could provide a high-speed quality control solution.

This test includes a measure of empty packaging without a lens or any saline fluid present. Once packaging thickness is measured, a second (this time unopened) packet was measured with saline fluid and lens present. Results show that device is able to recognise lens in closed packaging.

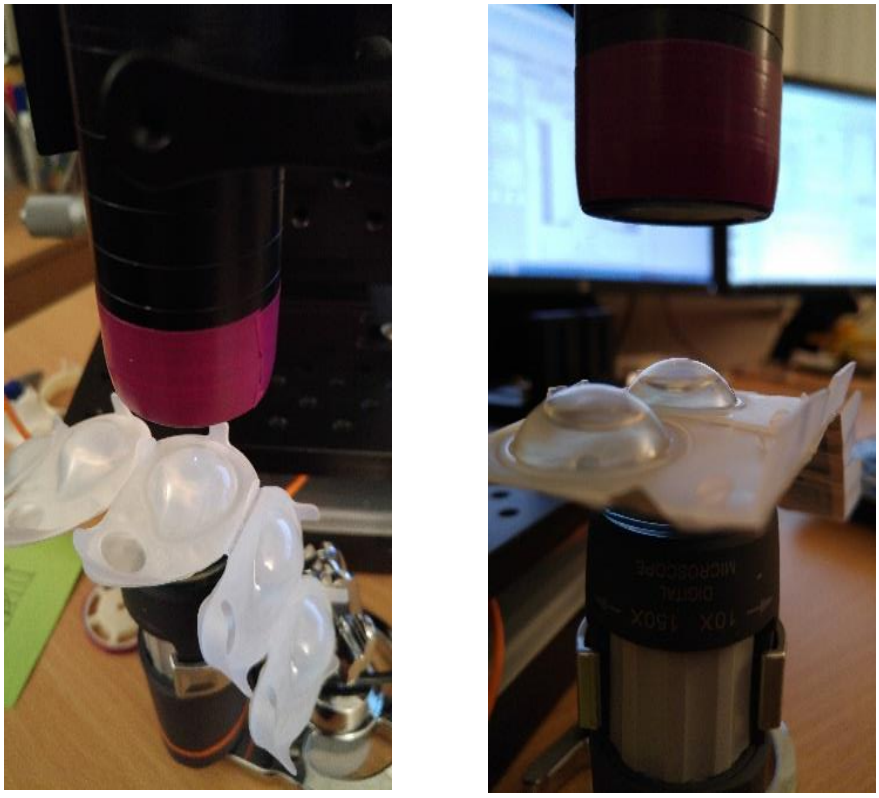

Figure 3-18: Micro Epsilon confocalDT IFC2451 controller with 3mm sensor focused on lens in unopened packaging

Table 3-11: Controller and probe combinations tested under experiment F

	Micro Epsilon ConfocalDT				Precitec		
Controller	IFC 2451		IFC2461		CHRocodile SE		
Probe	0.3mm	3mm	0.3mm	3mm	2mm	12mm	180µm

3.11.1. Experiment F Results

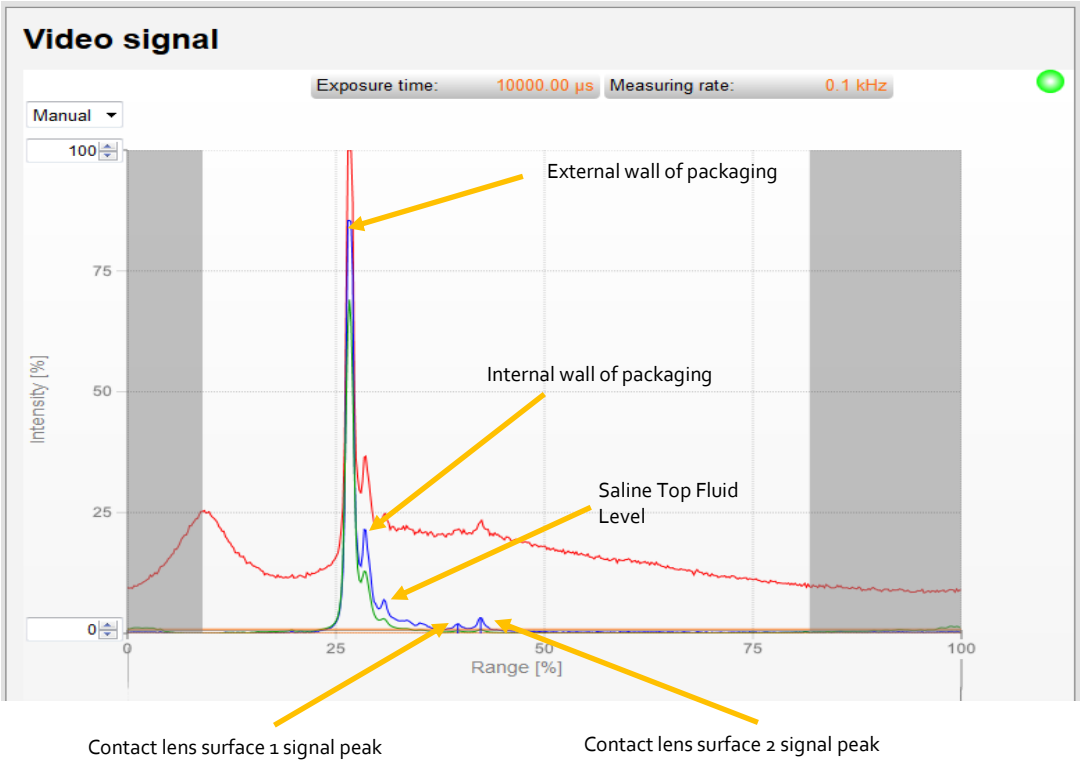

Figure 3-19: Screenshot of ConfocalDT data capture showing the various points through the contact lens packaging at which a surface is recognised. As signal travels deeper through various materials, signal strength rapidly decreases

Detection of CL presence in closed packaging was successfully accomplished by the Micro Epsilon confocalDT IFC 2415 controller. Two J&J 1 Day Acuvue Moist lenses of +6.00 and -1.00 power in unopened packets were evaluated. Thickness values of 0.13756 mm was obtained for the +6.00 lens, whereas a distance from packaging to lens top surface of 0.815417 mm was registered for the second lens. These readings need to be taken into context as the random nature of the lens positioning within the packaging does not guarantee that central lens region will be directly centred with the zenith of the packaging. What is important in this test is the ability of the instrument to recognise that a detectable surface exists within the saline fluid in unopened packaging. Reliable thickness readings would require a complete redesign of common contact lens packaging to ensure identical lens positions between packets. Similar experiments were repeated with CHRocodile SE chromatic in combination with the 12 mm probe and the instrument was capable of recognising a J&J Acuvue Oasys for Presbyopia +4.00 lens in unopened packaging. Interferometric measurement was unsuccessful, but no doubt the short probe working distance (180µm) was the primary reason for the failed reading. Custom probes could be designed to overcome such shortcomings but that is outside the scope of this work.

3.12. Experiment G: B- Scanning Model Eye

Simple one directional scanning as used in the above tests provides useful data in a single, Z-space dimension, but does not provide a picture of the entire eye and crucial details can easily be missed. A three axis, movable stage device was built combining OBE with Nanotech (*Feldkirchen, Germany*) stepper motors which was controlled through a custom programmed LabView interface (*National Instruments, Texas, United States*) which allowed the 3 mm probe head to follow the circular profile of an object that was being measured. Refractive index used was 1.48, acrylic. It was quickly recognised that B- scanning would not be currently possible with existing equipment on human subjects due to the large dimensions of the machine and the relatively close working distance requirements. Instead the profile of a model eye cornea, was selected as a reasonable alternative for the first step in B-scanning exploratory work.

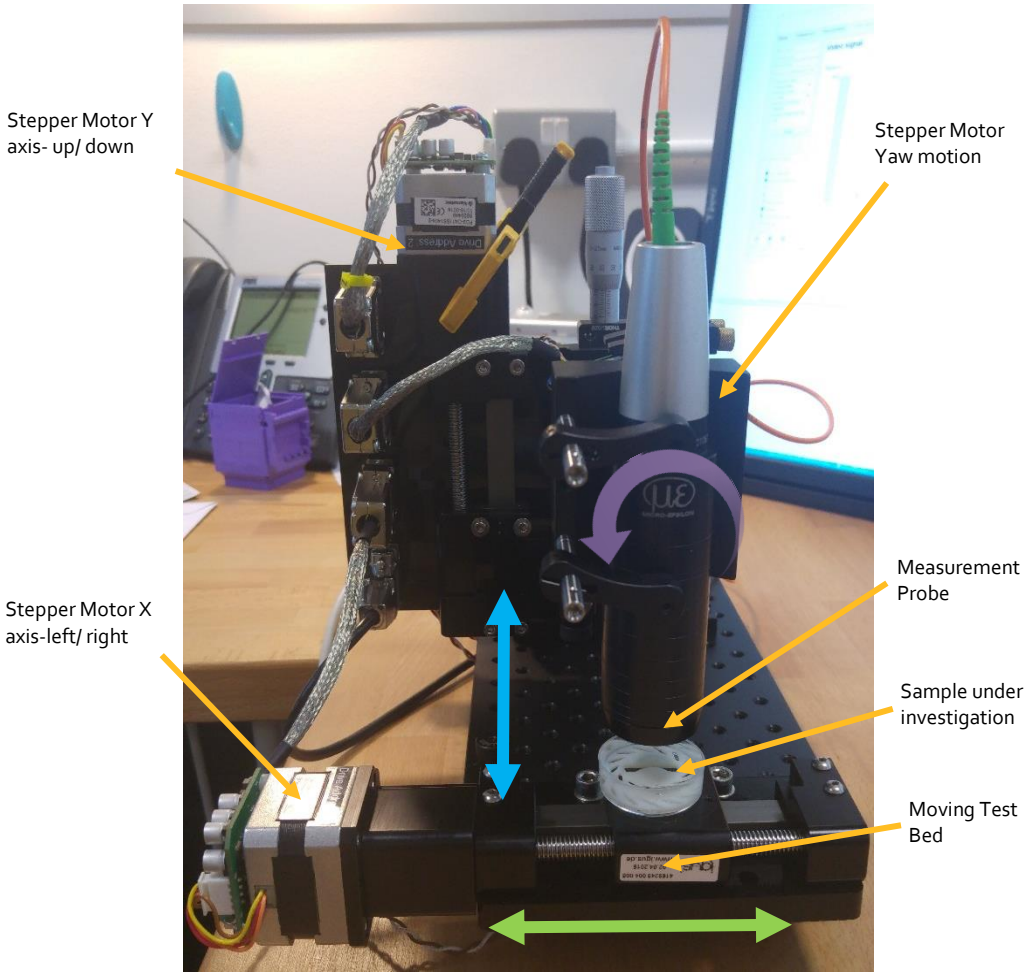

Figure 3-20: Custom built 3 axis b- scanning OBE platform controlled through LabView

Table 3-12: Controller and probe combinations tested under experiment G

	Micro Epsilon ConfocalDT				Precitec		
Controller	IFC 2451		IFC2461		CHRocodile SE		
Probe	0.3mm	3mm	0.3mm	3mm	2mm	12mm	180μm

Unfortunately, due to equipment rental restrictions, the CHRocodile SE instrument was not available during the B-scanning phase and no investigations were able to take place. From the confocal equipment the 3 mm probe was selected due to the working distance and measurement depth capability.

3.12.1. Experiment G Results

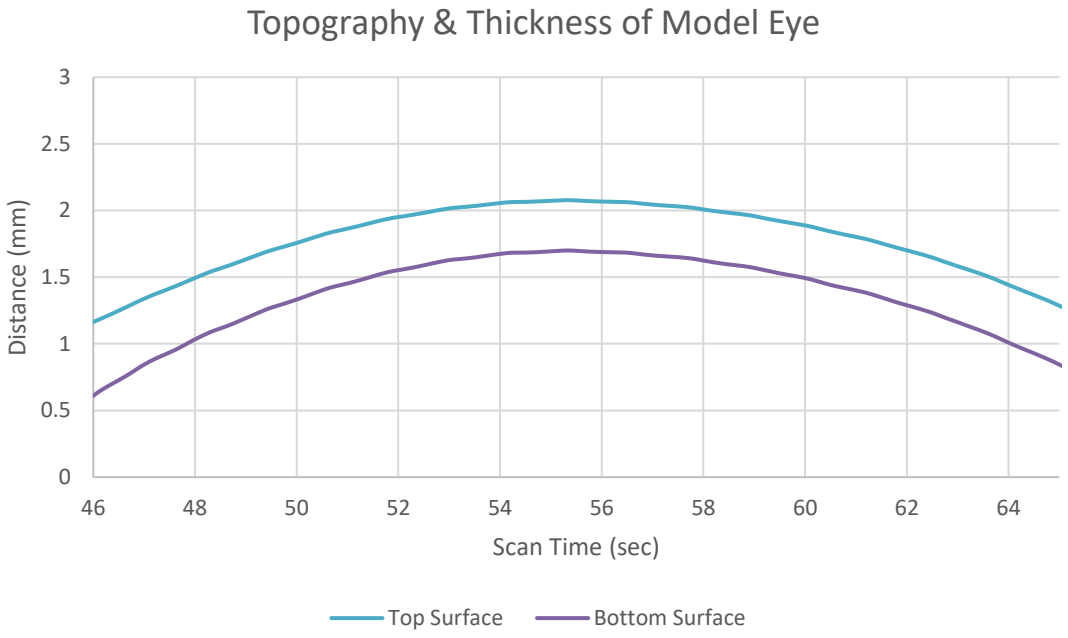

Figure 3-21: Model eye wall thickness profile

Scanning of the plastic model eye proved successful and a strong stable signal was achieved across the entire profile as seen in figure 3.19. The blue and purple lines show the contours of both the external and internal plastic corneal surface. As expected, they are smooth and continuous with a gradual increase and decrease in gradient that would reflect a true corneal profile. This successful experiment set the stage for further testing of B- scanning possibilities.

3.13. Experiment H: B- Scanning Porcine Eye

Experiment G was repeated but with a recently harvested porcine eye (< 12 hrs) as a sample in an attempt to understand measurement performance on tissue. Although the refractive index of the porcine eye was not known, the value was changed to 1.3371 to reflect the RI value of the human cornea. The purpose of this test was to gauge how deep the probe signal could penetrate into the eye and record various surfaces inside the eye during B- scanning moving conditions.

Table 3-13: Controller and probe combinations tested under experiment H

	Micro Epsilon ConfocalDT				Precitec		
Controller	IFC 2451		IFC2461		CHRocodile SE		
Probe	0.3mm	3mm	0.3mm	3mm	2mm	12mm	180µm

3.13.1. Experiment H Results

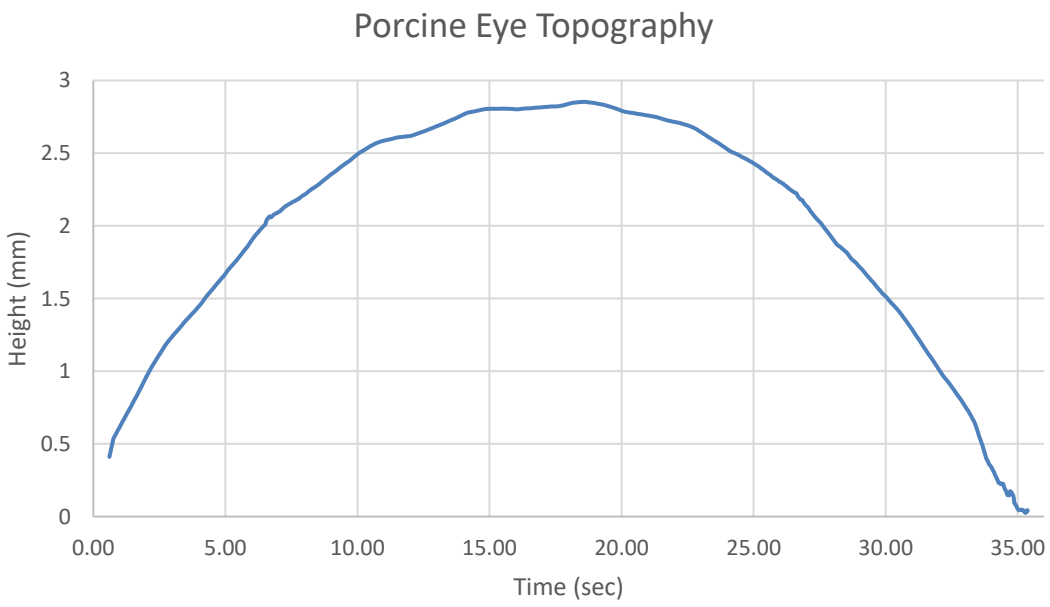

Figure 3-22: B- Scanning topography profile of porcine eye

Programming of the individual motor movement had to be precisely controlled as the probes needed to be held within a certain distance and angle to maintain acceptable tolerance. B- Scan results from the porcine eye yielded few results. A sample of the data captured is seen in figure 3.22. Only the top surface of the eye was measured and the profile itself is irregular and not symmetric. Although height values have been attained, they are simply distance in relation to the probe lens which is not particularly useful information.

Details within the eye were not measured, even under repeated attempts. This highlights the issues with using such technology in a B scanning application. For the second surface to be recognised a certain amount of data averaging needs to be factored in to the measurement. This fundamentally requires that the point of scan be held over the same area for several seconds for an average to be established. For a moving operation, such as B- scan, the point of measurement is constantly moving over the surface of the object. B- Scanning therefore is not recommended with this instrument as complex surfaces, such as the surface of the human cornea, would be better served by OCT technology which uses high speed galvanic mirrors to project the scanning path while keeping the probe stationary. Coupled with the weight of the probe and working distance requirements this technique is unsuitable for B- scanning application in its current form.

As the porcine eye aged it became cloudy and opaque which meant it was no longer suitable for testing. The porcine eye was treated in agreement with the Animal and Plant Health Agency APHA commercial movement of animal by-products and disposed of under Aston University guidelines.

3.14. Experiment I: B- Scanning Contact Lens Profile

The final experiment in B- scanning mode was to measure the profile of contact lenses submerged in saline solution. The lenses would be placed in a modified placeholder with a hollow channel running across the centre to prevent the signal from being confused with the plastic material holding the lens in position. Although difficult to distinguish, figure 3.23 shows a contact lens submerged in 0.9% saline solution being held in a centre position across the probe path. Probe was programmed on Labview to move across entire lens profile from bottom to top.

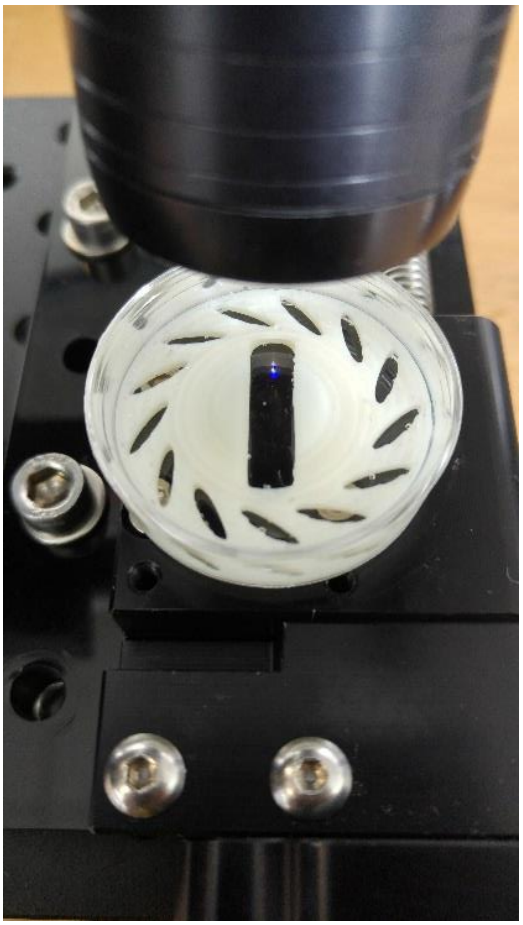

Figure 3-23: Modified placeholder with central channel allowing for contact lens to be held in a stable position during testing

Table 3-14: Controller and probe combinations tested under experiment I

	Micro Epsilon ConfocalDT				Precitec		
Controller	IFC 2451		IFC2461		CHRocodile SE		
Probe	0.3mm	3mm	0.3mm	3mm	2mm	12mm	180µm

3.14.1. Experiment I Results

Contact lens top and bottom profiles were visible in the centre of the lens but as the probe was moved to the periphery the signal was lost. This could be attributed to the lens periphery being submerged at progressively deeper depths below the saline solution leading to a decrease in signal strength returning to the probe. Other lenses produced similar results.

As mentioned earlier, the ConfocalDT controller uses sample averaging to generate reliable distance and thickness data. This may only work in a fixed mode of operation where the object and probe are held steady together but once movement is introduced the probe can no longer reliably measure a particular point on a curved surface due to the continuous passing of the material. The solution to this may require feedback signals to be returned from the controller to the stepper motors. Once a particular coordinate has been measured, a signal is sent to move the sample to the next point of measurement. Reliable thickness at each point would then be possible. Greater measurement exposure can be allowed for regions where signal strength is weak. Nevertheless, the proposed solution would add considerable time to any measurement program and the limits of what is reasonable to measure using this particular technology are now clear.

Table 3-15: List of all tests carried out by various controller/ probe combinations. Test descriptions in left column correspond to studies above

Experiment	Measurement Type	Instrument & Probe Combination						
		Micro Epsilon ConfocalDT IFC2451		Micro Epsilon ConfocalDT IFC2461		Precitec CHRocodile SE		
		0.3 mm	3 mm	0.3mm	3 mm	2 mm	12 mm	180 µm
A	Tear film thickness assessment	NP	NP	NP	NP	NP	NP	✓
B	Tear film thickness with artificial tears	-	-	NP	NP	NP	NP	✓
C	Tear film thickness with contact lenses	-	✓	-	-	✓	-	NP
D	Central corneal thickness & anterior chamber depth	-	✓	-	-	•	•	-
E	Contact lens thickness	-	-	-	✓	•	-	NP
F	Contact Lens recognition in unopened packaging	-	✓	-	-	-	✓	-
G	B- Scanning model eye	NP	-	-	-	-	-	-
H	B- Scanning porcine eye	NP	-	-	-	-	-	-
I	B- Scanning contact lens profile	NP	-	-	-	-	-	-

✓ *= Results Positive*

• *= Attempted, results inconclusive*

NP = Not Possible

- = Not Attempted

3.15. Discussion

Thorough evaluation of all controller and probe combinations have led to confident conclusions about the possibilities and limitations of the two low cost confocal and interferometric devices. Each instrument demonstrated strengths and weaknesses depending on application. Continuous TFT and thinning data has been collected in unprecedented detail over the course of a blink and subsequent open eye period. The value of 3.28 µm obtained through Precitec CHRocodile SE interferometric measurement corresponds within established measurements obtained through accepted methods [92, 97, 282]. Extremely close refractive indexes of anterior eye anatomy are crucial to clear unobstructed vision but cause both controllers to struggle to recognise individual surfaces and separate the TF from cornea. A more pressing issue is the small scanning area that is offered by the probes; a 9 µm spot diameter. There is little use in providing TF data on just the corneal apex as abnormalities may be occurring at different regions of the cornea or even sclera that will have an effect on TF stability [36]. Indeed, it is the upper region of the cornea that tends to frequently experience breakup- a region that is completely ignored by such a small spot size of both tested devices.

TF thinning rates varied from blink to blink and a value of $0.048 \pm 0.034\ \mu m^{-2}$ has been calculated as the average of this initial study. Kimball et al. placed air tight goggles on subjects to measure evaporation effect in an enclosed environment and achieved a mean $0.054 \pm 0.071\ \mu ms^{-1}$ evaporation rate in free air conditions [291]. This corresponds very closely to the acquired thinning results. With greater control over blinking behaviour and frequency, a clearer picture of exactly how these factors affect stability emerges, especially as this thickness is heavily dependent of blinking conduct [63, 261].

The exploratory testing conducted on TF was limited to a single healthy individual as tests were focused on equipment evaluation and feasibility of use rather than large scale data verification. Greater sample size is necessary to gain reliable baseline TF behaviour across healthy and diseased individuals. This may be possible in the theatre of research yet, coupled with the extremely short 180 µm working depth together with the considerable amount of patient training and perseverance required to maintain one's head completely stationary to capture data, the requirements are simply too great for common day to day assessment of raw tear thickness in real world patient diagnosis settings.

The insertion of CLs greatly aids the surface recognition and the TF can be identified and inspected far quicker. Although this now changes to an invasive category of measurement in healthy non- corrected subjects, it could be argued that daily contact lens wearers would

consider inserting CLs prior to TFT assessment as a norm and may even gain benefit as any results would reflect their standard conditions [292].

CLs had a considerable effect on TF thickness and this was dependent on which type of lens was inserted. Achieved thicknesses averaged for 2 seconds post blink ranged from 2.5 – 7.9 μm.

Chen et al. used a super luminescent diode based spectral domain OCT to view pre and post contact lens tear film thicknesses, reporting 1.7 ± 0.9 μm and 2.0 ± 1.5 μm respectively [93]. It has been proposed by Drone that TFT values change greatly at various points over an inserted contact lens and related research by Dos Santos et al.. and Schmoll et al. acquired TFT pre-contact lens values of 4.79 ± 0.88 μm and 5.1 ± 0.5 μm respectively [94, 96, 261]. Data acquired through the CHRocodile SE interferometric acquisition mode demonstrated that not only are tear film thicknesses different depending on lens material but that tear film thinning rates varied over the course of contact lens wear. Figure 3.11 and 3.12 are thinning rates for the same contact lens immediately after insertion and then 2 hrs later. A 0.199 μms^{-1} rate was recorded 2hrs after insertion as opposed to 0.074 μms^{-1} at the start of the wearing period.

All observations of TF characteristics, both with and without CLs, indicate the following general behaviours:

1. TF Thickness is variable after each blink and depends on prior conditions leading directly up to a particular blink instance. However, basal TF during typical conditions will refresh to roughly 2.7 – 4.5 μm post blink once TF has settled and spread over the ocular surface.
2. TF following a full blink will return close to nominal thickness, whereas quick partial blinks will temporarily boost the TF, but won't refresh the TFT to the same extent.
3. TF thinning will vary depending on the conditions before the latest blink (including but not exclusive to length of prior blink interval)
4. TF thickness and thinning rate is variable depending on CL material and may be subject to variation from patient to patient and duration of wear.

Compared with traditional interferometry, which is typically only capable of lipid layer assessment, or ultra- high resolution OCT which is far more expensive but offers faster scanning rates, the Precitec CHRocodile SE interferometric instrument is relatively low cost (sub £10,000)- significantly cheaper than OCT and readily available to purchase. Nevertheless, in the current off the shelf form it is not suitable for daily TF assessment. Precitec does offer probe

customisation and there is a probability that appropriate modification of the instrument can be tuned to better detect TF reflections and offer easier measurement, but further testing will be necessary to evaluate this.

Chromatic CL recognition can provide a robust substitute to existing OCT scanning techniques and even offers the potential of being capable of measuring the true dimensions of the CL as it is being worn by the patient. Since the inspected lens remain submerged in a native saline environment during measurement it can therefore retain its full hydrated profile. The Micro Epsilon system has proved capable for central contact lens thickness, but improvements to B-Scanning techniques need to be consolidated to potentially give full contact lens profile measurements.

The completion of this exploratory work has allowed for a greater understanding of the limits of this technology and can now lead to new avenues of anterior eye investigative study including;

a) Assessment and direct comparison on in vivo tear film thinning rates of various CL material compositions;
b) Assessment of tear film thickness and thinning rates in a multitude of environments such as hot, cold, light, dark or even humid or airplane type environments. Real world contemporary ocular examination is commonly conducted in relatively sterile clinical conditions that do not necessarily reflect the noisy, real- world environments that patients experience in day to day life. The compact size of the tested technology and ability to operate in a large range of conditions could provide insight into TF behaviour with regards to situational changes;
c) Comparisons of hard blinking to quick slow blinking patterns as well as tear film stability and retention over the CLs after different durations of wear or material compositions [63].
d) Effect of tear film thickness before and after certain activities such as screen usage and short sleep cycles [75]
e) Effect of medication and dry eye treatments on the recovery from dry eye disease and patient monitoring

It would be sensible to consider measurement of TF thickness as only one aspect of ocular fitness in the larger vector of assessments that need to be conducted to adequately diagnose pathology. Some subjects show signs of high tear osmolality, fast tear thinning and breakup, but at the same time be asymptomatic [136, 161]. Studies point to an estimated prevalence of DED of up to 33% of the world wide population, but with the definition of DED having to incorporate such a wide range of possible conditions of varying severities it is not surprising that even the

fundamental epidemiology varies depending on which country or territory one looks to, so much so that comprehensive statistics for the worldwide affected populations has not been fully gathered [18, 293]. This point can be extended to the tear film itself, which is a biological system with intrinsic variability with respect to what may be considered a “normal” thickness [282].

In conclusion, the low cost, non- contact chromatic or interferometric technology does provide huge potential for ocular health related applications. Both systems are of sufficiently low cost and small enough to mount on existing slit lamps and provided that the correct application is adopted that reflects the strengths of each instrument, these devices offer a viable low cost alternative to existing approaches and could lead to enhanced diagnosis and management of DED with further refinement.

4. Non-Contact Evaluation of the Anterior Eye

Ocular health does not depend solely on the condition of the tear film but also a complete myriad of physical properties of the human eye working in tandem to produce clear, sharp sight. Unlike common wet epithelia of the body, the nature of vision leaves the anterior eye exposed to the world, rendering it susceptible to many hazards ranging from physical injury to biological attack that may compromise sight. In the United States it is estimated that 2.4 million eye injuries occur annually [294] with an estimated 90% being preventable through the use of appropriate safety eyewear [295].

As our understanding of the complexities and structures of the eye have grown, so too have the number of techniques and instruments evolved and many practices have been developed to accurately assess the condition of the anterior eye, identify abnormalities and track disease or recovery progression [158, 286, 296, 297]. Non- contact forms of eye examination, although not always possible, tend to be the preferred method of observation [36, 122], thereby providing measurements that are not compromised by reflex reactions or unintended damage through touch. The inherent challenges of ocular observation is the need to identify small structures under difficult lighting and short working distances, all the while attempting to maintain reasonable patient comfort levels [232].

The first medium encountered by light entering the eye is the tear film which sits atop of the transparent, domed cornea. Accounting for roughly 40 of the total 60 dioptre power of the eye [46], the cornea is the primary refracting element of the eye. A supple crystalline lens suspended behind the pupil is the secondary optic and allows for precise focusing of the light through a process termed ‘accommodation’. Healthy, emmetropic eyes will produce a focal point of the image directly onto the surface of the retina at the rear of the eye giving clear vision.

It has been noted in previous chapters that compromised tear film dynamics may cause distortion to vision which may fluctuate in intensity throughout the day. However, it is defects of the cornea that give rise to common yet preventable cases of visual impairment such as myopia, which account for as much as 42% of visually compromised populations [7]. It is vital therefore that corneal topography is understood for many applications such as surgical intervention, contact lens fitting and refractive corrective surgeries.

Traditional corrective glasses, considered by some as undesirable and intrusive during activities such as athletics or sports, have been substituted by contact lenses which continue to gain

popularity and cosmetic appreciation [258, 290, 298]. Nevertheless the chore of inserting lenses coupled with potentially induced effects of dry eye [254] have led to the development of newer elective procedures such as Laser in Situ Keratomileusis (LASIK Surgery) [256, 299, 300] photorefractive keratectomy (PRK) [301] or the recently introduced Small Incision Lenticular Extraction (SMILE) procedure [302] to correct refractive error. Laser refractive surgery is generally accepted as a common and safe treatment for refractive correction and commonly co-occurring astigmatism but require pre-operative anterior eye examination to highlight characteristics of the cornea such as size, curvature, tear film quality and regions of astigmatism which would not have previously been apparent [303, 304]. By removing precise amounts of the stoma corneal layers through excimer lasers, myopic conditions can be corrected, but not without the risk of side effects.

While vision of most patients undergoing LASIK or PRK stabilised within 3 - 6 months post procedure [305, 306], patients of highly myopic eyes ranging from -6.00D to -10.00D have been known to experience regression up to 12 months after surgery completion [300]. Early LASIK procedures neglected the importance of pre- operative corneal thickness measurements recommended to be a minimum of 250- 300 µm [307]. Surgical intervention on thinner than recommended corneas have in some cases led to developing severe negative side effects such as corneal ectasias, irregular astigmatisms and profile steepening similar to those of keratoconus sufferers [308] due to compromised corneal structural integrity [309] .

Lack of awareness of dry eye and its association with corneal manipulation has led it to become the most common postoperative complaint of LASIK [299, 310], with between 20 to 40% of patients experiencing severe dry eye symptoms for at least six months following surgery [311]. The formation of a flatter region where material removal has taken place or central islands of steeper corneal tissue leading to compromised tear dynamics in this zone has been suggested [299, 312] as well as use of postoperative medications having a harmful effect on tear production [312]. The inherent cutting of the corneal flap also leads to severing of nerve endings within the cornea leading to reduced sensitivity and an ensuing reduced blinking rate [306, 313, 314].

Although technological advancements continue to offer patients new solutions to old problems, no progress is possible without comprehensive evaluation of the anterior eye pre and post intervention [232] to gain an appreciation of treatment success. Dry eye testing and corneal mapping have gained in popularity as their central role in overall ocular health has become more

appreciated over time. Table 4.1 lists various parameters that are necessary to be understood prior to reaching a confident diagnosis and aetiology of anterior eye disease/compromise.

Table 4-1: Common measurement parameters for corneal evaluation

Measurement	Application
Tear Breakup Time	Dry Eye Severity
Radius of curvature	Contact lens fitting
Refractive Power	Cataract Surgery IOL Lens Power selection
Elevation/ Astigmatism Profile	Ablation pattern for surgical correction
Corneal Thickness	Keratoconus/ corneal ectasia risk evaluation

4.1. Instruments for Corneal & Tear Film Evaluation

Slit projection and reflection methods are two techniques that are commonly employed by instrument manufacturers as they allow for high precision, non- contact assessment without disturbing the ocular surface [232].

4.1.1. Keratometers

One of the earliest instruments for objective corneal evaluation was the manual Keratometer [232]. First developed by Hermann von Helmholtz in 1854 [232], the instrument works by projecting illuminated mires on to the central 3 – 3.5 mm area of the corneal apex from which curvature and presence of astigmatism can be deduced [189, 315]. Furthermore by using a refractive index value of 1.3375, keratometers are able to estimate the refractive power of the cornea from the curvature measurement [316].

Keratometers can be manual or automatic in operation, however early versions assumed the cornea to be perfectly spherical, which it is not [317]. A correction factor is employed by newer hardware to give accurate shape reproduction over the entire surface which is essential for optimum contact lens sizing. Researchers Cronje- Dunn and Harris realised that Keratometer accuracy was influenced by tear film dynamics and from this were able to deduce tear film

breakup time as well as the presence of dry eye through hazy, distorted mires which were restored with each blink before once again becoming distorted [318, 319].

Over time new variations of keratometric measurement instrumentation have been conceived including the Javal- Schiŏtz, Helmholtz- Littmann and Sutcliffe type keratometers, each with different approaches to obtaining eye parameters and their own advantages and disadvantages. For example, the Hans Litterman instrument is considered the "gold standard" in keratometry as the measurement is not affected by imperfect mire focusing or through errors introduced by the accommodation of the physician's eye [232]. On the other hand, Javal – Schiŏtz keratometers are simpler in design and have observation systems without the need of moving parts but are susceptible to errors in measurement from incorrect patient positioning [232].

Recently, optoelectronic keratometers have been developed through the use of near infra- red LEDs arranged in a circular profile around a central camera aperture. Being mechanically simple with fewer components, electronic keratometers are typically combined with other ophthalmic devices to increase the tools at the disposal of the clinician. However, just as with the manual versions, all keratometers suffer from the universal flaw of a restricted projection method which confines evaluation to a small central 3.5 mm region of the cornea. Curvature, refractive power and tear film assessment are all limited to this small region and a comprehensive picture of ocular health is lacking.

4.1.2. Corneal Topographers

To increase the amount of data that can be gathered from the anterior eye, both the projection pattern and coverage area must increase which demands a new approach to instrument design.

In 1880, António Plácido da Costa was the first to use a large flat plate of concentric, retro illuminated black and white rings to qualitatively evaluate the corneal surface [232]. Reflections from the patients' eye were observed through a small opening in the centre of the disk and 'warps' in the reflections indicated corneal deformations such as the presence of astigmatism or possibly keratoconus. 1896 saw the first quantitative corneal evaluation by Alvar Gusllstrand who employed a microscope to measure distances between rings and develop the Gullstrand arc- step algorithms to reconstruct corneal shape [320]. Still in use today but in many alternative forms, the arc- step algorithm is an iterative process that uses a series of arcs from the corneal apex to periphery to calculate the corneal profile where the rings fall [321, 322].

Further improvements were made by Henri Dekking, who in 1930 modified the previously flat Placido disk arrangement into a new conical arrangement. This had the positive effect of projecting the placido rings further into the periphery of the domed cornea, thus giving greater area for observation. However, an unintended side effect was the introduction of shadows from the patient nose and eyelashes into the projection path, leading to large areas of the eye being unobservable due to no placido rings reaching these shadow zones.

It was not until the introduction of the Corneal Modelling system (CMS-1) in 1987 that a video camera and computer were coupled together for corneal measurement [232]. The CMS-1 was the first instrument that provided elementary colour coded corneal maps, but it was the Keraton (Opticon 2000), launched in 1993 that was capable of performing the arc- step algorithm which gave clinicians and surgeons the ability to precisely measure corneal curvature.

Modern topographers such as the Medmont E300 (*Medmont International, Nunawading, Australia*) launched in 1998, have been developed into large desktop based multi- function instruments capable of interpolating missing data points due to shadowing from the nose or lashes thereby overcoming early instrument shortfalls. Tolerances for refractive power measurement and corresponding radii of curvature are in the range of ±0.10 D and ±0.02 mm respectively [232]. Only keratometers can offer greater accuracy but remain restricted to the central 3.5mm of the cornea.

4.1.3. Non- invasive Tear Film Breakup Evaluation Techniques

Investigations into current ophthalmological NIBUT devices identify that there are two main techniques of non- invasive tear film analysis; white light retro illumination of a removable printed grid pattern and; fixed dimensioned, alternating black and white large placido disc with rear multi-colour mode illumination as regularly employed on the aforementioned corneal topographers.

Early subjective tear film analysis instruments were developed by Mengher et al. in 1984 using a white light source to illuminate a mesh pattern that was focused on the patient eye [323]. Upon blinking, the refreshed tear film is uniformly spread over the ocular surface with the projection sharp and focused, but over the course of seconds begins to degrade causing ruptures and distortions in the reflected pattern. At this point the test is concluded and break up time

recorded. Later instruments such as the Keeler Tearscope (*Keeler, Windsor, UK*) held transparent meshes which could be swapped out by clinicians to produce various patterns or removed entirely to provide simple white light interferometry of the tear film lipid layer. Although simple to perform, testing is extremely subjective with disagreements between clinicians common [187]. Surprisingly, such subjective observation techniques are still in use today and devices such as the Easy Tear View+ (*Easytear, Trento, Italy*) and CSO Polaris (*CSO, Florence, Italy*) hold appeal due to their relatively low cost and ability to be mounted directly to existing slit lamps during use – a preference of many practicing clinicians.

The second method uses placido disc projection of numerous concentric light and dark rings on to the cornea and analyses the spacing between rings to produce a topographic map [324]. Elevated regions of the cornea cause mires to appear further apart or even oval in shape thereby highlighting zones of corneal aberrations and astigmatism.

Topography instruments were originally used to provide corneal elevation mapping to supersede keratometers but evolved into multi-function tools which are typically larger devices and capable of objective measurement of several anterior eye parameters. Typical data captures anterior and posterior chamber elevations, corneal curvature and pachymetry which is useful for keratoconus, contact lens fitting and evaluating variations in corneal thickness prior to refractive surgery [325].

With regard to dry eye assessment, contemporary topographers use computer processing to capture details such as tear meniscus height, meibomian gland condition through infrared light, bulbar redness and, NIBUT [158]. Although methods may vary between manufacturers, modern anterior eye assessment devices are generally capable of comprehensive, objective anterior eye evaluation and reduce inter- clinician variability [326]. Advantages of NIBUT is the avoidance of fluorescein instillation which has been shown to impact tear break up time [326] and computer data capture allows for objective monitoring of disease progression [179]. However, there is a variation between obtained NIBUT values captured through NIBUT and FBUT techniques [326-328] as well as studies such as by Best et al. which showed an average difference of 12.35 seconds difference between the subjective Keeler Tearscope and the objective Oculus Keratograph instrument [189]. Intra device variation between manufactures and approaches is also a common issue [158] as shown in table 4.2.

Table 4-2: Average NIBUT results obtained from several leading tear film measurement devices in various levels of dry eye disease severity

Study	Instrument	Healthy Eyes NIBUT (sec)	Dry Eye NIBUT (sec)	Sensitivity / Specificity
Hong et al. [327]	Oculus Keratograph 5M	4.3 ± 0.3	2.0 ± 0.2	84.4 / 75.6
Gumus et al. [329]	Tomey RT7000	4.9 ± 1.6	2.4 ± 2.5 (Mild) 1.2 ± 1.8 (Moderate) 0.4 ± 0.5 (Severe)	82.2 / 88.0
Downie [328]	Medmont E300	19.4 ± 5.3	7.9 ± 4.9	81.5 / 94.4
Koh et al. [330]	Oculus Keratograph 5M	9.7 ± 6.7	4.6 ± 1.3	N/A

The introduction of diagnostic classifications by the National Eye Institute in 1995 and subsequent DEWs I and DEWs II workshops have led to major advancements in tear film understanding and disorder clarification. They have also helped standardised what may be considered to be a healthy or compromised tear film and which techniques to base these assumptions upon [185, 199].

Although NIBUT methods are well established in practice, they have reached an evolutionary plateau and suffer from many drawbacks, most notably from an inconsistent corneal coverage area and shadows from the nose and eyelashes rendering large regions of the projection void as the measurements are unable to be captured in these shadow zones [182]. The implementation of existing devices is rigid with ring spacing constrained, limited illumination options and many copycat designs between manufacturers. Each NIBUT instrument requires the patient to sit with their head on a chin and head rest such as those used with a slit lamp, which may be uncomfortable for older patients with posture problems and with the lack of portable alternatives meaning patients must always make the journey to the point of care. Secondly, the instruments are flawed the by the need to have a large conical head with large rings to achieve a projection over a sufficient part of the cornea. The working distance of the instrument (roughly 30cm) requires the projection brightness be increased to ensure a sufficiently bright reflection being created from the eye, thereby making the test experience rather uncomfortable and potentially inducing reflex tearing affecting results.

While the preference of one technique over others vary from region to region where legacies of historical practices and economics may influence contemporary methods at the granular level [164, 331], the desire to reveal the fundamental source of ocular dysfunctions and potentially save the vision of a patient are the same in the heart of healthcare professionals working in advanced countries such as Japan as they are in the depths of rural India.

The addition of computer analytics may have introduced the possibility of objective measurement of many anterior eye properties, nevertheless current devices are only capable of single point analysis meaning that individual test results are presented separately and combined on the basis of a risk assessment exercise. Final judgement is left up to the clinician which introduces subjectivity and bias into the diagnosis and disagreements even between experienced professionals is common.

4.2. Aims and Objectives

This chapter has reviewed the existing methods for evaluating anterior and dry eye assessment. The need for a new portable, low cost, multifunctional device which is capable of not only assessing NIBUT but also measurement of physical eye dimensions and provide superior imaging output is proposed.

A core specification list was compiled as the early guide for the design and composed of the following points:

- Non- contact, central corneal coaxial measurement
- Total production cost below £1,000
- Portable in nature
- Ability to record to various outputs, ideally including mobile phones
- Give rise to clearer images than possible with current technologies.

This chapter is the next step in the advancement of NIBUT measurement with the aim of achieving greater patient comfort, greater image quality and ultimately a consistent and repeatable measure of TFBUT.

4.3. Headset Slit Lamp and NIBUT Device

Dry eye evaluation devices of today are either large desktop-based instruments such as the Oculus Keratograph, Zeiss Atlas 9000, Medmont E300 or smaller equivalents like SBM Sistemi OSA, CSO Polaris and EasyTear View+. Varying levels of automation and measurement accuracy exist between models. Each form factor has strengths and weaknesses in usability which are inherent in their design. An example is patient positioning with respect to the instrument with large, stationary desktop-based systems requiring patients to be sat at a dedicated chin and head rest and focus their attention onto a central coloured LED located in the midpoint of the placido cone. This centres the eye during testing. However, patients with posture, mobility, hearing and concentration issues tend to struggle to be positioned correctly and follow instructions for accurate measurement to take place. This is especially true with young children.

Rather than continue to follow existing instrument projection concepts, a new approach in the form of a hands- free device designed around a mini projection system packaged within a patient wearable headset was conceived as a possible solution. The headset concept comprised of a high intensity Chip on Board LED light source that was condensed and passed through a 3 inch transparent LCD window hardwired to a local computer. Depending on the pattern being displayed on the LCD, the light was selectively passed through transparent regions into a collimating lens assembly before focusing lenses guided and magnified the projected image onto a two-way mirror behind which was positioned a digital camera. The mirror angle could be adjusted to ensure correct light incidence onto the patient eye.

A desktop proof of concept was assembled using Thor Labs OBE (*New Jersey, USA*) and can be seen in figure 4.1. This was later transposed into a tailor made headset composed of 3D printed and laser cut Perspex walls. This new headset was designed and created to hold the light source, LCD and lenses so that direct patient observation could take place and be recorded through the onboard camera.

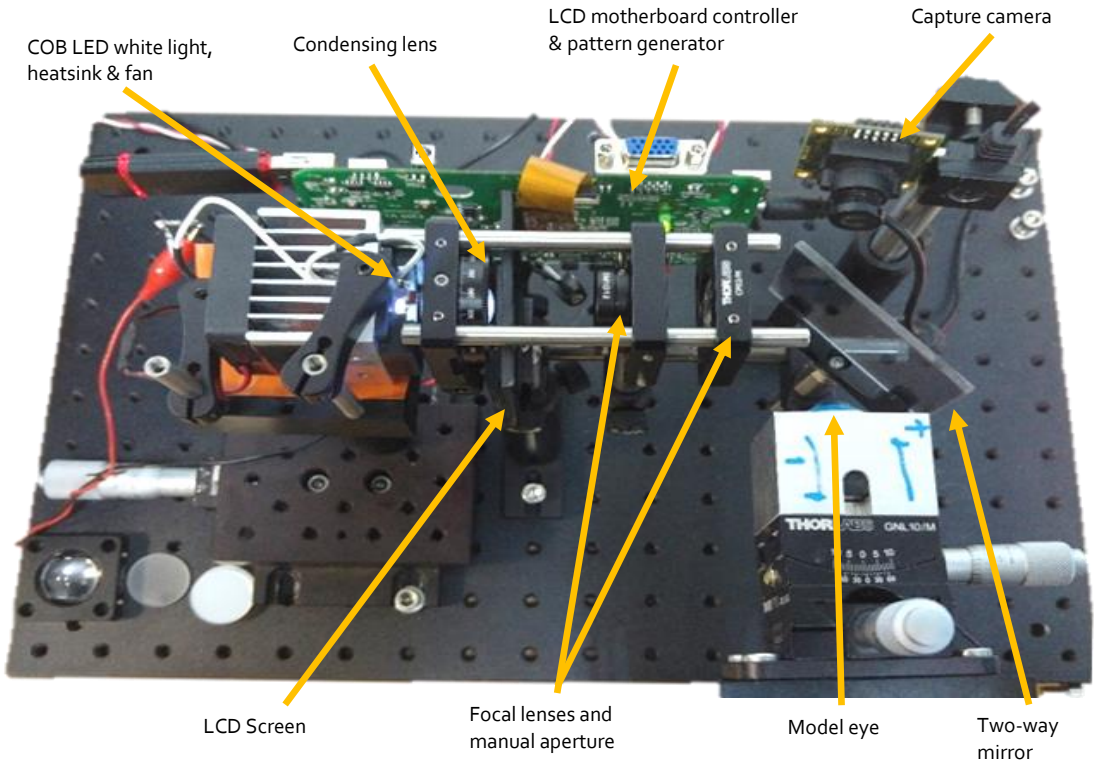

Figure 4-1: Early bench top concepts of LCD slit lamp and NIBUT instrument

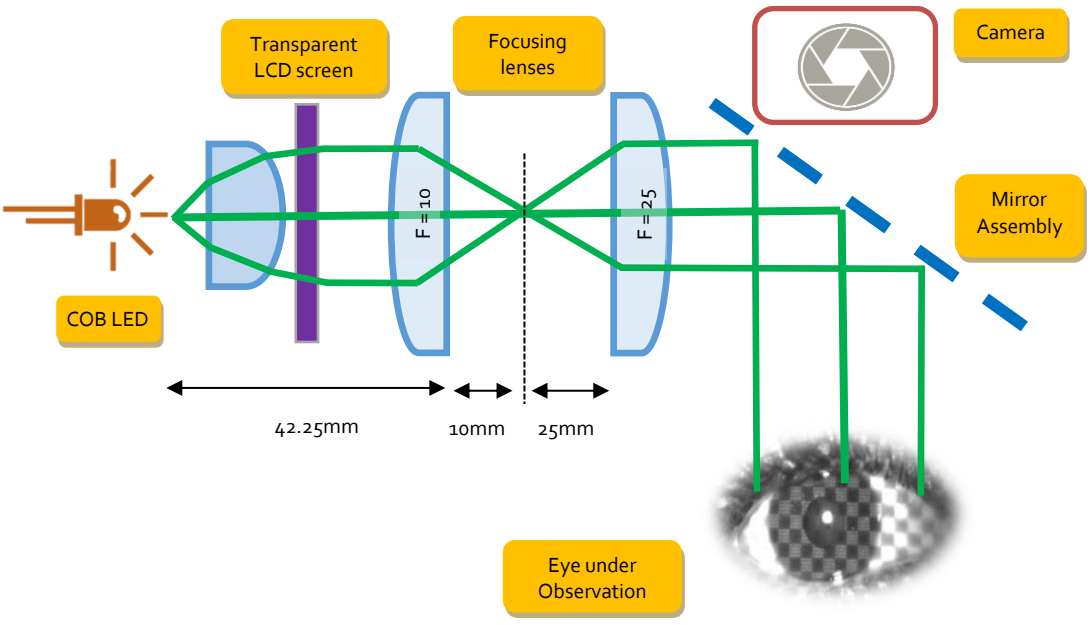

Figure 4-2: Headset slit lamp optical path and component diagram. Single LED providing point light source being collimated through 25.4mm ø, f= 10mm plano- convex lens. Separation of LED to lens is 42.25mm (LED to rear surface of lens). Light is collimated as it touched the LCD on the left face. LCD introduces distortion into light path and although still collimated as it leaves the right face, slowly begins to diffuse as we move further from the source. Projection on to model eye requires focusing lens (50mm ø, f= 25mm) to focus mires onto eyeball surface.

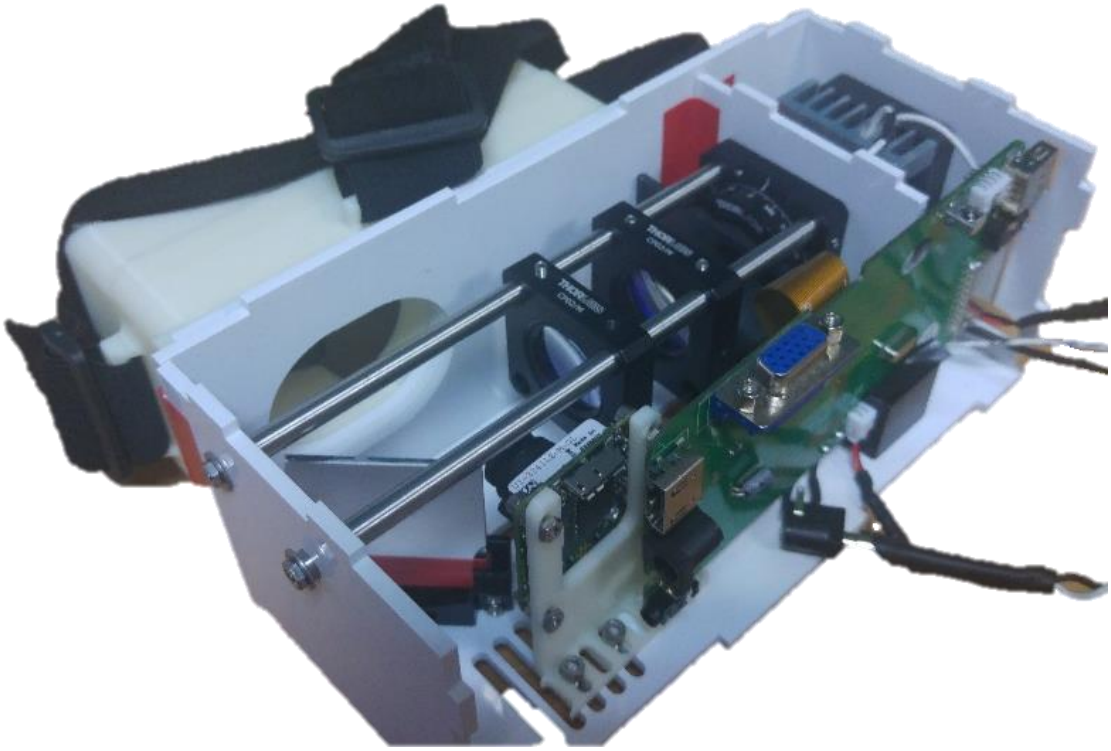

Figure 4-3: Slit lamp NIBUT prototype assembled in a wearable headset enclosure

4.3.1. Headset Hardware Specification

The majority of the headset slit lamp components were sourced from a repurposed mini projector system with the intention of mimicking its lighting and projection methods, only on a smaller scale with reduced working distance.

Table 4-3: Headset Slit Lamp hardware specification

Component	Specification
LCD Brightness	1800 lm
LCD Pixel Density	320x180
Contrast Ratio	500:1
Patient Working Distance	< 0.1m
Light Source	COB White LED
Power Source	12V, 1.5A
Camera Resolution	1.3MP
Connection	USB 2.0

4.3.2. Slit Lamp headset discussion

The prototype headset device proved surprisingly agile and extremely versatile with both projection capabilities and data capture. Many grid patterns were easily implemented and colour illumination was achieved through simple LCD manipulation, examples of which are shown in figure 4.4. Colour illumination could be useful for FBUT as well as identifying and distinguishing ring overlap in highly aberrated eyes as well as providing better clarity of ring warpage in dry eye testing modes. Due to the light source being projected directly in front of the eye as opposed from peripheral regions in present-day topographers, the LCD projection method allowed for zero nose and brow shadows to be present on the cornea- an issue which plagues computer algorithms and causes large regions of the image to be simply ignored. Figures 4.4 show variations in the capabilities of the device. Both colour and greyscale projections could be created and patterns changed instantly on demand without any need for mechanical movement. In addition, clear, high contrast projection was accomplished over the sclera which is typically overlooked during tear film breakup analysis and could provide useful insights into previously undocumented tear film behaviour.

Disappointingly there proved to be a major flaw in the current experimental setup with very little projection captured on the actual cornea once the equipment had been repackaged into the headset device. Looking closely at figure 4.4, the patterns are principally reflected from the Iris rather than the cornea itself. This is evident by the lack of reflection present within the dark pupil region. Figure 4.4a shows an image created using classic circular mires with a reflection present within the pupil region which was accomplished on the initial desktop test rig and shone on to a model eye. However, when the setup was installed into the close confinement of the headset, the short working distance to the eyeball required the use of stronger focusing lenses which were unavailable during the time of development. Unfortunately capture of tear film break up was not possible with the current equipment and although the author has great confidence in the potential of such a headset device, the learnings from this instrument have spawned a new method that could lead to a more comfortable user experience.

One of the central benefits to the headset device was the unique hands-free operation and enormous flexibility of projections that could be achieved on to the ocular surface. The headset device could be programmed to behave as a slit lamp with simple vertical/ horizontal patterns of any colour or dimension being displayed on the eye. Either fully diffuse illumination or coloured patterns are possible which would enable topical dye installation and observation.

Furthermore, corneal topography and non- invasive tear break up testing could be performed in perfectly dark conditions as the headset acts to block all external light sources.

Perhaps one of the greatest advantages of the headset form factor would be the ability to provide a comfortable platform for those with posture and mobility issues as theoretically this instrument could be used even on bedbound patients. There is also great potential to introduce eye tracking to the instrument which would relieve patients from needing to focus on a particular target and allow for the instrument to compensate for unintended eye movements during testing.

In summary the headset instrument has proven a strong first step in the design of a new anterior eye device and the knowledge gained from this first attempt will be continued into the next iteration.

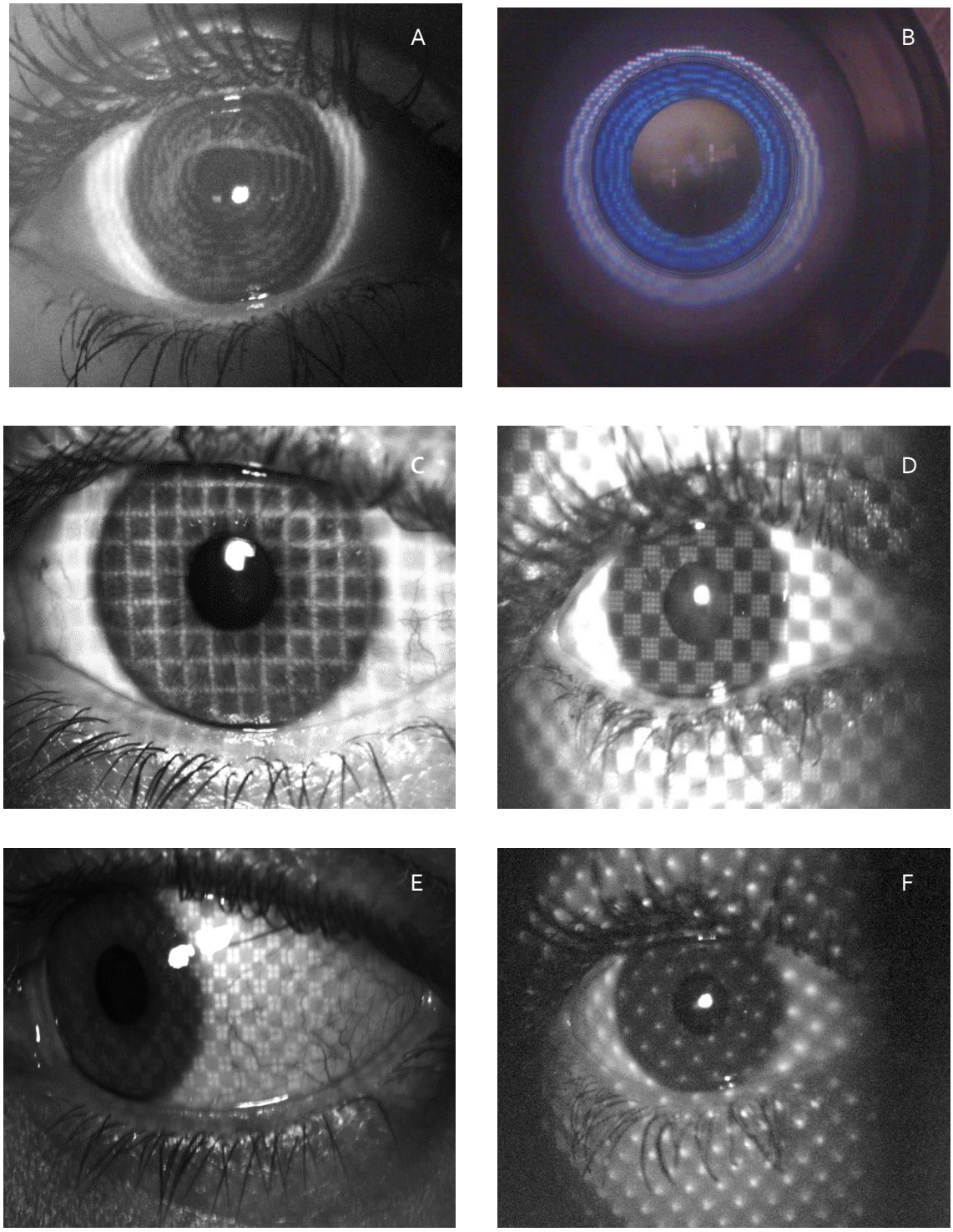

Figure 4-4: Headset slit lamp device demonstrating various projection modes. A) Circular mires B) Coloured circular mires on model eye C) Grid pattern D) Checkerboard pattern E) Checkerboard pattern on Sclera F) Dot Pattern

4.4. Development of the Anterior Eye Scope

A new concept will now be introduced which uses the phenomenon of persistence of vision to create virtual circular mires onto the tear film and allow for high contrast, superior image generation.

Human vision is the function of light focused on to the retina which causes a chemical stimulation and subsequent translation into electrical signals interpreted by the brain. The translation of chemical to electrical energy, although almost instantaneous, induces a delay of between 0.1 to 0.15 seconds which results in phantom image retention once that light source has been removed from the eye. As the eye cannot discriminate fluctuations in light faster than the retention period, any light changes faster than this retention period lead to overlapping images and give rise to continual, uninterrupted perception.

Persistence of vision is a common occurrence that takes advantage of image retention even when that moment has passed. By using a light source of a higher frequency than the refresh rate of the eye, the brain can be 'tricked' into seeing a moment that has in fact already passed and it is this method that will be used to create the mires that will be projected on to the eye undergoing TFBU analysis.

4.4.1. Device Development

Conventional NIBUT devices use a fixed pattern of white rings which is retro illuminated. Reflections of these mires are then camera captured and analysed by single point computer algorithms which only provide a single output based on the completed test.

The advancement of LED technology has now allowed extremely small LED units- known as surface mount devices (SMDs) to be manufactured at very low cost. Along with their small footprint is the added advantage of low power requirements and high luminosity. Several white SMD LEDs were mounted on a straight PCB 'blade' in a linear arrangement with surface connections between each running to a high- powered capacitor (0.47F @ 5.5v) that would provide power and a mass counter balance to the off- centre LED array during rotation. A 3D printed arm and housing complete with bearings and direct current (DC) motor connection was designed on Solidworks (*Dassault Systèmes, Vélizy-Villacoublay Cedex, France*) and printed using

a Statasys UPrint 3D printer (*Eden Prairie, Minnesota, US*). Early design iterations can be seen in figure 4.5 below.

The LED arm and motor were mounted on a temporary OBE setup, with a camera positioned off centre behind the blade for data capture. Once the DC motor was powered, the LED arm would undergo fast rotation around the central axis giving rise to the persistence of vision effect and a continuous ring pattern of perfect concentricity and high brightness was created, figure 4.5b.

In early device incarnations the placido rings, although bright, were thin and the recorded images skewed due to camera positioning being above centre from the axis of rotation. Speed of rotation also needed to be controlled as the refresh rate of camera must match that of the rotation speed to ensure a continuous 360° capture of the POV effect. These learnings were used to develop further iterations.

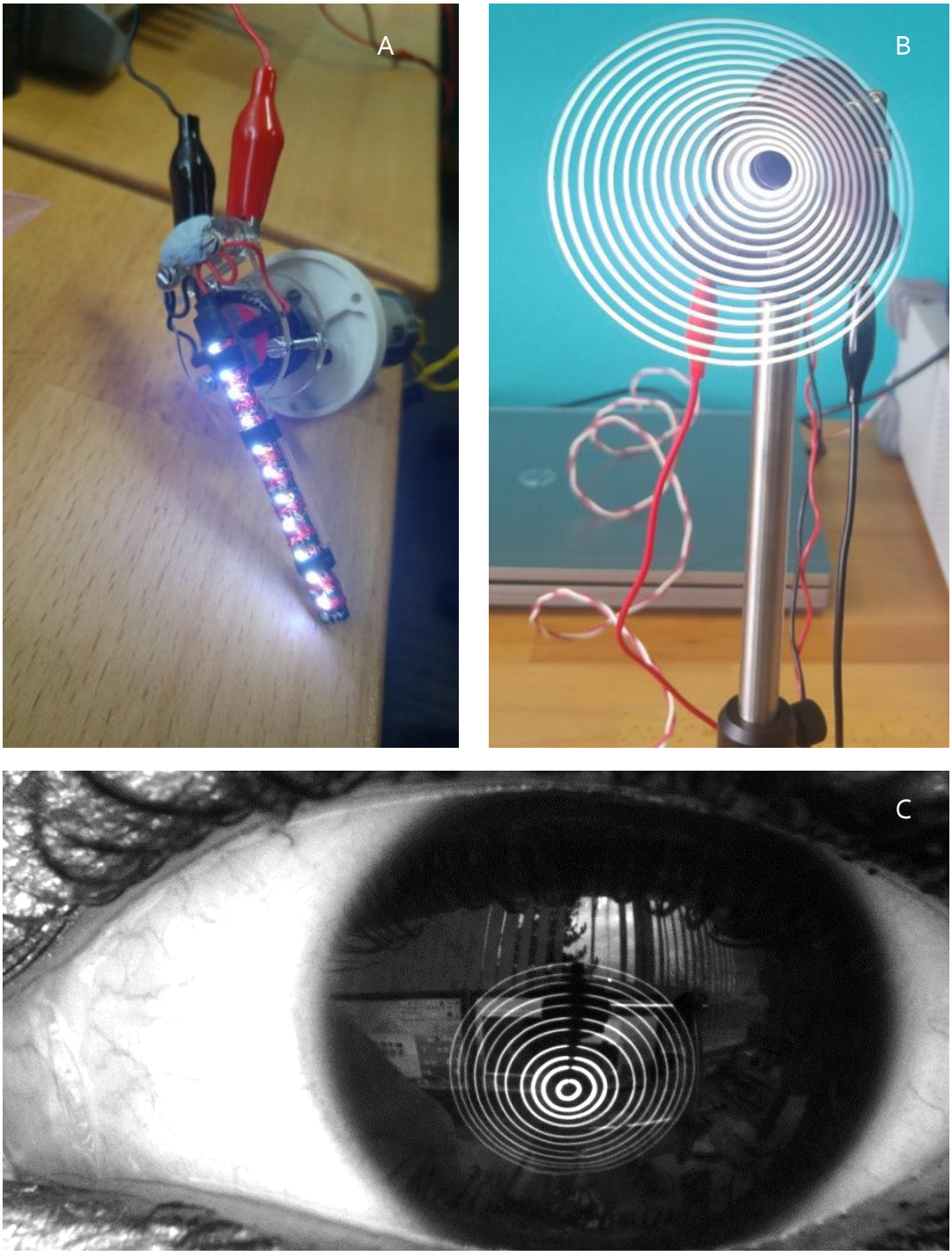

Figure 4-5: POV principle testing A) Row of SMD LEDs arranged in on a linear PCB attached to central motor shaft B) Blade rotating at 2,100 rpm to create persistence of vision effect C) LED reflection from tear film. Image is skewed due to camera offset from centre of rotation

4.4.2. Final Device

The final prototype device was a significant improvement over the original concepts with many issues needing to be overcome for precise, repeatable operation.

The prototype is a modular unit illustrated in figure 4.6 with multimode anterior eye assessment capabilities. New LED light blades have been designed on Proteus (*Labcenter Electronics, Grassington, UK*) and sent for manufacture to external suppliers. New colour combinations have been selected which include white light, Infra-red light, red light, and alternating blue/ white combinations. In addition, it has been possible to source SMD LEDs with integral diffusers allowing continuous, even illumination for general anterior eye imaging. This is particularly useful for topical dye (Lissamine green or Sodium Fluorescein) or general white light anterior eye observation where a uniformly illuminated eye is preferred to the broken pattern inherent of current topography systems due to their fixed ring spacing. To minimise electronic complexity, each LED light option was installed on its very own head cone which could be swapped onto the main body.

The main body encloses a DC motor connected to a central shaft pressed onto high speed bearings allowing low friction rotation. Individual LED heads are connected to the central shaft through magnetic connection which also provided the electrical terminals required to power the LEDs on the rotating cone.

There was an inherent need to stabilise the patient head in relation to the instrument and centralize the projection pattern on the cornea during testing. This was accomplished through a fixed cone enclosure, which sits proud of the rotating head and contacts with the patient brow during testing. Not only does this maintain the correct distance for the fixed lens camera to focus sharply on the cornea, but also provides a safety feature by preventing unintended patient contact with the spinning cone.

One of the greatest challenges was the need to engineer a tailor made high speed, low friction commutator capable of transferring power from the body of the device to the spinning LED blade. The speed of the motor rotation needed to be held constant- difficult to achieve when the onboard batteries begin to exhaust their power supply. LED brightness also needed to be controlled, especially with the ability to change PCB blade colours for various anterior eye tests (fluorescein viewing, IR capture or white light viewing) and each LED set requiring differing current driving values. Both issues were solved with the addition of individual buck boost circuitry contained within the body of a separate power unit that doubles up as the handle of

the device. Two versions of the handle have been created; one which holds AA batteries that allow for portable use of the instrument while the second is a mains powered version that is capable of being mounted onto a slit lamp for day to day clinical use where power is available. Each handle is interchangeable and held to the main body through magnetic connection.

The POV scope allows for three modes of data capture; a simple mono eye piece with magnification for use in subjective anterior eye observation; a camera option for direct computer recording and a phone adapter option which can take advantage of the abundance of modern mobile phones which are commonly equipped with high powered cameras capable of test recording. To keep all components together, a case was repurposed for device storage and transportation and shown in figure 4.7.

A B C

Figure 4-6: The POV Scope A) Rear view with magnifying eyepiece installed B) Front view, white rings C) POV Scope used in conjunction with slit lamp, connected to mains power

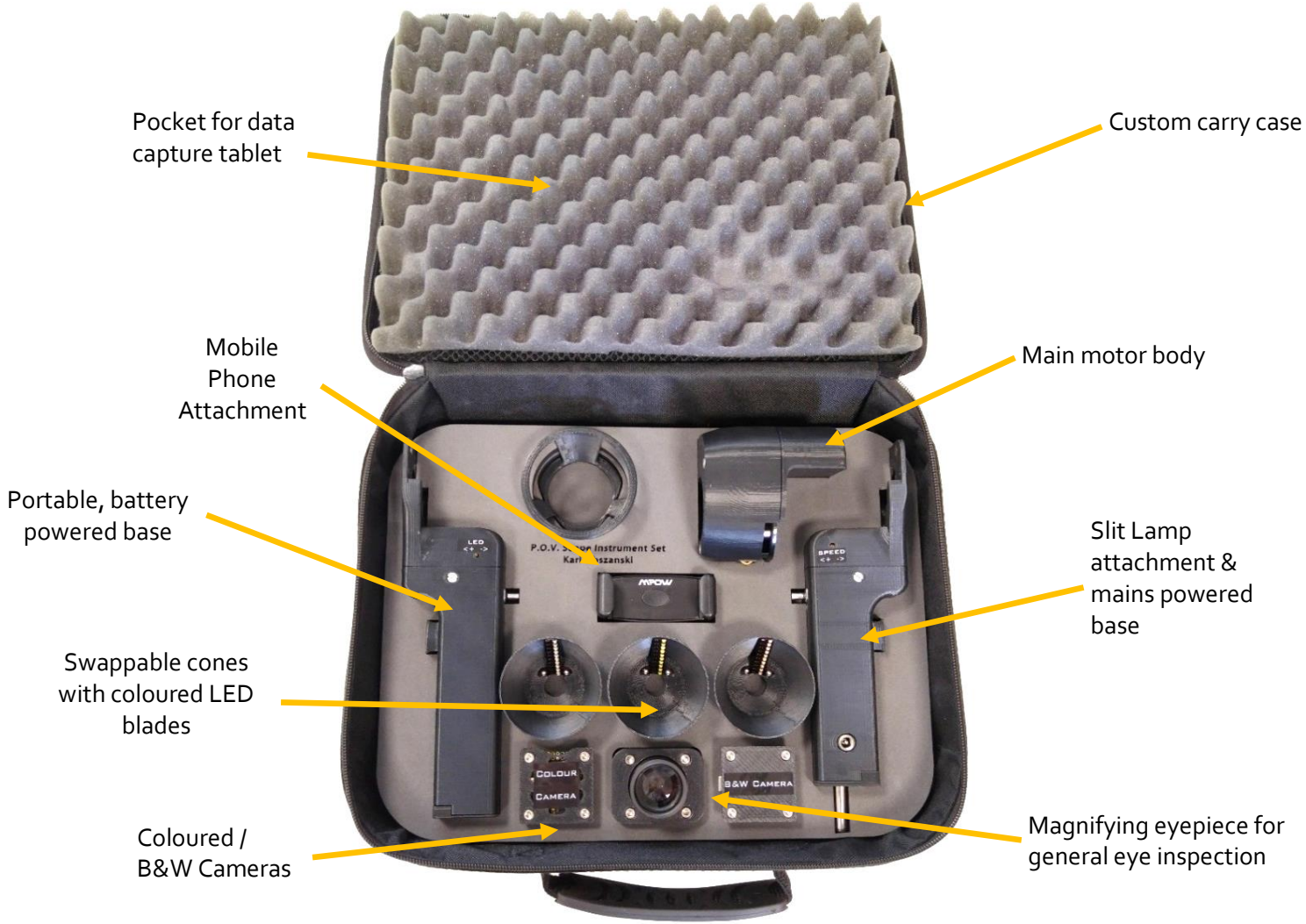

Figure 4-7: POV Scope with all accessories shown in portable case

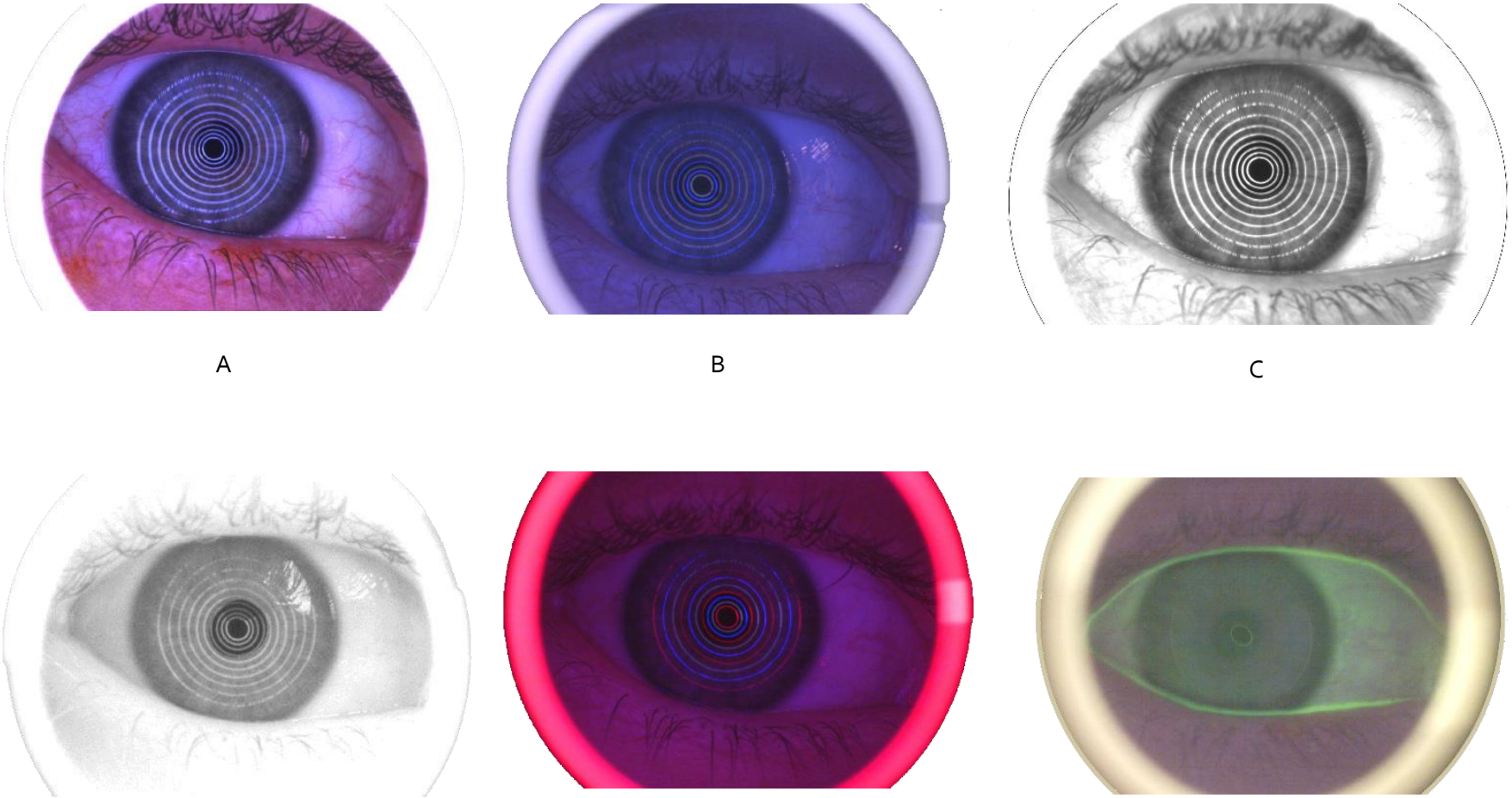

Figure 4-8: POV Scope projection capabilities A) White ring projection B) White & Blue Combination C) White rings, B&W camera D) IR Rings, IR Camera, E) Red & Blue rings F) Diffuse blue with yellow filter for tear film viewing

4.5. Study POV- A: Exploratory Comparison of NIBUT obtained through contemporary instruments against the newly developed POV Scope

The central aim of this exploratory study was to establish the consistency of the subjective POV Scope as compared to commercially available instruments and gain experience as to the function and acceptance of the new testing modality on a small cohort of patients.

The study was approved by Aston University Ethics Committee and conformed to all tenets of the Declaration of Helsinki. All clinical testing was conducted in the Aston University Vision Sciences centre. Six students aged 18 - 33 from the Aston University student body were recruited to attend a morning followed by an afternoon session on the same day of NIBUT testing. Once informed consent was obtained, each participant underwent five various tear film stability assessments on different instruments: Keeler Tearscope, CSO Polaris, EasyTear View+, Oculus Keratograph 5M and the POV Scope. Order of instrument testing was randomised between patients but kept consistent for both sessions. A two minute interval between tests was enforced to prevent eye fatigue leading to potential compromise of results in following assessments.

The Keeler, Polaris, Easy Tear View+ and POV Scope instruments were used in conjunction with a CSO camera slit lamp and hand-held timer. The participant was asked to blink twice and hold their eye open for as long as possible while the examiner monitored the reflection from the ocular surface for regions of pattern breakup. Being subjective in nature and to prevent bias, all test were conducted and recorded through means of a slit lamp camera during the test by a single clinician. After the event, recordings were played back and tear film break up deduced by the same examiner for both morning and afternoon sessions. Keratograph readings were calculated objectively by analysis of local regions of breakup and processed by onboard software. Software limits up to 25 seconds for each Keratograph test or up until patient blink. Each test was then repeated a further two times before moving on to the next instrument. Participants returned in the afternoon and tests conducted in the same order.

4.5.1. Study Results

The purpose of this study was to gain experience and understanding of the POV Scope in real world clinical settings. Images captured from the various instruments have been compared and typical capture examples from a single patient can be seen in figures 4.9 to 4.13 for comparison.

Usability and patient comfort to the new measurement method of the POV scope was asked. Although apprehensive about the spinning nature of the new device positioned close to the eye, once early measurements were completed many participants were perfectly comfortable with further testing.

Any data to be used for NIBUT measurement fundamentally depends on the clarity of the projection and corneal coverage of the instrument. Regions of the cornea where no projection is achieved are considered lost data as the clinician is blind to any tear break up that may be occurring in these areas. Lightly coloured iris', such as blue or green, naturally pose a difficult challenge to project upon as the white mires lose contrast against the light background and become problematic to distinguish in the 'noise' of the eye.

A large disparity between corneal coverage, quality of mires and concentricity of the instrument with respect to the eye exists. The Keeler Tearscope and CSO Polaris provided a relatively large coverage area, but mires are significantly fainter on the former instrument. Figure 4.9 demonstrates a gap in the mires due to incorrect mesh insertion and is noticeable in the one o'clock position. The instrument is also not centred on the eye giving a skewed projection particularly strong in the 9 to 12 o'clock regions.

A prime example of low corneal coverage is seen in Figure 4.10. Projection achieved on this participant from the EasyTear+ View instrument covers <50% of the total cornea and the outermost mires rapidly lose their illumination intensity the further they are from the centre of the projection. Within the small pupil region, the mires may appear bright, but an inverse relationship exists between pupil size and instrument brightness- the higher the brightness, the smaller the pupil. It may be appealing to simply increase the projection strength by increasing instrument brightness but would result in major pupil contraction and a loss of the ideal dark pupil region which offers greatest reflectance in the centre of the eye. Reflex tearing and patient discomfort are also most likely to increase.

Advanced instruments take advantage of this inverse relationship through the use of an infra-red light source as opposed to conventional white light. However, this is impossible to employ

in subjective instruments which require direct clinician observation as the clinicians themselves would not be able to see the mires during testing.

Images obtained from the Keratograph are much brighter, consistent and occupy a large corneal area. Nevertheless, this instrument suffers from a unique flaw due to its design and working distance. Shadow regions evident from the 3 to 5 o'clock positions in figure 4.12 are created by the patient's nose which blocks the mires from reaching the ocular surface. Further interruptions in the mires can be seen in broken/ intermittent superior and inferior regions of the cornea due to eyelashes. This is a major issue as software algorithms must immediately exclude these regions from their analysis, otherwise false positive results may be triggered. What initially looks like a large, clear corneal projection is progressively reduced to a relatively horizontal corridor stretching from the left to right of the eye.

Lastly, the POV Scope in figure 4.13 demonstrates a wide projection area and strong contrast of mires across the surface. A brighter section between 4 and 5 o'clock is the result of the speed of the blade revolution not being correctly matched to camera refresh rate causing over exposure in this part of the projection as overlap in rotation doubles the brightness in this zone. Evidence of tear breakup can be witnessed between the 2 and 3 o'clock regions with a break in the fourth mire from the centre.

Looking through all instruments in the line-up, top and bottom eyelash shadows are present on all the images but are not as easy to notice in on some instruments due to weak mire projections. The POV scope also generates such eyelash shadows which may require mathematical correction through interpolation in the future or outright exclusion should they pose an issue with data analysis. Unfortunately, eyelash influences are unavoidable no matter what instrument is used and are made worse through the use of makeup or false lash extensions.

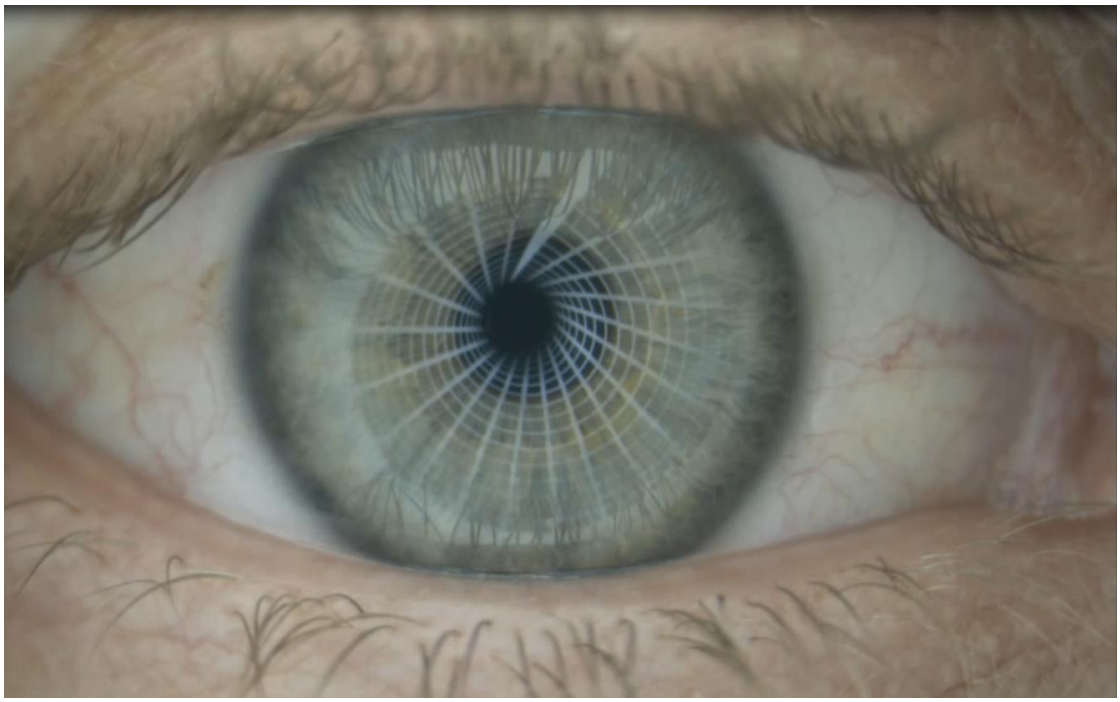

Figure 4-9: Keeler Tearscope NIBUT Capture. Mesh wrongly inserted giving rise to a twisted projection pattern. Gap in 1 o'clock position mesh pattern. White rings difficult to distinguish from blue/ green iris- especially towards the outer edges of the projection regions.

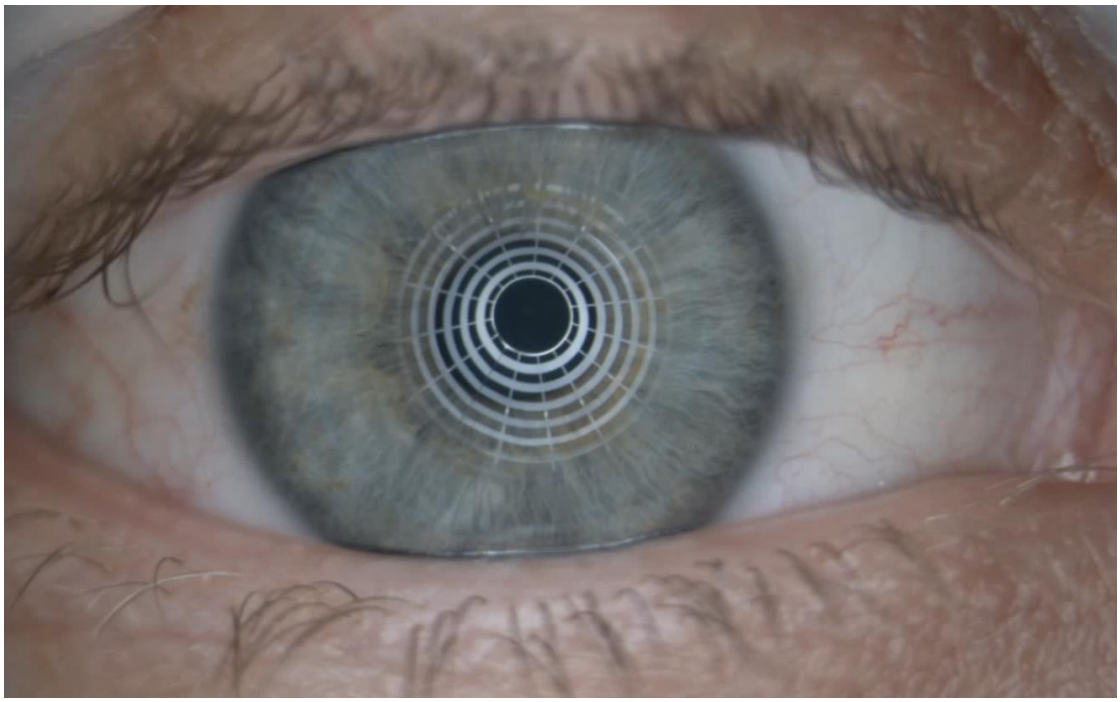

Figure 4-10: EasyTear View+ NIBUT Capture. Very small projection zone in the centre of the cornea. Low contrast in regions outside of dark pupil area making confident analysis of NIBUT difficult. Most likely cause is poor instrument positioning with regards to patient.

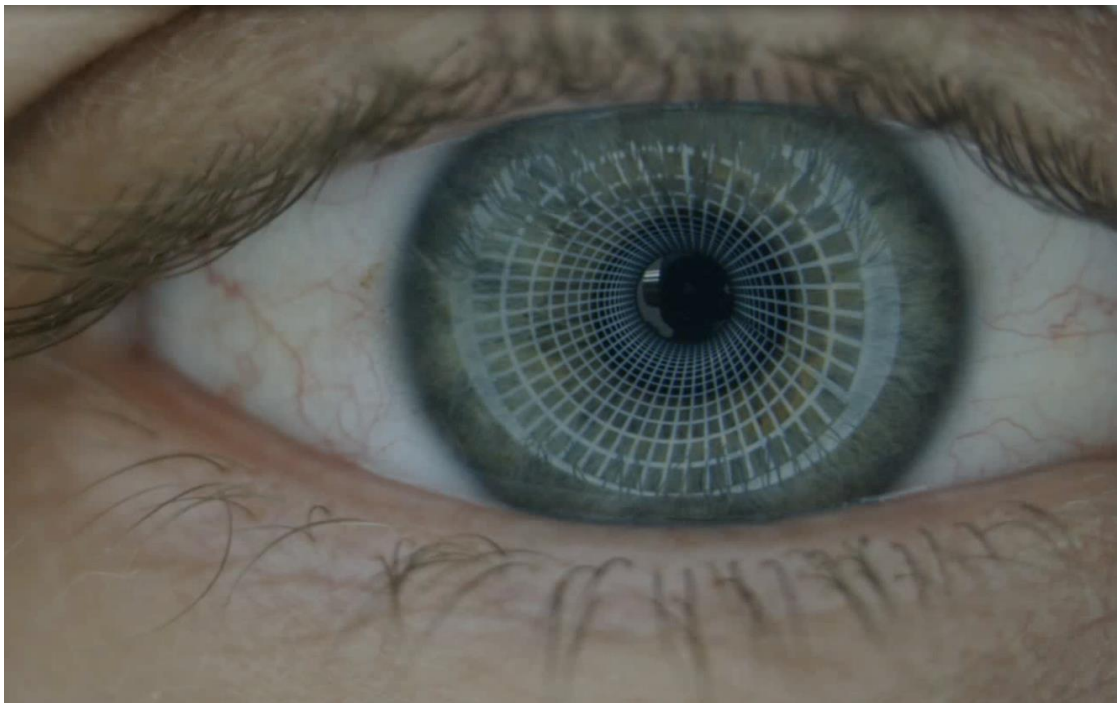

Figure 4-11: CSO Polaris NIBUT Capture. Large projection coverage with good pattern clarity all the way towards the periphery. Mesh wrongly inserted giving rise to large white regions from 1 to 5 and 8 to 11 o'clock position)

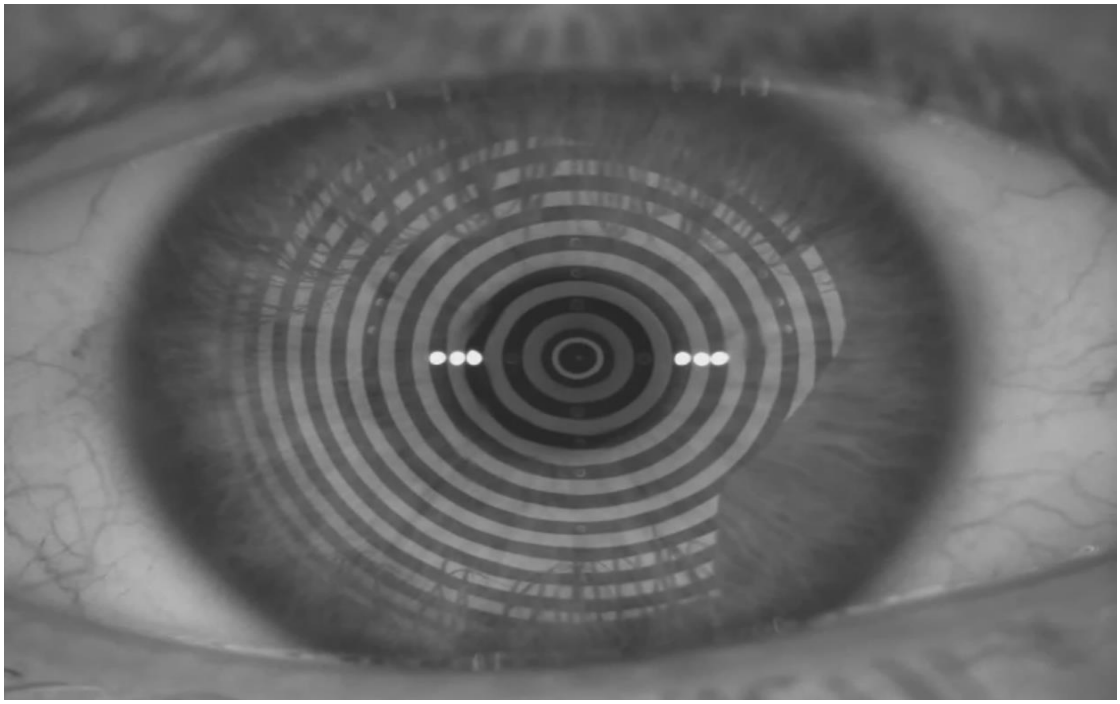

Figure 4-12: Oculus Keratograph 5M NIBUT capture. B&W capture as opposed to colour- boosts contrast on light coloured eye. Good coverage of cornea but strong artefacts present from top and bottom eyelashes. Nose shadow large in 3 to 5 o'clock region. Evidence of tear break up visible in 10 o'clock area, ring 3 from centre.

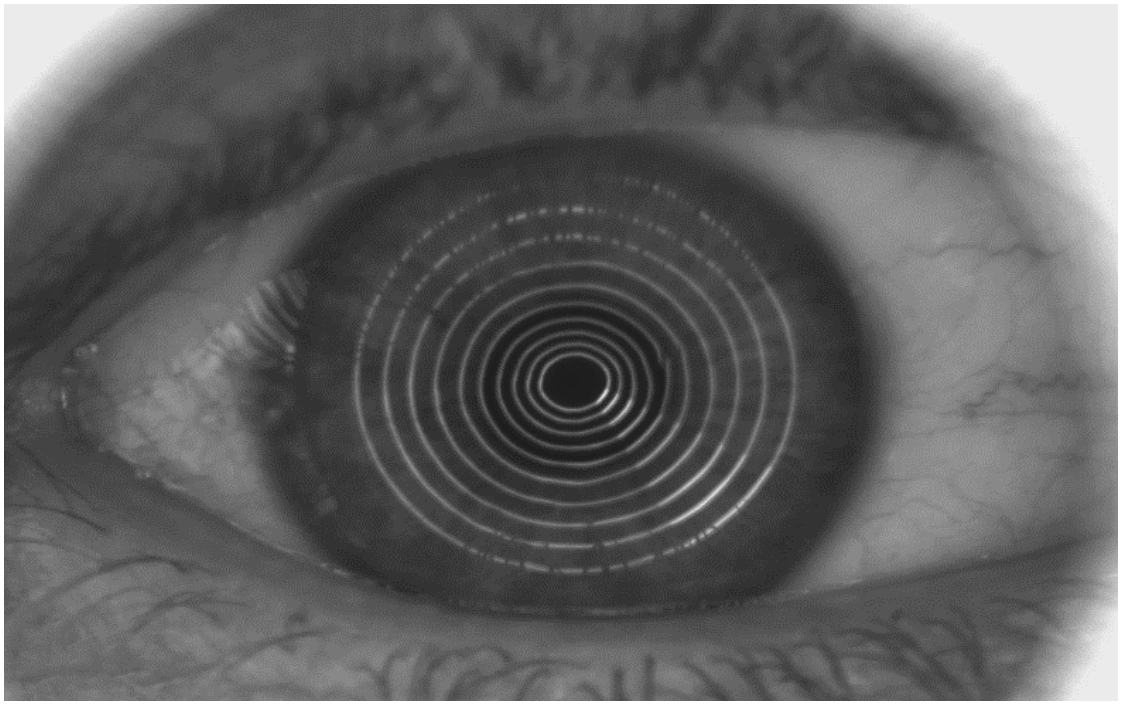

Figure 4-13: POV Scope NIBUT capture. Brighter region in 4 to 5 o'clock zone as discrepancy between rotation speed and camera shutter speed giving rise to double exposure. Good corneal coverage, strong contrast with bright rings making easy work of identifying projection. TFBU occurring in 2 o'clock position, ring 5 from centre.

Although sample size is small (6 participants, 3 measurements per patient), a Shapiro- Wilk test ($P > 0.05$) was conducted on a sample of the data to check for normality and returned a non-normal distribution indicating to non- parametric testing requirements. This is consistent with previous studies of a similar nature [196, 332]. All statistical testing conducted using SPSS software package (*IBM, Hampshire, England*).

Two Spearman correlation matrix's were calculated between morning and afternoon instrument results and can be seen in table 4.4. Significant variations ($P < 0.05$) between NIBUT measured on various instruments are highlighted in orange.

Table 4-4: Spearman's rank correlations between morning and afternoon sessions, n= 6.

Morning Testing

	Keeler Tearscope	CSO Polaris	EasyTear	Keratograph	POV Scope
Keeler Tearscope	1	0.26	0.63	0.35	0.15
CSO Polaris	-	1	0.64	0.61	-0.05
EasyTear View	-	-	1	0.67	-0.05
Keratograph	-	-	-	1	0.16
POV Scope	-	-	-	-	1

Afternoon Testing

	Keeler Tearscope	CSO Polaris	EasyTear	Keratograph	POV Scope
Keeler Tearscope	1	0.42	0.40	-0.02	0.29
CSO Polaris	-	1	0.52	0.52	0.22
EasyTear View	-	-	1	0.28	0.27
Keratograph	-	-	-	1	0.28
POV Scope	-	-	-	-	1

Performance between the new POV Scope and the existing instruments showed greater variation in the morning sessions than in the afternoon. Between both combinations of CSO Polaris vs POV Scope ($\rho < 0.05$) and Keeler Tearscope vs POV Scope ($\rho < 0.05$), significant differences between break up time results were recorded. A significant difference was also calculated between the Keratograph 5M compared to the Keeler Tearscope in the afternoon session ($\rho < 0.05$). Such inconsistencies highlight the problems with subjective measurement methods which give rise to results of questionable accuracy as measurement was undertaken through human observation and vital details are easier to miss, especially in cases of poor reflection and low corneal coverage. Mean NIBUT achieved from by the POV scope ($\sigma = 5.61$ seconds, S.D. ± 2.77) was lower than competing instruments with a lower maximum test time that the other four instruments suggesting additional factors in the measurement process.

Table 4-5: Descriptive statistics of various instruments and achieved TFBUT. n= 6

	Minimum	Maximum	Interquartile Range	Mean	Standard Deviation
Tearscope	4.44	14.7	5.44	8.63	3.57
Polaris	4.92	13.14	5.59	8.52	3.07
EasyTear View	4.05	15.1	6.49	8.13	4.01
Keratograph	4.86	19.7	7.85	9.73	5.45
POV	3.87	8.02	2.77	5.61	1.55

Due to the non-parametric nature of the results, Freidman paired wise tests with Bonferroni adjustment (due to multiple analysis being conducted on the small sample number), were implemented to measure overall agreement of NIBUT between instruments on all test subjects. Save for the EasyTear View+, significant differences have been discovered when the POV scope NIBUT times are compared with other instruments and are highlighted in orange in table 4.6.

Table 4-6: Freidman analysis between repeated results on NIBUT Measurement between instruments (n = 6)

Instrument A	Instrument B	Significance	Adjusted Significance
POV Scope	EasyTear View+	0.071	0.707
POV Scope	Tearscope	0.003	0.030
POV Scope	Polaris	0.000	0.005
POV Scope	Keratograph	0.001	0.008
EasyTear View+	Tearscope	0.245	1.000
EasyTear View+	Polaris	0.093	0.933
EasyTear View+	Keratograph	0.121	1.000
Tearscope	Polaris	0.606	1.000
Tearscope	Keratograph	0.699	1.000
Polaris	Keratograph	0.897	1.000

Although the projection pattern and coverage of the POV Scope is strong, readings suggest a consistent premature breakup of the tear film on this instrument as opposed to the others. Upon reflection this may be the result of the fundamental operation of the device as it requires high speed rotation of the LED cone to produce the POV effect and an unintended consequence is the disturbance of air around the eye. In effect the spinning LED is wafting air onto the eyeball promoting evaporative tear break up and skewing the results to a shorter NIBUT. LED cone redesign will need to take place for future tests.

Figure 4.14 shows Bland Altman plots, including mean values and 95% confidence limits, on individual NIBUT results calculated for each of the instruments compared with the POV Scope.

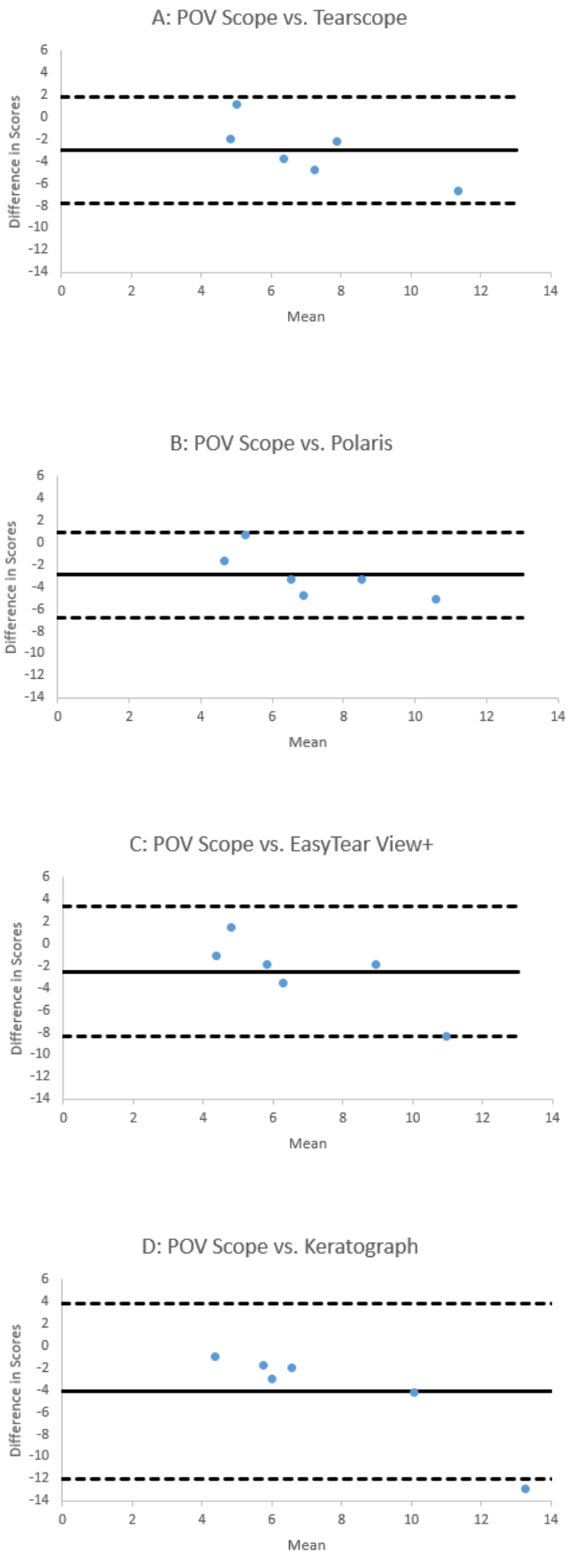

Figure 4-14: Bland Altman plots for each instrument compared with POV Scope, n=6.

Across the four comparisons there tends to be good general agreement between instruments when NIBUT values fall between 4 to 8 seconds. There spread is particularly concentrated with regards to POV Scope vs. Keratograph with exception to two outliers where divergence is noticeable in the longer test times. The remaining three instrument NIBUT values tend to be grouped in the 4 to 8 second region but with greater spacing. This is postulated to be a result of the subjective nature of the models being compared. Whereas the Keratograph is held to pre-defined computer algorithms which produce a predictable behaviour, the remaining instruments are at the mercy of interpretation from human decision making. It is therefore expected that comparison of two subjective measures will give rise to greater disparity (figures 4.14a to c) as opposed to an objective vs subjective measure, where one of the results are restrained objectively (figure 4.14d). It is this need to achieve greater confidence in obtained NIBUT values that drives the desire to improve instrument design and produce better projections that can be clearly recognised by objective computer algorithms and give consistent results.

Due to testing being separated across morning and afternoon sessions, an intra- class comparison was made between both visits totalling 60 readings across both sessions. As expected, table 4.7 shows a very strong correlation between both sets of results which is due to the same examiner being present across both periods. Any difference between morning and afternoon sessions cannot solely be contributed to just examiner bias but must also consider that the actual tear break up times experienced by participants can vary between sessions depending on their activity during the interval.

Table 4-7: Interclass correlation between morning and afternoon sessions

Session	N	Mean	Std. Dev.
Morning	30	7.97	4.17
Afternoon	30	8.28	3.97

	95% Confidence Interval	
Intra- class Correlation	Lower Bound	Upper Bound
0.821	0.624	0.915

Current cohort size is small with only 6 participants, and limited reliance should be placed on the results. To reiterate this was an exploratory study on the usability and acceptance of the new projection method on real world patients rather than a full-scale comparison study and the newly identified unintended influences of the spinning LED cone should now be considered when developing the beta instrument.

Correctly defining appropriate statistical methods to employ is difficult with disagreements between researchers common. Any future studies will take advantage of GPower calculations to estimate necessary sample size and follow recommendations expressed by Armstrong et al. for appropriate study design and statistical analysis [333].

4.6. Discussion

The newly invented POV Scope has shown great potential as an original method for measurement of NIBUT. In April 2018 a patent was submitted for the recognition of the author as the inventor of the device and the author is pursuing avenues for the commercialisation of the technology.

The wide ranging incarnations of dry eye make it difficult to identify with many inconsistent signs, and there is a general apathy toward dry eye diagnosis and treatment because of this [16, 107, 131, 135]. Contemporary objective instruments perform single point tests which still require a final interpretation by clinicians. Technology has now evolved to allow for machine learning and artificial intelligence (AI) capabilities to be built into medical devices. It is the intention of the author to take advantage of these possibilities and develop an objective, early diagnosis device for dry eye and ocular surface disease without the need for experienced doctors for the interpretation of obscure results.

The POV prototype instrument is considered to be at Technology Readiness level 3 (TRL3) and it is envisaged by the author that there shall be two eventual devices born from the original prototype- the first being a stationary unit which can be used in conjunction with common slit lamps with patients presented on a chin rest, and the second being a modular device with interaction possible either through a tablet or mobile phone interface while being used to diagnose patients beyond the restricted confines of traditional clinics.

The existing prototype uses interchangeable heads for different coloured LED illumination systems which shall be upgraded to a single head unit with multi LED blade arrangements including RGB, IR, diffuse white and diffuse blue. Unlike present devices, the POV scope will be capable of adjusting the angle of the cone to match patient face profile. Younger patients tend to have smaller head and eye socket profiles than their adult counterparts. To ensure maximum corneal coverage and therefore data collection, the cone angle will be adjustable to ensure the device perfectly matches the patient it is being used on. Not only will this simplify usage but also expand the potential for the device to be capable of measurement of many dry eye indicators such as FBUT, NIBUT, Meibomian gland dysfunction and even corneal topography.

By being portable the POV scope can also be used to diagnose conditions in mobility restricted patients such as the elderly or isolated communities in the developing world where access to transport is difficult. A well-trained clinician may visit large communities and only the patient suffering for visual complication need be referred to hospital, thereby using limited resources in

a more efficient manner while reaching greater patient numbers. Indeed it has once been said that the challenge for eye care providers in the 21st century is finding innovative solutions to build capacity within servicers in the face of diminishing resources which maintaining delivery of high- quality care.

To help lower costs and to be accessible to developing markets, the portable unit will allow for data capture through a mobile phone camera which are now abundant and can be used to control the instrument through a dedicated application developed for onboard patient record keeping and data storage as well as providing usage instructions to the operator. Dry eye questionnaires can also be part of the app allowing for more data collection and diagnosis with a higher confidence in line with DEWS II guidelines [36].

A new test for EDE is also uniquely possible with the POV Scope. Contemporary eye tests are performed in clean, closed clinics which do not necessarily reflect real world patient experiences such as environmental and wind exposure. Therefore, it can be argued that test results are not a true reflection of conditions experienced by patients in their everyday lives. However, due to the spinning nature of the cone, a slight breeze may be induced onto the ocular surface that can mimic normal windy situations and there is potential for this to be able to classify the type of dry eye disease present (either evaporative or aqueous deficient) based of tear film break up under windy conditions. More testing is however required.

Finally, control of the spinning LEDs can allow for custom pattern generation and lighting density which opens great potential for additional device features. One such possibility may be slit lamp type examinations where a vertical slit of desired dimensions is created through manipulation of LED on/ off timings. Example of various possible POV scope projection is shown in figure 4.15. Undeniably the potential of this instrument is greater than just dry eye diagnosis and through development may become capable of complete anterior eye evaluation all in the palm of one's hand.

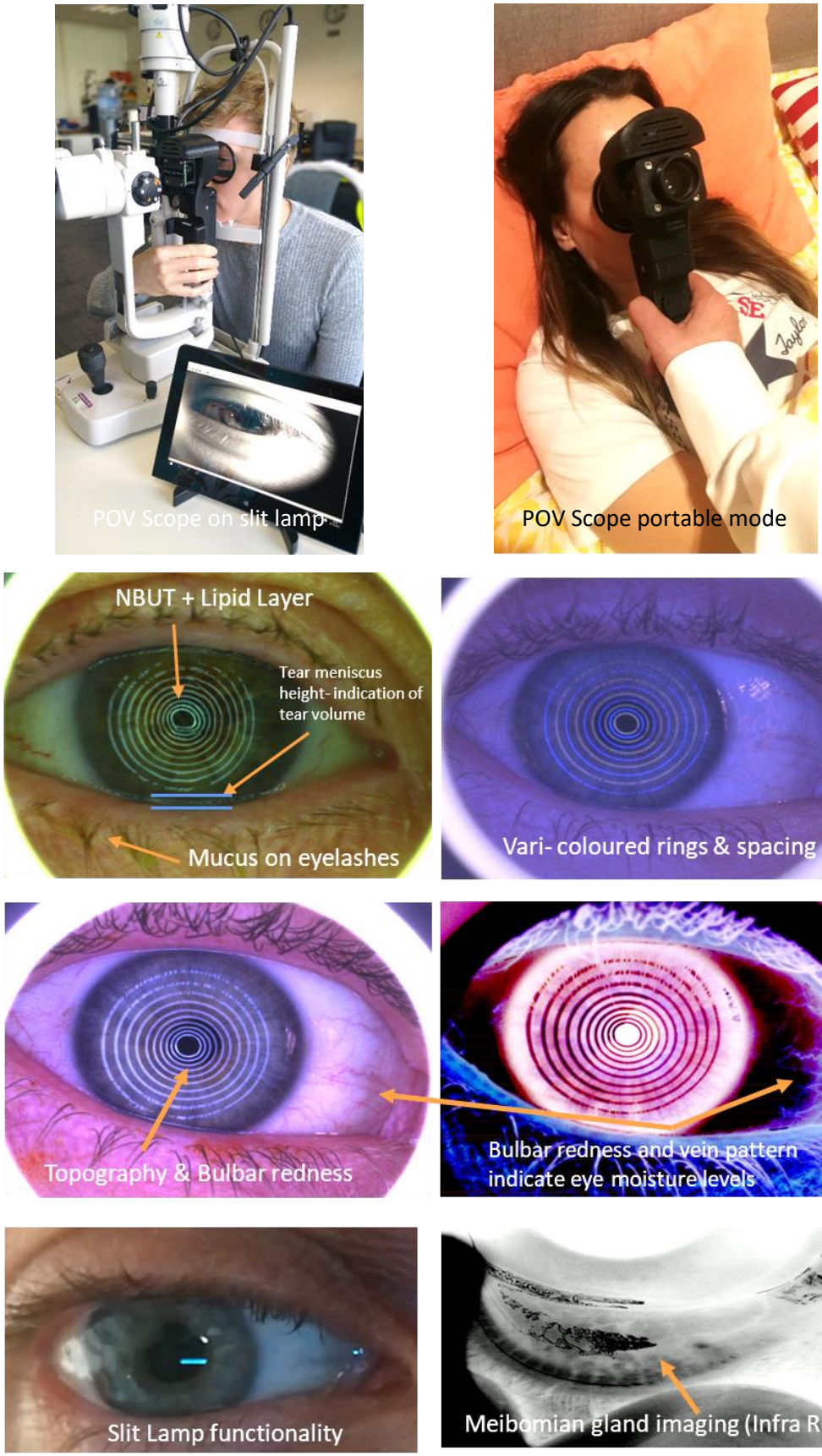

Figure 4-15: Examples of various images captured on POV Scope prototype

5. Thesis Conclusions

The irrevocable nature of advanced dry eye causes daily misery to millions of people [124, 149, 334, 335]. Seen as the chronic pain sufferers of the ophthalmic world, and with limited options for remedies, dry eye may sound rather trivial but the negative impact of one's life is substantial and often leaves patients with a choice between perpetual discomfort and pain, or the continual search for relief that is yet to be discovered [107]. To clinicians, the disease is equally frustrating with signs and symptoms not conclusively matching [135, 336] and options limited to mostly palliative care with newer treatments such as Intense Pulsed Light (IPL) and tear stimulation techniques (such as the Lipiflow System, iHeat WC) yet to prove consistent efficacy at reasonable cost [337-339].

Nelson et al. surveyed 70 dry eye sufferers and discovered the impact the disease had on their daily lives- table 5.1, with 27% of those asked indicating dry eye as the main reason for additional use of other medications – such as antibiotics and anti- inflammatory agents [107].

Table 5-1: Dry eye impact on quality of life. Data taken from A new look at dry eye disease and its treatments [107]

Quality of Life*	% of Dry Eye Patients Affected**
Lower confidence	38.6
Reduced leisure time	35.7
Daily activity frustration	34.3
Unhappy or depressed	25.7
Reduced work time	25.7
Missed outings	14.3
Change of work	12.9
Require help	11.4
Other	7.1
None of the above apply	22.9

Vision Related Activities***	% of Dry Eye Patients Affected
Driving at night	32.3
Reading	27.5
Working on computer/ bank machine	25.7
Watching television	17.9

** Any impact of symptoms*

*** Each patient allowed to indicate as many items as applicable*

**** Symptoms interfered with activities most of the time*

With the ever-increasing global population, growing exposure to visual display devices and millions of sufferers yet to be identified, dry eye is a health issue that has yet to be fully appreciated [145].

All the work contained within the preceding chapters of the thesis have focused on researching current mainstream diagnostic techniques, recognising strengths and limitations, and then pushing the boundaries for the betterment of early stage dry eye recognition. Ocular health is universally important and it is hoped that solutions proposed will cater for sufferers on all ranges of the global societal spectrum especially the often overlooked developing world populations. It is clear from the work contained within this thesis that new frontiers have been reached in addressing the growing global problems surrounding dry eye and its' reliable, early diagnosis.

Chapter 2- High Performance filters, introduced a new inexpensive approach to fluorescein imaging. Identified as one of the four key techniques for dry eye identification, and a favoured test among the professional community [122, 172], FBUT is central to dry eye diagnosis. FBUT is a low- cost technique and can be performed with minimal discomfort to the patient. Only a slit lamp with adequate filters is needed which although may be considered a trivial requirement for many developed countries, this is not always the case in poorer global regions. The author has identified that modern slit lamp filter performance is variable between manufacturers and a slow trend away from halogen to LED light sources may contribute further to disparity between examinations. Added to the fact that fluorescein observation is subjective, clinicians should have access to the best techniques available to science for the assessment of ocular health.

Blue filters are necessary to excite the fluorescein dye compound which has been instilled into the patients' eye. A companion yellow filter is used to exclude all wavelengths that fall outside of the fluorescein emission spectrum. The closer the excitation and emission filters are to ideal fluorescein the better viewing [173]. Glass filters have tended to be the preferred choice for fluorescein viewing due to the high precision with which particular colours can be tuned, but this leads to higher manufacturing costs. Optical clarity is also high and blue light hazard exposure is an important consideration.

A hands- free design was developed and plastic injection moulding manufacturing process selected. The base material was carefully chosen as polycarbonate. Although plastic dye colour is difficult to tune, final spectrum and transmission results of the both filters prove very favourable compared to glass equivalents. Due to large discrepancies between white light

sources, two blue filters were developed- one for halogen and one for LED light sourced slit lamps. 93% and 97% of ideal fluorescein coverage has been achieved, however poor transmissivity of 20 to 30% has compromised ultimate filter performance. A white diffuse filter to allow general anterior eye observation shared the same form factor and also provided positive results.

A clip-on yellow emission filter was developed separately to the blue and white filters. The mechanical requirements of filter operation forced the material selection to being polycarbonate once again. Although not ideal for optical clarity, viewing performance was high and fluorescence contrast strong. Bausch & Lomb have shown interest in distribution of the yellow filters and thus far 1,000 units have been manufactured and distributed globally, with a second 16,000 follow-up order being negotiated. Aston University optometry students have been using the filters as part of their slit lamp training in live situations.

It must be mentioned that although the blue and yellow filters work well separately, when used together performance is significantly lacking. The close excitation and emission spectra of 480 and 520 nm constrict the amount of contrast available to just a 40 nm window. Areas of differing fluorescence are difficult to distinguish from each other and this is exacerbated by the lower 20 – 30% transmissivity caused by the 3 mm cross sectional thickness of the blue filters simply meaning that less light reaches the patient eye. To compound this, there is a large region of blue and yellow filter overlap in the 500 nm region which effectively cancels out any fluorescence in this area. All these factors combine to diminish viewing and may only be improved upon by creating thinner filters with a greater and sharper separation between the blue and yellow colours.

Finally, with production costs below £1 per unit for either blue or yellow filters and performance matching, if not exceeding glass equivalents, solutions in chapter 2 serve as a reminder that expense is not always linked to performance.

Chapter 3- Non-contact approaches to tear film measurement explored the potential for low cost assessment of the physical tear film thickness and behaviour. Many common procedures for dry eye diagnosis, such as the aforementioned fluorescein instillation or osmolarity testing may disturb baseline homeostasis and skew results [183]. Various forms of dry eye have different effects on tear film dynamics, such as premature thinning and compromised composition. The search for a low-cost instrument that is capable of evaluating an invisible fluid

in the microns measurement range has until recently been beyond the possibilities of science, but would provide great insight into behaviour both pre- and post- treatment of the tear film. Extrinsic influences on dry eye such as contact lens wear or prescription medicine could be assessed. Current tear film thickness readings have been achieved through ultra- high resolution OCT with values between 2 to 5 µm viewed as healthy [93, 94]. High costs render such instruments prohibitively expensive for day to day use and as the tear film thickness is at the limit of their resolution, dynamic measurements are not obtainable.

Research focused on low cost off the shelf chromatic confocal and interferometric techniques produced by Micro Epsilon and Precitec respectively. Both instruments underwent a battery of tests on a range of anterior eye parameters including; in vivo tear film thickness measurement; in vivo pre and post contact lens tear film thickness measurement; corneal thickness; and ex vivo B- scanning possibilities.

Internationally recognised model eye values for refractive indexes were used, and consistent refractive indexes of biological materials fixed between tests. Results varied between interferometric and chromatic methods. Live tear film thickness measurements at the corneal apex were successfully achieved over a period of several blinks and clear thinning behaviour was observed over the course of the eye lid being open. This work has uncovered that it is not accurate to quote a single tear film thickness value as the fluid itself is highly dynamic and in a state of constant change. A thickness value obtained moments post blink was 3.28 µm with a thinning rate of 0.0507 μms^{-1}, both in line with existing literature [92, 97, 282]. Behaviour of tear film spreading and progressive thinning were observed for the first time and the effect of various blinking intermissions measured. The tear film is never stable and never truly at rest. Therefore, the author proposes that all future tear film thickness values should be quoted at one second after the eyelid has opened and only after several relaxed and natural complete blinks prior to measurement instance. This is sufficient time for the tear film to spread uniformly over the ocular surface and precede thinning actions which may significantly affect thickness. Secondly, tear thinning rates could be evaluated over the course of several blinks which themselves would give clinicians great awareness of tear stability and point to appropriate treatment pathways.

TFT values and thinning rates were significantly altered upon contact lens insertion, material composition and duration of wear. Such information would be a powerful tool to match dry eye suffers with appropriate lens material that promotes TF thickness and stability. No such insight currently exists, leaving patients to empirically experiment between lens material and subjectively judge personal comfort levels. Addition of eye drops resulted in a lower post-blink

TF thickness of 2.98 ± 0.243 µm, but with a slower thinning rate of 0.0185 μms^{-1}- slightly counter intuitive to expected findings which were anticipated to show an increase in tear film thickness through the addition of artificial tears.

Central corneal thickness was easily obtained but anterior chamber depth measurement proved harder due to signal attenuation through deeper layers of tissue penetration. Only one reading with the CHrocodile SE controller with 12 mm probe was successful but required much patience and a steady head. Even then it is unclear if the surfaces detected are indeed the ones that are thought to be as there is no camera present on the probe and likely surfaces must be inferred from expected values. Contact lens thickness measurement proved successful with the confocalDT 3 mm probe equipment and even recognition of CL in unopened packaging was possible which could easily translate into a new quality control method used in industry.

Investigations into B- Scanning capabilities were solely conducted with the confocalDT 2451 with 3mm probe as only this setup was available at the appropriate time. The custom 3- axis OBE rig was built specifically for this application and a plastic model eye, a porcine eye and submerged contact lens were evaluated. Out of the three samples only the plastic eye could be measured. Corneal thickness of the porcine eye proved unsuccessful due to the return signal of the probe being too weak for reliable measurement. The controller works by averaging many signals together to create a steady thickness value. The movement of the eye on the stage proved too much to lock onto a reading. A similar issue was encountered with the contact lens which was submerged in a saline solution that severely attenuated signal strength towards the lower depths where the periphery of the lens was found.

Several notable weaknesses of both Micro Epsilon confocalDT and Precitec CHRocodile SE instruments exist. The first is the restricted area over which scanning can take place; 6 – 40 µm spot diameter and an allowable tilt angle tolerance as low as ±5° depending on instrument and probe combinations. Added to this is the tiny working distance from probe face of only 3 – 180 µm for the Precitec interferometric probe. Such tight requirements severely restrict the usability of the instruments in clinical settings with day to day patients. It would simply be too difficult to correctly position the patient necessary for quick measurements and the author struggled for three weeks before readings were captured. Secondly, measurements were achieved at the corneal apex exclusively, but are blind to what may be happening in other regions of the ocular surface. To simply assume that TF thickness and thinning rates are uniform over the eyeball is incorrect. B- Scanning is possible, but not at the speed required to capture pseudo live data.

Up to this point all work was conducted with simple off the shelf probes and ready to use equipment. Both manufacturers offer custom probe designs based on user requirements which is the next step in the development of this technology. A close working partnership with the equipment supplier can yield a probe tailored exclusively to anterior eye evaluation requirements, larger scanning area and an overall better patient experience. Both manufacturers have expressed interest in such cooperation.

Chapter 4 – Non-contact evaluation of the anterior eye focused on NIBUT techniques centred on the projection and observation of mires on to the tear film. Degradation of projections reflected from the tear film give indications of stability and location of tear film breakup. Advanced contemporary instruments allow for the extraction of additional ocular information such as corneal topography, meibomian gland analysis, astigmatism, bulbar redness and other metrics. However, in addition to cost they suffer for many drawbacks, a lack of portability and large space requirements.

A completely new projection method based on the persistence of vision effect was conceived and developed into a functioning prototype and tested alongside contemporary instruments in an exploratory study consisting of six participants.

As opposed to conventional fixed projection systems such as the Oculus Keratograph or Medmont E300, the POV Scope is capable of changing its pattern, colour, spacing and angle of projection in relation to unique patient requirements. More tests can be conducted with a single instrument which occupies less space, is portable and a lower cost to produce.

The study demonstrated a mean tear film breakup time of 5.61 seconds, SD = 1.55 compared with 9.73 seconds, SD = 5.45 obtained with the industry leading Oculus Keratograph. Although the data showed a discrepancy between established instruments and the POV Scope, the reasons for this lie with the spinning cone prompting a blowing effect on to the eyeball inducing unintended evaporative tear film side effects. Refinements of the instrument continue, and the blowing can be eliminated through the introduction of a clear enclosure over the cone. A decision has been taken to spinout an Aston University company to develop the technology commercially. A patent application was submitted April 2018 and a dedicated dry eye diagnosis instrument will be developed closely following DEWS II diagnostic guidelines for evaluating the presence of dry eye [36]. Together with onboard machine learning and multi- testing capabilities, the POV Scope will be capable of providing dry eye questionnaires, NIBUT and FBUT.

In addition, Meibomian gland atrophy, bulbar redness, and tear meniscus height will all be evaluated through the onboard AI system to give a comprehensive assessment of anterior eye health and identify early dry eye conditions.

The portable nature of the instrument will disrupt the current provision of care. No longer will patients be required to make the journey to clinics for assessment. The instrument, being portable, will spare the old and immobile, typically the most susceptible to dry eye from travel. This will also be a great benefit to developing nations where populations tend to be scattered over large areas and beyond the reach of current care. It is the hope of the author that the POV Scope will indeed be the “go to” device for dry eye assessment.

5.1. Concluding Remarks

The journey to develop new approaches to anterior eye evaluation has been fruitful and shows that much room still exists to better serve patients. The complex nature of dry eye and its many incarnations leads to much frustration between clinicians who are not adequately equipped to provide comprehensive, reliable diagnosis, and growing numbers of patients which face little relief once the disease has taken hold.

It is the authors’ opinion that manufacturers offer as many testing regimes as possible and no single device exists that can be used to definitively identify dry eye without following DEWs II guidelines [39]. This may still be the case in years to come, but the work contained within this thesis has led to enhanced techniques that will enable greater direction to future instrument development and may one day lead to a single test that can accurately identify even early stage dry eye and allow for fast remedial action before the onset of permanent damage.

It can be said that this body of work is more reflective of an engineering rather than a clinical degree and that is apparent by the focus on device creation and unique applications of new techniques rather than large scale data collection. The natural next step for this completed work is to be continued by ophthalmologists with the intention to collect clinical data on the accuracy of diagnosis and further development work to take place that will bring the techniques discussed closer to real world applications and daily use. Further refinement of each technique should only take place by those close to understanding requirements of the end users and developing appropriately to meet their needs and satisfy patient expectations.

6. Bibliography

[1] RNIB, The State of the Nation Eye Health 2017: A Year in Review Royanl National Institue of Blind People, UK, 2017.
[2] K.F. Farrand, M. Fridman, I.Ö. Stillman, D.A. Schaumberg, Prevalence of Diagnosed Dry Eye Disease in the United States Among Adults Aged 18 Years and Older, American Journal of Ophthalmology 182 (2017) 90-98.
[3] N. Congdon, B. O'Colmain, C.C.W. Klaver, R. Klein, B. Munoz, D.S. Friedman, J. Kempen, H.R. Taylor, P. Mitchell, L. Hyman, G. Eye Dis Prevalence Res, Causes and prevalence of visual impairment among adults in the United States, Archives of Ophthalmology 122(4) (2004) 477-485.
[4] C.C.W. Klaver, R.C.W. Wolfs, J.R. Vingerling, A. Hofman, P. de Jong, Age-specific prevalence and causes of blindness and visual impairment in an older population - The Rotterdam Study, Archives of Ophthalmology 116(5) (1998) 653-658.
[5] S. Resnikoff, D. Pascolinia, S.P. Mariott, G.P. Pokharel, Global magnitude of visual impairment caused by uncorrected refractive errors in 2004, Bull. World Health Organ. 86(1) (2008) 63-70.
[6] World Health Organisation. International Statistical Classification of Diseases and Related Health Problems, 10th Revision (ICD-10). <http://apps.who.int/classifications/icd10/browse/2016/en#/H53-H54>, 2016 (accessed 4/4/18.).
[7] D. Pascolini, S.P. Mariotti, Global estimates of visual impairment: 2010, British Journal of Ophthalmology 96(5) (2012) 614-618.
[8] M.M. Abdull, C. Chandler, C. Gilbert, Glaucoma, "the silent thief of sight": patients' perspectives and health seeking behaviour in Bauchi, northern Nigeria, BMC Ophthalmol. 16 (2016) 9.
[9] R.L. Anderson, M.d.l.A. Ramos Cadena, J.S. Schuman, Glaucoma Diagnosis: From the Artisanal to the Defined, Ophthalmology Glaucoma 1(1) (2018) 3-14.
[10] D.M. Gibson, Frequency and predictors of missed visits to primary care and eye care providers for annually recommended diabetes preventive care services over a two-year period among U.S. adults with diabetes, Preventive Medicine 105 (2017) 257-264.
[11] C.o. Optometrists, Frequency of eye examinations. <https://guidance.college-optometrists.org/guidance-contents/knowledge-skills-and-performance-domain/the-routine-eye-examination/frequency-of-eye-examinations/>, 2018 (accessed 30/10/2018.2018).
[12] WHO, WHO | Visual impairment and blindness. <http://www.who.int/mediacentre/factsheets/fs282/en/>, 2016).
[13] M. Ibrahim, A. Bhandari, J.S. Sandhu, P. Balakrishnan, Making Sight Affordable (Part 1)-Aurolab Pioneers Production of Low-Cost Technology for Cataract Surgery, Innovations 41.
[14] L. Pezzullo, J. Streatfeild, P. Simkiss, D. Shickle, The economic impact of sight loss and blindness in the UK adult population, BMC Health Serv. Res. 18 (2018) 13.
[15] E.M. Chia, P. Mitchell, E. Rochtchina, A.J. Lee, R. Maroun, J.J. Wang, Prevalence and associations of dry eye syndrome in an older population: the Blue Mountains Eye Study, Clin. Exp. Ophthalmol. 31(3) (2003) 229-232.
[16] Globaldata, Dry Eye Syndrome- Global Drug Forecast and Market Assessment to 2024, 2015.
[17] S.C. Pflugfelder, A. Solomon, M.E. Stern, The diagnosis and management of dry eye - A twenty-five-year review, Cornea 19(5) (2000) 644-649.
[18] M.E. Johnson, P.J. Murphy, Changes in the tear film and ocular surface from dry eye syndrome, Progress in Retinal and Eye Research 23(4) (2004) 449-474.
[19] G.N. Foulks, K.K. Nichols, A.J. Bron, E.J. Holland, M.B. McDonald, J.D. Nelson, Improving Awareness, Identification, and Management of Meibomian Gland Dysfunction, Ophthalmology 119(10, Supplement) (2012) S1-S12.

[20] K. Attebo, P. Mitchell, R. Cumming, W. Smith, Knowledge and beliefs about common eye diseases, Aust. N. Z. J. Ophthalmol. 25(4) (1997) 283-287.
[21] O.S. Huang, Y.F. Zheng, W.T. Tay, P.P.C. Chiang, E.L. Lamoureux, T.Y. Wong, Lack of Awareness of Common Eye Conditions in the Community, Ophthalmic Epidemiol. 20(1) (2013) 52-60.
[22] A.S. Bruce, M.S. Loughnan, Anterior Eye Disease and Therapeutics A-Z, Churchill Livingstone2011.
[23] I.K. Gipson, The ocular surface: The challenge to enable and protect vision: The Friedenwald lecture, Investigative Ophthalmology & Visual Science 48(10) (2007) 4391-4398.
[24] M. Aramideh, B.W.O. Devisser, P.P. Deriese, L.J. Bour, J.D. Speelman, ELECTROMYOGRAPHIC FEATURES OF LEVATOR PALPEBRAE SUPERIORIS AND ORBICULARIS OCULI MUSCLES IN BLEPHAROSPASM, Brain 117 (1994) 27-38.
[25] I. Jalbert, M.C. Madigan, M. Shao, J. Ng, J. Cheng, D. Wong, C. McMonnies, Assessing the human lid margin epithelium using impression cytology, Acta Ophthalmologica 90(7) (2012) E547-E552.
[26] S. Fekrat, J.S. Weizer, All about your eyes, Durham, NC : Duke University Press, c2006.2006.
[27] K. Nakamori, M. Odawara, T. Nakajima, T. Mizutani, K. Tsubota, Blinking is controlled primarily by ocular surface conditions, American Journal of Ophthalmology 124(1) (1997) 24-30.
[28] M. Suzuki, M.L. Massingale, F. Ye, J. Godbold, T. Elfassy, M. Vallabhajosyula, P.A. Asbell, Tear Osmolarity as a Biomarker for Dry Eye Disease Severity, Investigative Ophthalmology & Visual Science 51(9) (2010) 4557-4561.
[29] W. Ngo, S. Srinivasan, L. Jones, Historical overview of imaging the meibomian glands, Journal of Optometry 6(6) (2013) 1-8.
[30] S. Mishima, D.M. Maurice, The oily layer of the tear film and evaporation from the corneal surface, Experimental Eye Research 1(1) (1961) 39-45.
[31] Eugene Wolff, The Anatomy of the Eye and Orbit, 4th (1954) 491.
[32] K.K. Nichols, G.N. Foulks, A.J. Bron, B.J. Glasgow, M. Dogru, K. Tsubota, M.A. Lemp, D.A. Sullivan, The International Workshop on Meibomian Gland Dysfunction: Executive Summary, Investigative Ophthalmology & Visual Science 52(4) (2011) 1922-1929.
[33] J.D. Nelson, J. Shimazaki, J.M. Benitez-del-Castillo, J.P. Craig, J.P. McCulley, S. Den, G.N. Foulks, The International Workshop on Meibomian Gland Dysfunction: Report of the Definition and Classification Subcommittee, Investigative Ophthalmology & Visual Science 52(4) (2011) 1930-1937.
[34] T. Chalkley, Your Eyes : A Book for Paramedical Personnel and the Lay Reader, 4th ed., Charles C. Thomas2000.
[35] I.A. Mackie, D.V. Seal, DIAGNOSTIC IMPLICATIONS OF TEAR PROTEIN PROFILES, British Journal of Ophthalmology 68(5) (1984) 321-324.
[36] J.S. Wolffsohn, R. Arita, R. Chalmers, A. Djalilian, M. Dogru, K. Dumbleton, P.K. Gupta, P. Karpecki, S. Lazreg, H. Pult, B.D. Sullivan, A. Tomlinson, L. Tong, E. Villani, K.C. Yoon, L. Jones, J.P. Craig, TFOS DEWS II Diagnostic Methodology report, Ocular Surface 15(3) (2017) 539-574.
[37] X.R. Zhang, Q.S. Li, B. Liu, H.M. Zhou, H.M. Wang, Z.Y. Zhang, M.H. Xiang, Z.M. Han, H.D. Zou, In Vivo Cross-Sectional Observation and Thickness Measurement of Bulbar Conjunctiva Using Optical Coherence Tomography, Investigative Ophthalmology & Visual Science 52(10) (2011) 7787-7791.
[38] I.K. Gipson, Y. Hori, P. Argüeso, Character of Ocular Surface Mucins and Their Alteration in Dry Eye Disease, The Ocular Surface 2(2) (2004) 131-148.
[39] M.D.P. Willcox, P. Argueso, G.A. Georgiev, J.M. Holopainen, G.W. Laurie, T.J. Millar, E.B. Papas, J.P. Rolland, T.A. Schmidt, U. Stahl, T. Suarez, L.N. Subbaraman, O.O. Ucakhan, L. Jones, TFOS DEWS II Tear Film Report, Ocular Surface 15(3) (2017) 366-403.
[40] N.A. McBrien, A. Gentle, Role of the sclera in the development and pathological complications of myopia, Progress in Retinal and Eye Research 22(3) (2003) 307-338.

[41] M. Batterbury, B. Bowling, C. Murphy, Ophthalmology, Third Edition ed., Elsevier Health Sciences2009.
[42] H.S. Dua, L.A. Faraj, D.G. Said, T. Gray, J. Lowe, Human Corneal Anatomy Redefined A Novel Pre-Descemet's Layer (Dua's Layer), Ophthalmology 120(9) (2013) 1778-1785.
[43] A.J. Bron, P. Argueeso, M. Irkec, F.V. Bright, Clinical staining of the ocular surface: Mechanisms and interpretations, Progress in Retinal and Eye Research 44 (2015) 36-61.
[44] P. Rosenthal, I. Baran, D.S. Jacobs, Corneal Pain without Stain: Is it Real?, The Ocular Surface 7(1) (2009) 28-40.
[45] M.J. Doughty, M.L. Zaman, Human corneal thickness and its impact on intraocular pressure measures: A review and meta-analysis approach, Survey of Ophthalmology 44(5) (2000) 367-408.
[46] I.o. Physics, Dissectible model eye. <http://practicalphysics.org/dissectible-model-eye.html>, 2016 (accessed 21/07/2016.).
[47] F. Mantelli, J. Mauris, P. Argüeso, The ocular surface epithelial barrier and other mechanisms of mucosal protection: from allergy to infectious diseases, Current opinion in allergy and clinical immunology 13(5) (2013) 10.1097/ACI.0b013e3283645899.
[48] I.K. Gipson, P. Argueso, Role of mucins in the function of the corneal and conjunctival epithelia, in: K.W. Jeon (Ed.), International Review of Cytology - a Survey of Cell Biology, Vol 231, Elsevier Academic Press Inc, San Diego, 2003, pp. 1-+.
[49] M.E. Bramwell, G. Wiseman, D.M. Shotton, Electron-microscopic studies of the CA antigen, epitectin, Journal of Cell Science 86(1) (1986) 249-261.
[50] J.P. Craig, M.D.P. Willcox, P. Argüeso, C. Maissa, U. Stahl, A. Tomlinson, J. Wang, N. Yokoi, F. Stapleton, The TFOS International Workshop on Contact Lens Discomfort: Report of the Contact Lens Interactions With the Tear Film Subcommittee, Investigative Ophthalmology & Visual Science 54(11) (2013) TFOS123-TFOS156.
[51] I.G. Morgan, K. Ohno-Matsui, S.M. Saw, Ophthalmology 2 Myopia, Lancet 379(9827) (2012) 1739-1748.
[52] P.J. Foster, Y. Jiang, Epidemiology of myopia, Eye 28(2) (2014) 202-208.
[53] C. Nischler, R. Michael, C. Wintersteller, P. Marvan, L.J. van Rijn, J.E. Coppens, T. van den Berg, M. Emesz, G. Grabner, Iris color and visual functions, Graefes Archive for Clinical and Experimental Ophthalmology 251(1) (2013) 195-202.
[54] H. Hüsniye Telek, The Effects of Age Pupil Diameters at Different Light Amplitudes, 2018.
[55] B. Winn, D. Whitaker, D.B. Elliott, N.J. Phillips, FACTORS AFFECTING LIGHT-ADAPTED PUPIL SIZE IN NORMAL HUMAN-SUBJECTS, Investigative Ophthalmology & Visual Science 35(3) (1994) 1132-1137.
[56] S. Kasthurirangan, A. Glasser, Age related changes in the characteristics of the near pupil response, Vision Research 46(8) (2006) 1393-1403.
[57] M. Goel, R.G. Picciani, R.K. Lee, S.K. Bhattacharya, Aqueous humor dynamics: a review, The open ophthalmology journal 4 (2010) 52-9.
[58] M. Dubbelman, G.L. Van der Heijde, H.A. Weeber, G.F.J.M. Vrensen, Changes in the internal structure of the human crystalline lens with age and accommodation, Vision Research 43(22) (2003) 2363-2375.
[59] R.A. Weale, AGE AND THE TRANSMITTANCE OF THE HUMAN CRYSTALLINE LENS, J. Physiol.-London 395 (1988) 577-587.
[60] P.J.T. Shum, L.S. Ko, C.L. Ng, S.L. Lin, A BIOMETRIC STUDY OF OCULAR CHANGES DURING ACCOMMODATION, American Journal of Ophthalmology 115(1) (1993) 76-81.
[61] A. Glasser, M.C.W. Campbell, Presbyopia and the optical changes in the human crystalline lens with age, Vision Research 38(2) (1998) 209-229.
[62] R.B. Vajpayee, S. Joshi, R. Saxena, S.K. Gupta, Epidemiology of cataract in India: Combating plans and strategies, Ophthalmic Research 31(2) (1999) 86-92.

[63] H. Wong, I. Fatt, C.J. Radke, Deposition and thinning of the human tear film, J. Colloid Interface Sci. 184(1) (1996) 44-51.
[64] J.X. Huang, Q. Yuan, B.Y. Zhang, K. Xu, P. Tankam, E. Clarkson, M.A. Kupinski, H.B. Hindman, J.V. Aquavella, T.J. Suleski, J.P. Rolland, Measurement of a multi-layered tear film phantom using optical coherence tomography and statistical decision theory, Biomed. Opt. Express 5(12) (2014) 4374-4386.
[65] J.I. Prydal, P. Artal, W. Hong, F.W. Campbell, STUDY OF HUMAN PRECORNEAL TEAR FILM THICKNESS AND STRUCTURE USING LASER INTERFEROMETRY, Investigative Ophthalmology & Visual Science 33(6) (1992) 2006-2011.
[66] Y. Danjo, M. Nakamura, T. Hamano, MEASUREMENT OF THE PRECORNEAL TEAR FILM THICKNESS WITH A NONCONTACT OPTICAL INTERFEROMETRY FILM THICKNESS MEASUREMENT SYSTEM, Jpn. J. Ophthalmol. 38(3) (1994) 260-266.
[67] R.J. Braun, Dynamics of the Tear Film, in: S.H. Davis, P. Moin (Eds.), Annual Review of Fluid Mechanics, Vol 44, Annual Reviews, Palo Alto, 2012, pp. 267-297.
[68] F.J. Holly, M.A. Lemp, TEAR PHYSIOLOGY AND DRY EYES, Survey of Ophthalmology 22(2) (1977) 69-87.
[69] M.G. Doane, Abnormalities of the structure of the superficial lipid layer on the in vivo dry-eye tear film, Advances in Experimental Medicine and Biology 350 (1994) 489-493.
[70] S. Khanal, T.J. Millar, Nanoscale phase dynamics of the normal tear film, Nanomed.-Nanotechnol. Biol. Med. 6(6) (2010) 707-713.
[71] P.E. King-Smith, E.A. Hinel, J.J. Nichols, Application of a Novel Interferometric Method to Investigate the Relation between Lipid Layer Thickness and Tear Film Thinning, Investigative Ophthalmology & Visual Science 51(5) (2010) 2418-2423.
[72] D.R. Korb, C.A. Blackie, "Dry Eye" Is the Wrong Diagnosis for Millions, Optometry and Vision Science 92(9) (2015) E350-E354.
[73] J.P. Craig, K.K. Nichols, E.K. Akpek, B. Caffery, H.S. Dua, C.K. Joo, Z.G. Liu, J.D. Nelson, J.J. Nichols, K. Tsubota, F. Stapleton, TFOS DEWS II Definition and Classification Report, Ocular Surface 15(3) (2017) 276-283.
[74] A.J. Bron, J.M. Tiffany, S.M. Gouveia, N. Yokoi, L.W. Voon, Functional aspects of the tear film lipid layer, Experimental Eye Research 78(3) (2004) 347-360.
[75] J.P. Craig, A. Tomlinson, Importance of the lipid layer in human tear film stability and evaporation, Optometry and Vision Science 74(1) (1997) 8-13.
[76] W. Mathers, Evaporation from the ocular surface, Experimental Eye Research 78(3) (2004) 389-394.
[77] C. Garcia-Resua, M.J.G. Fernandez, M.F.G. Penedo, D. Calvo, M. Penas, E. Yebra-Pimentel, New Software Application for Clarifying Tear Film Lipid Layer Patterns, Cornea 32(4) (2013) 538-546.
[78] P.E. King-Smith, K.S. Reuter, R.J. Braun, J.J. Nichols, K.K. Nichols, Tear Film Breakup and Structure Studied by Simultaneous Video Recording of Fluorescence and Tear Film Lipid Layer Images, Investigative Ophthalmology & Visual Science 54(7) (2013) 4900-4909.
[79] J. Shimazaki, E. Goto, M. Ono, S. Shimmura, K. Tsubota, Meibomian gland dysfunction in patients with Sjögren syndrome11No author has any proprietary interest in the marketing of this material, Ophthalmology 105(8) (1998) 1485-1488.
[80] A.J. Bron, The Doyne Lecture - Reflections on the tears, Eye 11 (1997) 583-602.
[81] M. Rolando, M. Zierhut, The ocular surface and tear film and their dysfunction in dry eye disease, Survey of Ophthalmology 45 (2001) S203-S210.
[82] L. Zhou, S.Z. Zhao, S.K. Koh, L. Chen, C. Vaz, V. Tanavde, X.R. Li, R.W. Beuerman, In-depth analysis of the human tear proteome, Journal of Proteomics 75(13) (2012) 3877-3885.
[83] M. Azkargorta, J. Soria, C. Ojeda, F. Guzmán, A. Acera, I. Iloro, T. Suárez, F. Elortza, Human Basal Tear Peptidome Characterization by CID, HCD, and ETD Followed by in Silico and in Vitro

Analyses for Antimicrobial Peptide Identification, Journal of Proteome Research 14(6) (2015) 2649-2658.
[84] I.A. Butovich, Meibomian glands, meibum, and meibogenesis, Experimental Eye Research 163 (2017) 2-16.
[85] T.L. Kessler, H.J. Mercer, J.D. Zieske, D.M. McCarthy, D.A. Dartt, STIMULATION OF GOBLET CELL MUCOUS SECRETION BY ACTIVATION OF NERVES IN RAT CONJUNCTIVA, Curr. Eye Res. 14(11) (1995) 985-992.
[86] J.X. Huang, H.B. Hindman, J.P. Rolland, In vivo thickness dynamics measurement of tear film lipid and aqueous layers with optical coherence tomography and maximum-likelihood estimation, Optics Letters 41(9) (2016) 1981-1984.
[87] S. Martinez-Conde, J. Otero-Millan, S.L. Macknik, The impact of microsaccades on vision: towards a unified theory of saccadic function, Nature Reviews Neuroscience 14(2) (2013) 83-96.
[88] K. Tsubota, S. Hata, Y. Okusawa, F. Egami, T. Ohtsuki, K. Nakamori, Quantitative videographic analysis of blinking in normal subjects and patients with dry eye, Archives of Ophthalmology 114(6) (1996) 715-720.
[89] N. Fogt, P.E. King-Smith, G. Tuell, Interferometric measurement of tear film thickness by use of spectral oscillations, Journal of the Optical Society of America a-Optics Image Science and Vision 15(1) (1998) 268-275.
[90] D.A. Benedetto, D.O. Shah, H.E. Kaufman, The instilled fluid dynamics and surface chemistry of polymers in the preocular tear film, Investigative ophthalmology & visual science 14(12) (1975) 887-902.
[91] S. Mishima, Some Physiological Aspects of the Precorneal Tear Film, 1965.
[92] P.E. King-Smith, B.A. Fink, N. Fogt, K.K. Nichols, R.M. Hill, G.S. Wilson, The thickness of the human precorneal tear film: Evidence from reflection spectra, Investigative Ophthalmology & Visual Science 41(11) (2000) 3348-3359.
[93] Q. Chen, J.H. Wang, A.Z. Tao, M.X. Shen, S.L. Jiao, F. Lu, Ultrahigh-Resolution Measurement by Optical Coherence Tomography of Dynamic Tear Film Changes on Contact Lenses, Investigative Ophthalmology & Visual Science 51(4) (2010) 1988-1993.
[94] V.A. dos Santos, L. Schmetterer, M. Groschl, G. Garhofer, D. Schmidl, M. Kucera, A. Unterhuber, J.P. Hermand, R.M. Werkmeister, In vivo tear film thickness measurement and tear film dynamics visualization using spectral domain optical coherence tomography, Opt. Express 23(16) (2015) 21043-21063.
[95] P.A. Wozniak, D. Schmidl, A.M. Bata, K. Fondi, K.J. Witkowska, V.A. dos Santos, C. Baar, K.I. Room, J. Nepp, I. Baumgartner, A. Popa-Cherecheanu, G. Garhofer, R.M. Werkmeister, L. Schmetterer, Effect of different lubricant eye gels on tear film thickness as measured with ultrahigh-resolution optical coherence tomography, Acta Ophthalmologica 95(4) (2017) E307-E313.
[96] T. Schmoll, A. Unterhuber, C. Kolbitsch, T. Le, A. Stingl, R. Leitgeb, Precise Thickness Measurements of Bowman's Layer, Epithelium, and Tear Film, Optometry and Vision Science 89(5) (2012) E795-E802.
[97] R.M. Werkmeister, A. Alex, S. Kaya, A. Unterhuber, B. Hofer, J. Riedl, M. Bronhagl, M. Vietauer, D. Schmidl, T. Schmoll, G. Garhofer, W. Drexler, R.A. Leitgeb, M. Groeschl, L. Schmetterer, Measurement of Tear Film Thickness Using Ultrahigh-Resolution Optical Coherence Tomography, Investigative Ophthalmology & Visual Science 54(8) (2013) 5578-5583.
[98] J.E. McDonald, Surface Phenomena of the Tear Film, American Journal of Ophthalmology 67(1) (1969) 56-64.
[99] D.G. Green, B.R. Frueh, J.M. Shapiro, Corneal thickness measured by interferometry, Journal of the Optical Society of America 65(2) (1975) 119-23.
[100] E. Hosaka, T. Kawamorita, Y. Ogasawara, N. Nakayama, H. Uozato, K. Shimizu, M. Dogru, K. Tsubota, E. Goto, Interferometry in the Evaluation of Precorneal Tear Film Thickness in Dry Eye, American Journal of Ophthalmology 151(1) (2011) 18-23.e1.

[101] J.P. Craig, J.D. Nelson, D.T. Azar, C. Belmonte, A.J. Bron, S.K. Chauhan, C.S. de Paiva, J.A.P. Gomes, K.M. Hammitt, L. Jones, J.J. Nichols, K.K. Nichols, G.D. Novack, F.J. Stapleton, M.D.P. Willcox, J.S. Wolffsohn, D.A. Sullivan, TFOS DEWS II Report Executive Summary, Ocular Surface 15(4) (2017) 802-812.
[102] B. Miljanović, R. Dana, D.A. Sullivan, D.A. Schaumberg, Impact of Dry Eye Syndrome on Vision-Related Quality of Life, American Journal of Ophthalmology 143(3) (2007) 409-415.e2.
[103] J.H. Yu, C.V. Asche, C.J. Fairchild, The Economic Burden of Dry Eye Disease in the United States: A Decision Tree Analysis, Cornea 30(4) (2011) 379-387.
[104] M.A. Lemp, RECENT DEVELOPMENTS IN DRY EYE MANAGEMENT, Ophthalmology 94(10) (1987) 1299-1304.
[105] M.A. Lemp, M.A. Mahmood, H.H. Weiler, ASSOCIATION OF ROSACEA AND KERATOCONJUNCTIVITIS SICCA, Archives of Ophthalmology 102(4) (1984) 556-557.
[106] K.K. Nichols, C.G. Begley, B. Caffery, L.A. Jones, Symptoms of ocular irritation in patients diagnosed with dry eye, Optometry and Vision Science 76(12) (1999) 838-844.
[107] J.D. Nelson, H. Helms, R. Fiscella, Y. Southwell, J.D. Hirsch, A new look at dry eye disease and its treatment, Advances in Therapy 17(2) (2000) 84-93.
[108] A.J. Bron, C.S. de Paiva, S.K. Chauhan, S. Bonini, E.E. Gabison, S. Jain, E. Knop, M. Markoulli, Y. Ogawa, V. Perez, Y. Uchino, N. Yokoi, D. Zoukhri, D.A. Sullivan, TFOS DEWS II pathophysiology report, Ocular Surface 15(3) (2017) 438-510.
[109] T. Schlote, G. Kadner, N. Freudenthaler, Marked reduction and distinct patterns of eye blinking in patients with moderately dry eyes during video display terminal use, Graefe's Archive for Clinical and Experimental Ophthalmology 242(4) (2004) 306-312.
[110] W.J. Yang, Y.N. Yang, J. Cao, Z.H. Man, J. Yuan, X. Xiao, Y.Q. Xing, Risk Factors for Dry Eye Syndrome: A Retrospective Case-Control Study, Optometry and Vision Science 92(9) (2015) E199-E205.
[111] L.L. Tan, P. Morgan, Z.Q. Cai, R.A. Straughan, Prevalence of and risk factors for symptomatic dry eye disease in Singapore, Clinical and Experimental Optometry 98(1) (2015) 45-53.
[112] M.J. Doughty, D. Fonn, D. Richter, T. Simpson, B. Caffery, K. Gordon, A patient questionnaire approach to estimating the prevalence of dry eye symptoms in patients presenting to optometric practices across Canada, Optometry and Vision Science 74(8) (1997) 624-631.
[113] J.J. Nichols, C. Ziegler, G.L. Mitchell, K.K. Nichols, Self-reported dry eye disease across refractive modalities, Investigative Ophthalmology & Visual Science 46(6) (2005) 1911-1914.
[114] C.G. Begley, R.L. Chalmers, G.L. Mitchell, K.K. Nichols, B. Caffery, T. Simpson, R. DuToit, J. Portello, L. Davis, Characterization of ocular surface symptoms from optometric practices in North America, Cornea 20(6) (2001) 610-618.
[115] A. Sommer, Xerophthalmia and vitamin a status, Progress in Retinal and Eye Research 17(1) (1998) 9-31.
[116] E.M. Hay, E. Thomas, B. Pal, A. Hajeer, H. Chambers, A.J. Silman, Weak association between subjective symptoms of and objective testing for dry eyes and dry mouth: results from a population based study, Annals of the Rheumatic Diseases 57(1) (1998) 20.
[117] J.P. McCulley, G.F. Sciallis, MEIBOMIAN KERATOCONJUNCTIVITIS, American Journal of Ophthalmology 84(6) (1977) 788-793.
[118] J.J. Nichols, G.L. Mitchell, P.E. King-Smith, Thinning rate of the precorneal and prelens tear films, Investigative Ophthalmology & Visual Science 46(7) (2005) 2353-2361.
[119] E. Knop, N. Knop, T. Millar, H. Obata, D.A. Sullivan, The International Workshop on Meibomian Gland Dysfunction: Report of the Subcommittee on Anatomy, Physiology, and Pathophysiology of the Meibomian Gland, Investigative Ophthalmology & Visual Science 52(4) (2011) 1938-1978.

[120] F. Stapleton, M. Alves, V.Y. Bunya, I. Jalbert, K. Lekhanont, F. Malet, K.S. Na, D. Schaumberg, M. Uchino, J. Vehof, E. Viso, S. Vitale, L. Jones, TFOS DEWS II Epidemiology Report, Ocular Surface 15(3) (2017) 334-365.
[121] M.A. Lemp, C. Baudouin, J. Baum, M. Dogru, G.N. Foulks, S. Kinoshita, P. Laibson, J. McCulley, J. Murube, S.C. Pflugfelder, M. Rolando, I. Toda, The definition and classification of dry eye disease: Report of the Definition and Classification Subcommittee of the international Dry Eye WorkShop (2007), Ocular Surface 5(2) (2007) 75-92.
[122] K.K. Nichols, J.J. Nichols, K. Zadnik, Frequency of Dry Eye Diagnostic Test Procedures Used in Various Modes of Ophthalmic Practice, Cornea 19(4) (2000) 477-482.
[123] D.A. Schaumberg, R. Dana, J.E. Buring, D.A. Sullivan, Prevalence of Dry Eye Disease Among US Men Estimates From the Physicians' Health Studies, Archives of Ophthalmology 127(6) (2009) 763-768.
[124] D.A. Schaumberg, D.A. Sullivan, J.E. Buring, M.R. Dana, Prevalence of dry eye syndrome among US women, American Journal of Ophthalmology 136(2) (2003) 318-326.
[125] A.J. Lee, J. Lee, S.-M. Saw, G. Gazzard, D. Koh, D. Widjaja, D.T.H. Tan, Prevalence and risk factors associated with dry eye symptoms: a population based study in Indonesia, British Journal of Ophthalmology 86(12) (2002) 1347-1351.
[126] V. Council, Digital Eye Strain Report, Eyes Overexposed: The digital device dilema, Vision Council, 225 Reinekers Lane Suite 700, Alexandria, VA 22314, 2016, p. 14.
[127] C. Blehm, S. Vishnu, A. Khattak, S. Mitra, R.W. Yee, Computer vision syndrome: A review, Survey of Ophthalmology 50(3) (2005) 253-262.
[128] I. Morgan, K. Rose, How genetic is school myopia?, Progress in Retinal and Eye Research 24(1) (2005) 1-38.
[129] L. Sorbara, T. Simpson, S. Vaccari, L. Jones, D. Fonn, Tear turnover rate is reduced in patients with symptomatic dry eye, Contact Lens and Anterior Eye 27(1) (2004) 15-20.
[130] K. Tsubota, Tear dynamics and dry eye, Progress in Retinal and Eye Research 17(4) (1998) 565-596.
[131] O.D. Schein, B. MuÑOz, J.M. Tielsch, K. Bandeen-Roche, S. West, Prevalence of Dry Eye Among the Elderly, American Journal of Ophthalmology 124(6) (1997) 723-728.
[132] S.E. Moss, R. Klein, B.E.K. Klein, Prevalence of and risk factors for dry eye syndrome, Archives of Ophthalmology 118(9) (2000) 1264-1268.
[133] P.-Y. Lin, S.-Y. Tsai, C.-Y. Cheng, J.-H. Liu, P. Chou, W.-M. Hsu, Prevalence of dry eye among an elderly Chinese population in Taiwan: The Shihpai Eye Study, Ophthalmology 110(6) (2003) 1096-1101.
[134] H. Hassan, K. Mehdi, K. Ahmad, E.M. Hassan, M. Shiva, S. Mohammad, F. Akbar, Prevalence of dry eye syndrome in an adult population, Clinical & Experimental Ophthalmology 42(3) (2014) 242-248.
[135] C.A. McCarty, A.K. Bansal, P.M. Livingston, Y.L. Stanislavsky, H.R. Taylor, The epidemiology of dry eye in Melbourne, Australia11Consumable items for the dry eye examinations were provided by Smith & Nephew, Melbourne, Australia, and Alcon Australia, Sydney, Australia, Ophthalmology 105(6) (1998) 1114-1119.
[136] B.D. Sullivan, L.A. Crews, E.M. Messmer, G.N. Foulks, K.K. Nichols, P. Baenninger, G. Geerling, F. Figueiredo, M.A. Lemp, Correlations between commonly used objective signs and symptoms for the diagnosis of dry eye disease: clinical implications, Acta Ophthalmologica 92(2) (2014) 161-166.
[137] G.N. Foulks, Challenges and Pitfalls in Clinical Trials of Treatments for Dry Eye, The Ocular Surface 1(1) (2003) 20-30.
[138] S. Narayanan, W.L. Miller, T.C. Prager, J.A. Jackson, N.E. Leach, A.M. McDermott, M.T. Christensen, J.P.G. Bergmanson, The diagnosis and characteristics of moderate dry eye in non-contact lens wearers, Eye and Contact Lens 31(3) (2005) 96-104.

[139] K. Tsubota, I. Toda, Y. Yagi, Y. Ogawa, M. Ono, K. Yoshino, Three different types of dry eye syndrome, Cornea 13(3) (1994) 202-209.
[140] T. Hikichi, A. Yoshida, Y. Fukui, T. Hamano, M. Ri, K. Araki, K. Horimoto, E. Takamura, K. Kitagawa, M. Oyama, Y. Danjo, S. Kondo, H. Fujishima, I. Toda, K. Tsubota, PREVALENCE OF DRY EYE IN JAPANESE EYE CENTERS, Graefes Archive for Clinical and Experimental Ophthalmology 233(9) (1995) 555-558.
[141] P. Versura, V. Profazio, M. Cellini, A. Torreggiani, R. Caramazza, Eye discomfort and air pollution, Ophthalmologica 213(2) (1999) 103-109.
[142] C.G. Begley, R.L. Chalmers, L. Abetz, K. Venkataraman, P. Mertzanis, B.A. Caffery, C. Snyder, T. Edrington, D. Nelson, T. Simpson, The relationship between habitual patient-reported symptoms and clinical signs among patients with dry eye of varying severity, Investigative Ophthalmology & Visual Science 44(11) (2003) 4753-4761.
[143] K.K. Nichols, G.L. Mitchell, K. Zadnik, The repeatability of clinical measurements of dry eye, Cornea 23(3) (2004) 272-285.
[144] B.D. Sullivan, D. Whitmer, K.K. Nichols, A. Tomlinson, G.N. Foulks, G. Geerling, J.S. Pepose, V. Kosheleff, A. Porreco, M.A. Lemp, An Objective Approach to Dry Eye Disease Severity, Investigative Ophthalmology & Visual Science 51(12) (2010) 6125-6130.
[145] Globaldata, Dry Eye Syndrome: Epidemiology Forecast to 2026, 2018.
[146] Y. Jie, L. Xu, Y.Y. Wu, J.B. Jonas, Prevalence of dry eye among adult Chinese in the Beijing Eye Study, Eye 23 (2008) 688.
[147] M. Uchino, Y. Nishiwaki, T. Michikawa, K. Shirakawa, E. Kuwahara, M. Yamada, M. Dogru, D.A. Schaumberg, T. Kawakita, T. Takebayashi, K. Tsubota, Prevalence and Risk Factors of Dry Eye Disease in Japan: Koumi Study, Ophthalmology 118(12) (2011) 2361-2367.
[148] J. Vehof, D. Kozareva, P.G. Hysi, C.J. Hammond, Prevalence and risk factors of dry eye disease in a British female cohort, British Journal of Ophthalmology 98(12) (2014) 1712-1717.
[149] E. Viso, M.T. Rodriguez-Ares, F. Gude, Prevalence of and Associated Factors for Dry Eye in a Spanish Adult Population (The Salnes Eye Study), Ophthalmic Epidemiol. 16(1) (2009) 15-21.
[150] L. Farris, Tear Osmolarity- A New Gold Standard?, Lacrimal Gland, Tear Film, and Dry Eye Syndromes (1994) 495-503.
[151] M.E. Johnson, P.J. Murphy, Temporal changes in the tear menisci following a blink, Experimental Eye Research 83(3) (2006) 517-525.
[152] J.H. Lee, P.M. Hyun, The reproducibility of the Schirmer test, Korean J Ophthalmol 2(1) (1988) 5-8.
[153] C. Jacobi, A. Jacobi, F.E. Kruse, C. Cursiefen, Tear Film Osmolarity Measurements in Dry Eye Disease Using Electrical Impedance Technology, Cornea 30(12) (2011) 1289-1292.
[154] A.M. Masmali, S. Al-Qhtani, T.M. Al-Gasham, G.A. El-Hiti, C. Purslow, P.J. Murphy, Application of a new grading scale for tear ferning in non-dry eye and dry eye subjects, Contact Lens & Anterior Eye 38(1) (2015) 39-43.
[155] I. Jalbert, F. Stapleton, E. Papas, D.F. Sweeney, M. Coroneo, In vivo confocal microscopy of the human cornea, British Journal of Ophthalmology 87(2) (2003) 225-236.
[156] B. Golebiowski, E. Papas, F. Stapleton, Assessing the sensory function of the ocular surface: Implications of use of a non-contact air jet aesthesiometer versus the Cochet-Bonnet aesthesiometer, Experimental Eye Research 92(5) (2011) 408-413.
[157] D.R. Iskander, M.J. Collins, Applications of high-speed videokeratoscopy, Clinical and Experimental Optometry 88(4) (2005) 223-231.
[158] R. Lee, S. Yeo, H.T. Aung, L. Tong, Agreement of noninvasive tear break-up time measurement between Tomey RT-7000 Auto Refractor-Keratometer and Oculus Keratograph 5M, Clinical Ophthalmology 10 (2016) 1785-1790.
[159] M.T.M. Wang, P.J. Murphy, K.J. Blades, J.P. Craig, Comparison of non-invasive tear film stability measurement techniques, Clinical and Experimental Optometry 101(1) (2018) 13-17.

[160] C. Purslow, J. Wolffsohn, The relation between physical properties of the anterior eye and ocular surface temperature, Optometry and Vision Science 84(3) (2007) 197-201.
[161] A.A. Abusharha, E.I. Pearce, The Effect of Low Humidity on the Human Tear Film, Cornea 32(4) (2013) 429-434.
[162] H. Pult, B.H. Riede-Pult, Non-contact meibography: Keep it simple but effective, Contact Lens & Anterior Eye 35(2) (2012) 77-80.
[163] H. Pult, C. Purslow, P.J. Murphy, The relationship between clinical signs and dry eye symptoms, Eye 25(4) (2011) 502-510.
[164] D.R. Korb, Survey of preferred tests for diagnosis of the tear film and dry eye, Cornea 19(4) (2000) 483-486.
[165] R.M. Schiffman, M.D. Christianson, G. Jacobsen, J.D. Hirsch, B.L. Reis, Reliability and validity of the ocular surface disease index, Archives of Ophthalmology 118(5) (2000) 615-621.
[166] C.G. Begley, B. Caffery, R.L. Chalmers, G.L. Mitchell, G. Dry Eye Invest Study, Use of the dry eye questionnaire to measure symptoms of ocular irritation in patients with aqueous tear deficient dry eye, Cornea 21(7) (2002) 664-670.
[167] K.K. Nichols, J.J. Nichols, G.L. Mitchell, The reliability and validity of McMonnies dry eye index, Cornea 23(4) (2004) 365-371.
[168] R.A. de, Sr, Lacrimation in normal eyes, A.M.A. Archives of Ophthalmology 49(2) (1953) 185-189.
[169] G. Savini, P. Prabhasawat, T. Kojima, M. Grueterich, E. Espana, E. Goto, The challenge of dry eye diagnosis, 2008.
[170] N. García-Porta, A. Mann, V. Sáez-Martínez, V. Franklin, J.S. Wolffsohn, B. Tighe, The potential influence of Schirmer strip variables on dry eye disease characterisation, and on tear collection and analysis, Contact Lens and Anterior Eye 41(1) (2018) 47-53.
[171] M.S. NORN, DESICCATION OF THE PRECORNEAL FILM, Acta Ophthalmologica 47(4) (1969) 865-880.
[172] A.W. Turner, C.J. Layton, A.J. Bron, Survey of eye practitioners' attitudes towards diagnostic tests and therapies for dry eye disease, Clin. Exp. Ophthalmol. 33(4) (2005) 351-355.
[173] R.C. Peterson, J.S. Wolffsohn, C.W. Fowler, Optimization of Anterior Eye Fluorescein Viewing, American Journal of Ophthalmology 142(4) (2006) 572–575.e2.
[174] J.W. McLaren, R.F. Brubaker, Light sources for fluorescein fluorophotometry, Appl. Opt. 22(18) (1983) 2897-2905.
[175] R.H. Rengstorff, Precorneal tear film - breakup time and location in normal subjects, American Journal of Optometry and Physiological Optics 51(10) (1974) 765-769.
[176] M.J.P.D. Collins, D.R.P.D. Iskander, A.B.S.O. Saunders, S.B.S.O. Hook, E.B.S.O. Anthony, R.B.S.O. Gillon, Blinking Patterns and Corneal Staining Eye & Contact Lens: Science & Clinical Practice 32(6) (2006) 287-293.
[177] D.R. Korb, J.V. Greiner, J. Herman, Comparison of fluorescein break-up time measurement reproducibility using standard fluorescein strips versus the Dry Eye Test (DET) method, Cornea 20(8) (2001) 811-815.
[178] P. Cho, B. Brown, I. Chan, R. Conway, M. Yap, Reliability of the Tear Break-Up Time Technique of Assessing Tear Stability and the Locations of the Tear Break-Up in Hong Kong Chinese, Optometry and Vision Science 69(11) (1992) 879-885.
[179] S.M. Cox, K.K. Nichols, J.J. Nichols, Agreement between Automated and Traditional Measures of Tear Film Breakup, Optometry and Vision Science 92(9) (2015) E257-E263.
[180] P. Cho, L. Leung, A. Lam, A. Choi, Tear break-up time: clinical procedures and their effects, Ophthalmic and Physiological Optics 18(4) (1998) 319-324.
[181] T. Kojima, R. Ishida, M. Dogru, E. Goto, Y. Takano, Y. Matsumoto, M. Kaido, Y. Ohashi, K. Tsubota, A new noninvasive tear stability analysis system for the assessment of dry eyes, Investigative Ophthalmology & Visual Science 45(5) (2004) 1369-1374.
[182] N.A. Listed, The Ocular Surface, The Ocular Surface 5(2) (April 2007).

[183] L.S. Mengher, A.J. Bron, S.R. Tonge, D.J. Gilbert, Effect of fluorescein instillation on the pre-corneal tear film stability, Curr. Eye Res. 4(1) (1985) 9-12.
[184] I. Toda, J. Shimazaki, K. Tsubota, Dry eye with only decreased tear break-up time is sometimes associated with allergic conjunctivitis, Ophthalmology 102(2) (1995) 302-309.
[185] S.C. Pflugfelder, S.C.G. Tseng, O. Sanabria, H. Kell, C.G. Garcia, C. Felix, W. Feuer, B.L. Reis, Evaluation of subjective assessments and objective diagnostic tests for diagnosing tear-film disorders known to cause ocular irritation, Cornea 17(1) (1998) 38-56.
[186] A.J. Bron, V.E. Evans, J.A. Smith, Grading of corneal and conjunctival staining in the context of other dry eye tests, Cornea 22(7) (2003) 640-650.
[187] J.J. Nichols, K.K. Nichols, B. Puent, M. Saracino, G.L. Mitchell, Evaluation of Tear Film Interference Patterns and Measures of Tear Break-Up Time, Optometry and Vision Science 79(6) (2002) 363-369.
[188] M. Elliott, H. Fandrich, T. Simpson, D. Fonn, Analysis of the repeatability of tear break-up time measurement techniques on asymptomatic subjects before, during and after contact lens wear, Contact Lens and Anterior Eye 21(4) (1998) 98-103.
[189] N. Best, L. Drury, J.S. Wolffsohn, Clinical evaluation of the Oculus Keratograph, Contact Lens & Anterior Eye 35(4) (2012) 171-174.
[190] G.V. Bahr, Könnte die Flussigkeitsabgang durch die Cornea von physiologischer Bedeutung sein, Acta Ophthalmologica 19(2) (1941) 125-134.
[191] V.Y. Bunya, N.M. Fuerst, M. Pistilli, B.E. McCabe, R. Salvo, I. Macchi, G.S. Ying, M. Massaro-Giordano, Variability of Tear Osmolarity in Patients With Dry Eye, JAMA Ophthalmol. 133(6) (2015) 662-667.
[192] TearLab, TearLab Osmolarity System: User Manual, TearLab Corporation, San Diego, California, 2012.
[193] A. Keech, M. Senchyna, B.D. Sullivan, M.A. Lemp, L.W. Jones, M.J. Brubaker, Impact of Time Between Collection on Human Tear Film Fluid Osmolarity, Investigative Ophthalmology & Visual Science 51(13) (2010) 4174-4174.
[194] P. Versura, V. Profazio, E.C. Campos, Performance of Tear Osmolarity Compared to Previous Diagnostic Tests for Dry Eye Diseases, Curr. Eye Res. 35(7) (2010) 553-564.
[195] S. Khanal, T.J. Millar, Barriers to clinical uptake of tear osmolarity measurements, British Journal of Ophthalmology 96(3) (2012) 341-344.
[196] A. Kingsnorth, Technological Enchancesments to Optometric Clinical Tests, ophthalmic Engineering, Aston University, England, 2015.
[197] P.D. O'Brien, L.M.T. Collum, Dry eye: Diagnosis and current treatment strategies, Curr. Allergy Asthma Rep. 4(4) (2004) 314-319.
[198] E. Uchiyama, J.D. Aronowicz, I.A. Butovich, J.P. McCulley, Pattern of vital staining and its correlation with aqueous tear deficiency and meibomian gland dropout, Eye and Contact Lens 33(4) (2007) 177-179.
[199] S.C. Pflugfelder, Differential diagnosis of dry eye conditions, Advances in dental research 10(1) (1996) 9-12.
[200] A. Behrens, J.J. Doyle, L. Stern, R.S. Chuck, P.J. McDonnell, D.T. Azar, H.S. Dua, M. Hom, P.M. Karpecki, P.R. Laibson, M.A. Lemp, D.M. Meisler, J.M. del Castillo, T.P. O'Brien, S.C. Pflugfelder, M. Rolando, O.D. Schein, B. Seitz, S.C. Tseng, G. van Setten, S.E. Wilson, S.C. Yiu, S. Dysfunctional Tear Syndrome, Dysfunctional tear syndrome - A Delphi approach to treatment recommendations, Cornea 25(8) (2006) 900-907.
[201] A.A.o.O.C.E.D. Panel, Preferred Practice Pattern- Dry Eye Syndrome, American Academy of Ophthalmology, 2013.
[202] M.S. Norm, Vital staining of cornea and conjunctiva, Eye Ear Nose and Throat Monthly 50(8) (1971) 294-&.
[203] W.D. Mathers, J.A. Lane, M.B. Zimmerman, Tear film changes associated with normal aging, Cornea 15(3) (1996) 229-234.

[204] J.A. Eliason, D.M. Maurice, Staining of the conjunctiva and conjunctival tear film, The British Journal of Ophthalmology 74(9) (1990) 519-522.
[205] M.S. NORN, CONGO RED VITAL STAINING OF CORNEA AND CONJUNCTIVA, Acta Ophthalmologica 54(5) (1976) 601-610.
[206] R.P.G. Feenstra, S.C.G. Tseng, What is actually stained by rose-bengal, Archives of Ophthalmology 110(7) (1992) 984-993.
[207] EdmundOpticsUK, Optics and Optical instrument annual catalogue, 2016, p. 133.
[208] B.H. Jeng, Diagnostic Techniques in Ocular Surface Disease. <https://clinicalgate.com/diagnostic-techniques-in-ocular-surface-disease/>, 2015 (accessed 14/06/2019.).
[209] F.J. Manning, S.R. Wehrly, G.N. Foulks, Patient tolerance and ocular surface staining characteristics of lissamine green versus rose bengal, Ophthalmology 102(12) (1995) 1953-1957.
[210] J. Kim, G.N. Foulks, Evaluation of the effect of lissamine green and rose bengal on human corneal epithelial cells, Cornea 18(3) (1999) 328-332.
[211] D.R. Korb, J.P. Herman, V.M. Finnemore, J.M. Exford, C.A. Blackie, An evaluation of the efficacy of fluorescein, rose bengal, lissamine green, and a new dye mixture for ocular surface staining, Eye & Contact Lens-Science and Clinical Practice 34(1) (2008) 61-64.
[212] P. Hamrah, F. Alipour, S. Jiang, J.H. Sohn, G.N. Foulks, Optimizing evaluation of Lissamine Green parameters for ocular surface staining, Eye 25(11) (2011) 1429-1434.
[213] M. Guillon, C. Maissa, Bulbar conjunctival staining in contact lens wearers and non lens wearers and its association with symptomatology, Contact Lens and Anterior Eye 28(2) (2005) 67-73.
[214] N. Efron, N.A. Brennan, P.B. Morgan, T. Wilson, Lid wiper epitheliopathy, Progress in Retinal and Eye Research 53 (2016) 140-174.
[215] N. Knop, D.R. Korb, C.A. Blackie, E. Knop, The Lid Wiper Contains Goblet Cells and Goblet Cell Crypts for Ocular Surface Lubrication During the Blink, Cornea 31(6) (2012) 668-679.
[216] D.R. Korb, J.P. Herman, C.A. Blackie, R.C. Scaffidi, J.V. Greiner, J.M. Exford, V.M. Finnemore, Prevalence of Lid Wiper Epitheliopathy in Subjects With Dry Eye Signs and Symptoms, Investigative Ophthalmology & Visual Science 50(13) (2009) 4640-4640.
[217] D.S. Mishra, Corneal staining procedure <https://www.slideshare.net/DrSamarthMishra/corneal-staining-procedure>, 2016 (accessed 21/01/2019.).
[218] S. Vahedi, M. Hessen, Dealing with Dry Eye: In the Present and in the Offing. <https://www.reviewofoptometry.com/article/dealing-with-dry-eye-in-the-present-and-in-the-offing>, 2016 (accessed 14/06/2019.).
[219] Jennifer P. Craig, James S. Wolffsohn, M.T.M. Wang, Making the Diagnosis with the TFOS DEWS II. <http://www.reviewofcontactlenses.com/article/making-the-diagnosis-with-the-tfos-dews-ii>, 2018 (accessed 21/01/2019.).
[220] F. Haurowitz, G. Braun, Zur Kalkverätzung der Cornea, hoppe-seyler's zeitschrift für physiologische chemie $V 123.
[221] P.B. Morgan, C. Maldonado-Codina, Corneal staining: Do we really understand what we are seeing?, Contact Lens & Anterior Eye 32(2) (2009) 48-54.
[222] C. Micallef, P. Cuschieri, Ocular infections due to contaminated solutions, Ophthalmologica 215(5) (2001) 337-350.
[223] S. Kyei, D. France, K. Asiedu, Microbial contamination of multiple-use bottles of fluorescein ophthalmic solution, Clinical and Experimental Optometry 102(1) (2019) 30-34.
[224] J.J. Nichols, P.E. King-Smith, E.A. Hinel, M. Thangavelu, K.K. Nichols, The Use of Fluorescent Quenching in Studying the Contribution of Evaporation to Tear Thinning, Investigative Ophthalmology & Visual Science 53(9) (2012) 5426-5432.
[225] F.H.F.M. Wiederholt, Human precorneal tear film pH measured by microelectrodes, Graefe's Archive for Clinical and Experimental Ophthalmology 218(3) (1982) 2.

[226] D.H. Lee, H.-J. Sung, D.-W. Han, M.-S. Lee, G.H. Ryu, M. Aihara, K. Takatori, J.-C. Park, In vitro bioassay of endotoxin using fluorescein as a pH indicator in a macrophage cell culture system, Yonsei Med J 46(2) (2005) 268-274.
[227] J. Murube, Fluorescein: The Most Commonly Used Surfocular Vital Stain, Ocular Surface 11(3) (2013) 144-149.
[228] Research in Dry Eye: Report of the Research Subcommittee of the International Dry Eye WorkShop (2007), The Ocular Surface 5(2) (2007) 179-193.
[229] J.S. Wolffsohn, R.C. Peterson, Anterior ophthalmic imaging, Clinical and Experimental Optometry 89(4) (2006) 205-214.
[230] N. Tanabe, K. Go, Y. Sakurada, M. Imasawa, F. Mabuchi, T. Chiba, K. Abe, K. Kashiwagi, A Remote Operating Slit Lamp Microscope System Development and its Utility in Ophthalmologic Examinations, Methods of Information in Medicine 50(5) (2011) 427-434.
[231] B. Wagner, Eye examination with the slit lamp, in: C.Z.M. AG, G.S. 51-52, Jena, Germany (Eds.) Germany 2001.
[232] M. Kaschke, K.-H. Donnerhacke, M.S. Ril, Optical Devices in Ophthalmology and Optometry: Technology, Design Principles and Clinical Applications, 2014.
[233] Topcon, SL- D Series Digital Slit Lamp, Europe, 2018.
[234] B.L.A.o.V. Care, Aston Fluorescein Enchancement Filter, 2009, p. 3.
[235] Medical Expo - Slit Lamp Suppliers. <http://www.medicalexpo.com/medical-manufacturer/slit-lamp-3410.html>, 2018 (accessed 15/10/2018.).
[236] W. Dawson, T. Nakanishi-Ueda, D. Armstrong, D. Reitze, D. Samuelson, M. Hope, S. Fukuda, m. Matsuishi, T. Ozawa, T. Ueda, R. Koide, Local Fundus Response to Blue (LED and Laser) and Infrared (LED and Laser) Sources, Experimental Eye Research 73(1) (2001) 137-147.
[237] H.R. Taylor, S. West, B. Munoz, F.S. Rosenthal, S.B. Bressler, N.M. Bressler, THE LONG-TERM EFFECTS OF VISIBLE-LIGHT ON THE EYE, Archives of Ophthalmology 110(1) (1992) 99-104.
[238] P.V. Algvere, J. Marshall, S. Seregard, Age-related maculopathy and the impact of blue light hazard, Acta Ophthalmologica Scandinavica 84(1) (2006) 4-15.
[239] R.W. Young, Solar-radiation and age-related macular degeneration, Survey of Ophthalmology 32(4) (1988) 252-269.
[240] J.W. McLaren, R.F. Brubaker, Light-sources for fluorescein fluorophotometry, Appl. Opt. 22(18) (1983) 2897-2905.
[241] J.W.T. Ham, J.J.J. Ruffolo, H.A. Mueller, A.M. Clarke, M.E. Moon, Histologic analysis of photochemical lesions produced in rhesus retina by short-wave-length light, Investigative Ophthalmology & Visual Science 17(10) (1978) 1029-1035.
[242] W.T. Ham, Jr., H.A. Mueller, J.J. Ruffolo, Jr., A.M. Clarke, Sensitivity of the retina to radiation damage as a function of wavelength, Photochem Photobiol 29(4) (1979) 735-43.
[243] J.L. Calkins, B.F. Hochheimer, S.A. D'Anna, Potential hazards from specific ophthalmic devices, Vision Research 20(12) (1980) 1039-1053.
[244] L.M. Rapp, S.C. Smith, Morphologic comparisons between rhodopsin-mediated and short-wavelength classes of retinal light damage, Investigative Ophthalmology & Visual Science 33(12) (1992) 3367-3377.
[245] Medlamps, Medlamps- Medical & Scientific Replacement Light Bulbs. <https://www.medlamps.co.uk/optical-lamps-and-bulbs/slit-lamp-bulbs.html>, 2018 2018).
[246] A. Optical, Ophthalmic Supply; Slit Lamps Bulbs. <http://armstrongoptical.com/ophthalmicsupply-slit-lamp-bulbs/>, 2018 (accessed 22/10/2018.2018).
[247] S.K. Ng, K.H. Loo, Y.M. Lai, C.K. Tse, Color Control System for RGB LED With Application to Light Sources Suffering From Prolonged Aging, IEEE Trans. Ind. Electron. 61(4) (2014) 1788-1798.
[248] W.S. Beich, Plastic Optics: Specifying Injection-Molded Polymer Optics. <http://www.photonics.com/EDU/Handbook.aspx?Tag=Optics&AID=25487>, 2016 (accessed 16/6/2016.).

[249] Curbell, Research & Compare Materials. <https://www.curbellplastics.com/Research-Solutions/Materials/Compare-Material-Properties>, 2018 (accessed 19/10/2018.2018).
[250] M. Biron, 4 - Detailed Accounts of Thermoplastic Resins, in: M. Biron (Ed.), Thermoplastics and Thermoplastic Composites (Second Edition), William Andrew Publishing2013, pp. 189-714.
[251] T.Y. Su, S.W. Chang, C.J. Yang, H.K. Chiang, Direct observation and validation of fluorescein tear film break-up patterns by using a dual thermal-fluorescent imaging system, Biomed. Opt. Express 5(8) (2014) 2614-2619.
[252] P.N. Dilly, Structure and function of the tear film, in: D.A. Sullivan (Ed.), Lacrimal Gland, Tear Film, and Dry Eye Syndromes: Basic Science and Clinical Relevance, Plenum Press Div Plenum Publishing Corp, New York, 1994, pp. 239-247.
[253] P.E. King-Smith, J.J. Nichols, K.K. Nichols, B.A. Fink, R.J. Braun, Contributions of evaporation and other mechanisms to tear film thinning and break-up, Optometry and Vision Science 85(8) (2008) 623-630.
[254] J.J. Nichols, L.T. Sinnott, Tear film, contact lens, and patient-related factors associated with contact lens-related dry eye, Investigative Ophthalmology & Visual Science 47(4) (2006) 1319-1328.
[255] J.J. Walline, Myopia Management in Young People, The ACLM Contact Lens Year Book 2013 (2012) 6.
[256] C. McAlinden, Corneal refractive surgery: past to present, Clinical and Experimental Optometry 95(4) (2012) 386-398.
[257] L. Dias, R.E. Manny, E. Weissberg, K.D. Fern, Myopia, contact lens use and self-esteem, Ophthalmic & physiological optics : the journal of the British College of Ophthalmic Opticians (Optometrists) 33(5) (2013) 573-580.
[258] K.N. Research, Ophthalmic Goods & Services- Market Update 2014, 2014.
[259] N. Pritchard, D. Fonn, DEHYDRATION, LENS MOVEMENT AND DRYNESS RATINGS OF HYDROGEL CONTACT-LENSES, Ophthalmic and Physiological Optics 15(4) (1995) 281-286.
[260] A. Jordan, J. Baum, J.L. Wobig, BASIC TEAR FLOW - DOES IT EXIST, Ophthalmology 87(9) (1980) 920-930.
[261] M.G. Doane, AN INSTRUMENT FOR INVIVO TEAR FILM INTERFEROMETRY, Optometry and Vision Science 66(6) (1989) 383-388.
[262] P.E. King-Smith, B.A. Fink, N. Fogt, Three interferometric methods for measuring the thickness of layers of the tear film, Optometry and Vision Science 76(1) (1999) 19-32.
[263] N. Yokoi, A. Komuro, Non-invasive methods of assessing the tear film, Experimental Eye Research 78(3) (2004) 399-407.
[264] J. Drescher, W. Stork, S. Hey, A. Gundlach, K.D.M. Glaser, C. Kreiner, Non-contact measurement of intraocular pressure using a modified Michelson interferometer, in: P.O. Rol, K.M. Joos, F. Manns, B.E. Stuck, M. Belkin (Eds.), Ophthalmic Technologies Ix, Proceedings Of, Spie-Int Soc Optical Engineering, Bellingham, 1999, pp. 104-113.
[265] D.N. Wang, S. Chen, K.T.V. Grattan, A.W. Palmer, A low coherence ''white light'' interferometric sensor for eye length measurement, Rev. Sci. Instrum. 66(12) (1995) 5464-5468.
[266] D. Huang, E.A. Swanson, C.P. Lin, J.S. Schuman, W.G. Stinson, W. Chang, M.R. Hee, T. Flotte, K. Gregory, C.A. Puliafito, J.G. Fujimoto, OPTICAL COHERENCE TOMOGRAPHY, Science 254(5035) (1991) 1178-1181.
[267] A. Konstantopoulos, P. Hossain, D.F. Anderson, Recent advances in ophthalmic anterior segment imaging: a new era for ophthalmic diagnosis?, British Journal of Ophthalmology 91(4) (2007) 551-557.
[268] M.E. Brezinski, J.G. Fujimoto, Optical coherence tomography: high-resolution imaging in nontransparent tissue, IEEE Journal of Selected Topics in Quantum Electronics 5(4) (1999) 1185-1192.
[269] D.T.E. Drew, The Development of Novel Instrumentation to further the Research in the Field, Opthalmic Engineering, Aston University, England, 2012.

[270] F. Forooghian, C. Cukras, C.B. Meyerle, E.Y. Chew, W.T. Wong, Evaluation of time domain and spectral domain optical coherence tomography in the measurement of diabetic macular edema, Investigative Ophthalmology & Visual Science 49(10) (2008) 4290-4296.
[271] A.J. Tatham, New Swept-Source OCT for Glaucoma: Improvements and Advantages, Review of Ophthalmology (2014) 8.
[272] G. Baikoff, H.J. Jodai, G. Bourgeon, Measurement of the internal diameter and depth of the anterior chamber: IOLMaster versus anterior chamber optical coherence tomographer, Journal of Cataract and Refractive Surgery 31(9) (2005) 1722-1728.
[273] H. McKee, C. Ye, M. Yu, S. Liu, D.S.C. Lam, C.K.S. Leung, Anterior Chamber Angle Imaging With Swept-Source Optical Coherence Tomography: Detecting the Scleral Spur, Schwalbe's Line, and Schlemm's Canal, Journal of Glaucoma 22(6) (2013) 468-472.
[274] C. Kent, Making the Most of Anterior Segment OCT. <https://www.reviewofophthalmology.com/article/making-the-most-of-anterior-segment-oct>, 2011 (accessed 28/07/2016.).
[275] J.S. Wolffsohn, L.N. Davies, Advances in ocular imaging, Expert Review of Ophthalmology 2(5) (2014) 755-767.
[276] MicroEpsilon, Measurement Product Guide 2015, Micro Epsilon, 2015.
[277] P. Optronik, Optical Sesnsors, 2014.
[278] P. Optronik, Optical Probes, 2014.
[279] J.M. Tiffany, Refractive index of meibomian and other lipids, Curr. Eye Res. 5(11) (1986) 887-889.
[280] J. Schwiegerling, Field Guide to Visual and Ophthalmic Optics, 2004.
[281] J.P. Craig, P.A. Simmons, S. Patel, A. Tomlinson, REFRACTIVE-INDEX AND OSMOLALITY OF HUMAN TEARS, Optometry and Vision Science 72(10) (1995) 718-724.
[282] Y.Q. Bai, J.J. Nichols, Advances in thickness measurements and dynamic visualization of the tear film using non-invasive optical approaches, Progress in Retinal and Eye Research 58 (2017) 28-44.
[283] S.I. Brown, D.G. Dervichian, Hydrodynamics of blinking: In vitro study of the interaction of the superficial oily layer and the tears, Archives of Ophthalmology 82(4) (1969) 541-547.
[284] P. Wolkoff, J.K. Nojgaard, P. Troiano, B. Piccoli, Eye complaints in the office environment: precorneal tear film integrity influenced by eye blinking efficiency, Occup. Environ. Med. 62(1) (2005) 4-12.
[285] R. Mapstone, C.V. Clark, DIURNAL-VARIATION IN THE DIMENSIONS OF THE ANTERIOR-CHAMBER, Archives of Ophthalmology 103(10) (1985) 1485-1486.
[286] B. Lackner, G. Schmidinger, S. Pieh, M.A. Funovics, C. Skorpik, Repeatability and reproducibility of central corneal thickness measurement with Pentacam, Orbscan, and ultrasound, Optometry and Vision Science 82(10) (2005) 892-899.
[287] J.A. Izatt, M.R. Hee, E.A. Swanson, C.P. Lin, D. Huang, J.S. Schuman, C.A. Puliafito, J.G. Fujimoto, MICROMETER-SCALE RESOLUTION IMAGING OF THE ANTERIOR EYE IN-VIVO WITH OPTICAL COHERENCE TOMOGRAPHY, Archives of Ophthalmology 112(12) (1994) 1584-1589.
[288] J. Wang, M. Abou Shousha, P. M., K. L., Y. C.L., S.H., M. Shen, L. Cui, V. Hurmeric, C. Du, D. Zhu, Q. Chen, M. Li, Ultra-high resolution optical coherence tomography for imaging the anterior segment of the eye, Ophthalmic surgery, lasers & imaging : the official journal of the International Society for Imaging in the Eye 42 (2011) 15-27.
[289] S.T. Fontana, R.F. Brubaker, VOLUME AND DEPTH OF THE ANTERIOR-CHAMBER IN THE NORMAL AGING HUMAN-EYE, Archives of Ophthalmology 98(10) (1980) 1803-1808.
[290] ACLM, Association of Contact Lens Manufactureres Contact Lens Year Book 2013, 2013.
[291] S.H. Kimball, P.E. King-Smith, J.J. Nichols, Evidence for the Major Contribution of Evaporation to Tear Film Thinning between Blinks, Investigative Ophthalmology & Visual Science 51(12) (2010) 6294-6297.

[292] N. Best, L. Drury, J.S. Wolffsohn, Predicting success with silicone-hydrogel contact lenses in new wearers, Contact Lens & Anterior Eye 36(5) (2013) 232-237.
[293] J.D. Nelson, J.P. Craig, E.K. Akpek, D.T. Azar, C. Belmonte, A.J. Bron, J.A. Clayton, M. Dogru, H.S. Dua, G.N. Foulks, J.A.P. Gomes, K.M. Hammitt, J. Holopainen, L. Jones, C.K. Joo, Z.G. Liu, J.J. Nichols, K.K. Nichols, G.D. Novack, V. Sangwan, F. Stapleton, A. Tomlinson, K. Tsubota, M.D.P. Willcox, J.S. Wolffsohn, D.A. Sullivan, TFOS DEWS II Introduction, Ocular Surface 15(3) (2017) 269-275.
[294] P.B. America, The scope of the eye injury problem, United States, 2010, p. 2.
[295] P. Blindness, Preventing Eye Injuries. <https://www.preventblindness.org/preventing-eye-injuries>, 2018 (accessed 19/11/2018.).
[296] M.W. Belin, D. Litoff, S.J. Strods, S.S. Winn, R.S. Smith, The PAR Technology Corneal Topography System, Refractive & corneal surgery 8(1) (1992) 88-96.
[297] A.F. Fercher, W. Drexler, C.K. Hitzenberger, T. Lasser, Optical coherence tomography - principles and applications, Reports on Progress in Physics 66(2) (2003) 239-303.
[298] P.B. Morgan, N. Efron, Demographics of UK contact lens prescribing, Contact Lens and Anterior Eye 31(1) (2008) 50-51.
[299] S.A. Melki, D.T. Azar, LASIK Complications: Etiology, Management, and Prevention, Survey of Ophthalmology 46(2) (2001) 95-116.
[300] S.G. Farah, D.T. Azar, C. Gurdal, J. Wong, Laser in situ keratomileusis: Literature review of a developing technique, Journal of Cataract and Refractive Surgery 24(7) (1998) 989-1006.
[301] S.L. Trokel, R. Srinivasan, B. Braren, EXCIMER LASER-SURGERY OF THE CORNEA, American Journal of Ophthalmology 96(6) (1983) 710-715.
[302] W. Sekundo, K.S. Kunert, M. Blum, Small incision corneal refractive surgery using the small incision lenticule extraction (SMILE) procedure for the correction of myopia and myopic astigmatism: results of a 6 month prospective study, British Journal of Ophthalmology 95(3) (2011) 335-339.
[303] L. Buratto, M. Ferrari, Indications, techniques, results, limits, and complications of laser in situ keratomileusis, Current Opinion in Ophthalmology 8(4) (1997) 59-66.
[304] A. Sugar, C.J. Rapuano, W.W. Culbertson, D. Huang, G.A. Varley, P.J. Agapitos, V.P. de Luise, D.D. Koch, Laser in situ Keratomileusis for myopia and astigmatism: Safety and efficacy - A report by the American Academy of Ophthalmology, Ophthalmology 109(1) (2002) 175-187.
[305] A.S. Chayet, K.K. Assil, M. Montes, M. Espinosa-Lagana, A. Castellanos, G. Tsioulias, Regression and its mechanisms after laser in situ keratomileusis in moderate and high myopia, Ophthalmology 105(7) (1998) 1194-1199.
[306] A.J. Kanellopoulos, I.G. Pallikaris, E.D. Donnenfeld, S. Detorakis, K. Koufala, H.D. Perry, Comparison of corneal sensation following photorefractive keratectomy and laser in situ keratomileusis, Journal of Cataract and Refractive Surgery 23(1) (1997) 34-38.
[307] L.E. Probst, J.J. Machat, Mathematics of laser in situ keratomileusis for high myopia, Journal of Cataract and Refractive Surgery 24(2) (1998) 190-195.
[308] S.D. McLeod, T.A. Kisla, N.C. Caro, T.T. McMahon, Iatrogenic keratoconus: Corneal ectasia following laser in situ keratomileusis for myopia, Archives of Ophthalmology 118(2) (2000) 282-284.
[309] L.T. Nordan, Keratoconus: Diagnosis and Treatment, International Ophthalmology Clinics 37(1) (1997).
[310] I. Toda, LASIK and the ocular surface, Cornea (2008).
[311] A. Denoyer, E. Landman, L. Trinh, J.-F. Faure, F. Auclin, C. Baudouin, Dry Eye Disease after Refractive Surgery: Comparative Outcomes of Small Incision Lenticule Extraction versus LASIK, Ophthalmology 122(4) (2015) 669-676.
[312] J.B. Lee, C.H. Ryu, J.H. Kim, E.K. Kim, H.B. Kim, Comparison of tear secretion and tear film instability after photorefractive keratectomy and laser in situ keratomileusis, Journal of Cataract and Refractive Surgery 26(9) (2000) 1326-1331.

[313] W.S. Kim, J.S. Kim, Change in corneal sensitivity following laser in situ keratomileusis, Journal of Cataract and Refractive Surgery 25(3) (1999) 368-373.
[314] J.C. Erie, J.W. McLaren, D.O. Hodge, W.M. Bourne, Recovery of corneal subbasal nerve density after PRK and LASIK, American Journal of Ophthalmology 140(6) (2005) 1059-1064.
[315] A.K.C. Lam, A HAND-HELD KERATOMETER, Ophthalmic and Physiological Optics 15(3) (1995) 227-230.
[316] W.A. Douthwaite, Contact Lens Optics & Lens Design, Butterworth-Heinemann 2005.
[317] J.H. Massig, E. Lingelbach, B. Lingelbach, Videokeratoscope for accurate and detailed measurement of the cornea surface, Appl. Opt. 44(12) (2005) 2281-2287.
[318] J. Veys, J. Meyler, I. Davies, Assessment of Corneal Contour, Essential Contact Lens Practice, Johnson & Johnson- The Vision Care Institute, 2008, p. 10.
[319] S. Cronje-Dunn, W.F. Harris, Keratometric variation: the influence of a fluid layer, Ophthalmic and Physiological Optics 16(3) (1996) 234-236.
[320] P.J. Timoney, C.S. Breathnach, Allvar Gullstrand and the slit lamp 1911, Irish J. Med. Sci. 182(2) (2013) 301-305.
[321] F. Cavas-Martínez, E. De la Cruz Sánchez, J. Nieto Martínez, F.J. Fernández Cañavate, D.G. Fernández-Pacheco, Corneal topography in keratoconus: state of the art, Eye and vision (London, England) 3 (2016) 5-5.
[322] P. P. Van Saarloos, I. J. Constable, Improved Method for Calculation of Corneal Topography for Any Photokeratoscope Geometry, 1992.
[323] L.S. Mengher, A.J. Bron, S.R. Tonge, D.J. Gilbert, A non-invasive instrument for clinical-assessment of the pre-corneal tear film stability, Curr. Eye Res. 4(1) (1985) 1-7.
[324] Z.G. Liu, A.J. Huang, S.C. Pflugfelder, Evaluation of corneal thickness and topography in normal eyes using the Orbscan corneal topography system, British Journal of Ophthalmology 83(7) (1999) 774-778.
[325] T. Swartz, L. Marten, M. Wang, Measuring the cornea: the latest developments in corneal topography, Current Opinion in Ophthalmology 18(4) (2007) 325-333.
[326] M.E. Johnson, P.J. Murphy, The Effect of Instilled Fluorescein Solution Volume on the Values and Repeatability of TBUT Measurements, Cornea 24(7) (2005) 811-817.
[327] J.X. Hong, X.H. Sun, A.J. Wei, X.H. Cui, Y.M. Li, T.T. Qian, W.T. Wang, J.J. Xu, Assessment of Tear Film Stability in Dry Eye With a Newly Developed Keratograph, Cornea 32(5) (2013) 716-721.
[328] L.E. Downie, Automated Tear Film Surface Quality Breakup Time as a Novel Clinical Marker for Tear Hyperosmolarity in Dry Eye Disease, Investigative Ophthalmology & Visual Science 56(12) (2015) 7260-7268.
[329] K. Gumus, C.H. Crockett, K. Rao, E. Yeu, M.P. Weikert, M. Shirayama, S. Hada, S.C. Pflugfelder, Noninvasive Assessment of Tear Stability with the Tear Stability Analysis System in Tear Dysfunction Patients, Investigative Ophthalmology & Visual Science 52(1) (2011) 456-461.
[330] S. Koh, C. Ikeda, H. Fujimoto, Y. Oie, T. Soma, N. Maeda, K. Nishida, Regional Differences in Tear Film Stability and Meibomian Glands in Patients With Aqueous-Deficient Dry Eye, Eye & Contact Lens-Science and Clinical Practice 42(4) (2016) 250-255.
[331] M. Darien B. Gaw, Bernard Gil O. Tinio, MD, A Simplified Xeroscope for the Noninvasive Measurement of Tear Break-up Time, Philippine Journal of OPHTHALMOLOGY (40) (2015) 18-23.
[332] W.Z. Lan, L.X. Lin, X. Yang, M.B. Yu, Automatic Noninvasive Tear Breakup Time (TBUT) and Conventional Fluorescent TBUT, Optometry and Vision Science 91(12) (2014) 1412-1418.
[333] R.A. Armstrong, L.N. Davies, M.C.M. Dunne, B. Gilmartin, Statistical guidelines for clinical studies of human vision, Ophthalmic and Physiological Optics 31(2) (2011) 123-136.
[334] B. Munoz, S.K. West, G.S. Rubin, O.D. Schein, H.A. Quigley, S.B. Bressler, K. Bandeen-Roche, S.E.E.S. Team, Causes of blindness and visual impairment in a population of older Americans - The Salisbury Eye Evaluation Study, Archives of Ophthalmology 118(6) (2000) 819-825.

[335] S.E. Moss, R. Klein, B.K. Klein, Prevalence of and risk factors for dry eye syndrome, Archives of Ophthalmology 118(9) (2000) 1264-1268.
[336] O.D. Schein, B. Munoz, J.M. Tielsch, K. BandeenRoche, S. West, Prevalence of dry eye among the elderly, American Journal of Ophthalmology 124(6) (1997) 723-728.
[337] S.S. Lane, H.B. DuBiner, R.J. Epstein, P.H. Ernest, J.V. Greiner, D.R. Hardten, E.J. Holland, M.A. Lemp, J.E. McDonald, 2nd, D.I. Silbert, C.A. Blackie, C.A. Stevens, R. Bedi, A new system, the LipiFlow, for the treatment of meibomian gland dysfunction, Cornea 31(4) (2012) 396-404.
[338] C.A. Blackie, C.A. Coleman, E.J. Holland, G. LipiFlow Study, The sustained effect (12 months) of a single-dose vectored thermal pulsation procedure for meibomian gland dysfunction and evaporative dry eye, Clinical Ophthalmology 10 (2016) 1385-1395.
[339] C.A. Blackie, A.N. Carlson, D.R. Korb, Treatment for meibomian gland dysfunction and dry eye symptoms with a single-dose vectored thermal pulsation: a review, Current Opinion in Ophthalmology 26(4) (2015) 306-313.